UILU-ENG-78-2022

CIVIL ENGINEERING STUDIES
STRUCTURAL RESEARCH SERIES NO. 455

INELASTIC RESPONSE OF REINFORCED CONCRETE COLUMNS SUBJECTED TO TWO-DIMENSIONAL EARTHQUAKE MOTIONS

By
M. I. H. SUHARWARDY
D. A. PECKNOLD

Technical Report of Research
Supported by the
NATIONAL SCIENCE FOUNDATION (RANN)
under Grants
ENV 75-08456
ENV 77-07190

DEPARTMENT OF CIVIL ENGINEERING
UNIVERSITY OF ILLINOIS
at URBANA-CHAMPAIGN
URBANA, ILLINOIS

OCTOBER 1978

ILU-ENG-78-2022

INELASTIC RESPONSE OF REINFORCED CONCRETE COLUMNS SUBJECTED TO TWO-DIMENSIONAL EARTHQUAKE MOTIONS

by

M.I.H. Suharwardy
D. A. Pecknold

University of Illinois
Urbana, Illinois

October 1978

BIBLIOGRAPHIC DATA SHEET	1. Report No. UILU-ENG-2022	2.	3. Recipient's Accession No. PB291207
4. Title and Subtitle: INELASTIC RESPONSE OF REINFORCED CONCRETE COLUMNS SUBJECTED TO TWO-DIMENSIONAL EARTHQUAKE MOTIONS			5. Report Date: October 1978 6.
7. Author(s): M.I.H. Suharwardy, D. A. Pecknold			8. Performing Organization Rept. No. SRS 455
9. Performing Organization Name and Address: University of Illinois at Urbana-Champaign Urbana, Illinois 61801			10. Project/Task/Work Unit No. 11. Contract/Grant No. ENV 75-08456 ENV 77-07190
12. Sponsoring Organization Name and Address: NATIONAL SCIENCE FOUNDATION (RANN)			13. Type of Report & Period Covered 14.

15. Supplementary Notes

16. Abstracts: This study was undertaken to determine the effects of two-dimensional earthquake motion on reinforced concrete (R/C) columns. An analytical model to represent the shear-deflection-axial load relationship of R/C columns is developed from stress-strain relations of steel and concrete. Improved hysteresis model for steel included the Bauschinger effect and the model for concrete included the deterioration of strength and stiffness under cyclic loading. The lumping of concrete at the end sections for calculating moment-curvature relationships in conjunction with an assumed curvature distribution along the column leads to an efficient procedure for the calculation of the shear-deflection-axial load relationship for R/C columns. The analytical model compares favorably with experimental results for both uniaxial and biaxial loading conditions. The analytical model predicts significant changes in the strength, energy absorption capacity and accumulated damage responses of the column under biaxial deformations as compared to the corresponding responses under uniaxial deformations.

17. Key Words and Document Analysis. 17a. Descriptors

Biaxial bending, Columns, Cyclic loading, Earthquake engineering, Hysteresis, Inelastic response, Nonlinear dynamic analysis, Reinforeced concrete, Two-dimensional interaction.

17b. Identifiers/Open-Ended Terms

17c. COSATI Field/Group

18. Availability Statement	19. Security Class (This Report)	21. No. of Pages
Release Unlimited	UNCLASSIFIED	226
	20. Security Class (This Page) UNCLASSIFIED	22. Price PC A10 MF A01

FORM NTIS-35 (REV. 10-73) ENDORSED BY ANSI AND UNESCO. THIS FORM MAY BE REPRODUCED USCOMM-DC 8265-P74

ACKNOWLEDGMENT

This thesis was prepared under the supervision of Professor David A. W. Pecknold, whose guidance and encouragement are deeply appreciated.

The study is based upon research supported by the National Science Foundation under Grant Nos. GI-29934 and ENV75-08456.

Any opinions, findings, and conclusions or recommendations expressed in this thesis are those of the author and do not necessarily reflect the views of the National Science Foundation.

TABLE OF CONTENTS

		Page
1.	INTRODUCTION	1
	1.1 General	1
	1.2 Brief Review of Previous Investigations	3
	1.3 Object and Scope	7
2.	ANALYTICAL MODEL	10
	2.1 Introductory Remarks	10
	2.2 Stress-Strain Relations	13
	2.3 Development of the Analytical Model	18
	2.3.1 Moment-Curvature-Axial Load Relationship	19
	2.3.2 Shear-Deflection-Axial Load Relationship	29
	2.4 Comparisons with Experiments	38
	2.5 Characteristics of the Proposed Analytical Model	42
	2.6 Concluding Remarks	49
3.	DYNAMIC RESPONSE UNDER EARTHQUAKE MOTION	51
	3.1 Introductory Remarks	51
	3.2 Earthquake Characteristics	53
	3.3 System Characteristics	56
	3.4 Results and Discussion of Dynamic Response	57
	3.4.1 T = 0.4 Systems under Design Strength Earthquakes	58
	3.4.2 Effect of System Period	62
	3.4.3 Effect of Earthquake Strength	64

Page

3.5 Effect of Axial Load 65

3.6 Effect of Material Hysteresis Rules . . 68

3.7 Concluding Remarks 71

4. CONCLUSIONS 73

REFERENCES 79

APPENDIX

A MATERIAL HYSTERESIS RULES 183

B CALCULATION OF MOMENT-CURVATURE-AXIAL LOAD RELATIONS 189

C CALCULATION OF SHEAR-DEFLECTION-AXIAL LOAD RELATIONS 193

D PROCEDURE FOR DYNAMIC ANALYSIS 198

E NOTATIONS 206

LIST OF TABLES

Table		Page
2.1	Two-Dimensional Curvature Histories (Fig. 2.19)	84
2.2	Properties of Test Specimens	85
2.3	Two-Dimensional Displacement Histories for Takizawa's Tests (Fig. 2.37)	86
3.1	System Properties	87
3.2	Maximum Displacement Response of Systems with Design Strength	88
3.3	Effect of Strength on Maximum Displacement Response	89
3.4	System Properties for Different Axial Loads	90
3.5	Maximum Displacement Response for Different Axial Loads, T = 0.4, Taft Record	91

LIST OF FIGURES

Figure		Page
2.1	Schematic Diagram of Proposed Hysteresis Model for Reinforcing Steel	92
2.2	Comparison of Proposed Hysteresis Model for Reinforcing Steel with Experiment, Specimen 5 (Ref. 2)	93
2.3	Comparison of Proposed Hysteresis Model for Reinforcing Steel with Experiment, Specimen 8 (Ref. 2)	94
2.4	Comparison of Proposed Hysteresis Model for Reinforcing Steel with Experiment and with Kent's Model, Specimen 25 (Ref. 13) .	95
2.5	Schematic Diagram of Proposed Hysteresis Model for Concrete	96
2.6	Comparison of Proposed Hysteresis Model for Concrete with Experiment (Ref. 28) . .	97
2.7	Comparison of Proposed Hysteresis Model for Concrete with Experiment, Specimen AC2-09 (Ref. 12)	98
2.8	Discretization of Concrete Area for 'Exact' Integration	99
2.9	Discretization of Concrete Area for 'Proposed' Integration	100
2.10	Points on Axial Load-Moment Interaction Diagram Matched to Obtain Areas and Locations of Lumped Concrete for Proposed Integration Scheme	101
2.11	Comparison of 'Exact' and 'Proposed' Integration, Circular Column, Axial Load-Moment Interaction, for Steel Ratios of 1, 2, 3, 4, 5 and 6%	102

Figure		Page
2.12	Comparison of 'Exact' and 'Proposed' Integration, Square Column, Axial Load-Moment Interaction, for Steel Ratios of 1, 2, 3, 4, 5 and 6%	103
2.13	Comparison of 'Exact' and 'Proposed' Integration, Circular Column, Moment-Curvature Relationship, for Steel Ratios of 1, 2, 3, 4, 5 and 6%	105
2.14	Comparison of 'Exact' and 'Proposed' Integration, Square Column, Moment-Curvature Relationship, for Steel Ratios of 1, 2, 3, 4, 5 and 6%	106
2.15	Test Columns Used for Analytical Cyclic Response Study	107
2.16	Comparison of 'Exact' and 'Proposed' Integration, Test Columns, Axial Load-Moment Interaction	108
2.17	Comparison of 'Exact' and 'Proposed' Integration, Circular Test Column, Moment-Curvature Relationship, Cyclic Loading	109
2.18	Comparison of 'Exact' and 'Proposed' Integration, Square Test Column, Moment-Curvature Relationship, Cyclic Loading . .	112
2.19	Two-Dimensional Curvature Histories Used to Compare 'Exact' and 'Proposed' Integration in Calculating Moment-Curvature Relationships	114
2.20	Comparison of 'Exact' and 'Proposed' Integration, Circular Test Column, Moment-Curvature Relationship, Two-Dimensional Cyclic Loading, Curvature History 1	115
2.21	Comparison of 'Exact' and 'Proposed' Integration, Circular Test Column, Moment-Curvature Relationship, Two-Dimensional Cyclic Loading, Curvature Histories 2 and 3	116

Figure		Page
2.22	Column Segments and Assumed Curvature Distribution Along Column	117
2.23	Assumed Curvature Distribution Along Column at Different Stages of Loading . .	118
2.24	Cracking and Yield Curves for Determination of Cracking or Yielding at a Section	119
2.25	Two-Dimensional Displacement Histories Used for Comparing Assumed and Calculated Moment-Curvature Relationships Along Column	120
2.26	Comparison of Assumed and Calculated Moment-Curvature Relationships Along Column Used in Deflection Calculations, Circular Column, Two-Dimensional Displacement History 1, Direction 1 . . .	121
2.27	Comparison of Assumed and Calculated Moment-Curvature Relationships Along Column Used in Deflection Calculations, Circular Column, Two-Dimensional Displacement History 1, Direction 2 . . .	122
2.28	Comparison of Assumed and Calculated Moment-Curvature Relationships Along Column Used in Deflection Calculations, Square Column, Two-Dimensional Displacement History 1, Direction 1 . . .	123
2.29	Comparison of Assumed and Calculated Moment-Curvature Relationships Along Column Used in Deflection Calculations, Square Column, Two-Dimensional Displacement History 1, Direction 2 . . .	124
2.30	Comparison of Assumed and Calculated Moment-Curvature Relationships Along Column Used in Deflection Calculations, Circular Column, Two-Dimensional Displacement History 2, Direction 1 . . .	125

Figure		Page
2.31	Comparison of Assumed and Calculated Moment-Curvature Relationships Along Column Used in Deflection Calculations, Circular Column, Two-Dimensional Displacement History 3, Direction 1 . . .	126
2.32	Comparison of Assumed and Calculated Moment-Curvature Relationships Along Column Used in Deflection Calculations, Circular Column, One-Dimensional with P = 0	127
2.33	Comparison of Assumed and Calculated Moment-Curvature Relationships Along Column Used in Deflection Calculations, Circular Column, One-Dimensional with Varying Axial Load	128
2.34	Comparison of Analytical and Experimental Moment-Curvature Relationships, Aoyama's Tests (Ref. 3)	129
2.35	Comparison of Analytical and Experimental Moment-Curvature Relationship, Karlsson's Specimen BK5 (Ref. 11)	130
2.36	Comparison of Analytical and Experimental Moment-Displacement Relationship, Karlsson's Specimen BK5 (Ref. 11)	131
2.37	Nominal Two-Dimensional Displacement Histories for Takizawa's Tests (Ref. 34) .	132
2.38	Comparison of Analytical and Experimental Shear-Deflection Relationship, Takizawa's Tests (Ref. 34)	133
3.1	Acceleration Records of Earthquakes Used in Study, Scaled to 1.0 g Peak Acceleration	135
3.2	20 Second Elastic Response Spectra, El Centro Record, Scaled to 1.0 g Peak Acceleration, 0%, 2%, 5% and 20% Damping .	136

Figure		Page
3.3	20 Second Elastic Response Spectra, Taft Record, Scaled to 1.0 g Peak Acceleration, 0%, 2%, 5% and 20% Damping	137
3.4	Principal Directions and Variances of Earthquake Records Used, Scaled to 1.0 g Peak Acceleration	138
3.5	Design Strength of Systems Compared with Required Strength of Elasto-Plastic Systems Subjected to El Centro and Taft Records, Calculated for $\mu = 4$	139
3.6	Displacement Response, T = 0.4 System, El Centro Record	140
3.7	Shear-Displacement Response, T = 0.4 System, El Centro N-S Record	141
3.8	Shear-Displacement Response, T = 0.4 System, El Centro E-W Record	142
3.9	2D Displacement Response of T = 0.4 System to the El Centro Record	143
3.10	2D Shear Response of T = 0.4 System to the El Centro Record	144
3.11	Centroidal Strain-Time History, T = 0.4 System, El Centro Record	145
3.12	Input and Hysteresis Energy-Time History, T = 0.4 System, El Centro Record .	146
3.13	Displacement Response, T = 0.4 System, Taft Record	147
3.14	Shear-Displacement Response, T = 0.4 System, Taft S69E Record	148
3.15	Shear-Displacement Response, T = 0.4 System, Taft N21E Record	149
3.16	2D Displacement Response of T = 0.4 System to the Taft Record	150

Figure		Page
3.17	2D Shear Response of T = 0.4 System to the Taft Record	151
3.18	Centroidal Strain-Time History, T = 0.4 System, Taft Record	152
3.19	Input and Hysteresis Energy-Time History, T = 0.4 System, Taft Record	153
3.20	Displacement Response, T = 0.2 System, El Centro Record	154
3.21	Displacement Response, T = 0.8 System, El Centro Record	155
3.22	Displacement Response, T = 1.6 System, El Centro Record	156
3.23	Displacement Response, T = 0.2 System, Taft Record	157
3.24	Displacement Response, T = 0.8 System, Taft Record	158
3.25	Displacement Response, T = 1.6 System, Taft Record	159
3.26	Maximum Displacement Response of Systems with Design Strength, El Centro Record . .	160
3.27	Maximum Displacement Response of Systems with Design Strength, Taft Record	161
3.28	Effect of P-Δ on Displacement Response, T = 0.4 System, Taft S69E Record	162
3.29	Effect of P-Δ on Displacement Response, T = 0.4 System, Taft N21E Record	163
3.30	Effect of System Strength on Maximum Displacement Response, El Centro Record . .	164
3.31	Effect of System Strength on Maximum Displacement Response, Taft Record . . .	165
3.32	Shear Displacement Response, P = - 562 kips, T = 0.4 System, Taft S69E Record	166

Figure		Page
3.33	Shear-Displacement Response, P = - 562 kips, T = 0.4 System, Taft N21E Record	167
3.34	Effect of Axial Load on Displacement Response, T = 0.4 System, Taft S69E Record	168
3.35	Effect of Axial Load on Displacement Response, T = 0.4 System, Taft N21E Record	169
3.36	Effect of Axial Load on Maximum Displacement Response, T = 0.4 System, Taft Record	170
3.37	Shear-Displacement Response of Edge Columns Subjected to 1D Displacement Response of T = 0.8 Interior Column to El Centro, N-S Record	171
3.38	Shear-Displacement Response of Edge Columns Subjected to 1D Displacement Response of T = 1.6 Interior Column to El Centro, N-S Record	172
3.39	Shear-Displacement Response, Bilinear Steel, 3% Hardening Slope, P = - 562, T = 0.4 System, Taft S69E Record	173
3.40	Shear-Displacement Response, Bilinear Steel, 3% Hardening Slope, P = - 562, T = 0.4 System, Taft N21E Record	174
3.41	Shear-Displacement Response, Bilinear Steel, 1.5% Hardening Slope, P = - 562, T = 0.4 System, Taft S69E Record	175
3.42	Shear-Displacement Response, Bilinear Steel, 1.5% Hardening Slope, P = - 562, T = 0.4 System, Taft N21E Record	176
3.43	Effect of Hardening Slope of Bilinear Steel on Displacement Response, P = - 562, T = 0.4 System, Taft S69E Record	177

Figure		Page
3.44	Effect of Hardening Slope of Bilinear Steel on Displacement Response, P = - 562, T = 0.4 System, Taft N21E Record	178
3.45	Shear-Displacement Response, Concrete Confined by Ties, Ω = 40, P = - 562, T = 0.4 System, Taft S69E Record	179
3.46	Shear-Displacement Response, Concrete Confined by Ties, Ω = 40, P = - 562, T = 0.4 System, Taft N21E Record	180
3.47	Effect of Concrete Confinement on Displacement Response, P = - 562, T = 0.4 System, Taft S69E Record	181
3.48	Effect of Concrete Confinement on Displacement Response, P = - 562, T = 0.4 System, Taft N21E Record	182
D.1	Flow-Chart of Calculation Procedure for Single Time Step	205

1. INTRODUCTION

1.1 General

The dynamic response of a structure to a given motion is dependent upon its strength, stiffness, and damping and hysteretic energy absorption capacities. Each of these characteristics of the structure can change significantly when it is subjected to concurrent earthquake motions in more than one direction. This change is a result of interaction between the resisting mechanisms in different directions.

The components of earthquake motion in different directions have been found to be nearly uncorrelated (14). It is, therefore, unlikely that the components of the ground motion are simultaneously large. As a consequence, the effect of concurrent earthquake motions in different directions on an elastic structure will be small, because the elastic response in the different directions will be uncorrelated.

For structural response in the inelastic range, however, the response in any particular direction could significantly change the characteristics of the structure in other directions due to inelastic interaction, thereby changing the response of the structure in that direction. This interaction, and thus the change in the properties of a structure in a given direction, increases with the increase in the level of inelasticity the structure undergoes.

Inelastic response of structures to medium and strong earthquakes is implicit in the designs specified by modern building codes (23, 36, 37). The effects of multidirectional interaction on the response of earthquake resistant structures should, therefore, be investigated to determine whether extra provisions should be made in future building codes for the simultaneous occurrence of earthquake motions in different directions.

In framed buildings the effect of the multidirectional nature of the earthquake is most pronounced in the columns. They are subjected to biaxial bending due to the two orthogonal components of the horizontal earthquake motion and the torsional earthquake motion, and are subjected to time dependent axial loads because of overturning moments and vertical earthquake motion.

Recent investigations (18, 20, 21) have related the end forces and end displacements of the column, referred to in this study as the shear-deflection relationship, using theory of plasticity formulations to show the importance of interaction effects in the response of columns subjected to the two orthogonal horizontal components of the ground motion.

For the uniaxial case these plasticity formulations reduce to a bilinear idealization of the shear-deflection relationship. Bilinear hysteresis loops do not realistically represent uniaxial cyclic behavior of reinforced concrete columns (29). Therefore, a different formulation is required

to model the uniaxial cyclic behavior of reinforced concrete columns and to extend it to the biaxial case. A study of the effects of two-dimensional earthquake motion on reinforced concrete columns can then be made.

1.2 Brief Review of Previous Investigations

A significant number of studies, both experimental and analytical, have been made on the behavior of reinforced concrete columns and frames subjected to one-dimensional earthquake motion (29). Studies on the two-dimensional behavior of such columns and frames are, however, very few.

Takiguchi and Kokusho (31) tested several square reinforced concrete sections under cyclic deformations in one direction and constant bending moment in the orthogonal direction. It was reported that significant changes, depending on the amplitude of the cyclic deformation, occurred in the bending moment response in the direction cycled and in the displacement response in the constant moment direction. Takizawa and Aoyama (34) tested a set of square reinforced concrete columns under complex uniaxial and biaxial displacement paths. Considerable strength and energy absorption changes were observed in columns subjected to biaxial loading when compared to those loaded with uniaxial projections of the biaxial deformation paths.

Analytical studies on the two-dimensional behavior of reinforced concrete columns have essentially utilized two types

of models. The first model used by most investigators (18, 20, 21, 22, 26, 32, 34) considers the columns to be a class of structural elements whose shear-deflection relationship can be modeled by use of yield surfaces and rules of plasticity (6) or their modifications (16, 39). The second model used in some studies (1, 19, 31), develops the shear-deflection relationship of the reinforced concrete column from stress-strain relationships of steel and concrete by considering the column to be composed of discrete filaments and assuming a curvature distribution along the length of the column.

Nigam (18) using the first type of model, studied the two dimensional behavior of single mass systems supported on fixed-fixed columns with elastic-perfectly-plastic properties subjected to steady-state and earthquake excitations. Under steady-state sinusoidal excitation peak responses for the biaxial case with an input phase difference of 30° occurred at lower exciting frequencies than for the uniaxial case and were much amplified at these frequencies in comparison to the uniaxial case. Under earthquake type excitations the biaxial interaction effects were found to be important for short period systems only. Pecknold (21) using a similar formulation studied the effect of system strength and fundamental period on the biaxial response of single mass systems. The biaxial effects were found to increase, in most cases, with a decrease in the system strength. The biaxial effects significantly increased

the system response whenever gravity (P-Δ) effects were included in the formulation and the uniaxial ductility was large. Padilla (20) included strain hardening in his formulation and found it to be an important parameter. He also studied biaxial effects on several five story framed structures under earthquake excitation and found a major redistribution of energy dissipation, in buildings of usual proportion, from the girders to the columns if biaxial interaction was included. It was also suggested that the biaxial effects in conjunction with P-Δ would have been critical for some designs if a sufficiently long duration of the earthquake record was used.

In a recent publication Takizawa and Aoyama (34) have extended several one-dimensional shear-deflection hysteresis rules for reinforced concrete columns to two-dimensions using a plasticity formulation similar to Mroz's (16) method of fields of work-hardening. This procedure was used to extend the 'degrading trilinear' and the 'non-degrading bilinear and trilinear' hysteresis rules of the uniaxial case to two-dimensions. The 'degrading trilinear' hysteresis rule models uniaxial experimental data quite well (30), and its extension to two dimensions was shown to model, to a fair degree, the qualitative behavior observed in experiments (34). These biaxial models for shear-deflection relationships were used to study two-dimensional response of single mass systems under earthquake excitations. It was reported that biaxial effects could

substantially increase the displacement response of the system, and that for any given system the biaxial effects were sensitive to the hysteresis rules used (being largest for the 'degrading trilinear' model), the degree of inelasticity which the system undergoes, the earthquake record used and the cross-correlation between the two components of the earthquake record (33). In a later study Takizawa (32) included the effects of gravity and deteriorating strength in the formulation. Although for the systems studied, the effects of P-Δ and deteriorating strength were not significant under uniaxial excitation, they became critical under biaxial excitation.

Takiguchi and Kokusho (31), and Okada et al. (19) used the second type of model, developing the shear-deflection relationship from assumed stress-strain relations for steel and concrete and making assumptions about the distribution of strain over the section and curvature over the length of the column. The analytical model was reported to match experimental data fairly well showing the same basic characteristics as observed in the tests. Aktan (1) used a similar analytical model to study the behavior of single mass systems under biaxial earthquake excitation. It was concluded in the study that if uniaxial displacement responses exceeded about twice the crushing deflection the biaxial displacement responses may be substantially higher.

In summary, the results obtained by previous investigators have one common conclusion, that the two-dimensional

effects can be significant for some systems. However, the extensive results obtained by Takizawa (32, 33, 34) to determine the factors which influence the magnitude of this effect are based on models developed from empirical extensions of theory of plasticity which may not adequately represent reinforced concrete column behavior. Aktan's model (1) was developed from the stress-strain properties of steel and concrete, but only limited results were obtained because of excessive computational costs. This study was undertaken to develop a computationally more efficient model which can adequately represent reinforced concrete column behavior so that the applicability of Takizawa's results to reinforced concrete columns can be verified.

1.3 Object and Scope

The study reported herein had two specific objectives, which were:

1. To develop a computationally efficient procedure, which would model the basic characteristics of the shear-deflection relationship, as observed experimentally, of reinforced concrete columns subjected to uniaxial shears and axial load, and which can be extended, by a consistent formulation, to model the same relationship for reinforced concrete columns subjected to biaxial shears;

2. To study the effect of two-dimensional earthquake motion on the response of reinforced concrete columns, as compared to their response to one-dimensional earthquake motion, and to ascertain the influence of various factors, relating both to earthquake characteristics and system characteristics, on this comparison.

The shear-deflection model for reinforced concrete columns is developed from stress-strain relationships of constituent materials by assuming the distribution of strain over the section and the distribution of curvature along the length of the column. Hysteresis and deterioration in concrete strength due to cycling and strain-hardening and the Baushinger effect in steel are accounted for. Effect of bar slip is not explicitly taken into account. Creep and shrinkage effects are neglected. Shear and anchorage failures, and large reductions in shear strength due to insufficient lateral reinforcement are excluded from the formulation.

Chapter 2 describes the development of the shear-deflection model. The calculated stress-strain relationships for steel and concrete, moment-curvature relationships of reinforced concrete sections, and shear-deflection relationships of reinforced concrete elements are also compared with experimental results of previous investigations.

Chapter 3 describes the results of the dynamic analyses. The dynamic analyses were limited to single mass systems

supported on fixed-fixed columns. Responses of the columns to both one- and two-dimensional earthquake motions were calculated. Scaled time-histories of the horizontal components of the El Centro 1940 and Taft 1952 earthquakes were used. A wide range of initial system periods and earthquake strength were studied and the effect of these variables on the two-dimensional response as compared to the one-dimensional response observed. The effects of P-Δ, and different and varying axial loads in influencing the two-dimensional responses were studied. The effect of material hysteresis rules was also briefly investigated.

In the last chapter, general conclusions resulting from the present study are presented.

2. ANALYTICAL MODEL

2.1 Introductory Remarks

The object of this chapter is to develop a mathematical model for the calculation of shear-deflection-axial load relationship of reinforced concrete columns subjected simultaneously to biaxial shears and axial load. This model is used in Chapter 3 to predict the behavior of fixed-fixed reinforced concrete columns subjected to two-dimensional earthquake motions.

Previous investigators have used two types of models for calculating the shear-deflection relationship of reinforced concrete columns subjected to uniaxial shear and axial load.

The first type of models are characterized by a set of rules to determine directly the shear-deflection relationship for a column under a given axial load. These set of rules are formulated to predict the basic characteristics of the experimentally observed shear-deflection relationship. These type of models include the bilinear, bilinear degrading (4), trilinear degrading (30), Ramberg-Osgood (10) and so on.

The second type of models are developed from the basic stress-strain relations for steel and concrete using principles of mechanics with assumptions about strain and curvature distributions or displacement distributions. In the more general form, this type includes finite element modeling of the column (40).

In the simpler form,moment-curvature relationships are obtained at a number of sections along the length of the column by dividing the sections into layers of steel and concrete and tracing stress-strain histories of these layers as the loading progresses (13, 15). These type of models have two major drawbacks. Firstly, only flexural and axial load behavior of reinforced concrete columns is understood to a degree that it may be analytically synthesized. Therefore, shear deformations and deformations arising from bond and anchorage slips are either neglected or gross assumptions about them are made. Secondly, the amount of computation required and the data to be monitored in using such models is very large.

Both types of models have been extended to predict behavior of reinforced concrete columns under biaxial shears and axial load. Since very few experiments in this area have been reported, the basic characteristics of two-dimensional shear-deflection behavior of reinforced concrete columns have not yet been determined. The first type of models have, therefore, been extended to two-dimensions using concepts of plasticity, such as yield surfaces and flow rules (20, 34). A theoretical or experimental basis for use of such flow rules for reinforced concrete columns has yet to be established. The second type of models can be extended to two-dimensions without involving any new concepts. The column is now divided into filaments instead of layers (1) or into three-dimensional

finite elements instead of two-dimensional ones. However, the drawbacks of such models, noted earlier for uniaxial shear, are even greater for the two-dimensional case. The amount of computation and data monitored increases by an order of magnitude or more. Also, the effects of shear deformation and bond and anchorage slips in two dimensions can only be guessed at, since experimental data on these are unavailable.

A model of the second type was developed for this study. Shear-deflection relationships for the column under biaxial shears and axial load were calculated from moment-curvature relationships at the end section of the column by making assumptions on the distribution of curvatures along the length of the column. The moment-curvature relationships were calculated from stress-strain relations for steel and concrete. The concrete area at the end sections was lumped at a few discrete points on the section to reduce the amount of computation.

The model was developed with the object of obtaining the same characteristics with respect to strength and energy absorption in the calculated relationship for shear-deflection as observed experimentally for uniaxial shears, and using the same assumptions to obtain the relationship for biaxial shears. No attempt was made to predict failure of the column. Experimental data in this area, especially for the biaxial case, is insufficient for failure of the column to be modeled.

The analytical model developed here is restricted to columns restrained against rotations at both ends. A more general model can be developed based on the same concepts as used in this study. However, a more complex numerical procedure would be required, because of the increase in the number of variables. This will increase the amount of computations considerably.

The stress-strain relations for steel and concrete used in the study are given in Section 2.2. The development of the model is described in Section 2.3. In Section 2.4 the model is compared with some available experimental data. The characteristics of the model under axial load and biaxial shears are discussed in Section 2.5

2.2 Stress-Strain Relations

a) Steel

The calculated moment-curvature relationship of a reinforced concrete section is dependent to a large degree on the stress-strain relations used for steel (13, 15). The basic characteristics to be modeled to accurately represent the stress-strain behavior of reinforcing steel for earthquake type loadings are yielding and strain hardening for the first quarter cycle, and the non-linear Bauschinger effect for subsequent cycles. The Bauschinger effect reduces the apparent yield stress for cyclic

loading after first yielding has occurred. For earthquake type loading where only few large strain excursions occur, fatigue effects may be neglected. Strain rate may increase the initial yield stress slightly, but its effect on cyclic behavior is little known and it is neglected in this study.

A number of expressions are available for calculation of stress-strain relationships for reinforcing steel (2 , 13, 27). Modified forms of Ramberg-Osgood relations have been used by Kent (13) and Aktan, et al. (2). These relations fit fairly well the data from which they are derived. The basic problem in using the Ramberg-Osgood curve is that it gives the strain in terms of the stress and to obtain stresses from strains an iterative procedure has to be followed.

In this study after the initial elastic-perfectly-plastic branch of the stress-strain diagram, strain hardening and the unloading and reloading curves are modeled by an expression suggested recently by Richard and Abbott (24). The expression in its general form is

$$\sigma = \frac{(1 - \alpha)\,\varepsilon}{(1 + (\frac{\varepsilon}{\beta})^{n})^{1/n}} + \alpha\,\varepsilon \qquad (2.1)$$

where σ and ε are some normalized stress and strain, respectively, measured from the point of reversal and α, β and n are constants which may depend on the previous strain history. The specific forms of this equation used in this study are given in

Appendix A where the rules used in obtaining the complete stress-strain relationship for steel are described. A schematic diagram of the proposed steel stress-strain relationship is shown in Fig. 2.1.

For this study α was assumed to be a constant and β and n were assumed to depend only on the maximum range of stress reached in previous loadings. The model as used here may, therefore, be said to have only limited memory.

The numerical parameters required in using the relationship given in Appendix A were evaluated for Grade 60 steel from data given in Ref. (2) and for Grade 40 steel from data given in Ref. (13). These values were used for all comparisons with experimental tests at the moment-curvature and load-deflection level. However, general applicability of these values is not claimed. Figs. 2.2, 2.3 and 2.4 show comparisons of the proposed analytical model with tests. The comparison is very good for the purposes of this study. Also shown in Fig. 2.4 for comparison is the analytical model of Kent (13).

b) Concrete

The effect of concrete hysteresis rules on the overall calculated cyclic behavior of reinforced concrete sections and elements is small (13, 15). The important characteristics to be modeled are the maximum compressive stress and the strain at which it occurs, the slope of the stress-strain curve after

maximum stress is reached (which is dependent on the degree of confinement), and cracking and crack closing.

A number of rules for calculating the stress-strain relations of concrete subjected to cyclic loading have been suggested (5, 12, 13, 28). The procedure used in this study is a simplified version of the hysteresis rules proposed by Darwin (5). The procedure as suggested is for biaxial cyclic loading of concrete. However, only uniaxial cyclic loading of concrete is considered in this study. The rules used in this study for determining the concrete stress-strain relations are described in Appendix A. A schematic diagram of the basic rules is shown in Fig. 2.5. The notations used in that figure are also defined in Appendix A.

The procedure is characterized by an envelope curve also used for monotonic loading and a set of rules for determining the stress-strain relations for cyclic loading. The rules for cyclic loading were obtained by Darwin (5) to match the energy absorbed and the number of cycles to failure observed in experiments. The rules were suggested only for unconfined concrete. However, since data on cyclic behavior of confined concrete is unavailable these rules are also used for confined concrete in this study.

The envelope curve in compression consists of three branches. The first branch, for loading from zero to maximum compressive stress, is the same for both confined and unconfined

concrete and is given by Hognestad's parabola (7). The second branch is a straight line with the slope dependent on the degree of confinement. The slope is assumed to be zero for spirally confined concrete. For concrete confined by rectilinear ties the formula (Eq. A.8 in Appendix A) as used by Wight (38) and originally suggested by Roy and Sozen (25) is used. For unconfined concrete it is assumed that stress drops down to 20% of maximum at a point where strain is four times the strain at maximum stress. The third branch is a straight line at a constant stress equal to maximum stress for spirally confined concrete and to 20% of maximum for concrete confined by rectilinear ties. The unconfined concrete is assumed to spall off after the strain reaches four times the strain at maximum stress.

In tension the concrete is assumed to be elastic-brittle material. A reduced elastic stiffness in tension is used if the concrete has previously been loaded in compression.

The effects of creep and shrinkage and any strain rate effects are ignored in the formulation.

The above model was compared with two experimental curves, and the comparisons are shown in Figs. 2.6 and 2.7. For purposes of this study the analytical model compares favorably with the experimental data.

It may be worth noting here that modeling concrete unloading and reloading by a single straight line with the same slope as the initial elastic slope did not change the

results of the dynamic analyses to any significant degree. However, a change in the slope of the softening branch of the envelope curve produced significant changes in the results of the dynamic analyses.

2.3 Development of the Analytical Model

The shear-deflection-axial load relationship of a reinforced concrete column is developed in this section. The model is used to calculate the resisting shears in an axially loaded column as it is displaced incrementally through a given set of two-dimensional relative lateral displacements between its ends. The axial load may be different in each step, and further, may be a function of the calculated shears.

The model as developed in this section is limited to circular and rectangular sections which are symmetrically reinforced. Also, it is limited to columns which are constrained against rotations at both ends.

The model is synthesized from the stress-strain relations of the constituent materials which were described in Sec. 2.2. These stress-strain relations are used to obtain the moment-curvature-axial load relationships at the end-sections of the column. The moment-curvature-axial load relationships of the end-sections are in turn used to calculate the shear-deflection-axial load relationship of the column.

In the following, the development of the moment-curvature-axial load relationship is described first, then, the development of the shear-deflection-axial load relationship is described.

2.3.1 Moment-Curvature-Axial Load Relationship

2.3.1.1 Development

Given a set of biaxial curvatures and an axial load, the resisting moments at a reinforced concrete section can be determined from a knowledge of the geometry of the section, the strain distribution over the section, the stress-strain properties of the materials constituting the section, and the strain history.

The usual procedure is to assume the shape of the strain distribution over the section, and then to find the strain distribution and the corresponding stress distribution which satisfy the given curvatures and the axial load. This last step may require iterations if the stress-strain properties are nonlinear. The integration of the first moments of the stresses over the area of the section gives the required resisting moments.

The nonlinear behavior of concrete in compression and cracking in tension, and the yielding and strain hardening in steel makes direct integration of the stresses over the section to obtain axial load and moments difficult. The problem is further compounded for cyclic loading when strain-history parameters for all points on the section must be known.

This problem has been attacked previously by dividing the concrete in the section into layers for uniaxial loading (13, 15), and into a two-dimensional mesh for biaxial loading (1). It is then assumed that the stress obtained at the centroid of any layer or any element of the mesh is constant over such layer or element. The strain-history parameters thus have to be kept for a fixed number of points on the section and the integrations for axial load and moments are obtained as summations.

A similar procedure is used in this study to obtain the moment-curvature-axial load relationship of a reinforced concrete section. The detailed calculation procedure is described in Appendix B. A linear variation of strain over the section is assumed. The same distribution of strain is used for both steel and concrete. This ignores bond slip between the two materials and averages the concentrated strains at the cracks in concrete. The stress-strain relationships for steel and concrete used are as detailed in Section 2.2. The actual strain values for a given set of curvatures and axial load are obtained by an iterative procedure which solves for the concrete strain at the centroid of the section to satisfy the given axial load.

The major difference from past procedures is in the discretization of concrete area for integration and for recording the strain history parameters. The previous procedures use the type of discretization shown in Figure 2.8 and is referred to

here as 'exact' integration. In the procedure proposed here, concrete area is lumped at nine prespecified locations on the section as shown in Figure 2.9 and referred to here as 'proposed' integration. This significantly reduces the amount of computation and space required to store strain history parameters. As is shown later in this subsection the effect of this lumping of the concrete area on the computed response of the section is very small. In the following the criteria and the procedure used in obtaining the locations and the areas of the lumped concrete on the section is described and then the behavior of reinforced concrete sections as predicted by the 'proposed' integration procedure is compared with the behavior predicted by the 'exact' integration procedure.

2.3.1.2 Procedure for Lumping Concrete Area

Different numbers and configurations of lumped concrete areas were tried and the number of concrete areas in the configuration shown in Fig. 2.9 were found to be the minimum to give acceptable results. It was found that matching the axial load-moment interaction diagram obtained from the 'proposed' and 'exact' integrations procedures gave excellent agreement between the cyclic moment curvature relationships obtained by the two procedures.

The axial load-moment interaction diagrams were first obtained using the 'exact' integration procedure. The limiting conditions were tension yielding in a steel bar or reaching of

maximum compressive stress in any concrete fiber. The interaction diagrams normalized with respect to the section size and the concrete strength are dependent on the shape of the section, the steel ratio and its arrangement, the concrete cover, the ratio of the yield stress of steel to the concrete strength, the ratio of steel yield strain to concrete strain at maximum stress, the shape of the concrete stress-strain curve up to maximum stress, and the moment direction.

Square and circular sections were used in this study. The steel ratio was varied from 1 to 6% using eight bars placed symmetrically as shown in Fig. 2.15 for the test columns. The concrete cover to the center of steel was varied from 0.05 to 0.2 of the depth. The ratio of steel yield stress to concrete strength was 60/5. The ratio of steel yield strain to concrete strain at maximum stress was 0.00207/0.0025. The concrete stress-strain curve up to maximum stress was assumed to be a parabola. Two different axes for the direction of the moment were considered for each of the sections. For the square sections one direction was parallel to the edge and the other along the diagonal. For the circular section the axes were 22 1/2° apart, since with eight bars the section is symmetrical about axes 22 1/2° apart.

The lumped concrete areas and their locations were determined to obtain the best fit for the points 1, 2, 3 and 4 on the axial load-moment interaction diagram shown in Fig. 2.10

for moments around each of the two axes shown. Point 2 is the balanced point when tension yielding in a steel bar occurs simultaneously with maximum compressive stress in any concrete fiber. Points 1 and 4 are matched exactly in this study by using the actual total concrete and steel areas.

For the circular section three unknowns, areas A_4 and A_5, and radius r_1 as shown in Fig. 2.9, have to be determined for any particular combination of geometric and material properties. Area A_5 can be written in terms of A_4 and the known total concrete area. Area A_4 and radius r_1 are determined to obtain the best fit for points 2 and 3 on the interaction diagram for each of the two moment directions considered. A value of r_1 is first chosen and using the same curvature as obtained in the 'exact' integration procedure A_4 is solved for to separately match axial load and moment at points 2 and 3 in each of the moment directions. This gives eight values for A_4. The process is repeated for different values of r_1, and the value of r_1 which gives the least dispersion for the value of A_4 is selected. The average value of A_4 corresponding to the selected value of r_1 is used.

For the square section of five unknowns, areas A_1, A_2 and A_3, and distances d_1 and d_2 as shown in Fig. 2.9, have to be determined. Area A_3 can be written in terms of A_1, A_2 and the known total concrete area. To obtain areas A_1, A_2 and distances d_1, d_2 the procedure was to select sets of d_1 and d_2

and using the same curvature as obtained by the 'exact' integration procedure solve for areas A_1 and A_2 to match the axial load and moment at points 2 and 3 in each of the moment directions. This gives four sets of areas A_1 and A_2. The process is repeated for different set of values for d_1 and d_2 and the set of values which gives the least dispersions for the values of A_1 and A_2 is selected. The average values obtained for A_1 and A_2 for the selected values of d_1 and d_2 are used.

It was found that the lumped concrete areas and their locations were dependent on the steel ratio and the concrete cover only to a very small degree. The average areas and their locations for concrete covers ranging from 0.05 to 0.2 of depth and steel ratios ranging from 1% to 6% are shown in Fig. 2.9.

As a consequence of the small dependence of these lumped concrete areas on the concrete cover and steel ratio, the values obtained for the square section can be used directly for rectangular sections. Also, these values can be used for different steel bar numbers and arrangements than the one they were obtained for, if the bars are symmetrically placed.

No distinction is made between unconfined and confined concrete for the lumped concrete areas. This does not affect the calculations for obtaining axial load-moment interaction diagrams, because the properties of the two kinds of concrete

up to maximum stress are assumed to be the same. However, it does affect the moment-curvature relationships after maximum compressive stress is reached in concrete. For this case the properties used for lumped concrete are an area-weighted average of the properties of confined and unconfined concretes. The two parameters that are averaged are the slope of the softening branch of the concrete curve and the ultimate stress at very large strains. The lumped concrete is then treated as confined concrete with averaged properties.

2.3.1.3 Comparison of 'Exact' and 'Proposed' Integration Procedures

The accuracy of the proposed model for the column section was checked by comparing the axial load-moment interaction diagrams and the moment-curvature relationships obtained by the 'exact' and the 'proposed' integration procedures.

For 'exact' integration procedure the square column section was divided into 144 concrete elements and the circular column section into 121 concrete elements as shown in Fig. 2.8. The outer two layers consisted of unconfined concrete. For 'proposed' integration procedure the concrete area was lumped at 9 locations on the section as shown in Fig. 2.9. The actual areas and location of steel were used in both procedures. For all comparisons 8 steel bars were arranged in the configuration shown in Fig. 2.15 for the test columns.

The stress-strain properties for steel and concrete given in Section 2.2, and described in detail in Appendix A were used for all comparisons.

A large number of comparisons were made between results obtained by the two procedures. As the loading complexity increased fewer sections were tested. The comparisons can be divided into four sets as follows:

i) Axial load-moment interaction diagrams are compared in Fig. 2.11 for circular sections and Fig. 2.12 for square sections. The concrete cover was varied from 0.05 to 0.2 of the depth. Although results for only 0.1 and 0.15d are shown, the results for other cover ratios were similar. (Other parameters used were the same for which the lumped concrete areas were obtained.) The comparison between the two procedures is excellent.

ii) Moment-curvature relationships for zero axial load and monotonic loading are compared in Fig. 2.13 for circular sections and Fig. 2.14 for square sections. Two different covers of 0.1 and 0.15 of depth were used. Both gave similar results and only the results for 0.1d cover are shown. All other parameters were the same as used for axial load-moment interaction comparisons. The circular columns were assumed to be spirally confined with a slope, $\Omega = 0$ for the descending branch of the concrete curve. The square columns were assumed to be so confined to give $\Omega = 40$ (strain at 20%

of maximum stress ε_{20} = - 0.0225, compared to strain at maximum stress ε_o = - 0.0025). The unconfined concrete for both sections had Ω = 107 (ε_{20} = - 0.01). The agreement of results for the circular section shown in Fig. 2.13 is excellent except for large steel ratios for one of the moment directions. For the square section the agreement of results shown in Fig. 2.14 is also good except for the post-yielding slope for moments applied about the diagonal.

iii) Uniaxial cyclic moment-curvature relationships are compared in Fig. 2.17 for a circular section and Fig. 2.18 for a square section under different axial loads. The test sections and the material properties used are shown in Fig. 2.15. The circular column has the same section as the interior columns in the Olive View Medical Center, heavily damaged during the San Fernando Earthquake of 1971. The square section was chosen to have the same area. The lateral confinement shown gives Ω = 0 for the confined concrete in the circular section and Ω = 17.2 (ε_{20} = - 0.042) for the square section. The axial load-moment interaction diagram for the two sections are given in Fig. 2.16. The balanced load for the circular section is approximately 750 kips. The axial loads for the different moment-curvature curves varied from 375 kips in tension to 1500 kips in compression. The loading history consisted of two cycles each to maximum curvatures of 3, 6 and 10 times the yield curvature for zero axial load.

As is seen from Fig. 2.17 for the circular section, the 'proposed' model compare extremely well with the 'exact' model. All basic characteristics - strength, shape of hysteresis loops, strain hardening slope are predicted quite well.

Not all computed curves for the square column are shown in Fig. 2.18. The comparison between 'proposed' and 'exact' is, however, similar to those shown. For a compressive axial load of P = - 1125 kips the proposed model shows a breakdown in strength for the larger curvature cycle. For P = 1500 kips both models showed similar breakdowns. This does not affect the use of this model, because it is recommended that columns designed with such confinement to resist lateral loads should not carry axial loads of more than half the balanced load.

iv) Biaxial cyclic moment-curvature relationship are shown in Figs. 2.20 and 2.21. Only results for the circular section are shown since the results for the square section are similar. The column section and material properties are the same as shown in Fig. 2.15. An axial load of P = - 750 kips was used. This is the estimated load on the interior column of the Olive View Medical Center. Three different two-dimensional curvature histories were used as shown schematically in Fig. 2.19 and given in Table 2.1. The projection of each of the curvature histories in Direction 1 is the same. The sequence of loading in Direction 1 is also shown in Fig. 2.19. It

consisted of two cycles to a maximum ductility of 6 (six times yield curvature at P = 0), then two cycles to a maximum ductility of 10, followed by two cycles to a maximum ductility of 6.

For Curvature History 1, Direction 2 was loaded only after loading in Direction 1 was completed. The results for both directions are shown in Fig. 2.20. The comparison between 'exact' and 'proposed' models is excellent. For Curvature History 2, loading in both directions progressed simultaneously but 90° out of phase. For Curvature History 3 one curvature was held constant at its maximum while the other was varied. Results for Direction 1 for both of these curvature histories are shown in Fig. 2.21. Results for Direction 2 were similar. The comparison for these two cases is also seen to be excellent.

These comparisons indicate that the computationally more efficient 'proposed' model for the column section gives results for the moment-curvature-axial load relationship which are similar to and show the same characteristics as those obtained from the 'exact' model.

2.3.2 Shear-Deflection-Axial Load Relationship

2.3.2.1 Development

The relative lateral displacements between the ends of a reinforced concrete column restrained against rotations at its ends arise basically due to flexural deformations and shear deformations. For most columns shear deformations are small

relative to the flexural deformations. They are neglected in this study. It is, however, impossible to completely restrain the column ends from rotating due to deformations of the joints and cumulative slips of the reinforcement at the face of the joints (anchorage slips). The column displacements arising due to joint deformation are small for a well proportioned joint. The displacement due to end rotations because of anchorage slips can, however, exceed displacements due to flexural deformations. It is difficult to synthesize anchorage slip behavior analytically especially for biaxial bending and it is assumed in this study that the columns are fixed-ended. It may, however, be noted here that comparisons made in Section 2.4 between experimental hysteresis loops and those predicted by the proposed model after assuming that displacements arising due to anchorage slips are proportional to those due to flexural deformation, were good.

One procedure for calculation of shear-deflection relationships of reinforced concrete columns is to use finite element type modeling of the column (40). A similar procedure was used by Aktan (1) who divided the column into a number of elements and assumed displacement distributions along the length of the element. However, because of the large amount of computations involved, the study was made using only one element which resulted in a linear curvature distribution along the length of the column. This will grossly overestimate the column deflection after yielding of the reinforcement.

The more usual procedure for calculation of the shear-deflection relationship of a column is to obtain the moment-curvature relationships at a number of sections along the length of the column, then from a knowledge of the bending moment distribution, the curvature distribution along the column length can be obtained which can be integrated twice to yield the displacements (13, 15). The disadvantage of this procedure is the amount of computation required because moment-curvature relations at a number of sections are needed. In addition, the displacements rather than the bending moments are known requiring prediction and iteration procedures to obtain the desired results.

A procedure similar to the above was used in this study. The amount of computation required was greatly reduced by assuming a curvature distribution along the length of the column, thus requiring the calculation of the moment-curvature relationships only at the end sections of the column.

Since lateral loads along the length of the column are not considered, the bending moment diagrams are linear in each of the two orthogonal directions considered. Also, since the ends are restrained against rotations the moments at opposite ends in each direction are equal and the points of contra-flexure for both directions are at mid-length of the column. Therefore only one-half of the column and only one end section is considered in this study.

The half column is divided into three segments, as shown in Fig. 2.22, in order to idealize the curvature distribution. The first segment is assumed to be uncracked and the curvature distribution along it is assumed to be linear. The second segment is assumed cracked but unyielded and the curvature distributions along it are assumed linear. The third segment is assumed to have yielded and the curvature distributions along it are assumed to be parabolic.

The lengths of the segments are determined by finding the sections where cracking or yielding have been initiated. The initiation of cracking or yielding at a section is indicated by the cracking and yield criteria shown in Fig. 2.24. For the circular column the curves are circular in the moment space, their size dependent on axial load. For the rectangular column, the cracking curve is diamond shaped in the moment space with size dependent on axial load. The yield curve is given by the equation

$$\left[\frac{|M_1|}{M_{y_1}} \right]^{\alpha} + \left[\frac{|M_2|}{M_{y_2}} \right]^{\alpha} = 1 \qquad (2.2)$$

where M_1 and M_2 are the two orthogonal moments at the section, M_{y_1} and M_{y_2} are the respective yield moments for the given axial load and α is a parameter varying between 1 and 2 depending on the axial load.

When the cracking or yield criterion at a section is found to be satisfied, the lengths of the segments are adjusted accordingly. It is assumed that the length of the uncracked segment can only decrease and that the length of the yielded segment can only increase as the loading progresses.

The two orthogonal curvatures at the end section are calculated from the end moments by using the moment curvature-axial load relationships developed in Section 2.3.1. Once the end curvatures and the segment lengths are known the lateral deflections in the two orthogonal directions can be determined independently of each other. As shown in Fig. 2.22 for each direction the moments m_1 and m_2 at the ends of segments 1 and 2 are calculated from the linear bending moment diagram. The curvature ϕ_1 corresponding to the moment m_1 is calculated using the uncracked slope, k_{cr} of the moment-curvature relationship in that direction. The curvature ϕ_2 corresponding to moment m_2 is calculated using k_y the secant slope up to yield of the moment-curvature relationship in that direction for that particular axial load. The parabola in Segment 3 is assumed to have the same slope at the junction with Segment 2 as the curvature diagram in Segment 2. After the curvature diagram in a particular direction is known the deflection can be calculated analytically by integrating it twice.

The above shear-deflection-axial load model is used in the dynamic study of Chapter 3. Since displacements are

specified in that analysis and moments have to be calculated, an iterative procedure is devised which predicts the end curvatures and thus the end moments, which in turn determine the curvature distribution resulting in the calculation of a set of displacements. If calculated displacements are different from those required, new curvatures are predicted and the process repeated. The complete procedure is detailed in Appendix C.

2.3.2.2 Analytical Check of Assumed Curvature Distribution

The shapes taken by the assumed curvature along the length of the half-column at different stages of loading are shown in Fig. 2.23. The assumption of a linear distribution of curvature in the uncracked segment is correct. The loading and unloading at each section along this segment is with the uncracked slope, k_{cr}. The assumption of a linear distribution of curvature in the segment which is cracked but unyielded will be analytically correct only if it is assumed that the moment-curvature relationship from cracking to yielding is a straight line and that cracking along the length of this segment is a continuous and not a discrete phenomenon. The average curvature in the actual case will not be very different from what is assumed and the overall effect on displacements of these assumptions may be neglected. The actual distribution of curvatures in the yielded segment is not known and may be quite

different from the parabolic distribution assumed. Calculations discussed below were made for several loading histories and the assumptions of a parabolic distribution of curvature in the yielded segment was found to be good. An analytical check showed that a linear distribution of curvature in the yielded segment was not a good assumption.

The analytical check consisted of comparing assumed moment-curvature relationships with calculated moment-curvature relationships at two sections in the yielded segment of the column. The loading consisted of prescribed relative displacement paths between the ends of the column. The assumed moment-curvature relationship at any section was obtained directly from the moment-curvature relationship calculated at the end section. The moments were calculated from the linear bending moment diagram and the curvatures from the assumed curvature distributions. The calculated moment-curvature relationships were calculated for the assumed curvatures using the moment-curvature relationship developed in Section 2.3.1. The two sections were the moment-curvature relationships are compared are located at distances of 0.025L and 0.075L from the end section. The column section and properties used were the same as used for the two-dimensional moment curvature study and are given in Fig. 2.15. Three different sets of loadings were used as follows:

i) Three different two-dimensional displacement histories shown in Fig. 2.25 were prescribed for both circular and square columns. The projection of each of the displacement histories in Direction 1 was the same. The axial load on the circular column was - 750 kip and on the square column - 375 kips.

Displacement History 1 consisted of cyclic loading in Direction 1 followed by cyclic loading in Direction 2. The shear-deflection relationship obtained, the moment-curvature relationship at the end-section and the assumed and calculated moment-curvature relationships at distances of 0.025L and 0.075L are shown for the circular column in Fig. 2.26 for Direction 1 and Fig. 2.27 for Direction 2. The agreement between assumed and calculated moment curvature relationships is found to be good. The same results are shown for the square column in Figs. 2.28 and 2.29 and the agreement for this case is also good.

Displacement History 2 consisted of simultaneous cyclic loading in the two directions with 90° phase difference. The results for the two directions and for the circular and square columns were similar and only the results for Direction 1 for the circular column are shown in Fig. 2.30. The agreement between calculated and assumed moment-curvature relationships is good.

Displacement History 3 consisted of cycling in the two directions alternately while one direction is kept at constant peak displacement. Results for Direction 1 for the circular column are shown in Fig. 2.31. The results for Direction 2 and for the square column were similar to the results shown. The agreement between the assumed and calculated moment-curvature relationships for the section at 0.025L is seen to be good, however, the assumed moment for one of the cycles for the section at 0.075L is somewhat larger than the calculated moment. This suggests that the actual curvature for that cycle at that section will be larger than predicted by the parabolic distribution.

ii) Circular columns were checked for axial loads of 0 and - 1500 kips and square columns for axial loads of 0 and - 750 kips. The displacement history used was the one-dimensional first half of Displacement History 1. The agreement between assumed and calculated moment-curvature relationships was similar to that shown for Direction 1 of Displacement History 1 in Fig. 2.26 for the circular column with axial load of - 750 kips and in Fig. 2.28 for the square column with axial load of - 375 kips. Only the results for 0 kips axial load for the circular column are shown in Fig. 2.32.

iii) A check was made using variable axial loads. $P = - 750 - 0.05 M$ was used for the circular column and $P = - 375 - 0.05 M$ for the square column. P being the axial

load in kips and M the moment at the end of the column in kip-in. Displacement history consisted of that used for the constant axial loads. The results for the circular column only are shown in Fig. 2.33. The results for the square column being similar. The overall agreement between the assumed and calculated moment-curvature relationships is seen to be good.

From the above comparisons for the different types of loadings it is seen that the assumption of a parabolic distribution of curvature in the yielded segment of the column is acceptable. It may be noted here, however, that the same circular and square columns were used for all of the different loading histories and the results may be influenced by section and material properties significantly different from those assumed.

2.4 Comparisons with Experiments

The analytical model developed in this study was compared with some experiments reported by previous investigators. The subject was to compare the shape of the analytical hysteresis curves with experimental curves. Curvature or displacement histories obtained in the experiments were prescribed as loading to obtain the analytical curves. Three different sets of experiments are used for the comparisons. The column properties used are given in Table 2.2. The sets of experiments and their comparisons with the analytical model are as follows:

a) Aoyama's Specimens A-1 and A-2 (Ref. 3)

These specimens consisted of simply supported beams with 12' spans. They were loaded laterally at two points giving a 6' constant moment region in the middle. The curvatures were obtained from the rotations in this region. Specimen A-1 had no axial load. Specimen A-2 had an axial load of - 36 kips which is less than half of the balanced load for the section. Analytical and experimental moment-curvature relationships for the first 1 1/4 cycles for these two specimens are compared in Fig. 2.34. The agreement between the two curves is seen to be very good.

b) Karlsson et al. Specimen BK5 (Ref. 11)

This specimen was modeled to be a half scale representation of the interior columns in the Olive View Medical Center. The specimen consisted of two cantilevers connected by a central stub. The lateral loading was applied simultaneously at the ends of the cantilevers, but in opposite directions. The central stub was constrained against rotation. The axial load was - 200 kips, approximately the balanced load of the section. The column section was 13" square, but the longitudinal steel was placed along a circular perimeter and the column was spirally confined. The proposed model for the section assumed the column to be circular, 13" in diameter, but with the area of concrete in the actual section.

The experimental moment-curvature relationship is compared in Fig. 2.35 with the proposed analytical and Aktan's analytical (1) models. The experimental curvatures are average rotations in a 13" reference length near the fixed end of the column. The proposed model is seen to be good and gives a much better agreement with the experimental curve than Aktan's model. The difference between the two analytical curves can largely be attributed to the Bauschinger effect in steel which is neglected in Aktan's model. The drop in strength after yielding in the first quarter cycle of the experimental curve was noticed only at one end of the specimen.

The experimental shear-deflection relationship for the other end of the specimen is compared with the proposed model in Fig. 2.36. Because of neglect of anchorage slip at the joint, and, to a much lesser degree, neglect of joint deformations and shear deformation of the column itself, the analytically predicted yield displacement was only 40% of the experimentally obtained displacement at yielding of steel. Flexural deformation to total deformation ratios of this magnitude are expected (29). To determine whether the analytical model can successfully predict the shape of the experimental shear-deflection curves, and whether the deflections due to anchorage slips can be assumed to be proportional to the deflections due to flexural deformations, deflections for the analytical model shown in Fig. 2.36 are multiplied by a factor

of 2.5. As is seen from the figure the proposed model predicts quite well the shape of the experimental hysteresis curve.

c) Takizawa and Aoyama's Specimen 3 and 4 (Ref. 34)

These specimens are part of the only available set of experiments in which biaxial lateral loadings introducing large inelastic deformations are used. The specimens were single cantilevers anchored into a reinforced concrete stub. An axial load of - 16.0 tons was applied. This is approximately 70% of the balanced load.

The nominal biaxial loading paths are shown in Fig. 2.37. The exact sequence is given in Table 2.3.

The experimental shear-deflection relationship for Direction 1 is compared in Fig. 2.38 with relationship obtained from the proposed model and Takizawa's model. For Specimen 3 shear-deflection curves for loading sequence 6 to 13 given in Table 2.3 are not shown in Fig. 2.38 for purposes of clarity. For these specimens the proposed model predicted only 50% of the displacements at yielding of steel, therefore, the displacements obtained from the proposed model are multiplied by a factor of 2.0. Takizawa's model is based on fields of work hardening, utilizing a number of yield surfaces, and uses the yield displacement as input to the model.

As is seen from the comparison the proposed model predicts very well the shape of the experimental curves and gives a much better fit than Takizawa's model.

2.5 Characteristics of the Proposed Analytical Model

The basic characteristics of the proposed model are discussed here. Emphasis is placed on those characteristics which are expected to influence the response of the column under moderate to strong uniaxial or biaxial earthquake motion. These characteristics include the strength, the post-yield slope of the shear-deflection or moment-curvature relationships, the overall shape of these relationships which affects their energy absorption capacity, and some index for the cummulative damage to the column.

It should be noted here that actual loading histories during an earthquake may be very different from the simplified histories used in this study. Nevertheless, it is expected that major characteristics of the model affecting response under actual loading conditions can still be observed.

Another limitation of the observed behavior in this study is due to the use of a single circular column and a single square column. The geometry and the material properties used for these columns, however, are expected to represent a large class of actually constructed columns. The properties of the test columns are shown in Figure 2.15.

The characteristics of the proposed model are discussed in two parts. First, the effect of different axial loads on uniaxial cyclic behavior is examined, then the behavior under biaxial cyclic loading is discussed.

a) Effect of Axial Loads

The effect of axial load was studied by comparison of results obtained for different and varying axial loads during analytic verification of the proposed model for moment-curvature relationship and shear-deflection relationship. The moment-curvature relationships are shown in Fig. 2.17 for the circular section and Fig. 2.18 for the square section. For the circular section the results shown are for axial loads from 375 kips in tension to 1500 kips in compression, and for the square section from 0 to 1125 kips in compression. The balanced load is approximately 750 kips. The shear-deflection results to be compared are shown in Figs. 2.26, 2.32 and 2.33 for axial loads of - 750 kips, 0 kips and - 750 - 0.05 M kips, respectively, where M is the end moment in kip-in.

The following observations can be made:

i) The strength at yielding of steel increases rapidly with increase in compressive axial load up to the balanced axial load beyond which it decreases gradually as shown in Fig. 2.17.

ii) The post-yield slope of the moment-curvature or the shear-deflection curve decreases continuously with increase in compressive axial load. This is more evident in the case of the shear-deflection curve because of the P-Δ effect. This decrease in slope directly influences stability under strong earthquake loading. Also the distribution of damage along the column is influenced. This is quite evident from a comparison of the

moment-curvature relations obtained at different sections along the length of the columns for different axial loads. Such a comparison between results for axial loads of - 750 k and 0 k can be made, for the circular column, through Figs. 2.26 and 2.32. It is seen that the deformations for the higher compressive axial load are concentrated at the end, whereas, the deformations are more widely distributed for the smaller axial load. A displacement of approximately 4 times the yield displacement required curvature ductilities of 12, 14 and 18 for axial loads of 0, - 750 and - 1500 kips respectively for the circular column, and of 11, 14 and 22 for axial loads of 0, - 375 and - 750 kips respectively, for the square column. It may be noted here that the decrease in the computed post-yield slope due to axial loads is much faster for the square column than for the circular column, because of differences in the assumed effects of concrete confinement.

iii) The shape of the hysteresis curve changes considerably as compressive axial loads are increased, as seen from Fig. 2.17. The curves are much different from the elastic-plastic or elastic-strain hardening curves assumed in many previous investigations. The hysteresis curves for column with axial tension can be fitted with a Ramberg-Osgood type relationship, but as axial compressive forces are added the curves deviate from this type of relationship due to crack closing in concrete. The hysteresis loops become thinner as compressive

axial loads are increased up to the balanced axial load after which they again start becoming wider.

For square columns, under axial loads larger than balanced load, and subjected to large amplitude cycles, a sudden change in the shape of the hysteresis curves is noticed, because of breakdown in the strength of the column. This breakdown is a result of the poorer confinement of concrete assumed for the square column with ties.

For columns with varying axial load which are a linear function of the moments assymmetric curves like the one shown in Fig. 2.31 is obtained. It resembles a curve with a much larger axial load on one side of the zero moment line, and a curve with a much smaller axial load on the other side. This type of varying axial load can result from overturning moments in a framed building. The variation being significant for edge columns.

iv) An accumulation of strain was observed due to cyclic loading of columns with axial loads. Although prediction of collapse of the column was not the objective in this study, this accumulation of strain may become an important index for studying collapse of columns. The accumulated strains at the end of loadings shown in Fig. 2.17, for the circular column, were 0.025, 0.007, 0.0, - 0.002, - 0.013 and - 0.029 for axial loads of 375, 0, - 375, - 750, - 1125 and - 1500 kips respectively. For the square column they were

0.014, 0.009, 0.0, - 0.002, - 0.047 and - 0.132 for the same axial loads. The rapid increase in the accumulated compressive strain in the square column, for axial loads above balanced, is again a consequence of poorer confinement of concrete, and is the reason for decay in the strength of these columns under large amplitude cycling. The curvature amplitude in the above calculations was the same for all columns and its maximum value was approximately ten times the yield curvature for no axial load.

b) Effect of Biaxial Lateral Loads

For analytical verification of the proposed model for biaxial lateral loadings, three different correlations between the two orthogonal loading directions were used. The three loading histories are shown in Fig. 2.19 and Fig. 2.25 for curvatures and displacements respectively. The basic characteristics of the biaxial behavior are observed from the results obtained for these loading histories.

The moment-curvature relationships are shown in Fig. 2.20 and 2.21, and the shear-deflection as well as the moment-curvature relationships at different sections are shown in Figs. 2.26-2.31. The results for Direction 1 for Loading history 1, shown in Fig. 2.20, 2.26 and 2.28 act as index for comparing uniaxial and biaxial results. The following observations can be made from the results computed for the three loading histories.

i) For Loading History 1, where Direction 2 is loaded after loading in Direction 1 is completed, the strength is reduced significantly only in the first cycle. As the amplitude of the cycles increases the same strength in Direction 2 is obtained as in Direction 1. This is seen by comparing the moment-curvature curves of the two directions in Fig. 2.20. For Loading History 2, where loadings in the two directions are simultaneous but 90° out of phase a drop in strength of about 20% is noted after the uniaxial first quarter cycle. This is seen from a comparison of top curves shown in Figs. 2.20 and 2.21. For Loading History 3, where the deformation in one direction is maintained at its peak while the other direction is being loaded or unloaded, the initial strength reached in the active direction is only slightly smaller than the uniaxial case, but it drops rapidly when the orthogonal direction becomes active. Drop in strength in the inactive direction of up to 70% are noted while the active direction goes through one cycle of loading. This is seen from a comparison of top curves of Fig. 2.20 with the bottom curves in Fig. 2.21. This drop in strength may significantly increase the displacement response under dynamic loading conditions.

ii) The post-yield slope of the hysteresis curves is decreased by the presence of loads in the orthogonal direction. This is reflected in the increase in curvature ductility requirements for a given displacement, for Displacement

Histories 2 and 3. This is seen from a comparison of Fig. 2.26 with Figs. 2.30 and 2.31. The curvature ductility required for the circular column, for a displacement of approximately 4 times the yield displacement, increased from 14 for the uniaxial case to 16 for Displacement History 2, and to 18 for Displacement History 3.

iii) The shape of the curves and their energy absorption capacity for the different type of biaxial loadings, except for Loading History 1, are quite different from the uniaxial case as can be seen from a comparison of the moment-curvature curves shown in Figs. 2.20 and 2.21. For Curvature History 2 it results in a thinning of the hysteresis loops, whereas for Curvature History 3 it has the opposite effect. This is a direct result of the correlation of the loadings in the two orthogonal direction.

iv) In all cases of biaxial loading significantly more damage of the column is indicated. This can be deduced from the significantly larger accumulation of axial strain under biaxial loading. For the results shown in Figs. 2.20 and 2.21, for the circular column with - 750 kips axial load, accumulated axial strain after uniaxial loading was - 0.002, but after biaxial loadings it was - 0.01, - 0.015 and - 0.023 for Curvature Histories 1, 2 and 3 respectively. For the square column under - 375 kips axial load the accumulated axial strains were - 0.0 for uniaxial loading and - 0.008, - 0.05 and - 0.10 for Curvature Histories 1, 2 and 3 respectively.

It is seen, therefore, that the effect of biaxial cyclic loading, on the strength of energy absorption capacity and the accumulated damage of a reinforced concrete column can be significant. The magnitude of this effect depends on the correlation between the loadings in the two directions.

2.6 Concluding Remarks

An analytical model for calculating the shear-deflection-axial load relationship of a reinforced concrete column, subjected to cyclic biaxial lateral loading, has been developed. The model is synthesized from the stress-strain relations of steel and concrete. Important characteristics of the cyclic stress-strain relations of these materials are accounted for. The model is used for calculating shears in the column as it is loaded incrementally through a set of biaxial lateral displacements and axial load. However, the results are independent of the size of the increments.

The moment-curvature relationships predicted by the model agree well with experimental data. However, displacements obtained in experiments are underestimated by the model. This is expected, because of anchorage slip of the reinforcement. Nevertheless, the shape of the experimental shear-deflection curves for both uniaxial and biaxial loadings are quite well predicted.

The model predicts significant changes in the strength, energy absorption capacity and accumulated damage of the reinforced concrete column when subjected to biaxial loadings as compared to uniaxial loadings. The magnitude of these changes depends on the correlation between the two directions of loading. Further experimental work is needed to confirm the above findings.

3. DYNAMIC RESPONSE UNDER EARTHQUAKE MOTION

3.1 Introductory Remarks

The response to earthquake motion of the analytical model, developed in the previous chapter for reinforced concrete columns, is studied in this chapter. The basic object of this study is to determine the effect on reinforced concrete columns of simultaneous two-dimensional earthquake motion in the horizontal plane.

Earthquake motion is multi-dimensional and in the inelastic range the responses of a structure in different directions are coupled. For the columns this coupling is especially significant. This necessitates an understanding of the response of columns to multi-dimensional earthquake motion and a study of the factors which influence such response.

As described in Section 1.2 previous investigators have studied two-dimensional behavior of columns subjected to earthquake motion using a variety of models and system parameters. One conclusion is common, that the effect of including two-dimensional interaction could be significant for some cases. However, further study is needed for a better understanding of the factors which determine the magnitude of this effect for a given system.

The effects of two-dimensional earthquake motion on reinforced concrete columns is studied herein by comparison of

biaxial responses with corresponding uniaxial responses. The influence of system strength and period, of different and varying axial loads, and of material hysteresis rules on the two-dimensional behavior are discussed.

The system studied here consists of a single mass supported on a reinforced concrete column represented by the analytical model proposed in the previous chapter. The column is assumed to be restrained against rotations at both ends. Only two translational degrees of freedom in the horizontal plane are considered for the mass. The effect of vertical earthquake motion is not considered in this study. Also the effect of any vertical motion of the mass due to axial shortening or lengthening is neglected. A constant axial load or one dependent on the resisting shears is assumed to act on the column.

The equations of motion for the system are given in Appendix D, where the detailed procedure used for the solution of these equations is also given. A step by step procedure assuming a linear variation of the response acceleration, is used for the integration of these equations in the time domain. The procedure requires iterations to satisfy the equations of motion. An average of 1.8 iterations were required to satisfy these equations with a tolerance of $\pm$ 0.0075 of the yield strength of the column. A constant time step of 0.02 seconds

and viscous damping equal to 2 % of critical was used for all calculations.

The study is limited by the use of only two earthquake records, El Centro 1940 and Taft 1952, and the use of a single set of column geometry and properties. Nevertheless, it is expected that the conclusions drawn herein are more widely applicable. The column dimensions and properties used are those shown in Fig. 2.15 for the circular section. This is similar to the interior column of the Olive View Medical Center which was heavily damaged in the San Fernando Earthquake of 1971 (8).

Section 3.2 discusses the characteristics of the earthquakes used in this study. Section 3.3 describes the systems studied. The results of the dynamic analyses are presented in Section 3.4, where the effect of two-dimensional earthquake motion is discussed and the influence of system period and earthquake strength are evaluated. Sections 3.5 and 3.6 discuss the effect of axial load and of material modelling on calculated dynamic response.

3.2 Earthquake Characteristics

The earthquake motions used in this study are the horizontal components of the El Centro 1940 and Taft 1952 earthquakes. Only the first 20 seconds of the recorded motions are used. The acceleration-time histories for El Centro N-S

(Direction 1) and E-W (Direction 2), and Taft S69E (Direction 1) and N21E (Direction 2) are shown in Fig. 3.1. The peak accelerations recorded during the earthquakes were scaled to 1.0 g. This results in peak accelerations of 1.0 g for El Centro N-S and Taft S69E, and of 0.61 g and 0.87 g for El Centro E-W and Taft N21E respectively. The elastic response spectra for the records such scaled are shown in Figs. 3.2 and 3.3. The spectral intensities computed from these spectra for periods from 0.1 to 2.5 seconds and a viscous damping of 20 % of critical are 91, 78, 83 and 79 inches for the scaled El Centro N-S and E-W, and Taft S69E and N21E records respectively.

The response of a structure to two-dimensional motion is also influenced by the correlation between the motion in the two directions. To study this correlation for the earthquake records used variances and covariances of the input records were computed as proposed by Kubo and Penzien (14) using the relation

$$\mathrm{cov}_{ij}(t_o,\Delta t) = \left\langle [a_i(t) - \bar{a}_i]\,[a_j(t) - \bar{a}_j] \right\rangle_{t_o - \frac{\Delta t}{2}}^{t_o + \frac{\Delta t}{2}} \qquad (3.1)$$

where $a_i(t)$ and $a_j(t)$ are the two input motions, $\bar{a}_i$ and $\bar{a}_j$ are their mean values over the duration of the records and $\mathrm{cov}_{ij}(t_o,\Delta t)$ is the covariance of the input motion at time t_o

averaged over a time interval Δt. For the present calculations Δt was taken as 5 seconds and covariances and variances were evaluated for discrete values of t_o spaced half a second apart. Also, Eq. 3.1 was slightly modified when computing covariances and variances for the first and last 2 seconds of the records by using time averaging intervals of less than 5 seconds which were not centered over t_o.

The computed variances and covariances for the records were used to obtain the principal directions and variances of the input motions in these directions. Figure 3.4 shows the principal directions and the variances of the scaled input records.

The following observations can be made from Fig. 3.4:

i) The strength of the two scaled earthquakes as measured by their maximum variances are about the same. However, the duration of strong motion is longer for the Taft earthquake.

ii) For the El Centro earthquake definite principal directions exist during the strong motion part of the records. Also, the recorded N-S direction is very near to the major principal direction. For the Taft earthquake, however, the motion is almost isotropic.

3.3 System Characteristics

The systems studied in this investigation consisted of single masses supported by fixed-fixed reinforced concrete columns. The properties of the systems studied to investigate the influence on dynamic response of system period and strength relative to the earthquake are given in Table 3.1. The circular section shown in Fig. 2.15 with a single set of material properties and a constant axial load of -750 kips was used for all systems given in Table 3.1. The axial load and material properties were varied only to study their influence on dynamic response as discussed later in Sections 3.5 and 3.6.

The system masses were varied to obtain different elastic periods, ranging from 0.2 to 1.6 seconds. The elastic periods were calculated using the secant stiffness of the column up to yield.

The earthquake strengths used were such as to give a wide range of maximum displacement responses ranging from less than 2 to over 10 times the yield displacement for one-dimensional motions. For studying the influence of system period, strength dependent on system period is used as indicated in Table 3.1. A yield shear ratio of $c = 0.24\ A_{max}/(T)^{2/3}$, where A_{max} is the peak acceleration of the earthquake and T the system period, is used to obtain the design strength. The yield shear ratio c is defined as the ratio of the yield shear to the weight of the system. This value is similar to that

recommended by the Applied Technology Council (35), for ductile reinforced concrete frames on stiff soils. It is expected that this value of the yield shear ratio will result in maximum response displacements of about four times the yield displacement under design strength earthquakes. A comparison is made in Fig. 3.5 between the assumed design strengths and the range of required strengths for elastoplastic systems calculated to give displacements of four times the yield displacement when subjected to the earthquake records used in this study. It is seen that the design strength is towards the lower end of this range except for 0.4 second period for which it is significantly weaker.

3.4 Results and Discussion of Dynamic Response

To study the effect of two-dimensional earthquake motion on reinforced concrete columns the single mass systems given in Table 3.1 were subjected to the El Centro and Taft earthquakes and their responses studied. In the following, first the response to design strength earthquakes of systems with elastic period of 0.4 sec is studied in detail, then the effect of system period and strength relative to earthquake intensity, on the conclusions drawn from that study, are examined.

3.4.1 T = 0.4 Systems under Design Strength Earthquakes

The complete results of the response of T = 0.4 second systems subjected to design strength El Centro earthquake are presented in Figs. 3.6 to 3.12, and to the Taft earthquake in Figs. 3.13 to 3.19. In each figure the two-dimensional response and the two corresponding one-dimensional responses are shown and compared. One-dimensional response refers to response of the column subjected to only one of the components of the earthquake. Two-dimensional response without interaction refers to the resultant of the two 1D responses of the column computed separately. This will give the effect of any correlation between the two components of the earthquake motion. Two-dimensional response with interaction refers to the response of the column subjected simultaneously to the two components of the earthquake.

For the El Centro earthquake as seen from Table 3.2 the maximum displacement responses were 8.7 and 7.54 inches in N-S and E-W directions respectively under one-dimensional excitation (yield displacement = 0.93 inches). The two 1D responses gave a resultant maximum in any direction of 8.7 in. The maximum response, however, increased to 19.95 in. when the column was subjected simultaneously to the two components of the earthquake. For the Taft earthquake the 1D maximums were 5.9 and 8.00 inches in S69E and N21E directions respectively. The two 1D responses gave a resultant maximum of 8.03 inches. However, the column became unstable when subjected to the two

components of the earthquake simultaneously. The results for this case are shown only for the first 9.98 seconds at which time the displacement had reached 25 times the yield displacement.

The following observations can be made from the results given above and those shown in Figs. 3.6 to 3.19 for the T = 0.4 second systems subjected to the two earthquakes:

i) The effect of two-dimensional motion on the maximum displacement response of the systems is significant. It results in an increase of 129 % over the 1D maximum displacement for the El Centro earthquake and leads to instability in the case of Taft earthquake.

ii) For these particular systems this increase is due primarily to the inelastic interaction in the two directions and not due to the correlation between the responses for the 1D cases. This is evident from the fact that the 2D maximum displacements without interaction for the two earthquakes are very nearly equal to the 1D maximum displacements for the corresponding earthquakes.

iii) A study of Figs. 3.6 and 3.13 showing the displacement-time responses reveals that the effective period of the system is increased considerably for the one-dimensional case whenever large amplitude cycles occur. Any further increase in the effective period due to two-dimensional motion is slight.

iv) The wave forms of the displacement responses for the 2D and the 1D cases are very similar for small and moderate amplitude cycles and most of the additional displacements for the 2D cases come from drifts accumulated over short intervals of time. It is suspected from studying the 1D force responses at these times that most of the additional drifts for the 2D cases occur when the 1D force responses in the two directions are simultaneously large. However, this observation needs further study.

v) The 2D displacement traces for the column top with and without interaction presented in Figs. 3.9 and 3.16 clearly show the random path taken by the column and, therefore, the difficulty of predicting 2D dynamic responses from a study of the responses of the column to a few prescribed displacement paths.

vi) Figures 3.7, 3.8, 3.14 and 3.15 which compare 1D and 2D shear-displacement responses show the difference in the resistances for the two cases. The significance of P-Δ effect is quite noticeable from the 2D shear-displacement responses.

vii) From the 2D shear response presented in Figs. 3.10 and 3.17 it is seen that when interaction is not considered the shears can be large in both directions simultaneously. The probability of this happening a given number of times during an earthquake for a particular system could very well be an index of the susceptibility of the system to increased

displacement response to two-dimensional earthquakes. Sufficiently large number of earthquakes or systems were not analyzed in this study for this to be definitely stated.

viii) The accumulation of axial strain under cyclic loading as noted in the static study is clearly seen from Figs. 3.11 and 3.18. Although the reliability of the numerical values for the strains is much less than those for the displacements, the trends are very well established. The effects of the very large accumulation of axial strains for the 2D cases as compared to the 1D cases should be experimentally investigated so that safe limits for 2D displacement response can be prescribed.

ix) Figures 3.12 and 3.19 present the input and hysteresis energy plots with respect to time for the systems under study. These plots were used as a check for the dynamic analyses procedure. The input energy should be the sum of the hysteresis energy, the damping loss and the kinetic energy in the system. The above plots were obtained from values at one second intervals and the energy check was found to be good.

It is seen from the figures that for the 2D cases the input and hysteresis energies are slightly less than the corresponding 1D cases, except for the Taft N21E direction. It should also be noted that the hysteresis energy for the 2D case for the Taft N21E direction, 4 seconds after the beginning of the earthquake, is larger than the input energy, although the

overall balance of energy for the two directions combined is correct. This is an indication of the redistribution of energy in the two directions under 2D excitation.

The above observations are made only from a study of systems of elastic period equal to 0.4 seconds and under design strength earthquakes. The effects of changing the period or the strength of the system, on these observations, are discussed in the following subsections.

3.4.2 Effect of System Period

The displacement response of systems with 0.2, 0.8 and 1.6 seconds period under design strength El Centro and Taft earthquakes are presented in Figs. 3.20 to 3.25. The maximum displacements and the time at which the maxima occurred are given in Table 3.2 and the maximum displacements are plotted in Figs. 3.26 and 3.27.

The 1D maximum displacements in each direction are given in Table 3.2 but only the greater of the two maxima is plotted as the 1D maximum in Figs. 3.26 and 3.27. The 2D without interaction refers to the resultant of the 1D responses. The maximum of this resultant response is obtained and plotted. The 2D with interaction under reduced strength earthquake refers to results obtained by multiplying the earthquake records by 0.77. This is equivalent to increasing the strength of the columns by 30 %.

The vertical arrow in Fig. 3.27 over the 0.8 second period for the 2D with interaction curve means that systems with periods shorter than 0.8 seconds, studied here, collapsed under 2D excitation.

The following observations can be made from these results.

i) The 2D with interaction displacement responses are larger than the maximum 1D displacement responses by 39 % to 160 % and for two systems (0.2 and 0.4 second systems under Taft earthquake) the 2D interaction leads to instability.

ii) The 2D without interaction response is larger than the maximum 1D response by zero to 31 %. It can be concluded, that for the systems studied, most of the 2D increased displacements resulted from inelastic interaction effect.

iii) Whether the magnitude of the increase is dependent on the period or on the maximum 1D ductility reached is not immediately evident from Figs. 3.26 and 3.27, since the larger increases occur for systems with large 1D ductility requirements. This is further investigated in the next subsection.

iv) When the earthquake strength is reduced to 0.77 of its value (or when the system strength is increased by 30 %) for 2D response calculations, then the 2D with interaction displacement response is less than the corresponding maximum 1D displacement response without the reduction in earthquake strength. This is true for all systems except for the T = 0.4

system under Taft earthquake for which the 2D response is still larger than the maximum 1D by 10 %. It can thus be concluded that 30 % increase in the strength of the system will bring the 2D response down to the level of the 1D response of the unstrengthened system. However, whether safe limits on displacements determined from uniaxial tests, and the basis for uniaxial design, are safe for biaxial loading has yet to be experimentally determined.

v) The above discussion has been for results of systems for which the effect of P-Δ was included. Table 3.2 also presents results for systems for which P-Δ was neglected. The results show the marked effect of P-Δ on 2D response. Without the P-Δ effect the increase of 2D response over 1D response was only 12 % to 67 %. The effect of P-Δ is evident from Figs. 3.28 and 3.29 where displacement response of 1D and 2D analyses with and without P-Δ are compared for the T = 0.4 system under the Taft earthquake. Although the effect of P-Δ on 1D response is negligible for this system its effect on 2D response is critical.

3.4.3 Effect of Earthquake Strength

Table 3.3 presents results for T = 0.4 and 1.6 second systems under different earthquake strengths. These results are also plotted in Figs. 3.30 and 3.31. The vertical arrows in the figures indicating that the system collapsed under the

next higher strength of the earthquake. The figures compare only the 2D results with and without interaction.

The following observations can be made from the figures:

i) The increase in 1D ductility demand generally results in an increase in the effect of 2D interaction on displacement response. This is quite well demonstrated by the results for the T = 0.4 systems. For the T = 1.6 systems this is not evident for the Taft earthquake. This may be a result of neglecting P-Δ for these systems.

ii) For stronger systems for which the 1D ductility requirements are about 2 times the yield displacement or less the 2D with interaction response is less than the 2D without interaction response. This may be a result of a redistribution of input energy, so that energy input in one particular direction is also dissipated in the orthogonal direction.

3.5 Effect of Axial Load

To determine the effect of axial load on dynamic response both constant and varying axial loads are studied. Firstly, the effect of constant axial loads on two dimensional response as compared to its effect on one-dimensional response is studied. After that the effect on the shear displacement behavior of the column with a varying axial load, dependent on the resisting shears, is studied.

a) The systems investigated for the constant axial load study are given in Table 3.4. Three different axial loads of -375, -562 and -750 kips were used. Only T = 0.4 systems under the Taft earthquake were investigated. The maximum displacements obtained are given in Table 3.5 and plotted in Fig. 3.36.

Changing the axial load on the column changes the post yield slope of the shear-deflection curve. For the cases under study the average post-yield slopes for uniaxial loads, up to a displacement of 8 times the yield displacement, were 7, 8.5 and 9 % of the secant slope up to yield, for the -750, -562 and -375 kips axial loads respectively, if P-Δ was neglected. With P-Δ, the same numbers were 3, 6 and 7 %.

The effect of this change in slope alone on 2D response as compared to 1D response can be studied by looking at the results for 2D with and without interaction with P-Δ neglected in Fig. 3.36. The 2D response with interaction is 46 % higher than the one without the interaction for the -750 kips axial load, whereas it is only 13 % higher for the -375 kips axial load.

When P-Δ is included in the analyses, the 2D response increases so rapidly with increases in compressive axial loads that the system with -750 kips axial load became unstable.

The effect of axial load on the shear-displacement response of the system can be seen by comparing Figs. 3.14 and

3.15 for the -750 kips axial load with Figs. 3.32 and 3.33 for -562 kips axial load. The beneficial effects of the lower compressive axial load are clearly seen.

Also, a comparison of the displacement-time response for axial loads of -562 and -375 kips made in Figs. 3.34 and 3.35 shows clearly that although the effect of axial load on 1D response is negligible its effect on 2D response is significant.

As would be expected the accumulated axial strain is significantly larger for the larger compressive axial loads. The larger of the two accumulated strains for 1D excitation were 0.0, -0.0016 and -0.0089 for axial loads of -375, -562 and -750 kips respectively. For 2D excitation they were -0.0016 and -0.015 for -375 and -562 kips axial load respectively, the -750 kips system becoming unstable.

b) For studying the effect of varying axial load in edge columns on the dynamic response of buildings, the shear-displacement response of edge columns is compared with that of the interior columns. The results obtained for T = 0.8 and T = 1.6 second systems with P = -750 kips under El Centro N-S records were used.

Assuming three bay frames, a height to width ratio of 1.3 and 3 for the T = 0.8 and T = 1.6 second buildings respectively, and a triangular distribution of lateral load over the height of the buildings, axial loads of P = $-750 \pm 2.5V$ and

$P = -750 \pm 5.7V$ were calculated for the edge columns of T = 0.8 T = 1.6 second buildings respectively. P = -750 kips was assumed as the gravity load.

Shear-displacement responses for these edge columns subjected to the computed displacement responses of the T = 0.8 and 1.6 systems to the El Centro N-S record are shown in Figs. 3.37 and 3.38. The shear-displacement responses of the interior column are also shown in these figures. The average shear for the two edge columns and the two interior columns was also computed and is shown in the figures.

It can be observed from the figures that although the shear-displacement response of the edge columns is significantly different from that of the interior column the average shear in the story is not greatly affected and, therefore, the effect on dynamic response of the building will not be significant. However, it is possible that the edge columns may suffer significantly more damage, because of the large variation of axial load supported by them.

3.6 Effect of Material Hysteresis Rules

For steel the effect of assumed material hysteresis rules was studied by using a bilinear model for the steel with 3 % and 1.5 % hardening. For concrete the effect of assumed material hysteresis rules was studied by modeling loading and unloading of concrete by a single straight line relationship

and in another case by assuming that the concrete was confined by ties such that the softening slope of the envelope curve, $\Omega = 40$.

For this study P = -562 kips was assumed and the Taft earthquake was used.

For purposes of comparison the shear-displacement response of this system using the proposed steel and concrete models are given in Figs. 3.32 and 3.33 and the displacement-time response by the solid lines in Figs. 3.34 and 3.35.

a) A comparison of Figs. 3.32, 3.39 and 3.41 computed for the proposed, the bilinear with 3 % hardening slope and the bilinear with 1.5 % hardening slope steel models respectively will show that the basic effect of the different modeling of steel on the shear-displacement response is in the post yield slope and in the case of the proposed model for steel in the smoother curve because of the Bauschinger effect. A similar comparison for the other direction of loading can be made by comparing Figs. 3.33, 3.40 and 3.42.

A comparison of the solid curves in Figs. 3.34 and 3.35 with the curves in Figs. 3.43 and 3.44 will show that the results of the proposed steel model are very similar to the results of the bilinear steel model with the 1.5 % hardening slope, so even though the shear-displacement response for the two cases look different the predicted maximum displacements are the same. It may, however, be noted that the average

hardening slope of the proposed steel model is 3 % but the bilinear steel model with 3 % hardening slope predicts only 60 % of the displacements for the 2D case. It can, therefore, be concluded that bilinear modeling for steel can be used, but that the equivalent hardening slope should be chosen to be smaller than for the real steel. The effect of the hardening slope on response is very small for the 1D case but significant for the 2D case, as shown in Figs. 3.43 and 3.44.

b) The effect of modeling concrete loading and unloading by a single line with a slope equal to the initial elastic slope was found to be slight. It increased the maximum 1D response by 5 % and the 2D response by 15 %.

The effect of assuming $\Omega = 40$ for the confined concrete instead of $\Omega = 0$ as was assumed for the spiral reinforcement was found to be significant. A comparison of Figs. 3.45 and 3.46 for $\Omega = 40$, with Figs. 3.32 and 3.33 for $\Omega = 0$ will reveal the beneficial effects of better confinement. A study of Figs. 3.47 and 3.48 shows that the effects of poorer confinement of concrete were large even for the 1D case and, therefore, proved to be critical for the 2D case causing the computed response to become unstable even with the smaller axial load of P = -562 kips.

As would be expected the poorer confinement of concrete led to a significant increase from -0.0016 to -0.079 in the accumulated axial strain for the 1D case. The 2D case with the poorer confinement became unstable.

3.7 Concluding Remarks

The responses to two-dimensional earthquake motion of systems consisting of a fixed-fixed reinforced concrete column supporting a single mass were calculated in this Chapter. The horizontal components of the El Centro 1940 and Taft 1952 earthquakes were used. The two-dimensional responses were compared with the corresponding one-dimensional responses.

Under design strength earthquakes resulting in one-dimensional displacements of the order of four or more times the yield displacement the two-dimensional displacements were significantly larger than the one-dimensional displacements and led to instability in some systems. The above results were found to be true for all system periods studied, which ranged from 0.2 to 1.6 seconds.

The magnitude of the two-dimensional interaction effect was found to be dependent on the strength of the earthquake. For strengths of the earthquake resulting in one-dimensional displacement responses of three or more times the yield displacement, the general trend was for the two-dimensional effect to be larger the stronger the earthquake. For earthquake strengths resulting in one-dimensional displacements of two or less times the yield displacement the trend was for the two-dimensional displacements to be less than the corresponding one-dimensional displacements.

It was found that a 30 % increase in the strength of the column for two-dimensional response resulted in displacements which were generally less than the corresponding one-dimensional response. However, whether a 30 % increase in strength of the column will result in a satisfactory design has yet to be studied experimentally, because significantly more damage in the biaxially loaded columns is predicted as compared to columns loaded uniaxially for the same level of displacement.

The effect of axial loads was found to be critical for most two-dimensional responses mainly because of the P-Δ effect even though their effect on most one-dimensional responses was insignificant.

The computed two-dimensional responses were found to be sensitive to changes in the post-yield slope of the shear-deflection relations, although one-dimensional responses were not greatly affected. Changes in the assumed material hysteresis rules which resulted in significant changes in the post-yield slope of the shear-deflection relations, also resulted in significant changes in the computed two-dimensional response. Thus a change in the hardening slope of steel or a change in the confinement of concrete had significant effect.

4. CONCLUSIONS

The conclusions drawn in this study are summarized herein under two general categories. The first category relates to conclusions about the modeling assumptions used in the development of the analytical model for reinforced concrete columns and its static behavior. The second category relates to conclusions about effects of two-dimensional earthquake motion on reinforced concrete column response.

a) The conclusions about the modeling assumptions and static response of the analytical model are:

1) The stress-strain model for reinforcing steel developed in this study gives an excellent match with experimental data. The reinforcing steel model which accounts for yielding, strain-hardening and the Bauschinger effect is important in reproducing realistic moment-curvature and shear-deflection relationships. However, the use of a bilinear steel model for dynamic analyses gave displacement responses similar to the proposed steel model if the hardening slope of the bilinear steel was assumed to be about half the average actual hardening slope.

2) For dynamic analyses only the strength and the softening slope of the concrete stress-strain curve was found to be important. The details of the hysteresis curve were

found to be unimportant. The softening slope of the concrete stress-strain curve is dependent on the degree of confinement of the concrete. Further experimental work is indicated to obtain this slope from the specified confinement especially for different amounts of spiral reinforcements under eccentric loading conditions.

3) The lumped concrete model developed in this study to represent the concrete in the section of a column reduces the computational cost for calculating moment-curvature relationships of the section from given material stress-strain curves by an order of magnitude. The lumped concrete model gives excellent comparisons for moment-curvature-axial load relationships of the section with those obtained by dividing the concrete into a two-dimensional mesh for two-dimensional loadings.

4) The assumed curvature distribution along the length of the column which allows the calculation of shear-deflection-axial load relationships from the moment-curvature relationships at the end sections of the column underestimates the experimental displacements. This is mainly due to the neglect of anchorage slip in the present study. However, the shape of the experimental shear-deflection relationship for both uniaxial and biaxial loadings is quite well predicted.

5) The analytical model predicts an accumulation of axial strain under cyclic loading of the column. This accumulated axial strain increases with increase in compressive axial loads and with poorer confinement of concrete. This predicted accumulated axial strain could be used as an indication of the amount of damage to the column.

6) The analytical model predicts significant changes in strength and energy absorption capacity when the column is loaded biaxially as compared to uniaxial loading. The magnitude of this change is dependent on the correlation between the loadings in the two directions. Biaxial loading also significantly increased the accumulation of axial strain under cyclic loading.

b) The conclusions about the effect of two-dimensional earthquake motion on reinforced concrete columns are:

1) Under design strength earthquakes resulting in one-dimensional displacement responses of four times the yield displacement or more, the two-dimensional responses of reinforced concrete columns were significantly higher. Increases in displacements from 39 to 160 % were noted, and some systems became unstable under two-dimensional excitation. The increases were mainly due to inelastic interaction in the columns.

2) The strength of the earthquake significantly influences the effect of two-dimensional motion. If the

one-dimensional response is greater than three times the yield displacement, an increase in displacement response under two-dimensional motion is expected; the increase being larger the stronger the earthquake. If the one-dimensional responses are less than two times the yield displacement, the corresponding two-dimensional responses are expected to be less than the one-dimensional responses.

3) A thirty percent increase in column strength for two-dimensional response reduced the displacements to one-dimensional response level. However, experimental work is indicated to define limits of safe behavior for two-dimensional loading of the column. The analytical model predicts significantly more damage to the column under biaxial loading compared to uniaxial loading for the same level of cyclic deformation.

4) A comparative study of the displacement-time response under one- and two-dimensional earthquakes reveals that the waveforms for the two cases are very similar, and that most of the additional displacements for the two-dimensional cases come from additional drifts accumulated over short intervals of time. It is suspected that these additional drifts occur when the shear response for the two one-dimensional cases are simultaneously large. The number of systems and earthquakes studied herein were not sufficient in number for a definitive statement to be made in this

regard. This conjecture would explain the greater susceptibility of shorter period systems to two-dimensional motion. Due to the larger number of cycles for the shorter period systems for a given duration of an earthquake, the probability of shear responses in the two directions being simultaneously large are greater, thus leading to additional drifts. This conjecture would also explain the greater effect of two-dimensional motions if the one-dimensional displacement responses are large. The larger the displacement response, the greater is the length of time for which shears are large. This increases the probability that the shear response in the two directions will be simultaneously large, thus leading to additional drifts.

5) The effect of axial load as manifested by the P-Δ effect is critical for two-dimensional response, even though it may appear to be unimportant for one-dimensional response.

6) Time-varying axial loads dependent on the resisting shears as would be obtained in edge columns due to overturning moments, result in significantly different shear-deflection relationships for the individual columns, and their safety should be further investigated. However, the average shear in the story is not much affected, therefore, a significant change in the dynamic response of the building is not indicated.

7) Changes in material hysteresis rules which significantly change the post-yield slope of the shear-deflection curve do also significantly change the two-dimensional response, even though the one-dimensional response may not be much affected.

In summary, the most important conclusions of this study are, that if a building is so proportioned that one-dimensional maximum displacement response of columns to earthquakes are larger than about three times the yield displacement, then a 30 % increase in the strength of the columns will result in two-dimensional maximum displacement responses about equal to the maximum one-dimensional displacements responses. If the one-dimensional maximum displacement responses are less than about two times the yield displacement then the two-dimensional effects may be neglected. If two systems with different periods are so designed to give similar one-dimensional displacement responses, then the two-dimensional effects will be similar irrespective of the system periods. The inclusion of gravity for calculating two-dimensional responses was found to be critical.

REFERENCES

1. Aktan, A. E., "Effects of Two-Dimensional Earthquake Motion on a Reinforced Concrete Column," thesis presented to the University of Illinois at Urbana-Champaign in partial fulfillment of the requirements for the degree of Doctor of Philosophy, 1973.

2. Aktan, A. E., Karlsson, B. I. and Sozen, M. A., "Stress-Strain Relationships of Reinforcing Bars Subjected to Large Strain Reversals," SRS No. 397, Civil Engineering Studies, University of Illinois at Urbana-Champaign, Illinois, June 1973.

3. Aoyama, H., "Moment-Curvature Characteristics of Reinforced Concrete Members Subjected to Axial Load and Reversal of Loading," Proceedings of the International Symposium on Flexural Mechanics of Reinforced Concrete, ACI, SP-12, pp. 183-212.

4. Clough, R. W. and Johnston, S. B., "Effect of Stiffness Degradation on Earthquake Ductility Requirements," Proceedings, Japan Earthquake Engineering Symposium, Tokyo, Oct. 1966, pp. 227-232.

5. Darwin, D., "Inelastic Model for Cyclic Biaxial Loading of Reinforced Concrete," thesis presented to the University of Illinois at Urbana-Champaign in partial fulfillment of the requirements for the degree of Doctor of Philosophy, 1974.

6. Drucker, D. C., "A More Fundamental Approach to Plastic Stress-Strain Relations," Proceedings, First U. S. National Congress of Applied Mechanics (Chicago, 1951), New York, 1952, p. 487.

7. Hognestad, E., "A Study of Combined Bending and Axial Load in Reinforced Concrete," University of Illinois Engineering Experiment Station, Bulletin Series No. 399, November, 1951.

8. Jennings, P. C., "Engineering Features of the San Fernando Earthquake, February 9, 1971," Earthquake Engineering Research Laboratory, California Institute of Technology, Pasadena, California.

9. Jennings, P. C. and Husid, R., "Collapse of Yielding Structures During Earthquakes," Journal of the Engineering Mechanics Division, ASCE, Vol. 94, No. EM5, October 1968, pp. 1045-1065.

10. Kaldjian, M. J. and Fan, W. R. S., "Earthquake Response of a Ramberg-Osgood Structure," Journal of the Structural Division, ASCE, Vol. 94, No. ST10, October 1968, pp. 2451-2465.

11. Karlsson, B. I., Aoyama, H. and Sozen, M. A., "Spirally Reinforced Concrete Columns Subjected to Loading Reversals Simulating Earthquake Effects," Proceedings of the Fifth World Conference on Earthquake Engineering, Rome, Italy, 1973.

12. Karsan, D. I., "Behavior of Plain Concrete Under Variable Load Histories," thesis presented to Rice University, Houston, Texas in partial fulfillment of the requirements for the degree of Doctor of Philosophy, 1968.

13. Kent, D. C., "Inelastic Behavior of Reinforced Concrete Members with Cyclic Loading," Ph.D. thesis presented to the University of Canterbury, Christchurch, New Zealand, 1969.

14. Kubo, T. and Penzien, J., "Characteristics of Three-Dimensional Ground Motions, San Fernando Earthquake," Review Meeting of the U. S.-Japan Cooperative Research Program on Earthquake Engineering with Emphasis on the Safety of School Buildings, University of Hawaii, Honolulu, Hawaii, August 1975.

15. Mark, K. M. S., "Nonlinear Dynamic Response of Reinforced Concrete Frames," thesis presented to the Massachusetts Institute of Technology, Cambridge, Massachusetts in partial fulfillment of the requirements for the degree of Doctor of Philosophy, 1976.

16. Mroz, Z., "An Attempt to Describe the Behavior of Metals under Cyclic Loads Using a More General Workhardening Model," Acta Mechanica, Vol. 7, 1969, pp. 199-212.

17. Newmark, N. M., "A Method of Computation for Structural Dynamics," Journal of the Engineering Mechanics Division, ASCE, Vol. 85, No. EM3, July 1959, pp. 67-94.

18. Nigam, N. C., "Inelastic Interactions in the Dynamic Response of Structures," thesis presented to the California Institute of Technology at Pasadena, California, in partial fulfillment of the requirements for the degree of Doctor of Philosophy, 1967.

19. Okada, T., Seki, M., Asai, S., "Response of Reinforced Concrete Columns to Bi-Directional Horizontal Force and Constant Axial Force," Bulletin of ERS, No. 10, Earthquake Resistant Structure Research Center, Institute of Industrial Science, University of Tokyo, 1976, pp. 30-36.

20. Padilla, R., "Non-linear Response of Framed Structures to Two-Dimensional Earthquake Motion," thesis presented to the University of Illinois at Urbana-Champaign in partial fulfillment of the requirements for the degree of Doctor of Philosophy, 1974.

21. Pecknold, D. A., "Inelastic Structural Response to 2D Ground Motion," Journal of the Engineering Mechanics Division, ASCE, Vol. 100, No. EM5, October 1974, pp. 949-963.

22. Pecknold, D. A. and Sozen, M. A., "Calculated Inelastic Structural Response to Uniaxial and Biaxial Earthquake Motions," Proceedings of the Fifth World Conference on Earthquake Engineering, Rome, Italy, 1973.

23. "Recommended Lateral Force Requirements and Commentary," Seismology Committee, Structural Engineers Association of California, San Francisco, California, 1973.

24. Richard, R. M. and Abbott, B. J., "Versatile Elastic-Plastic Stress-Strain Formula," Technical Note, Journal of the Engineering Mechanics Division, ASCE, Vol. 101, No. EM4, August 1975, pp. 511-515.

25. Roy, H. E. H. and Sozen, M. A., "Ductility of Concrete," Proceedings of the International Symposium on Flexural Mechanics of Reinforced Concrete, ACI, SP-12, pp. 213-235.

26. Selna, L. G., Morrill, K. B. and Ersoy, O. K., "Earthquake Response Analysis of the Olive View Hospital Psychiatric Day Clinic," International Journal of Earthquake Engineering and Structural Dynamics, Vol. 3, 1974, pp. 15-32.

27. Singh, A., Gerstle, K. H. and Tulin, L. G., "The Behavior of Reinforcing Steel under Reversed Loading," Journal ASTM, Materials Research and Standards, Vol. 5, No. 1, January 1965, pp. 12-17.

28. Sinha, B. P., Gerstle, K. H. and Tulin, L. G., "Stress-Strain Relations for Concrete Under Cyclic Loading," Journal ACI, Proc. V, 61, No. 2, 1964, pp. 195-211.

29. Sozen, M. A., "Hysteresis in Structural Elements," Applied Mechanics in Earthquake Engineering, AMD-8, ASME, 1974, pp. 63-98.

30. Takeda, T., Sozen, M. and Nielsen, N. N., "Reinforced Concrete Response to Simulated Earthquakes," Journal of the Structural Division, ASCE, Vol. 96, No. ST12, December 1970, pp. 2557-2573.

31. Takiguchi, K. and Kokusho, S., "Hysteretic Behavior of Reinforced Concrete Members Subjected to Bi-axial Bending Moments," Proceedings of the Sixth World Conference on Earthquake Engineering, New Delhi, India, 1977.

32. Takizawa, H., "Biaxial and Gravity Effects in Modelling Strong-Motion Response of R/C Structures," Proceedings of the Sixth World Conference on Earthquake Engineering, New Delhi, India, 1977.

33. Takizawa, H., "Biaxial Effects in Modelling Earthquake Response of R/C Structures," Technical Note, International Journal of Earthquake Engineering and Structural Dynamics, Vol. 4, 1976, pp. 609-620.

34. Takizawa, H. and Aoyama, H., "Biaxial Effects in Modelling Earthquake Response of R/C Structures," International Journal of Earthquake Engineering and Structural Dynamics, Vol. 4, 1976, pp. 523-552.

35. "Tentative Provisions for the Development of Seismic Regulations for Buildings," ATC Publication ATC 3-06, NBS Special Publication 510, NSF Publication 78-8, U. S. Government Printing Office, Washington, D. C., 1978.

36. "The National Building Code of Canada 1975," National Research Council of Canada, Ottawa, Canada.

37. "Uniform Building Code - 1976 Edition," International Conference of Building Officials, Whittier, California.

38. Wight, J. K., "Shear Strength Decay in Reinforced Concrete Columns Subjected to Large Deflection Reversals," thesis presented to the University of Illinois at Urbana-Champaign in partial fulfillment of the requirements for the degree of Doctor of Philosophy, 1973.

39. Ziegler, H., "A Modification of Prager's Hardening Rule," Quarterly of Applied Mathematics, Vol. 17, No. 1, April 1959, pp. 55-65.

40. Zienkiewicz, O. C., "The Finite Element Method in Engineering Science," McGraw-Hill, 1971.

Table 2.1 Two-Dimensional Curvature Histories (Fig. 2.19)

Sequence of Loading	Curvature History 1 (/in. 10^{-5})		Curvature History 2 (/in. 10^{-5})		Curvature History 3 (/in. 10^{-5})	
	Direction 1	Direction 2	Direction 1	Direction 2	Direction 1	Direction 2
0	0	0	0	0	0	0
1	96	0	96	0	96	0
2	- 96	0	0	96	96	96
3	96	0	- 96	0	- 96	96
4	- 96	0	0	- 96	- 96	- 96
5	160	0	96	0	96	- 96
6	- 160	0	0	96	96	96
7	160	0	- 96	0	- 96	96
8	- 160	0	0	- 96	- 96	- 96
9	160	0	96	0	96	- 96
10	- 96	0	160	0	96	0
11	96	0	0	160	160	0
12	- 96	0	- 160	0	160	160
13	96	0	0	- 160	- 160	160
14	0	0	160	0	- 160	- 160
15	0	96	0	160	160	- 160
16	0	- 96	- 160	0	160	160
17	0	96	0	- 160	- 160	160
18	0	- 96	160	0	- 160	- 160
19	0	160	96	0	160	- 160
20	0	- 160	0	96	160	0
21	0	160	- 96	0	96	0
22	0	- 160	0	- 96	96	96
23	0	160	96	0	- 96	96
24	0	- 96	0	96	- 96	- 96
25	0	96	- 96	0	96	- 96
26	0	- 96	0	- 96	96	96
27	0	96	96	0	- 96	96
28	0	0	0	0	- 96	- 96
29					96	- 96
30					96	0
31					0	0

Table 2.2 Properties of Test Specimen

Specimen	Aoyama's Specimen A-1 (Fig. 2.34)	Aoyama's Specimen A-2 (Fig. 2.34)	Karlsson's Specimen BK5 (Figs. 2.35 and 2.36)	Takizawa's Specimen 3 (Fig. 2.38)	Takizawa's Specimen 4 (Fig. 2.38)
Shear Span (L/2)	--	--	38 ins.	60 cm	60 cm
Section	6x12 ins.	6x12 ins.	13x13 ins.	20x20 cm	20x20 cm
Core	4.75x9.5 ins.	4.75x9.5 ins.	11.5 ins. dia.	16.2x16.2 cm	16.2x16.2 cm
Concrete					
σ_o	- 4.9 ksi	- 4.9 ksi	- 5.0 ksi	- 0.23 ton/cm^2	- 0.16 ton/cm^2
ε_o	- 0.0025	- 0.0025	- 0.0025	- 0.0025	- 0.0025
σ_t	0.4 ksi	0.4 ksi	0.45 ksi	0.02 ton/cm^2	0.015 ton/cm^2
Confinement	Rectilinear ties #3 at 6 ins.	Rectilinear ties #3 at 6 ins.	Spiral #3 at 1 5/8 ins.	Rectilinear ties 6 mm dia. at 5 cm	Rectilinear ties 6 mm dia. at 5 cm
Ω (confined)	107	107	0	65	65
Ω (unconfined)	107	107	107	107	107
Ω (average)	107	107	24	80	80
Steel	4 - #6	4 - #6	8 - #9	4 - 13 mm dia.	4 - 13 mm dia.
A_s	1.76 in.^{2}	1.76 in.^{2}	8 in.^{2}	5.08 cm^2	5.08 cm^2
σ_y	50 ksi	50 ksi	65 ksi	3.94 ton/cm^2	3.94 ton/cm^2

Table 2.3 Two-Dimensional Displacement Histories For Takizawa's Tests (Fig. 2.37)

Sequence of Loading	Specimen 3 Displacements (mm)		Specimen 4 Displacements (mm)	
	Direction 1	Direction 2	Direction 1	Direction 2
0	0	0	0	0
1	9	0	9	0
2	0	9	9.5	9
3	- 9	0	- 9.5	11.5
4	0	- 9	- 12	- 9.5
5	9	0	9	- 11.5
6	0	9	10.5	10
7	- 9	- 0.5	- 9	12.5
8	0	- 9	- 10.5	- 9.5
9	8.5	0	9	- 17
10	11.5	0	12	0.5
11	0	11.5	20	2
12	- 12	0	21.5	20
13	0	- 12.5	- 21	24.5
14	11.5	0	- 27.5	- 20
15	0	12	20	- 25.5
16	- 12	0		
17	0	- 11.5		
18	0	- 4.5		
19	0	- 20		
20	20	0		
21	- 1	20.5		
22	- 20.5	0		
23	0	- 20		

Table 3.1 System Properties

Period T (sec)	Yield Shear V_y (kips)	Yield Displacement u_y (in.)	Mass m (kip-sec^2/in.)	Yield Shear Ratio $c = V_y/mg$	Peak Acc. A_{max} (g)	c/A_{max} (/g)
0.2	131	0.93	0.143	2.37	3.37	0.70*
0.4	131	0.93	0.573	0.59	1.67	0.35
0.4	131	0.93	0.573	0.59	1.34	0.44*
0.4	131	0.93	0.573	0.59	1.00	0.59
0.4	131	0.93	0.573	0.59	0.67	0.88
0.4	131	0.93	0.573	0.59	0.50	1.18
0.4	131	0.93	0.573	0.59	0.34	1.75
0.8	131	0.93	2.29	0.148	0.53	0.28*
1.6	131	0.93	9.16	0.037	0.32	0.12
1.6	131	0.93	9.16	0.037	0.26	0.14
1.6	131	0.93	9.16	0.037	0.21	0.18*
1.6	131	0.93	9.16	0.037	0.16	0.23
1.6	131	0.93	9.16	0.037	0.11	0.34

* Referred to as systems with design strength.

Table 3.2 Maximum Displacement Response of Systems with Design Strength

Earthquake	Period T (sec)	c/A_{max} (/g)	P-Δ	Maximum Displacement (in.)				
				Elastic		Proposed Model		
						1D Response	2D Response	
				Direction 1	Direction 2	Direction 1	Direction 2	Without Interaction	With Interaction	With Interaction, Reduced Strength Earthquake[2]
El Centro	0.2	0.7	Yes	-	-	5.12 (2.18)[1]	2.17 (2.74)	5.12 (2.18)	8.93 (2.20)	2.86 (2.32)
			No	3.50	2.69	4.62 (2.18)	2.11 (2.74)	4.63 (2.18)	6.14 (2.18)	-
	0.4	0.44	Yes	-	-	8.70 (5.34)	7.54 (11.70)	8.70 (5.34)	19.95 (14.72)	6.74 (11.64)
			No	4.75	5.01	7.51 (1.96)	6.95 (11.68)	7.59 (1.96)	8.85 (11.68)	-
	0.8	0.28	Yes	-	-	5.01 (3.08)	4.28 (12.40)	5.97 (3.08)	6.98 (5.50)	4.97 (3.12)
			No	6.45	5.68	4.81 (3.06)	4.35 (12.36)	5.65 (3.06)	6.07 (3.10)	-
	1.6	0.18	Yes	-	-	3.57 (5.62)	3.56 (9.62)	4.34 (5.62)	4.97 (3.68)	3.10 (5.66)
			No	3.66	2.60	3.54 (5.60)	3.68 (9.58)	4.22 (5.60)	4.27 (3.62)	-
Taft	0.2	0.7	Yes	-	-	9.40 (6.72)	5.69 (9.18)	10.20 (6.74)	Unstable (7.06)	6.20 (14.66)
			No	4.31	3.52	7.10 (6.68)	5.55 (6.76)	8.60 (6.70)	8.89 (9.20)	-
	0.4	0.44	Yes	-	-	5.90 (6.80)	8.00 (14.40)	8.03 (14.40)	Unstable (9.98)	8.86 (19.30)
			No	5.52	6.16	6.47 (7.88)	6.72 (14.38)	7.01 (7.88)	10.23 (14.38)	-
	0.8	0.28	Yes	-	-	5.31 (4.00)	6.28 (9.54)	7.00 (9.54)	18.21 (19.60)	5.87 (6.54)
			No	7.50	7.46	5.22 (3,98)	5.36 (9,52)	6.00 (3.98)	8.99 (6.60)	-
	1.6	0.18	Yes	-	-	2.82 (8.18)	5.37 (4.62)	6.01 (4.68)	7.41 (6.62)	5.15 (6.62)
			No	6.81	3.33	2.72 (8.18)	4.84 (4.34)	5.20 (4.34)	6.67 (6.66)	-

Note: 1) Numbers in parenthesis are time in seconds when maximum displacement occurred.
For unstable systems it refers to time when displacement was 25 times the yield displacement. (Yield Disp. = 0.93 in.)

2) For 2D response with reduced earthquake strength, the earthquake record was multiplied by 0.77.
This is equivalent to increasing the column strength by 30 %.

Table 3.3 Effect of Strength on Maximum Displacement Response

Earthquake	Period T (sec)	c/A_{max} (/g)	P-Δ	Maximum Displacement (in.)			
				1D Response		2D Response	
				Direction 1	Direction 2	Without Interaction	With Interaction
El Centro	0.4	0.35	Yes	14.66	10.39	14.69	Unstable
	0.4	0.44	Yes	8.70	7.54	8.70	19.95
	0.4	0.59	Yes	5.54	4.25	5.84	6.74
	0.4	0.88	Yes	2.48	1.58	2.51	4.00
	0.4	1.18	Yes	1.91	1.82	1.95	1.71
	0.4	1.75	Yes	1.38	0.72	1.44	1.18
	1.6	0.12	No	4.98	7.95	8.08	10.54
	1.6	0.14	No	4.22	4.92	4.92	7.53
	1.6	0.18	No	3.54	3.68	4.22	4.27
Taft	0.4	0.35	Yes	10.34	13.45	15.10	Unstable
	0.4	0.44	Yes	5.90	8.00	8.03	Unstable
	0.4	0.59	Yes	4.87	4.90	5.10	8.86
	0.4	0.88	Yes	3.22	2.34	3.30	3.21
	0.4	1.18	Yes	2.64	2.20	2.76	2.46
	0.4	1.75	Yes	1.87	1.66	1.87	1.77
	0.4	0.35	No	7.74	9.49	9.56	17.42
	0.4	0.44	No	6.47	6.72	7.01	10.23
	0.4	0.59	No	4.62	4.76	4.93	5.47
	0.4	0.88	No	3.26	2.14	3.32	2.96
	1.6	0.12	No	5.43	9.87	10.90	11.19
	1.6	0.14	No	4.07	7.90	8.71	8.12
	1.6	0.18	No	2.72	4.84	5.20	6.67
	1.6	0.23	No	2.74	3.32	3.74	4.40
	1.6	0.34	No	2.11	2.04	2.29	2.44

Table 3.4 System Properties for Different Axial Loads

Period, T (sec)	Axial Load, P (kips)	Yield Shear, V_y (kips)	Yield Displacement, u_y (in.)	Mass, m (kip-sec^2/in.)	Yield Shear Ratio $c = V_y/mg$	Peak Acceleration A_{max} (g)	c/A_{max} (/g)	$\frac{P}{KL} = \frac{Pu_y}{V_y L}$
0.4	- 750	131	0.93	0.573	0.59	1.34	0.44	0.032
0.4	- 562	120	0.87	0.561	0.55	1.25	0.44	0.024
0.4	- 375	108	0.81	0.540	0.52	1.17	0.44	0.016

Table 3.5 Maximum Displacement Response for Different Axial Loads, T = 0.4, Taft Record

Axial Load, P (kips)	c/A_{max} (/g)	P-Δ	Maximum Displacement (in.)			
			1D Response		2D Response	
			Direction 1	Direction 2	Without Interaction	With Interaction
- 750	0.44	Yes	5.90	8.00	8.03	Unstable
		No	6.47	6.72	7.01	10.23
- 562	0.44	Yes	5.77	6.34	6.34	14.17
		No	5.79	6.13	6.30	7.50
- 375	0.44	Yes	5.45	6.02	6.02	7.52
		No	5.15	5.78	5.78	6.52

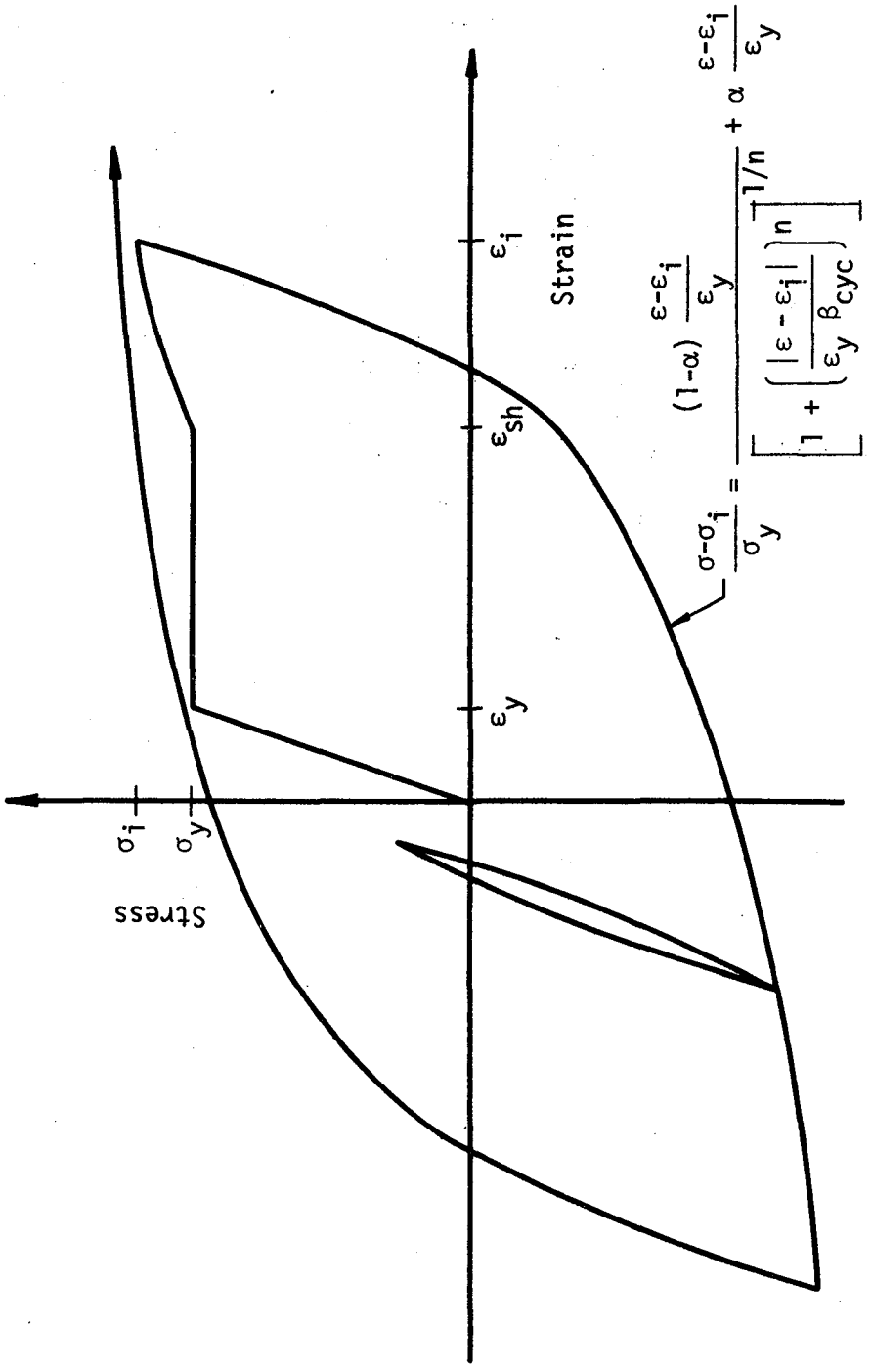

Fig. 2.1 Schematic Diagram of Proposed Hysteresis Model for Reinforcing Steel

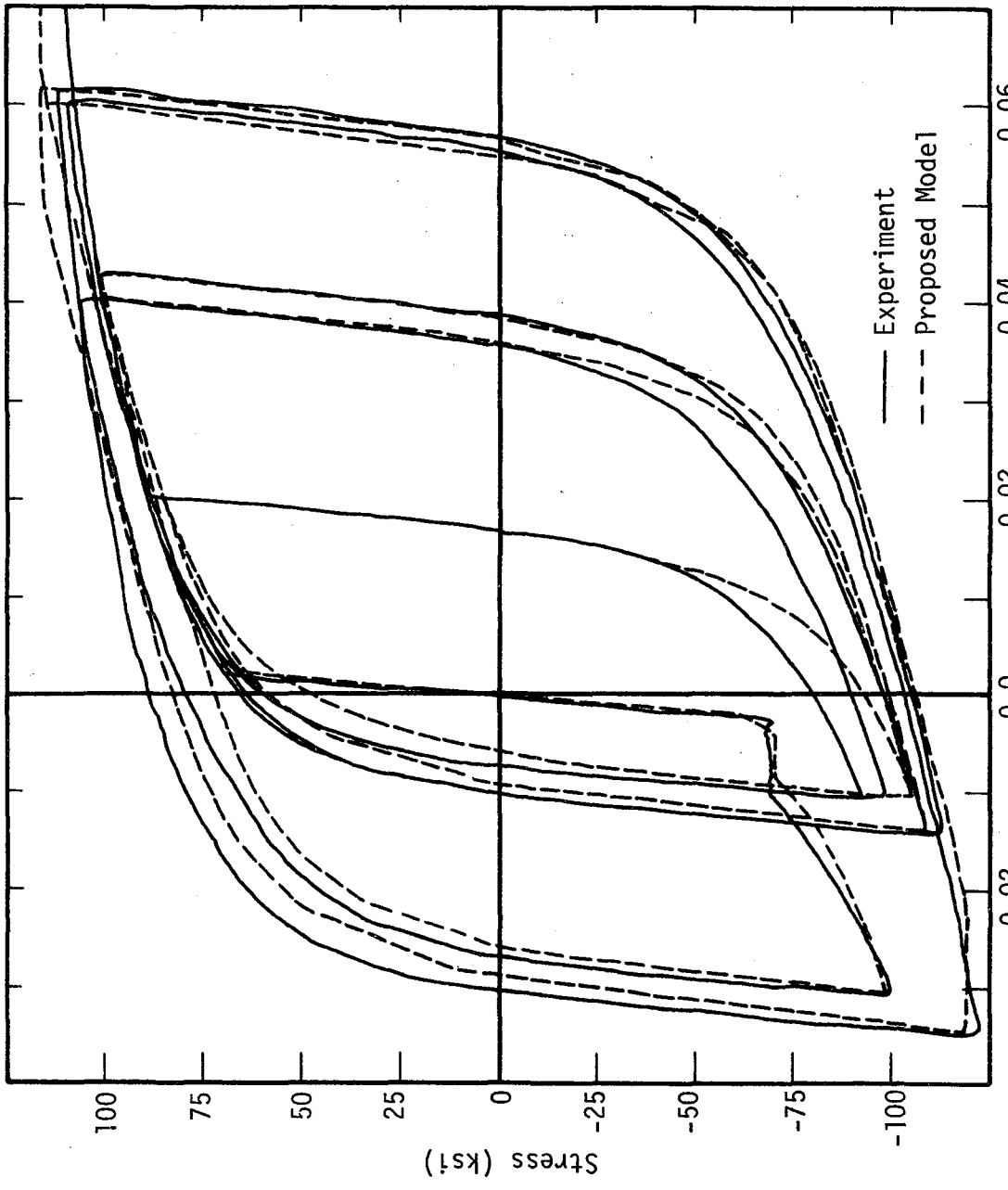

Fig. 2.2 Comparison of Proposed Hysteresis Model for Reinforcing Steel with Experiment, Specimen 5 (Ref. 2)

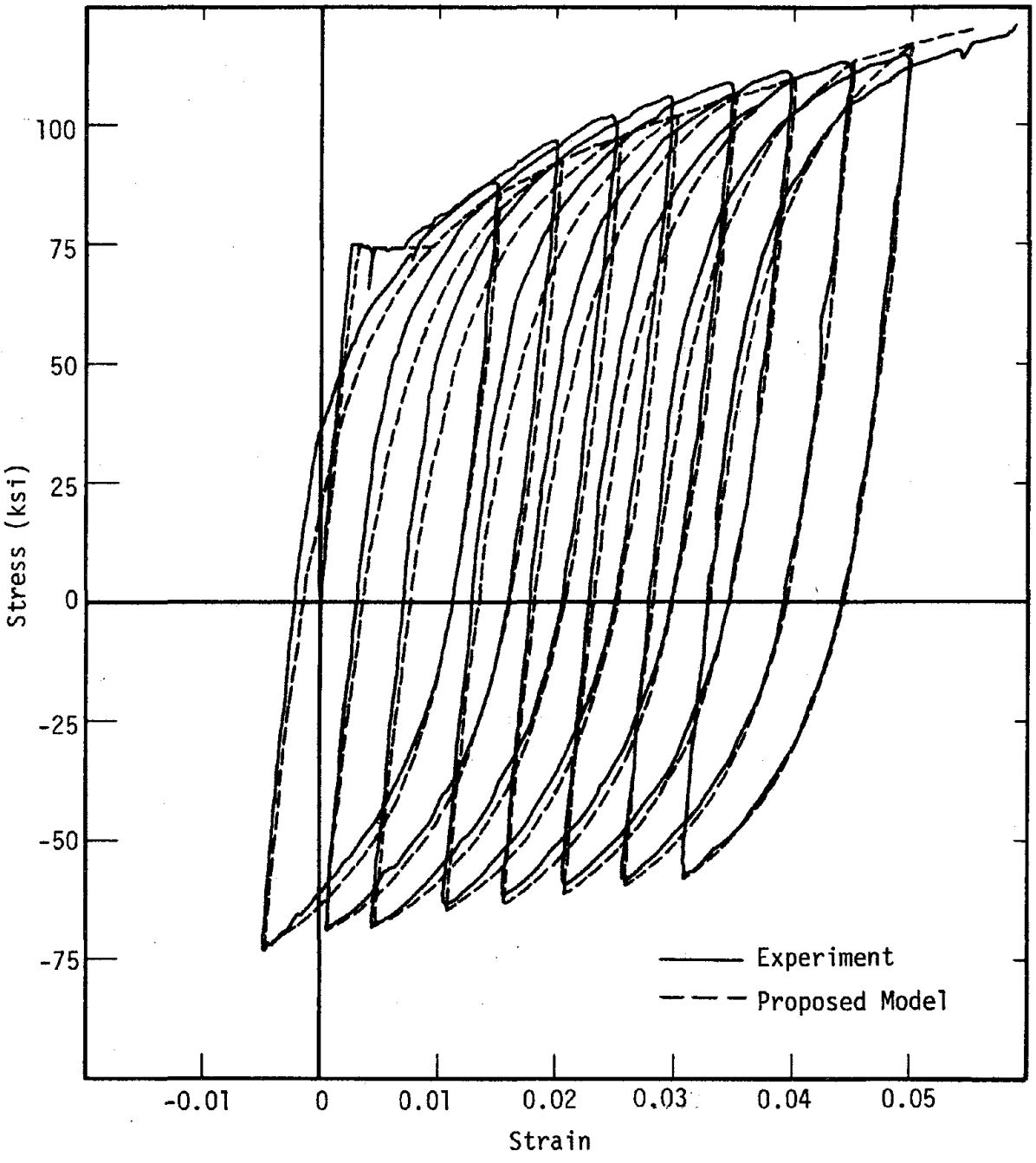

Fig. 2.3 Comparison of Proposed Hysteresis Model for Reinforcing Steel with Experiment, Specimen 8 (Ref. 2)

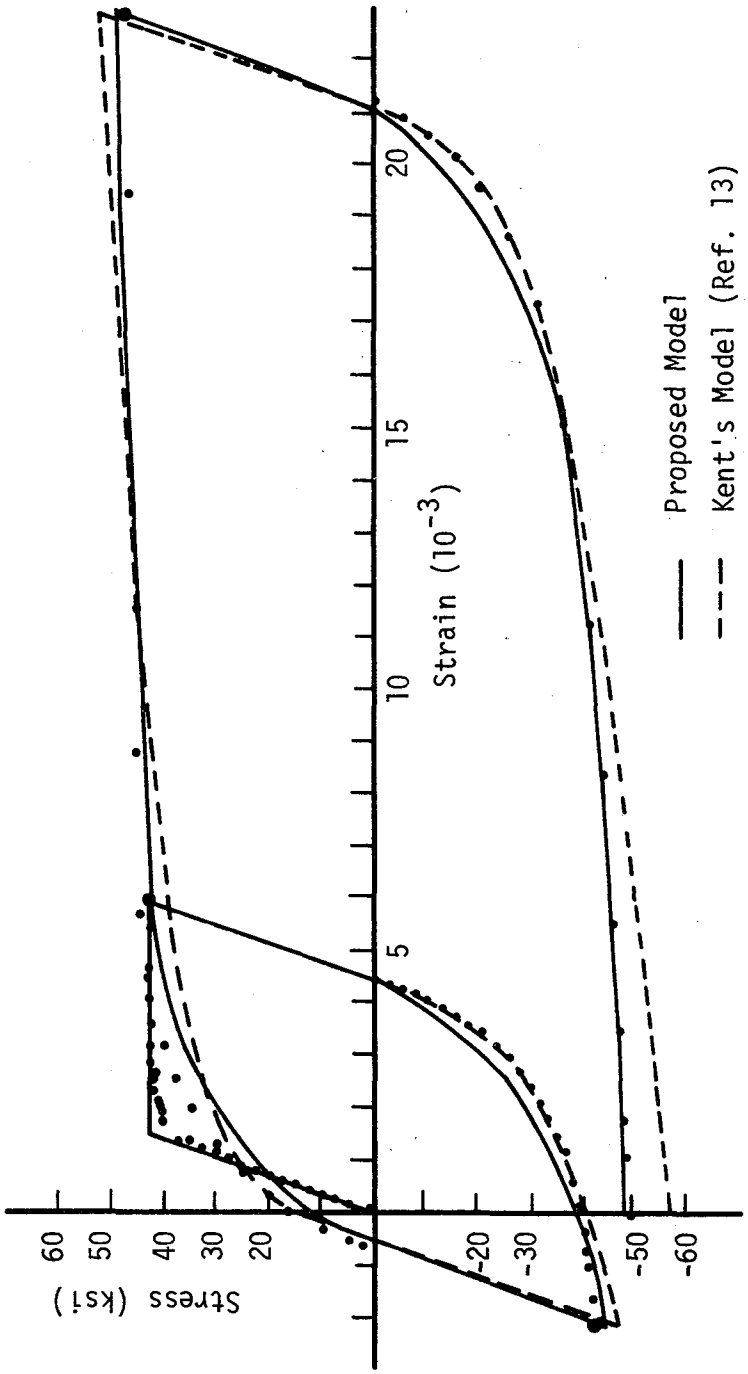

Fig. 2.4 Comparison of Proposed Hysteresis Model for Reinforcing Steel with Experiment and with Kent's Model, Specimen 25 (Ref. 13)

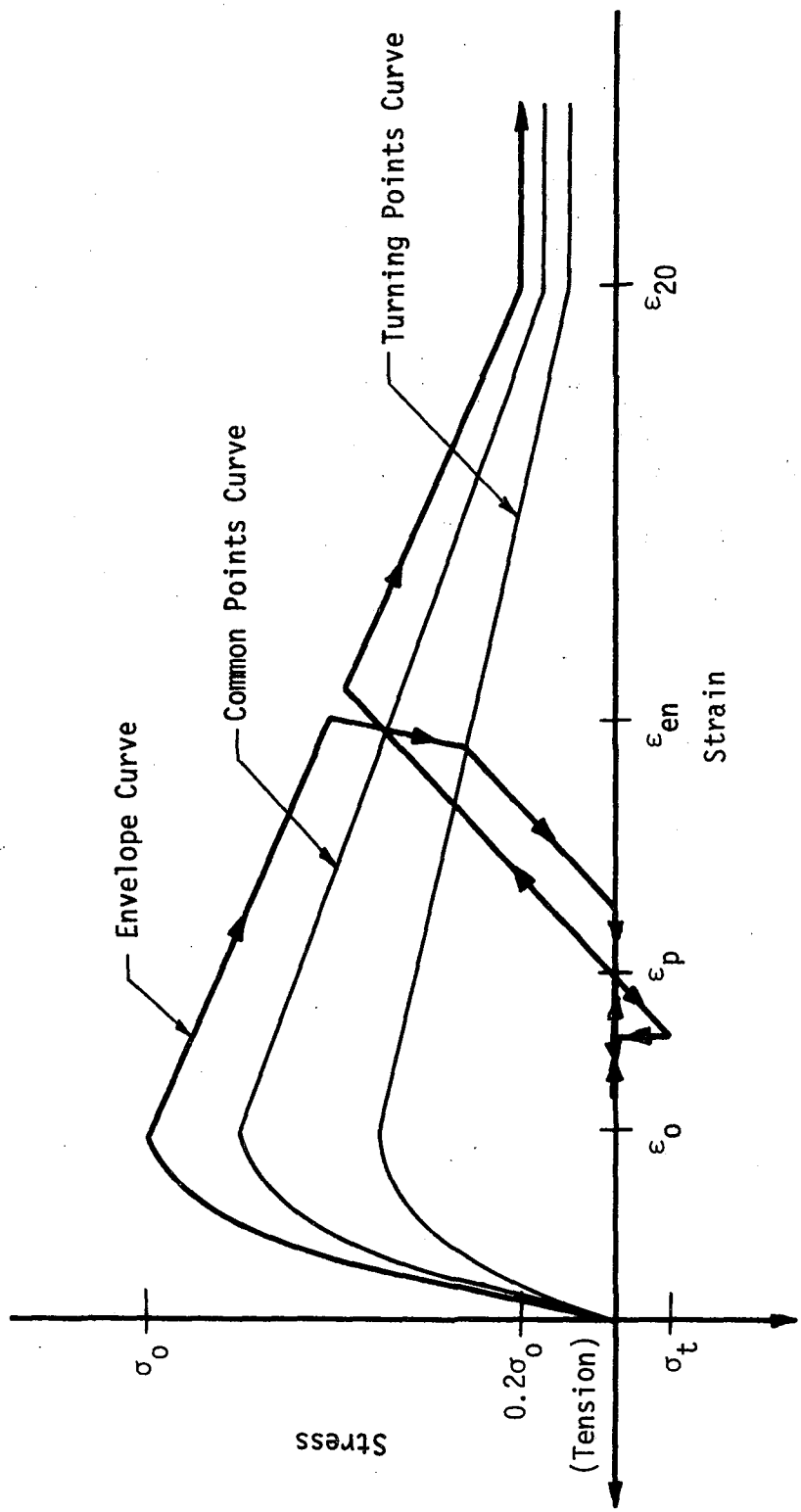

Fig. 2.5 Schematic Diagram of Proposed Hysteresis Model for Concrete

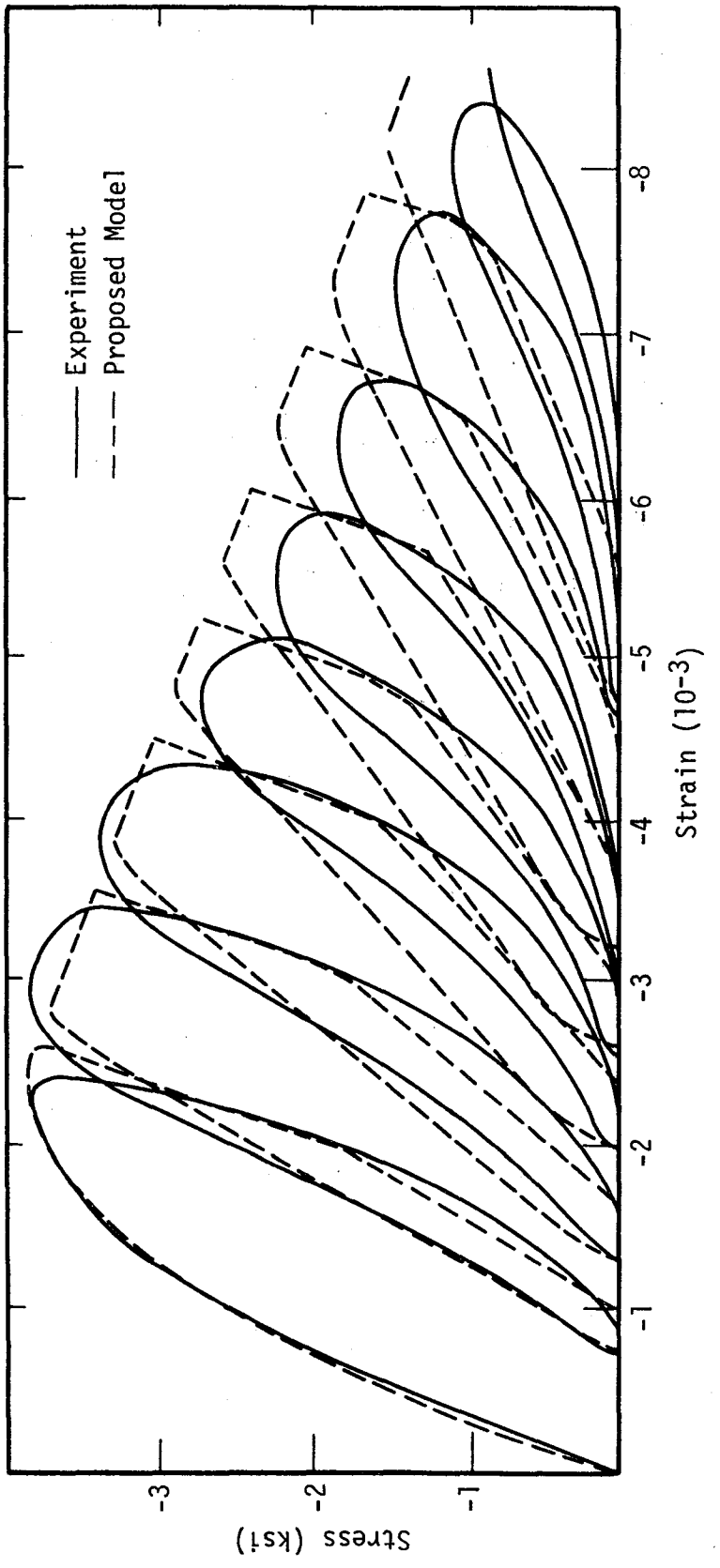

Fig. 2.6 Comparison of Proposed Hysteresis Model for Concrete with Experiment (Ref. 28)

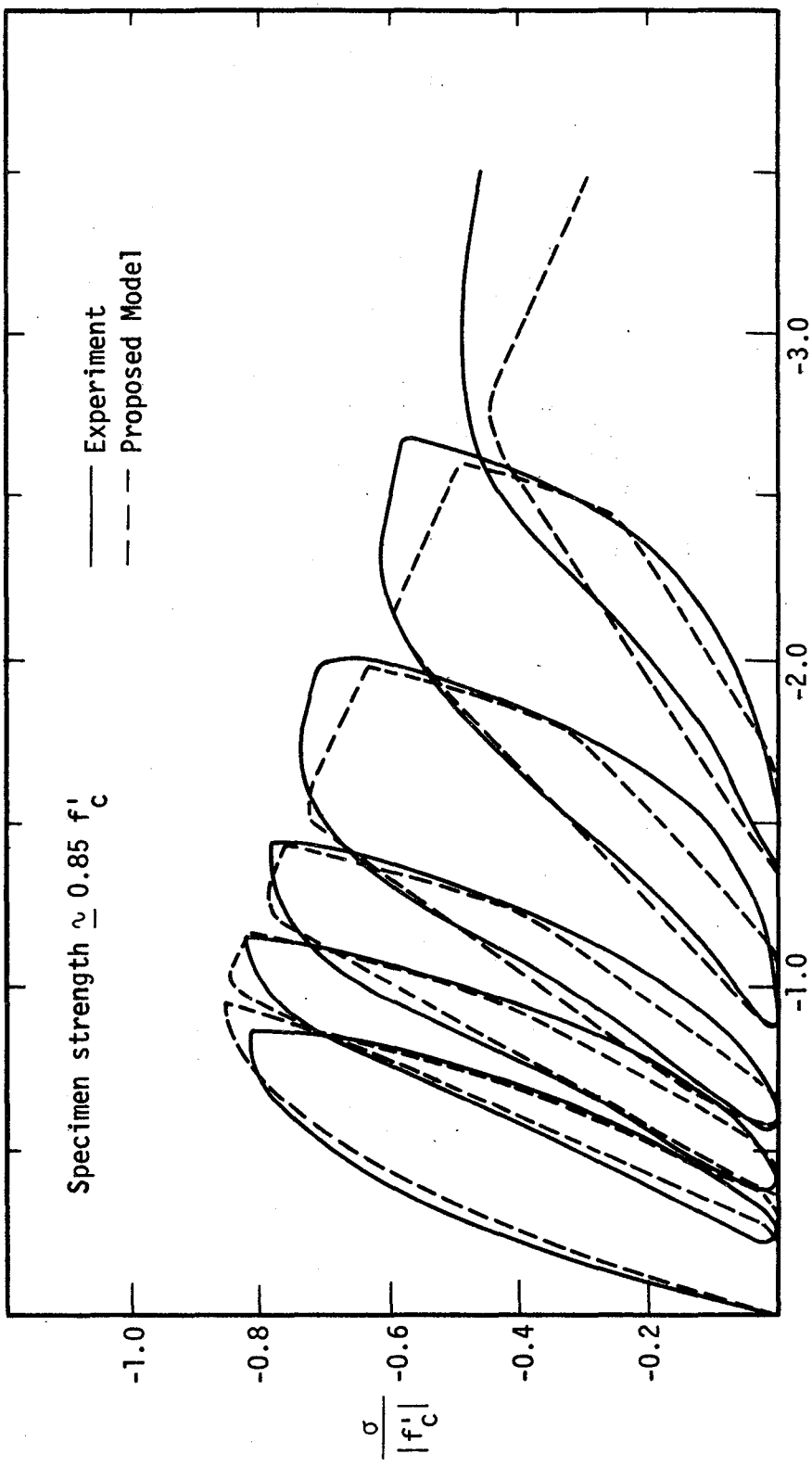

Fig. 2.7 Comparison of Proposed Hysteresis Model for Concrete with Experiment, Specimen AC2-09 (Ref. 12)

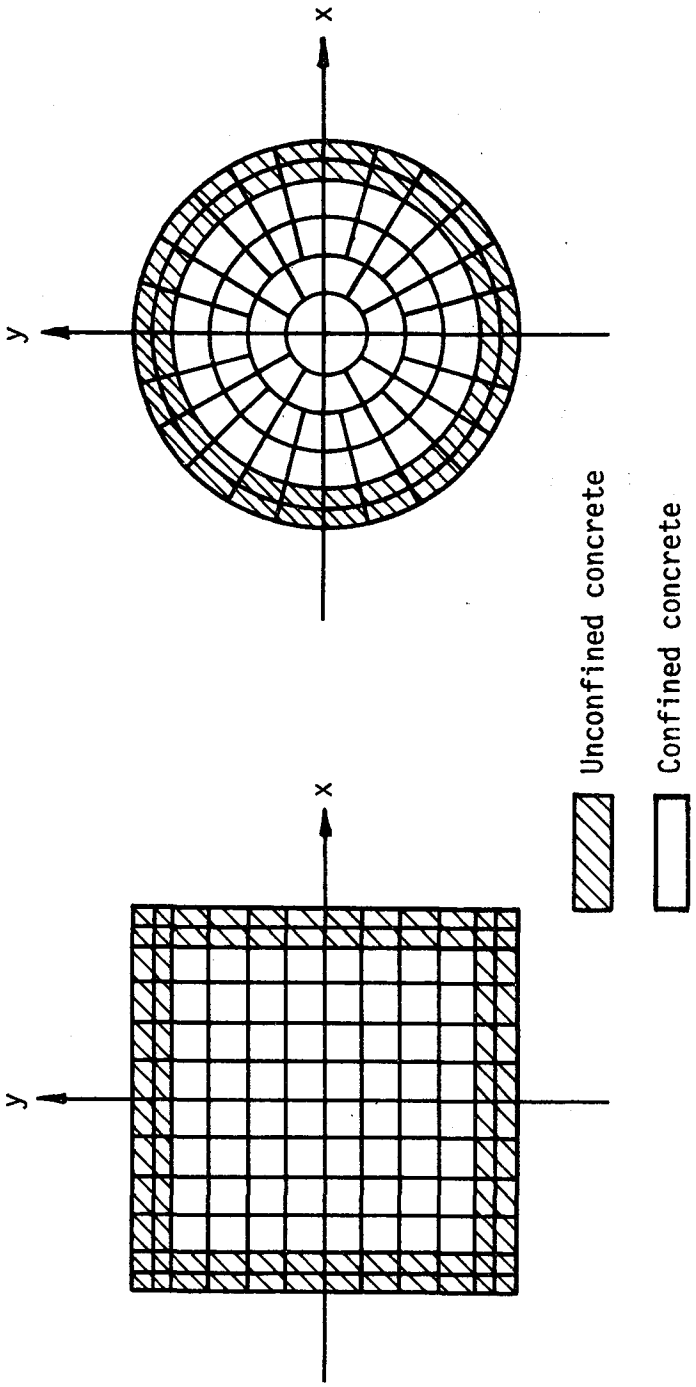

Fig. 2.8 Discretization of Concrete Area for 'Exact' Integration

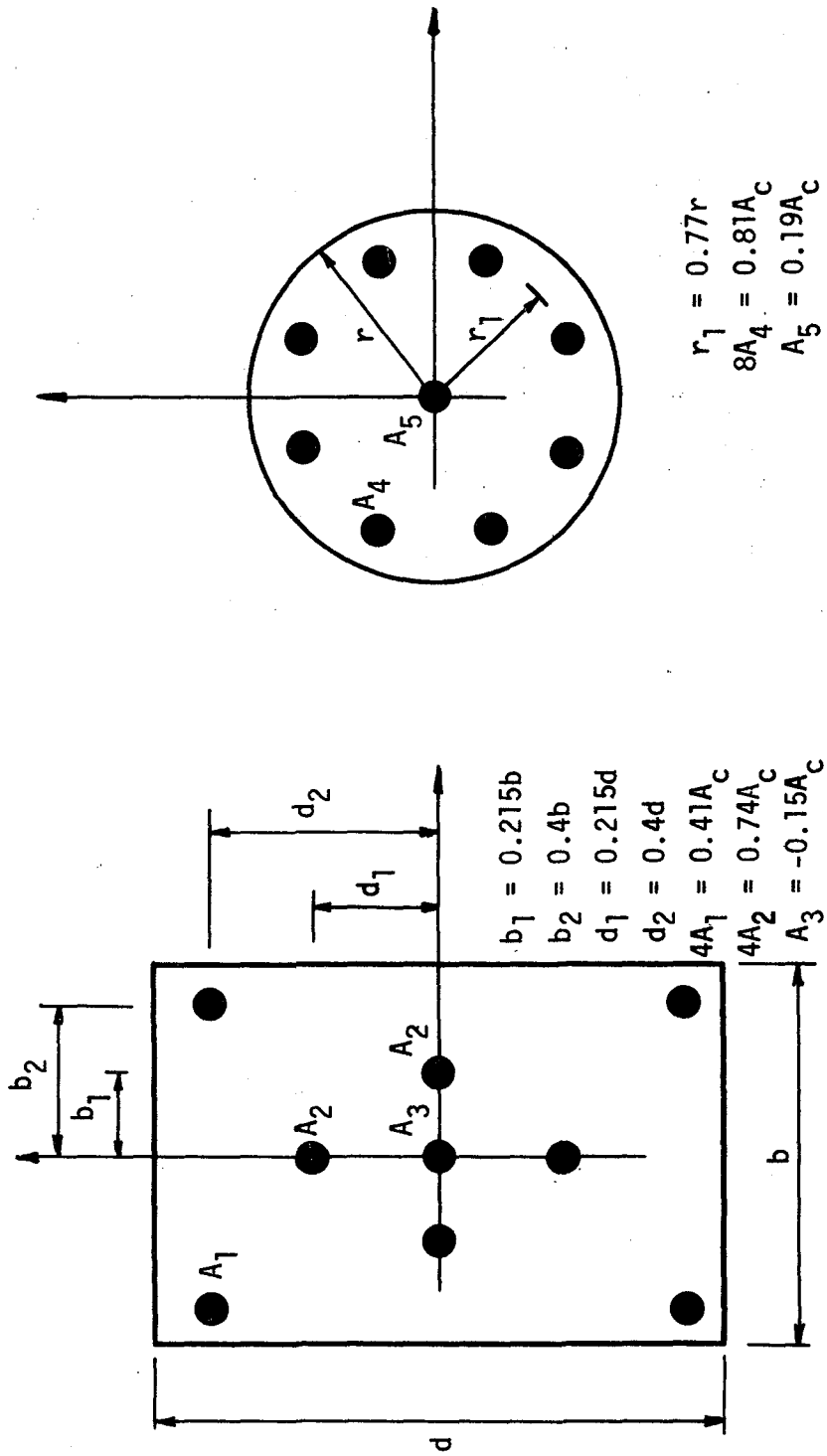

Fig. 2.9 Discretization of Concrete Area for 'Proposed' Integration

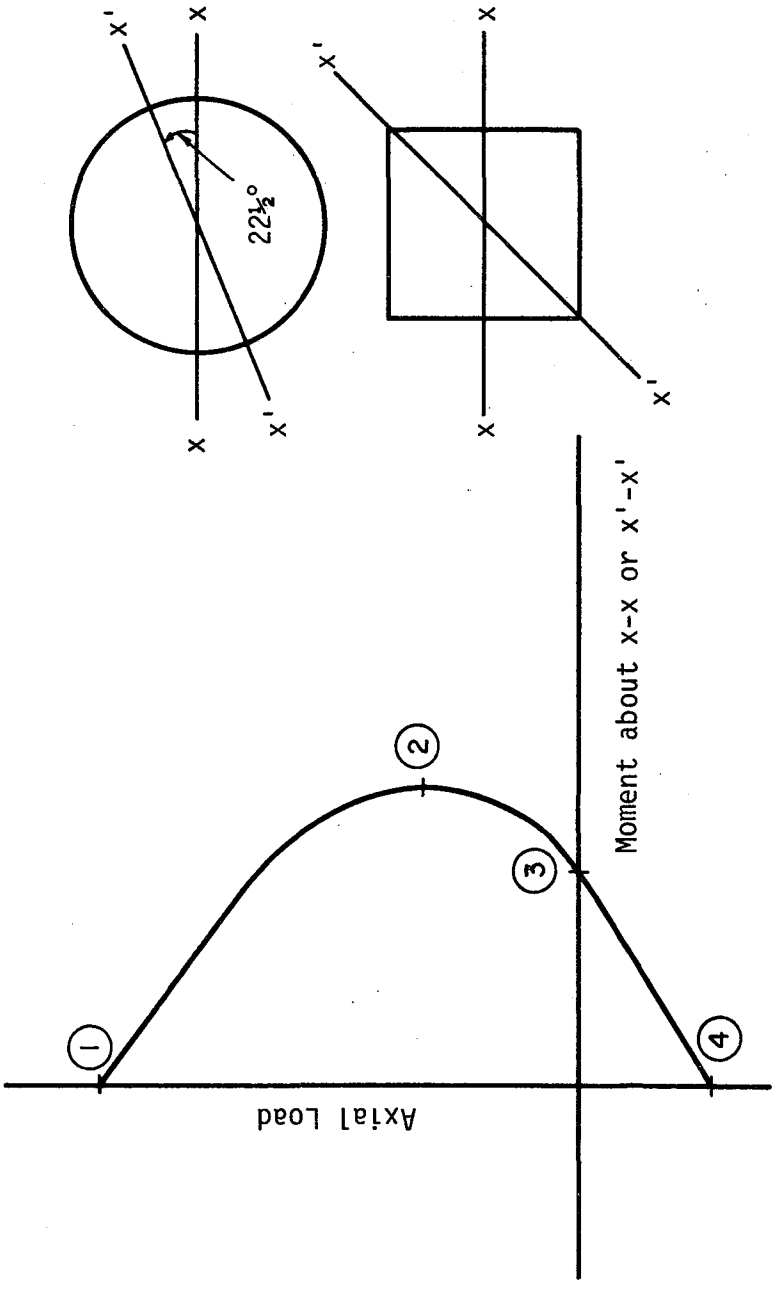

Fig. 2.10 Points on Axial Load-Moment Interaction Diagram Matched to Obtain Areas and Locations of Lumped Concrete for Proposed Integration Scheme

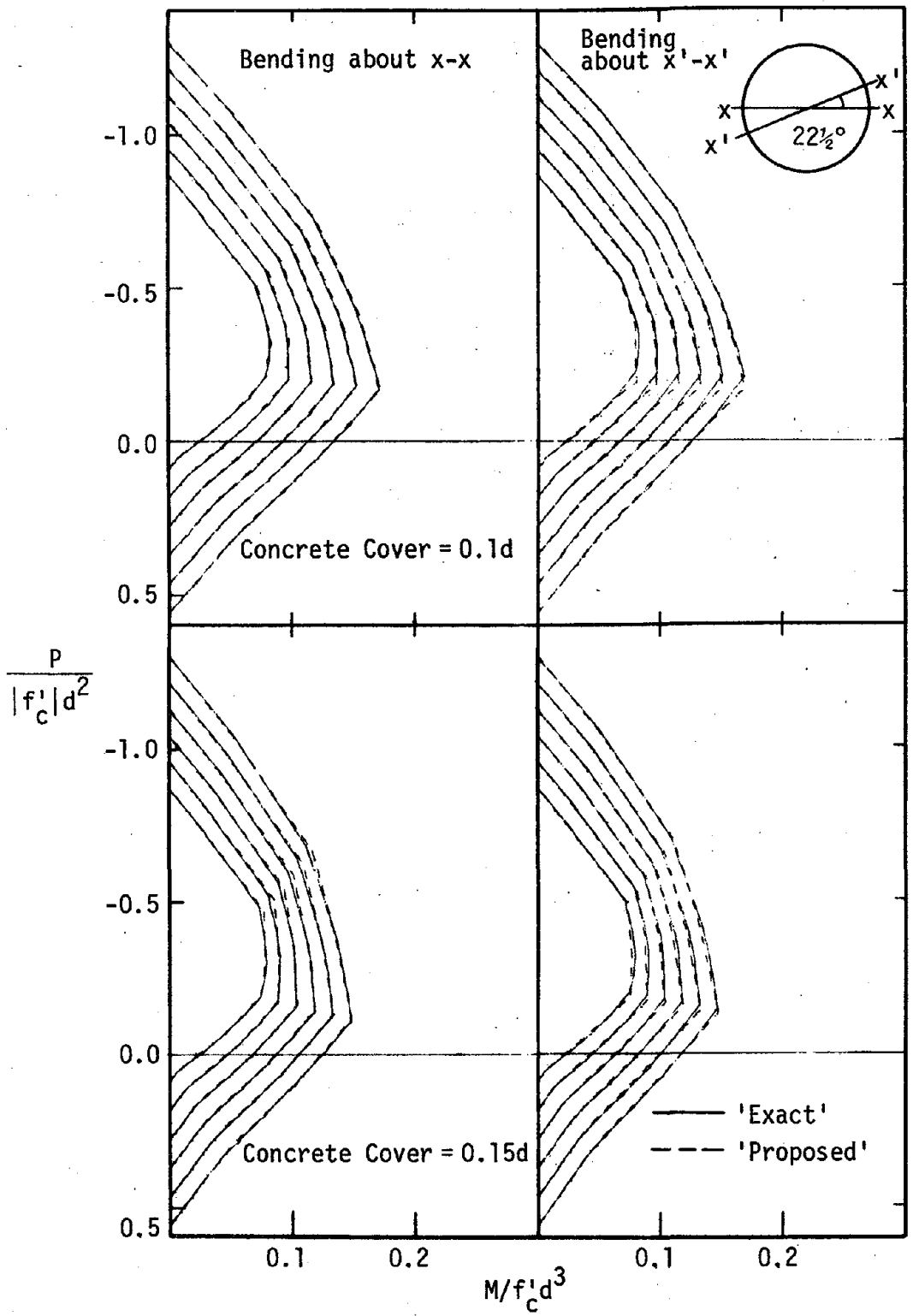

Fig. 2.11 Comparison of 'Exact' and 'Proposed' Integration, Circular Column, Axial Load-Moment Interaction, for Steel Ratios of 1, 2, 3, 4, 5 and 6%

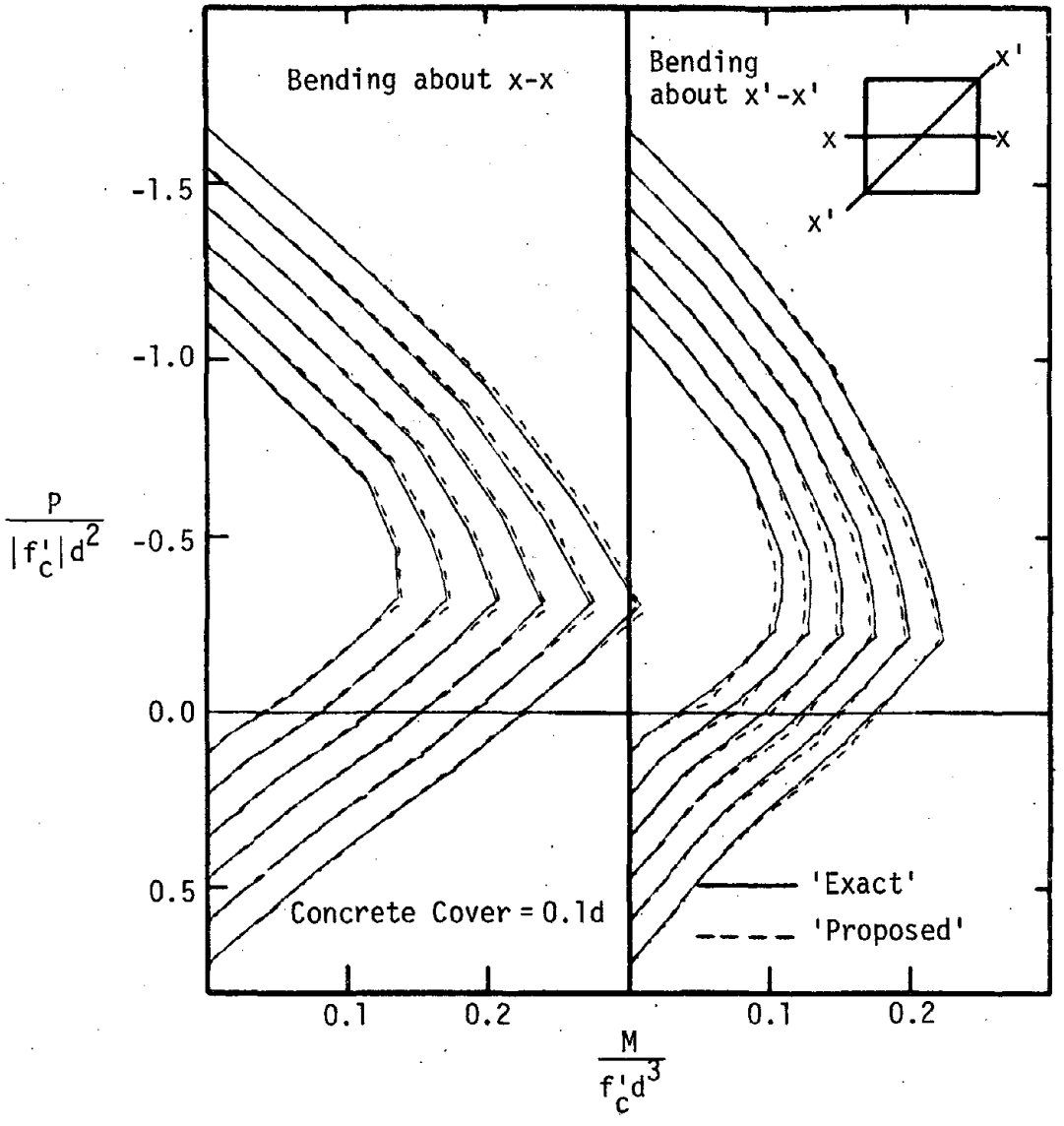

Fig. 2.12 Comparison of 'Exact' and 'Proposed' Integration, Square Column, Axial Load-Moment Interaction, for Steel Ratios of 1, 2, 3, 4, 5 and 6%

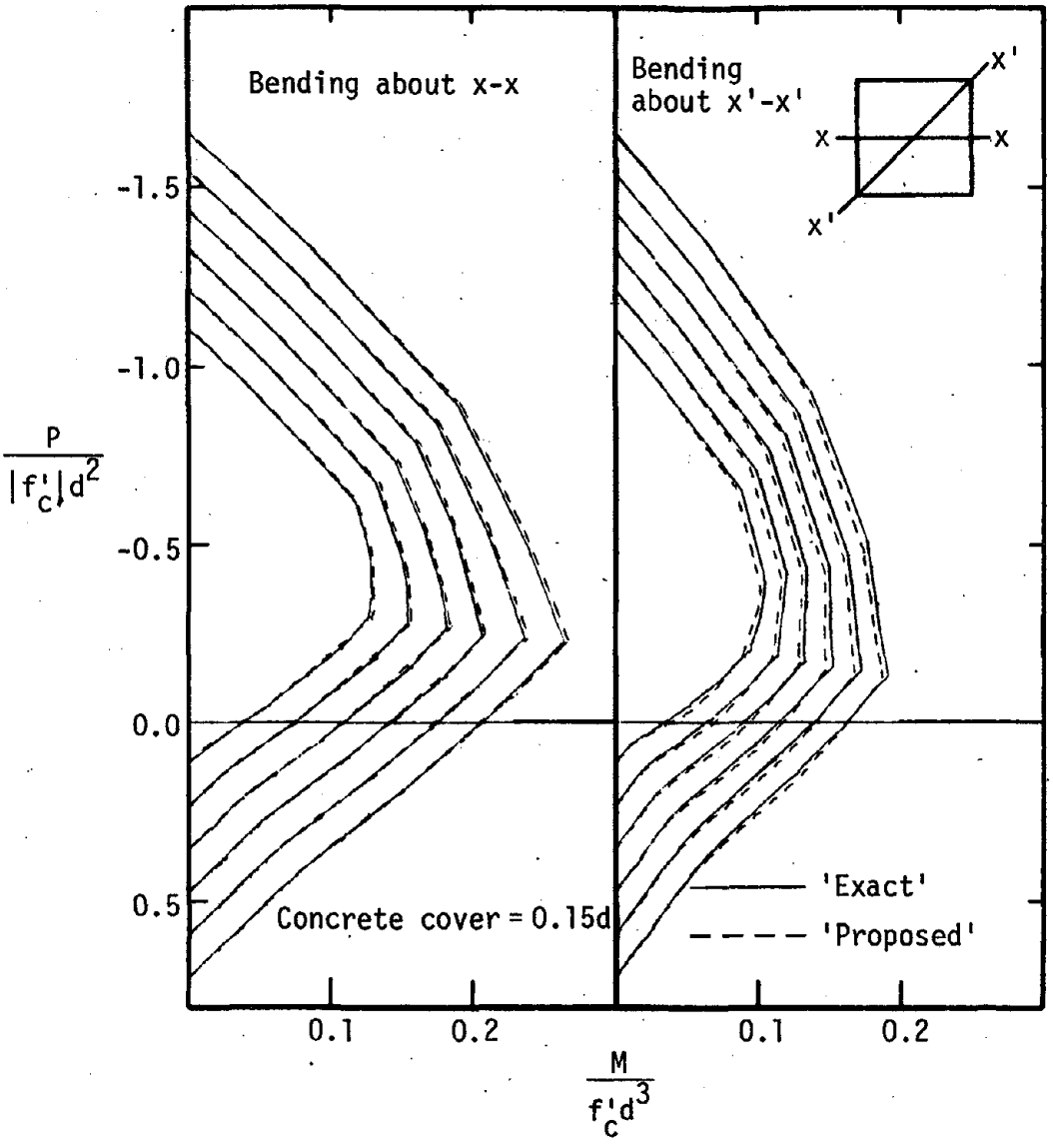

Fig. 2.12 (Continued)

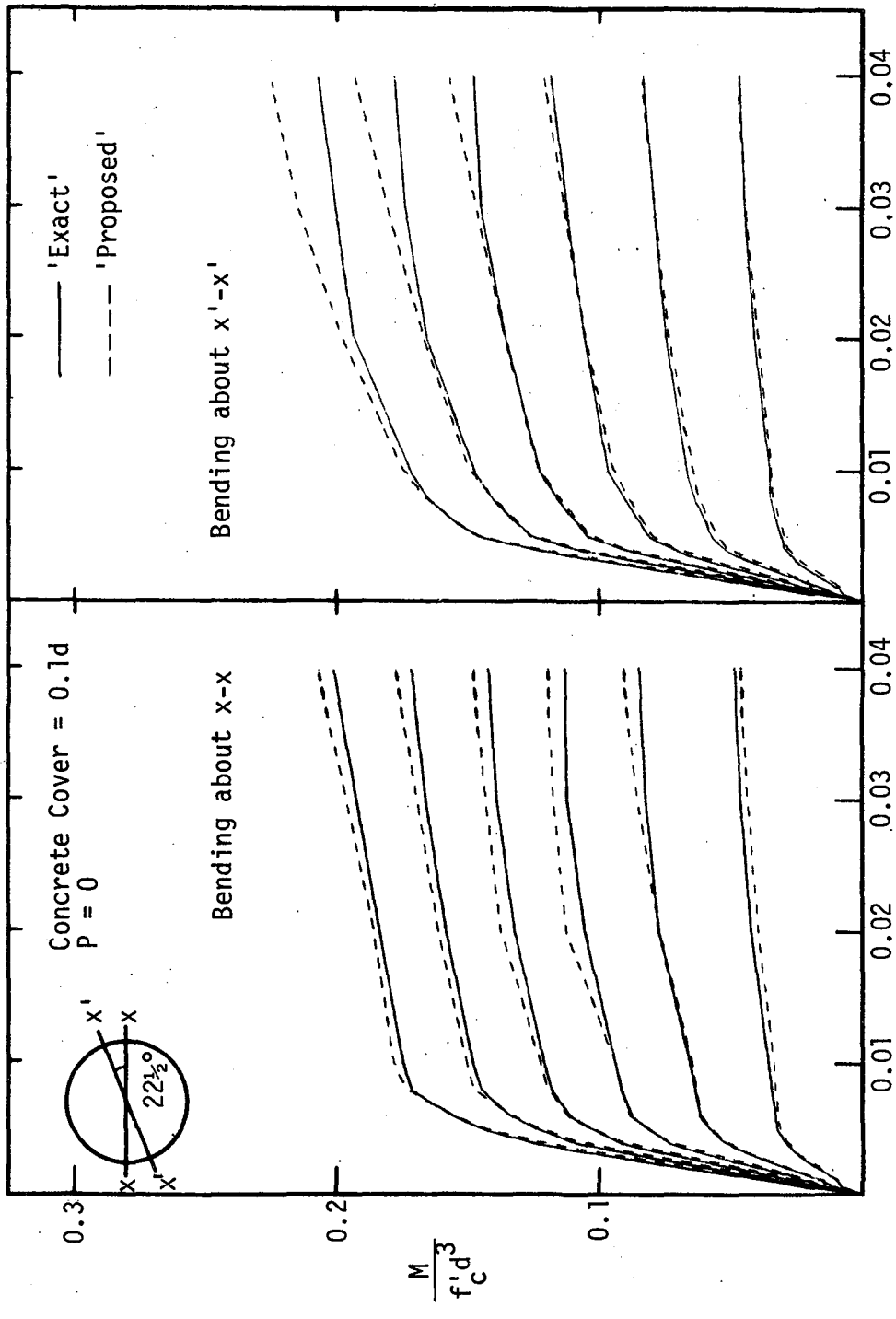

Fig. 2.13 Comparison of 'Exact' and 'Proposed' Integration, Circular Column, Moment–Curvature Relationship, for Steel Ratios of 1, 2, 3, 4, 5 and 6%

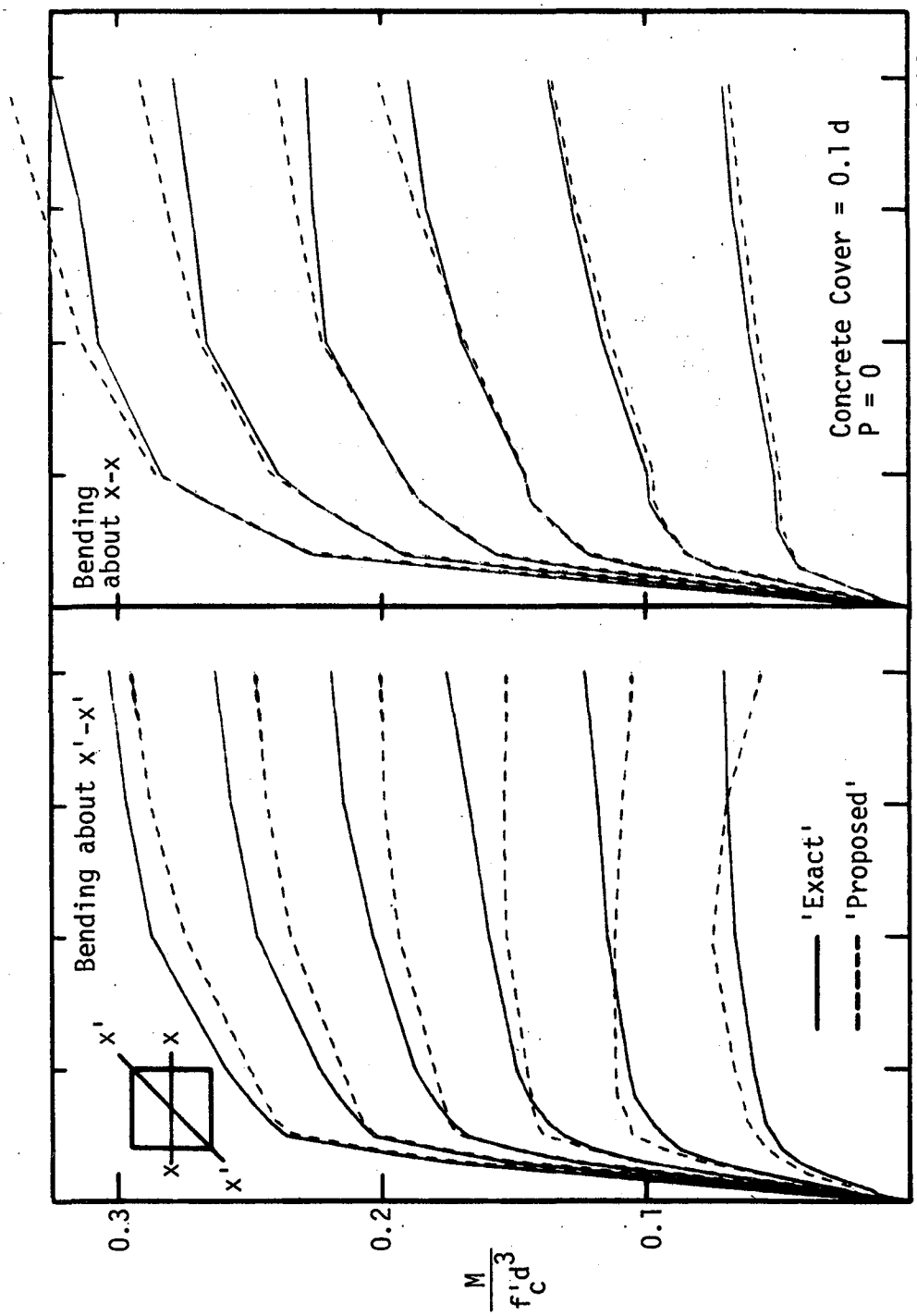

Fig. 2.14 Comparison of 'Exact' and 'Proposed' Integration, Square Column, Moment-Curvature Relationship, for Steel Ratios of 1, 2, 3, 4, 5 and 6%

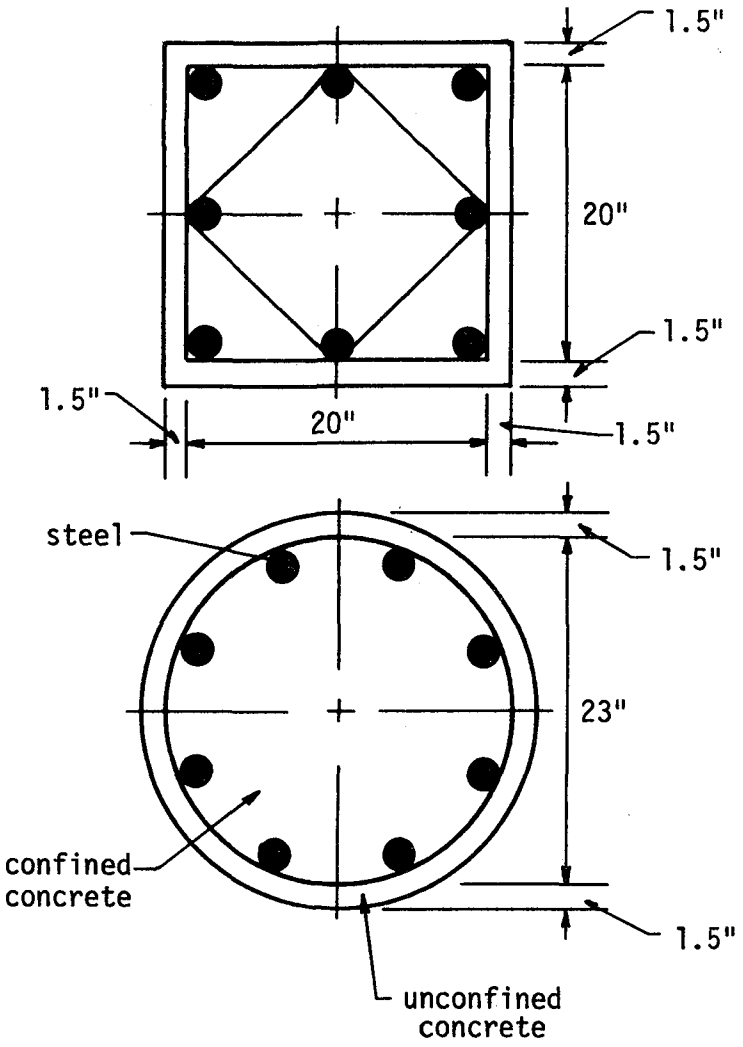

Height of Columns = 168"

Concrete:

σ_o = -5 ksi

ε_o = -0.0025

σ_t = 0.45 ksi

Longitudinal Steel:

8 #14 bars

σ_y = 60 ksi

Transverse Steel:

Circular Column 1/2" spiral @ 2 1/2"

Square Column 1/2" ties @ 2 1/2"

Fig. 2.15 Test Columns Used for Analytical Cyclic Response Study

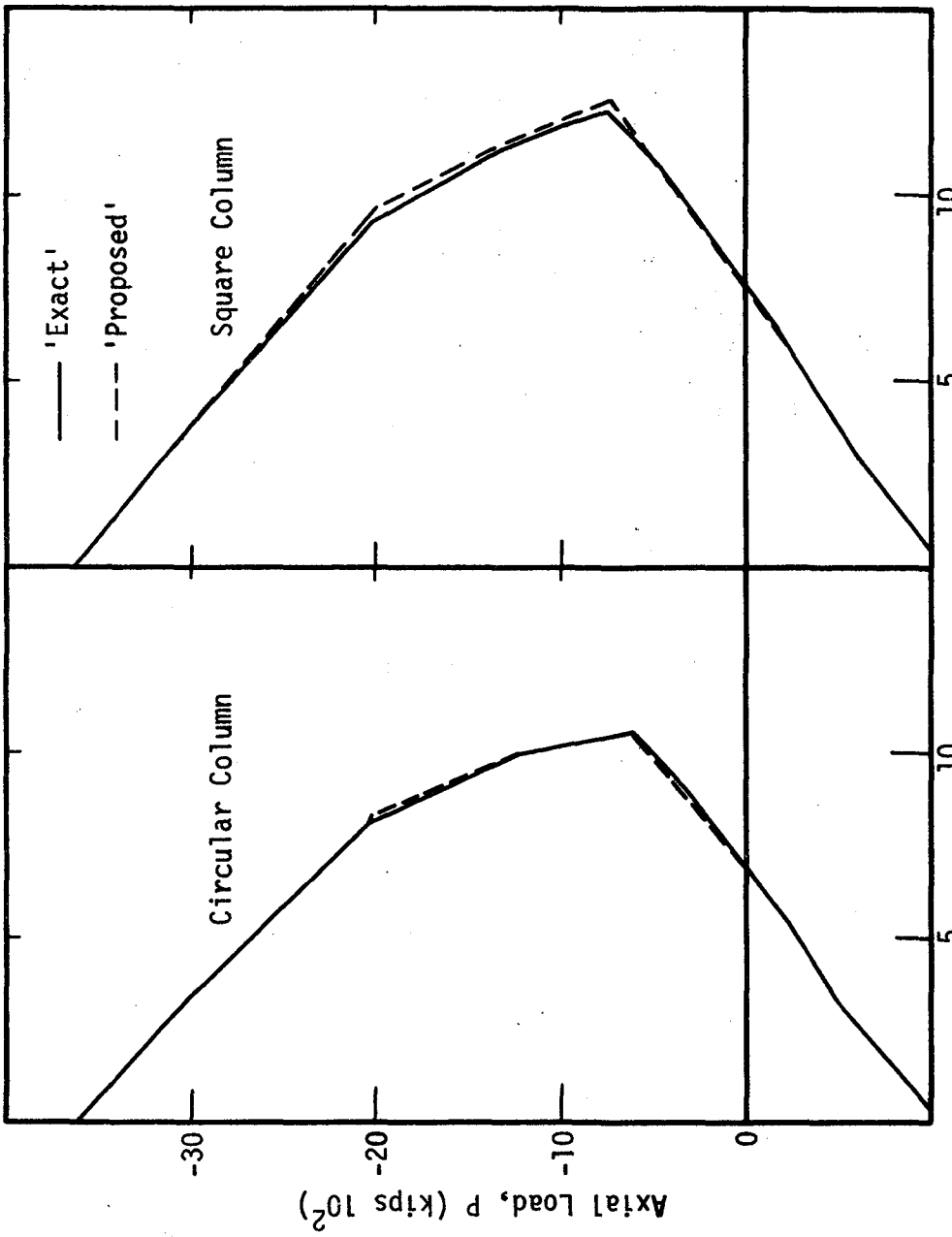

Fig. 2.16 Comparison of 'Exact' and 'Proposed' Integration, Test Columns, Axial Load-Moment Interaction

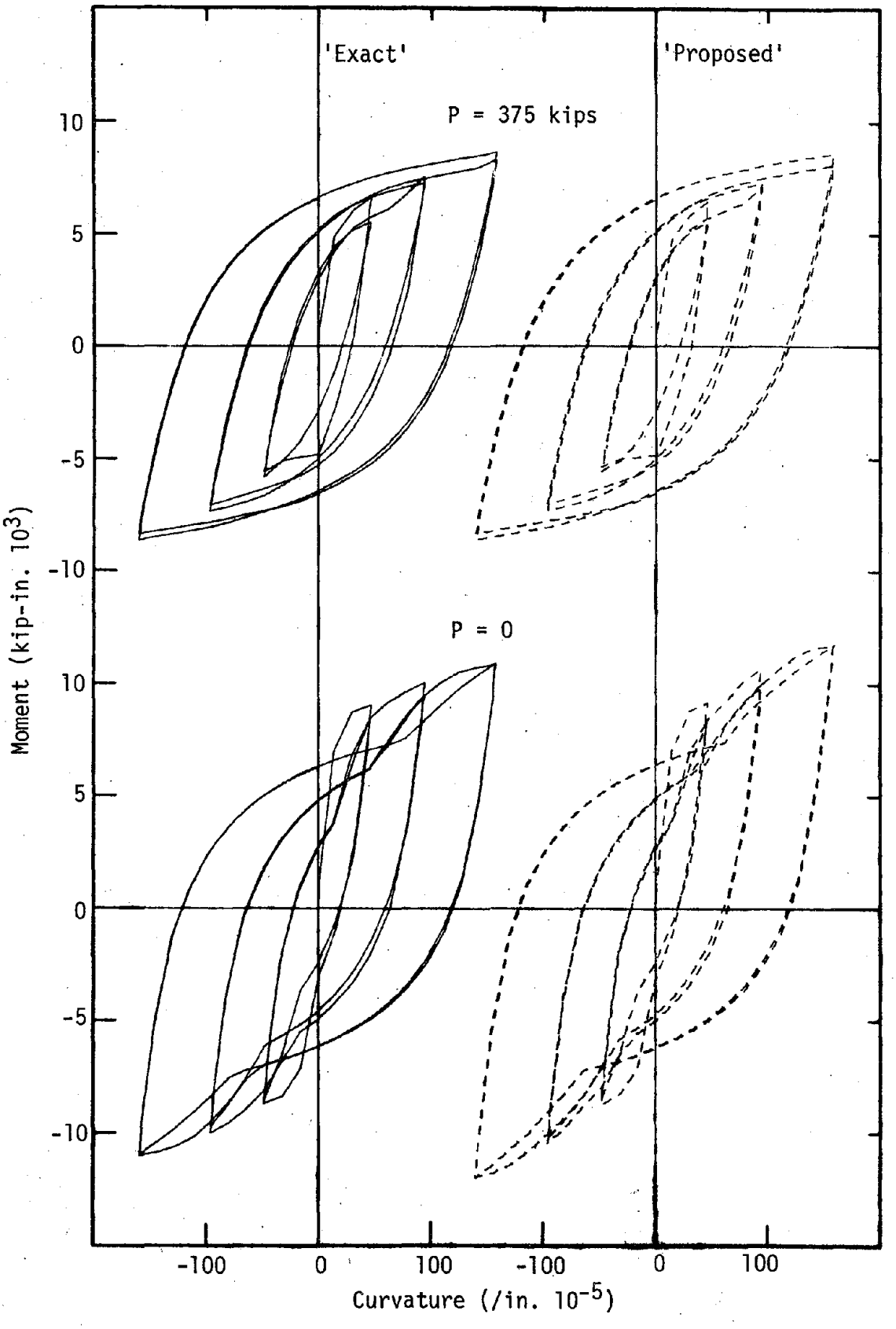

Fig. 2.17 Comparison of 'Exact' and 'Proposed' Integration, Circular Test Column, Moment-Curvature Relationship, Cyclic Loading

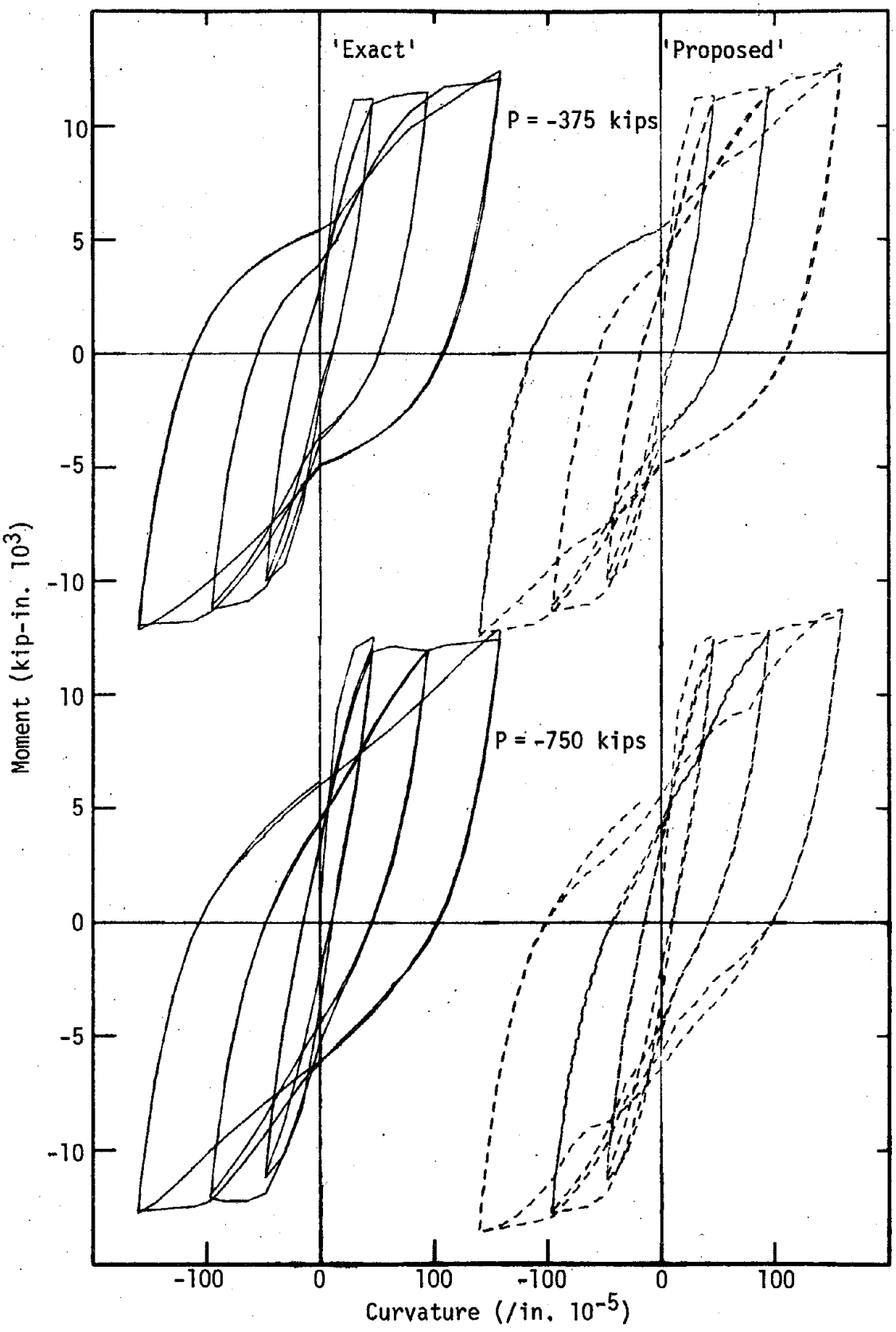

Fig. 2.17 (Continued)

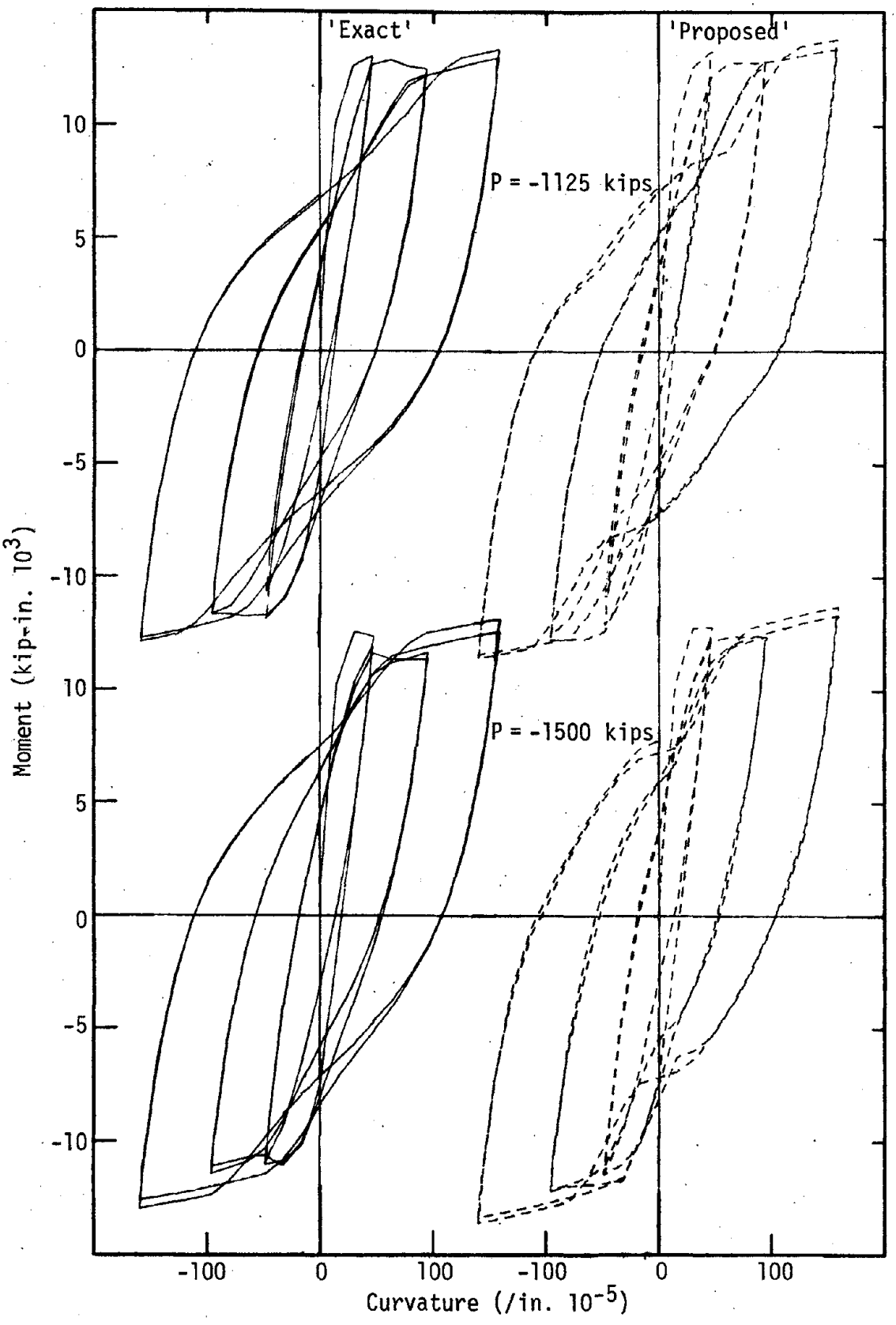

Fig. 2.17 (Continued)

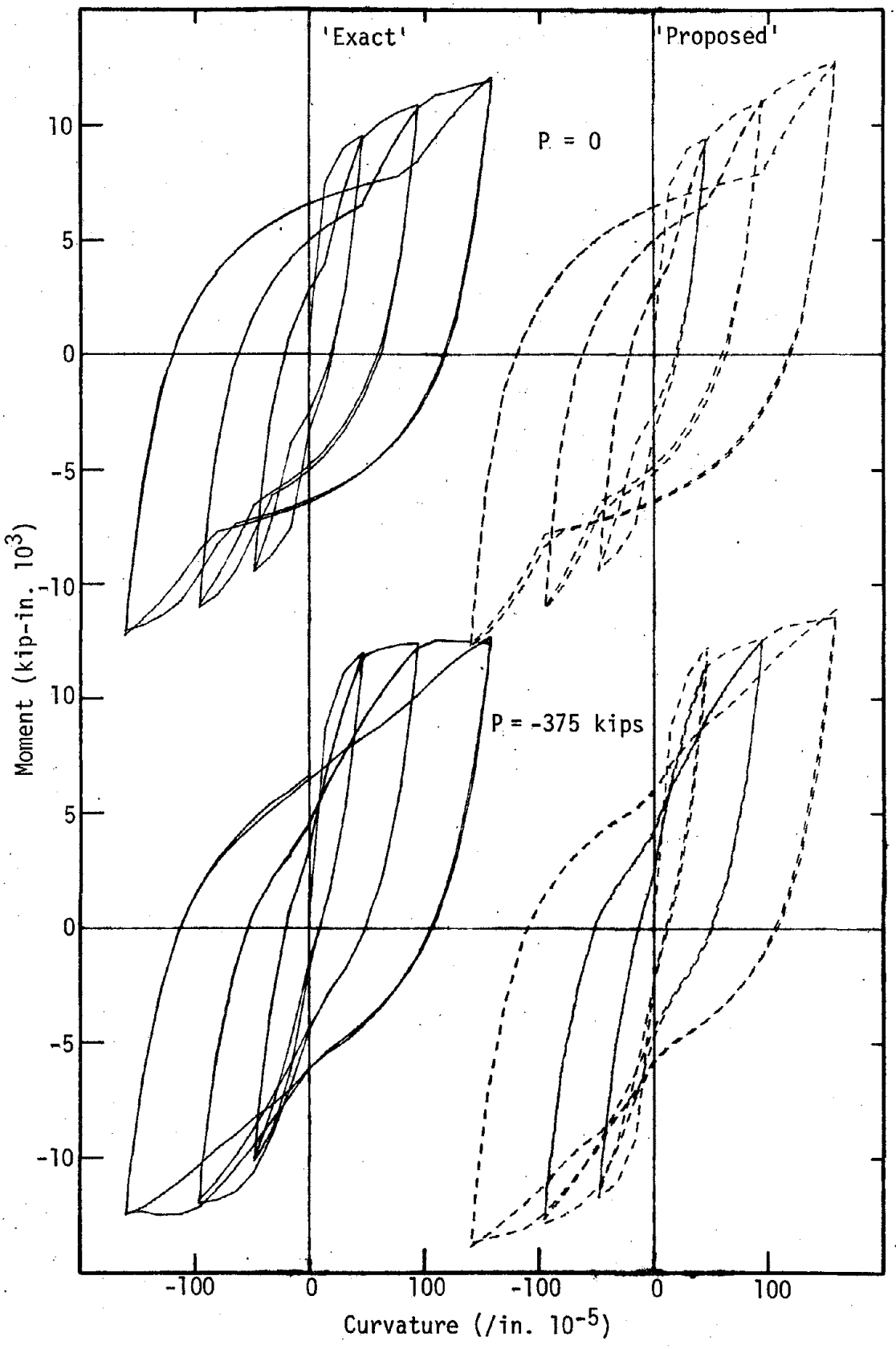

Fig. 2.18 Comparison of 'Exact' and 'Proposed' Integration, Square Test Column, Moment-Curvature Relationship, Cyclic Loading

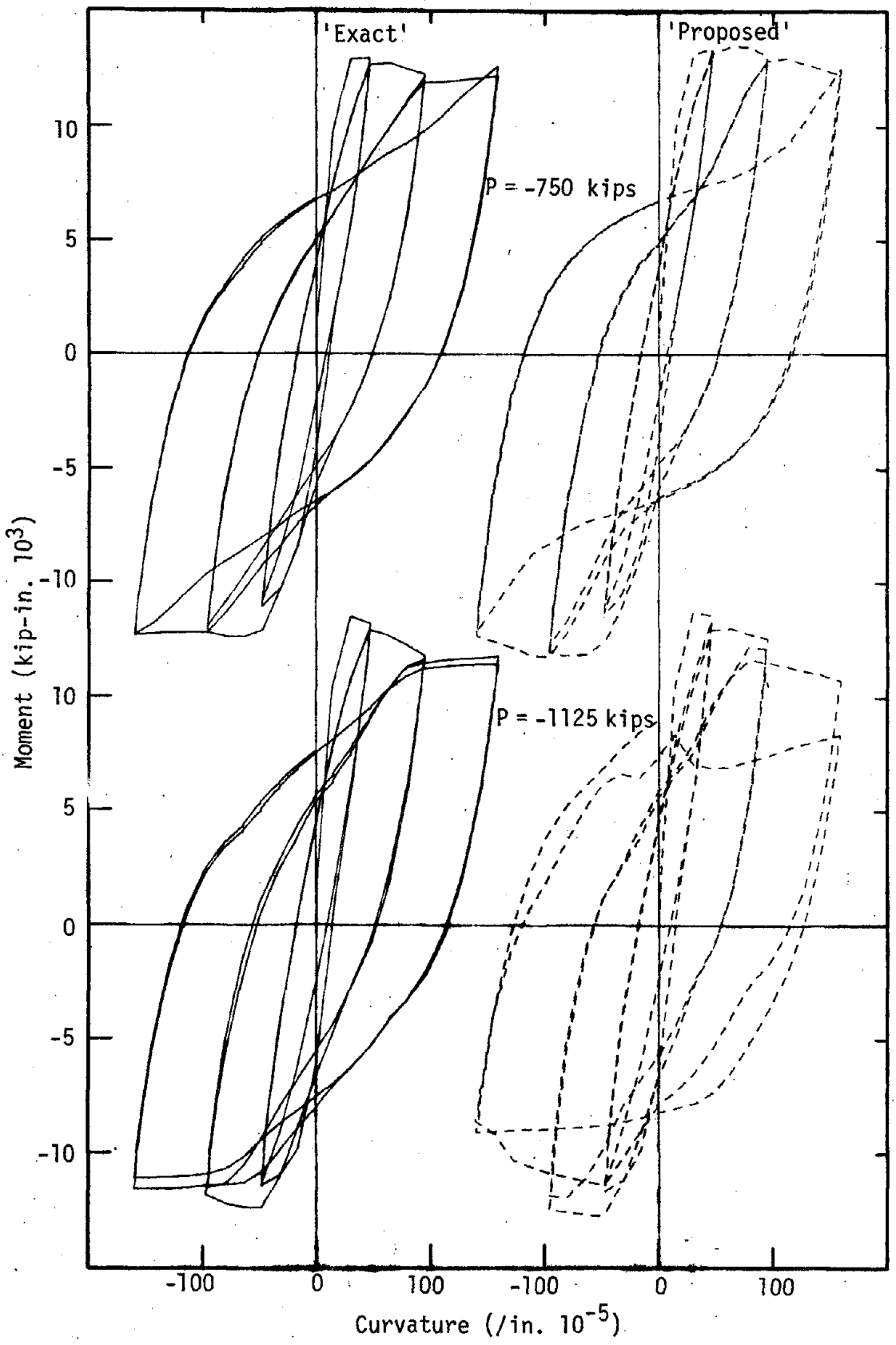

Fig. 2.18 (Continued)

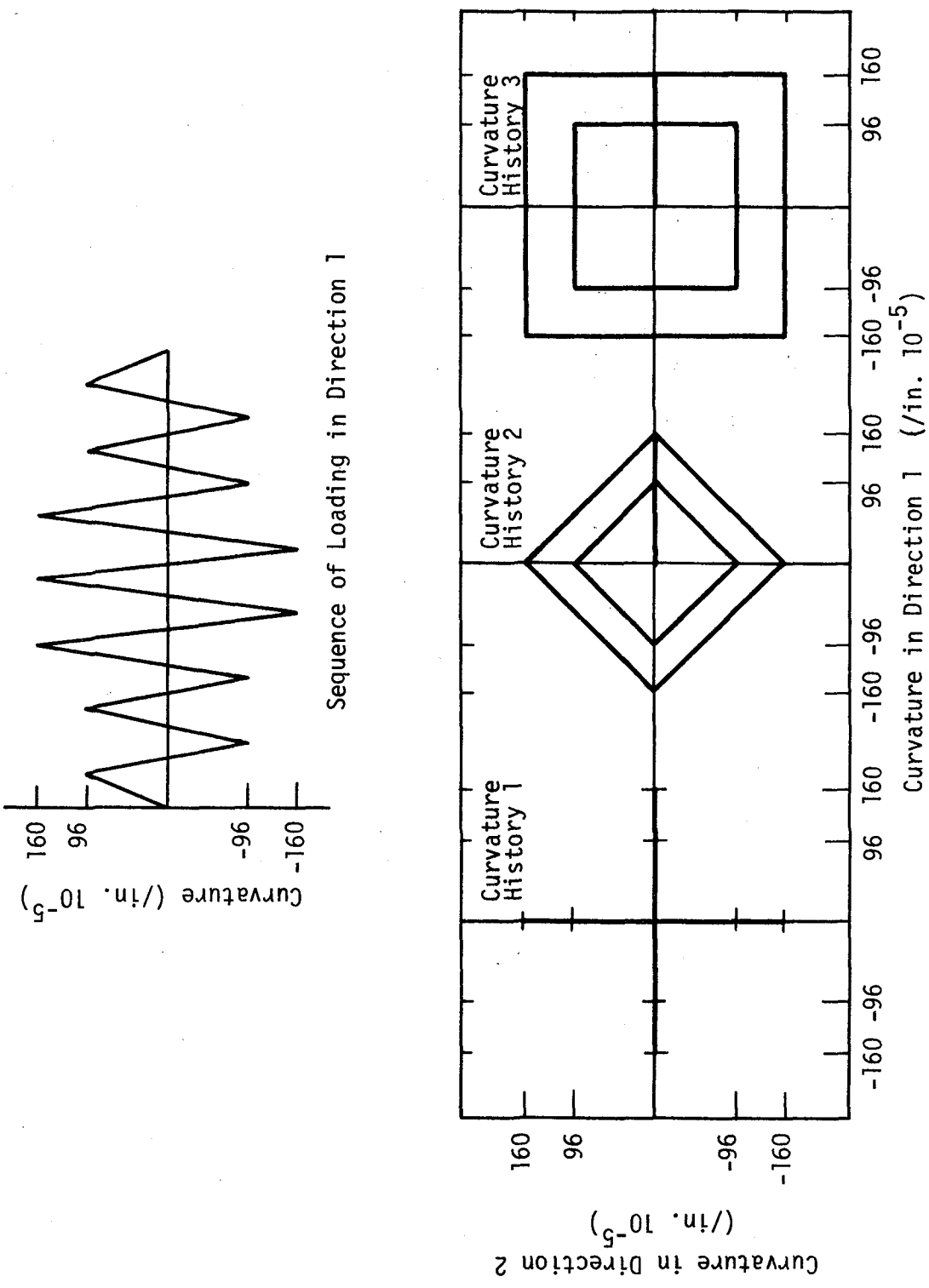

Fig. 2.19 Two-Dimensional Curvature Histories Used to Compare 'Exact' and 'Proposed' Integration in Calculating Moment-Curvature Relationships

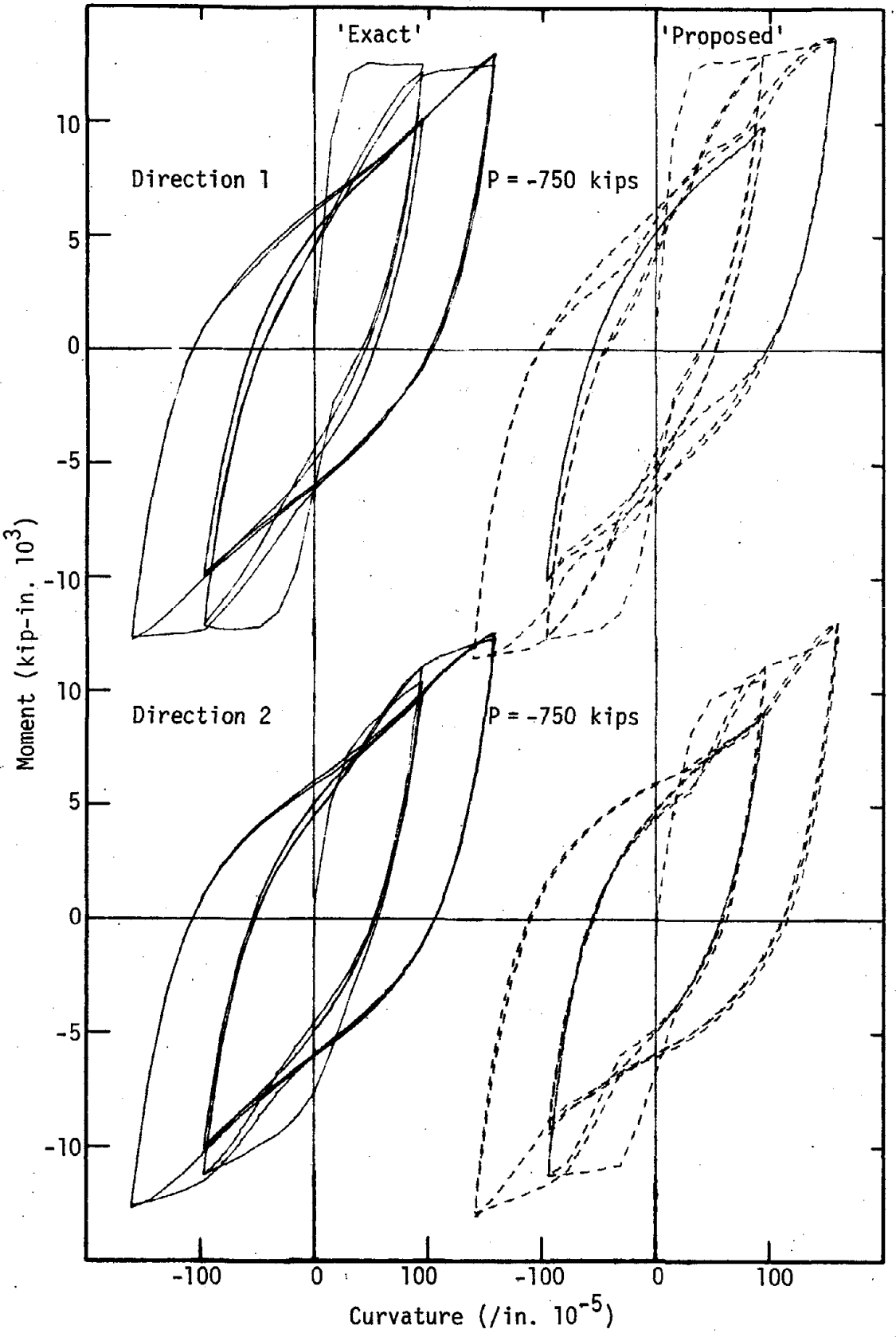

Fig. 2.20 Comparison of 'Exact' and 'Proposed' Integration, Circular Test Column, Moment-Curvature Relationship, Two-Dimensional Cyclic Loading, Curvature History 1

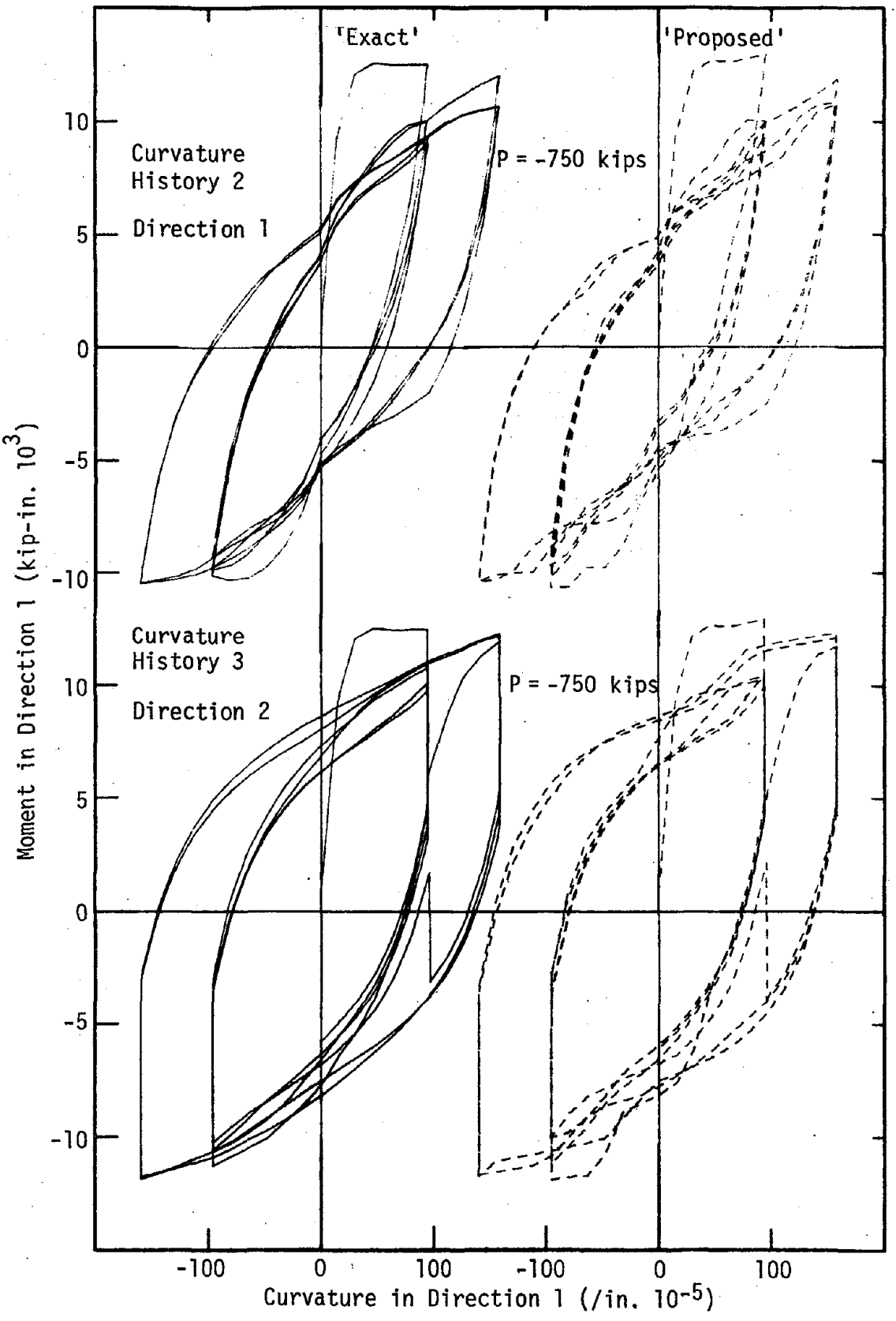

Fig. 2.21 Comparison of 'Exact' and 'Proposed' Integration, Circular Test Column, Moment-Curvature Relationship, Two-Dimensional Cyclic Loading, Curvature Histories 2 and 3

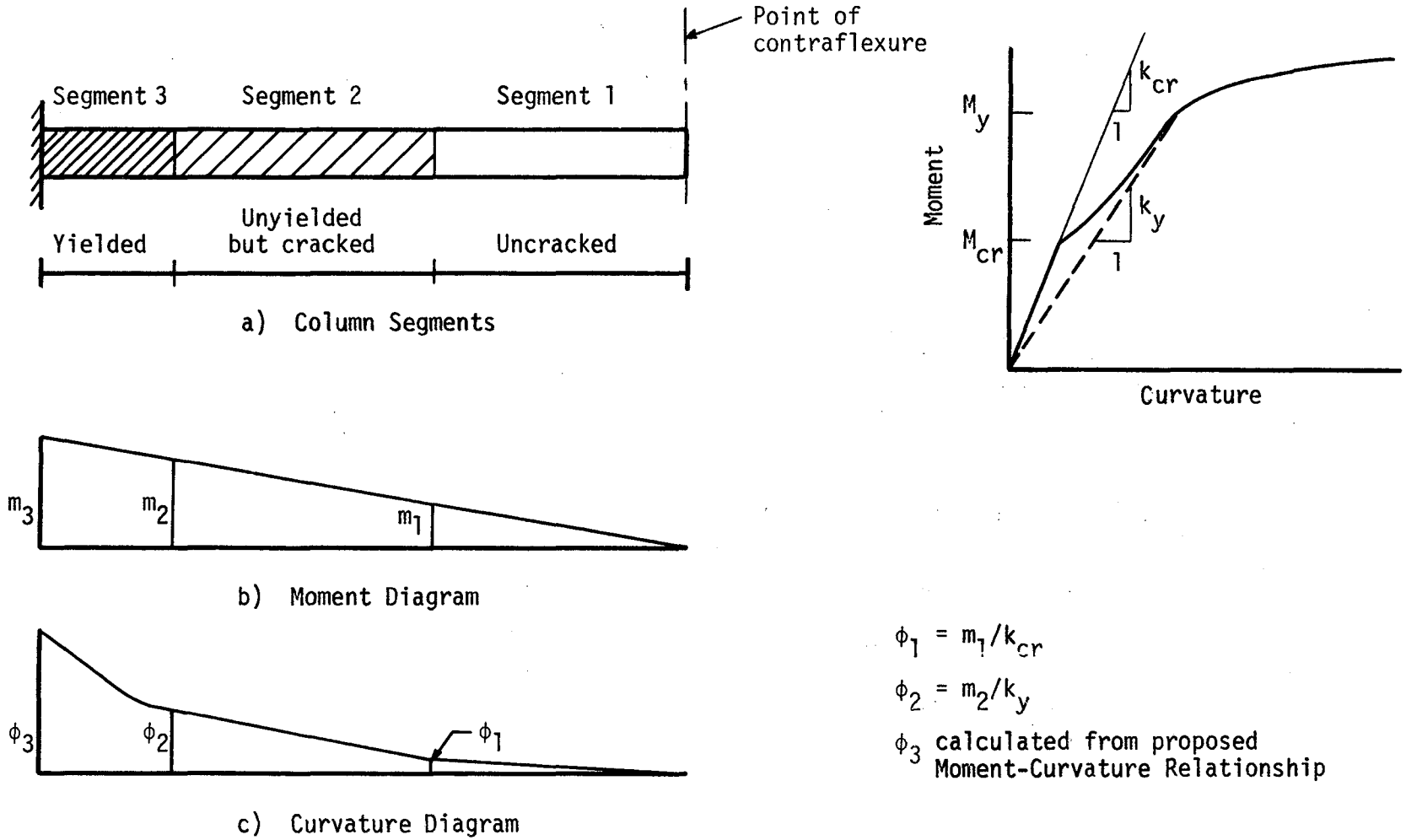

Fig. 2.22 Column Segments and Assumed Curvature Distribution Along Column

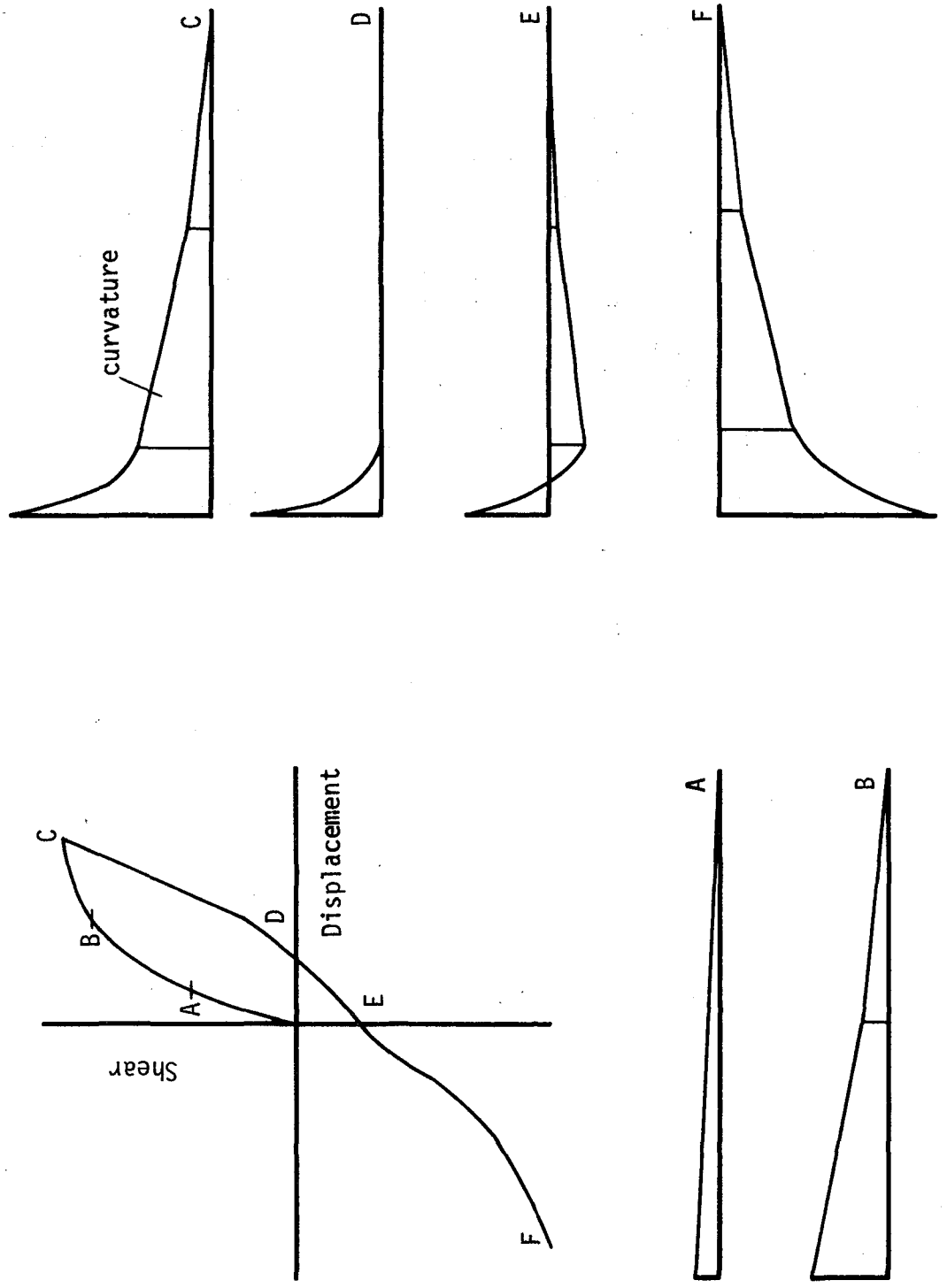

Fig. 2.23 Assumed Curvature Distribution Along Column at Different Stages of Loading

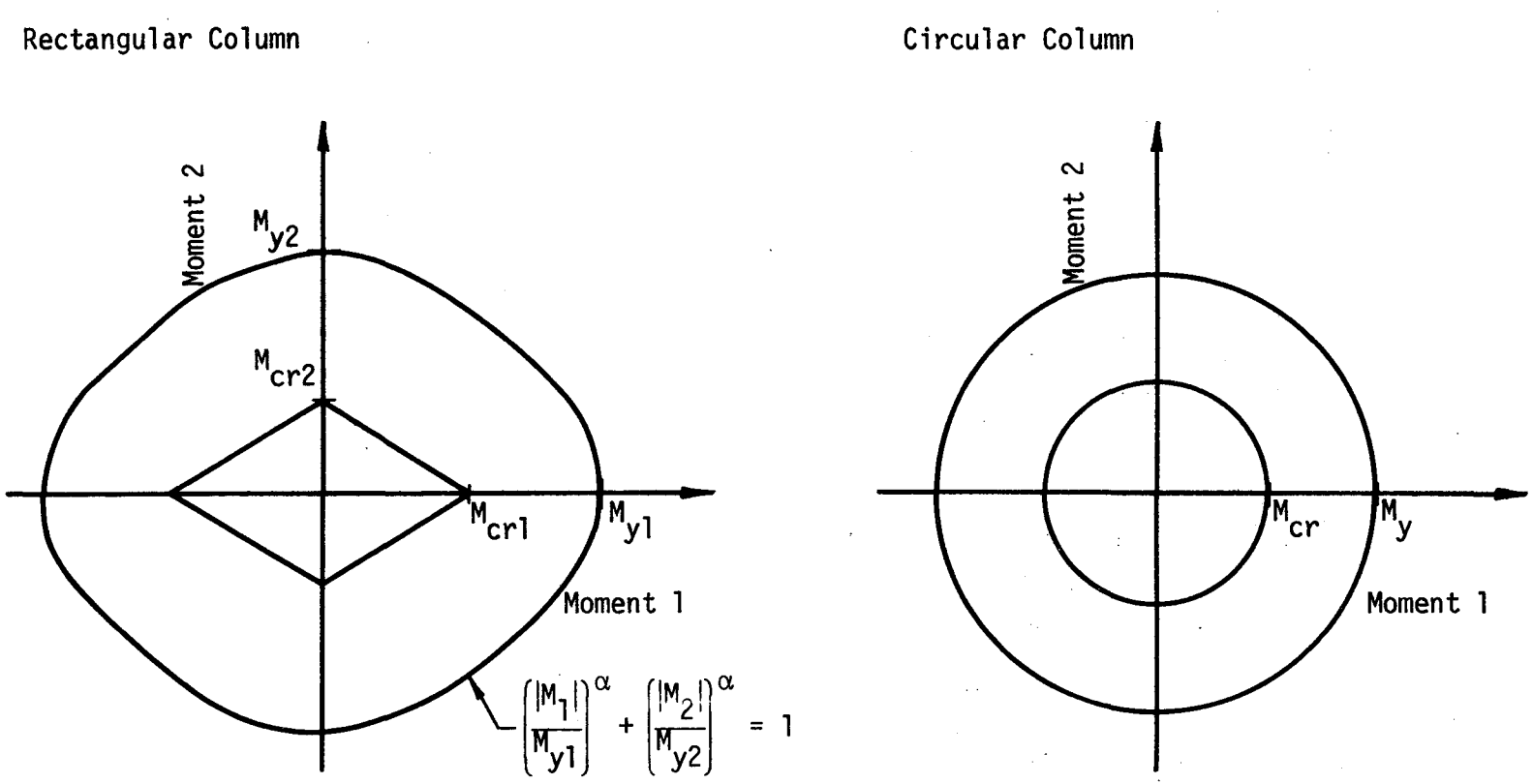

α depends on Axial Load
and varies between 1 and 2.

Fig. 2.24 Cracking and Yield Curves for Determination of Cracking or Yielding at a Section

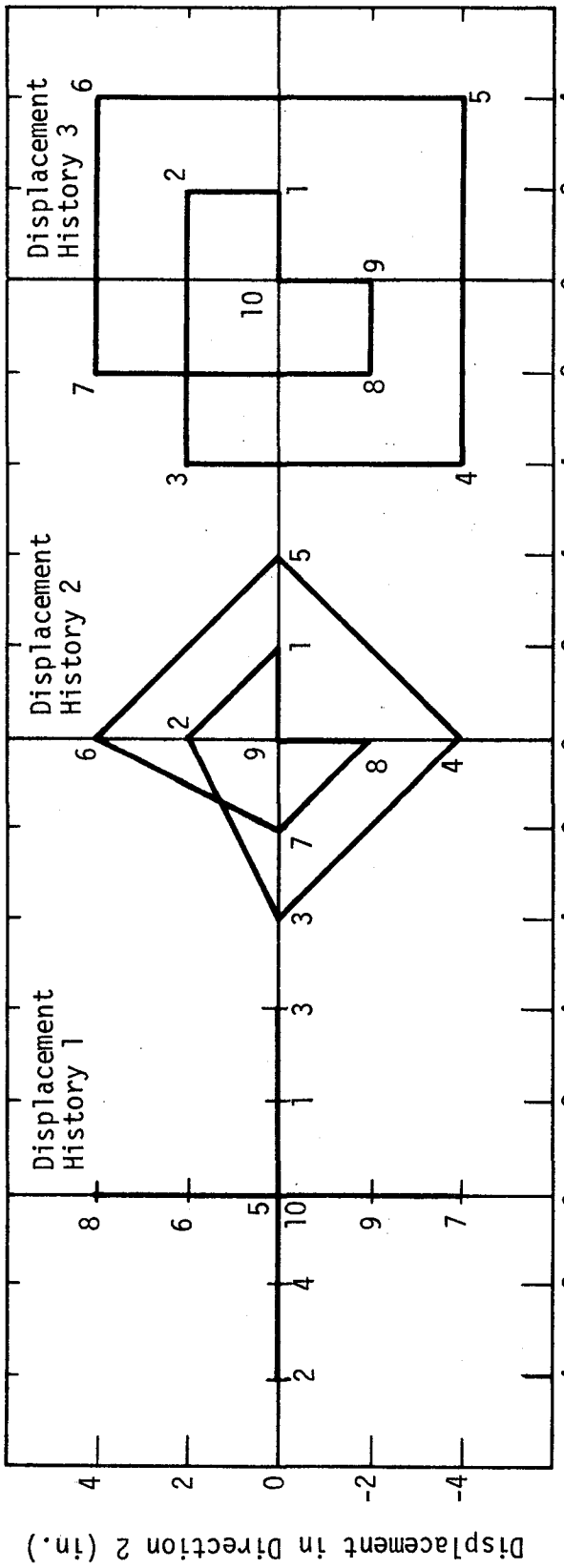

Fig. 2.25 Two-Dimensional Displacement Histories Used for Comparing Assumed and Calculated Moment-Curvature Relationships Along Column

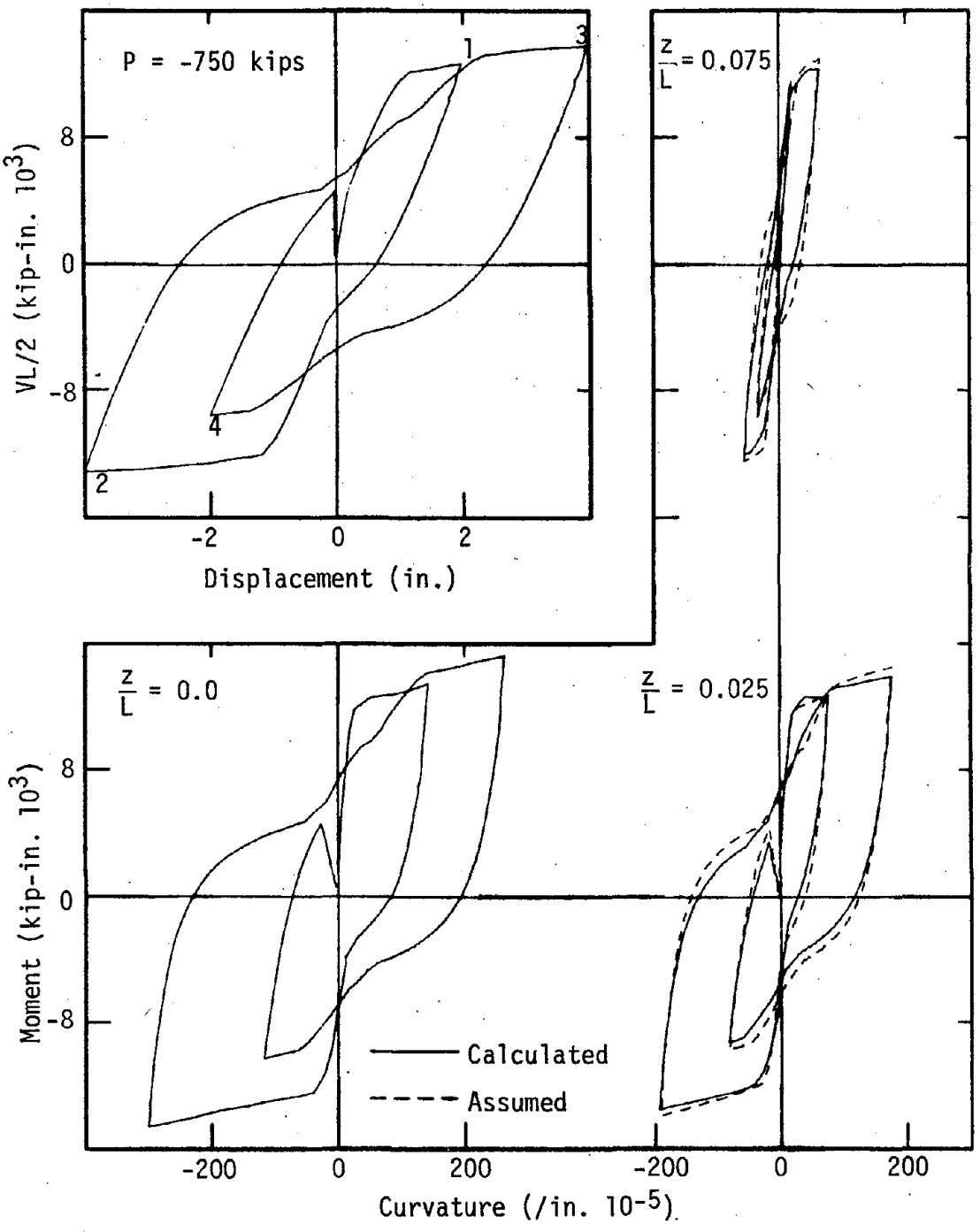

Fig. 2.26 Comparison of Assumed and Calculated Moment-Curvature Relationships Along Column Used in Deflection Calculations, Circular Column, Two-Dimensional Displacement History 1, Direction 1

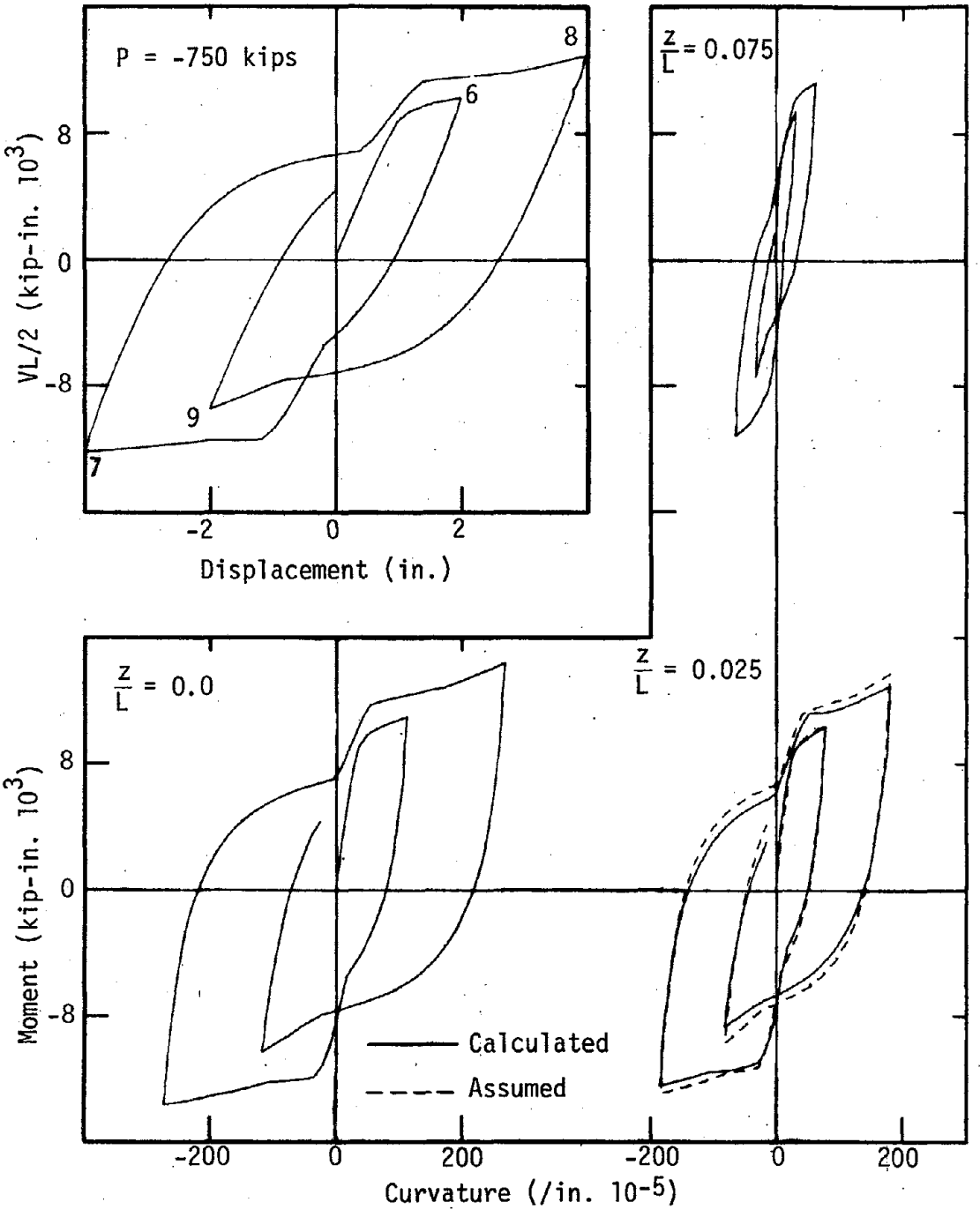

Fig. 2.27 Comparison of Assumed and Calculated Moment-Curvature Relationships Along Column Used in Deflection Calculations, Circular Column, Two-Dimensional Displacement History 1, Direction 2

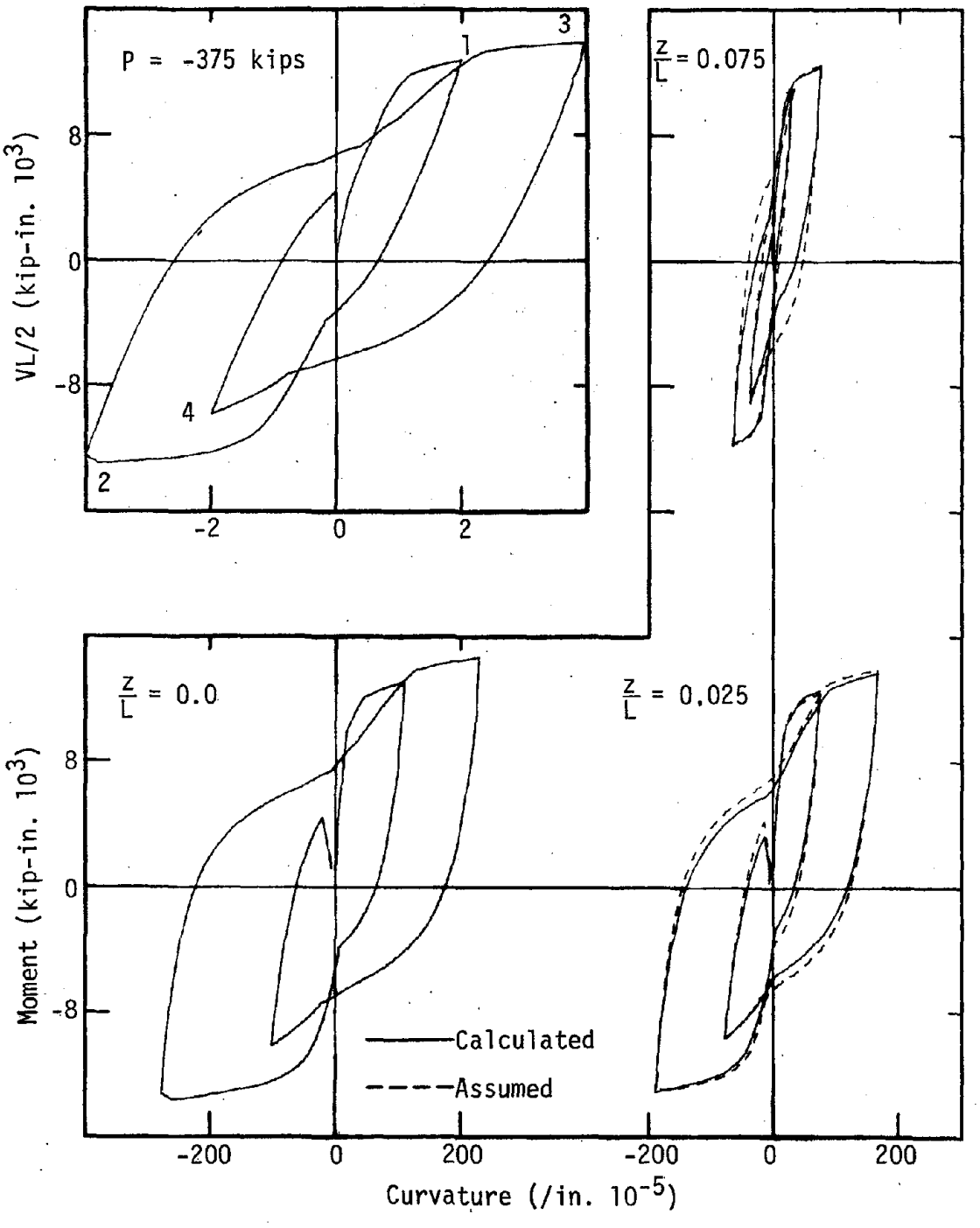

Fig. 2.28 Comparison of Assumed and Calculated Moment-Curvature Relationships Along Column Used in Deflection Calculations, Square Column, Two-Dimensional Displacement History 1, Direction 1

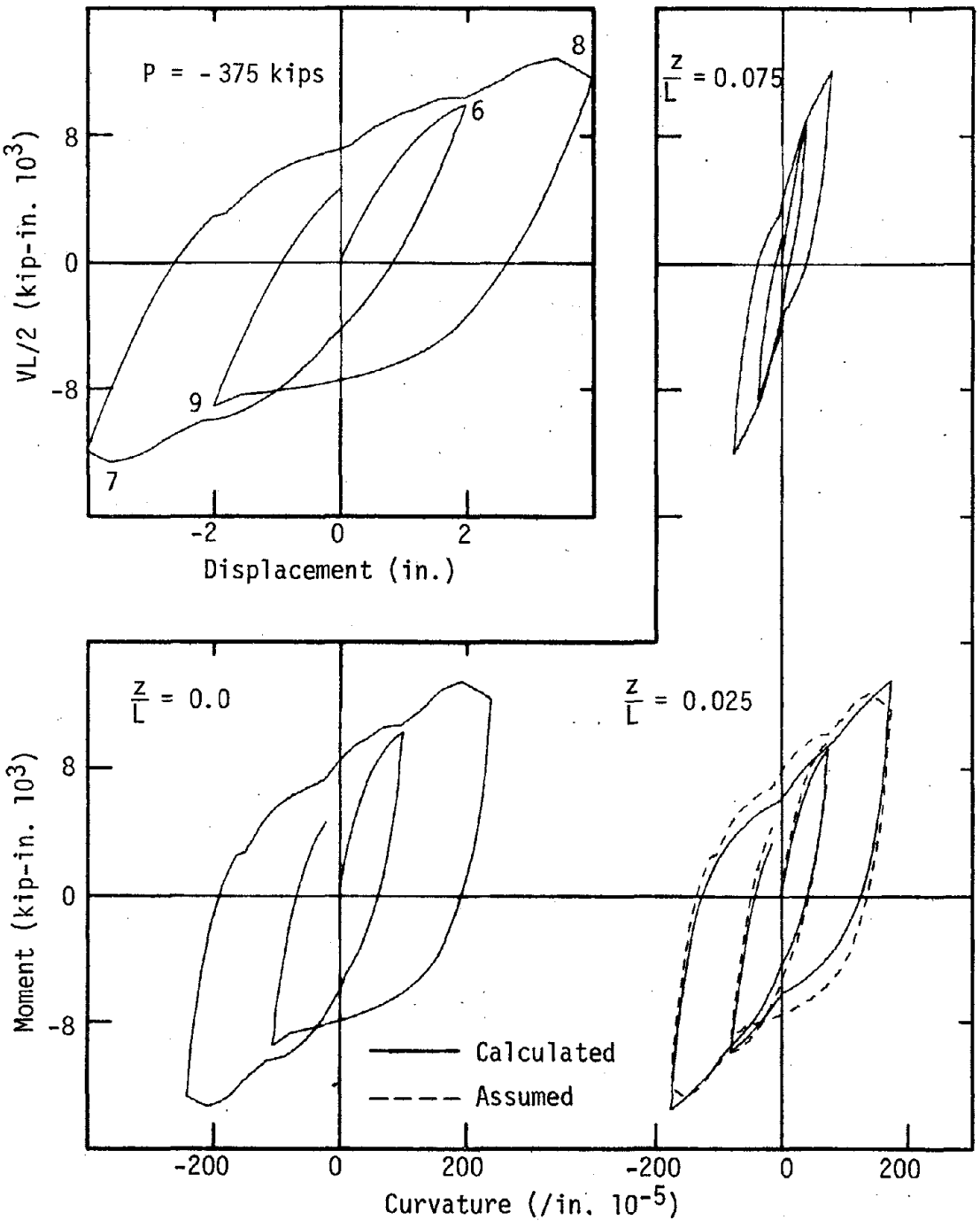

Fig. 2.29 Comparison of Assumed and Calculated Moment-Curvature Relationships Along Column Used in Deflection Calculations, Square Column, Two-Dimensional Displacement History 1, Direction 2

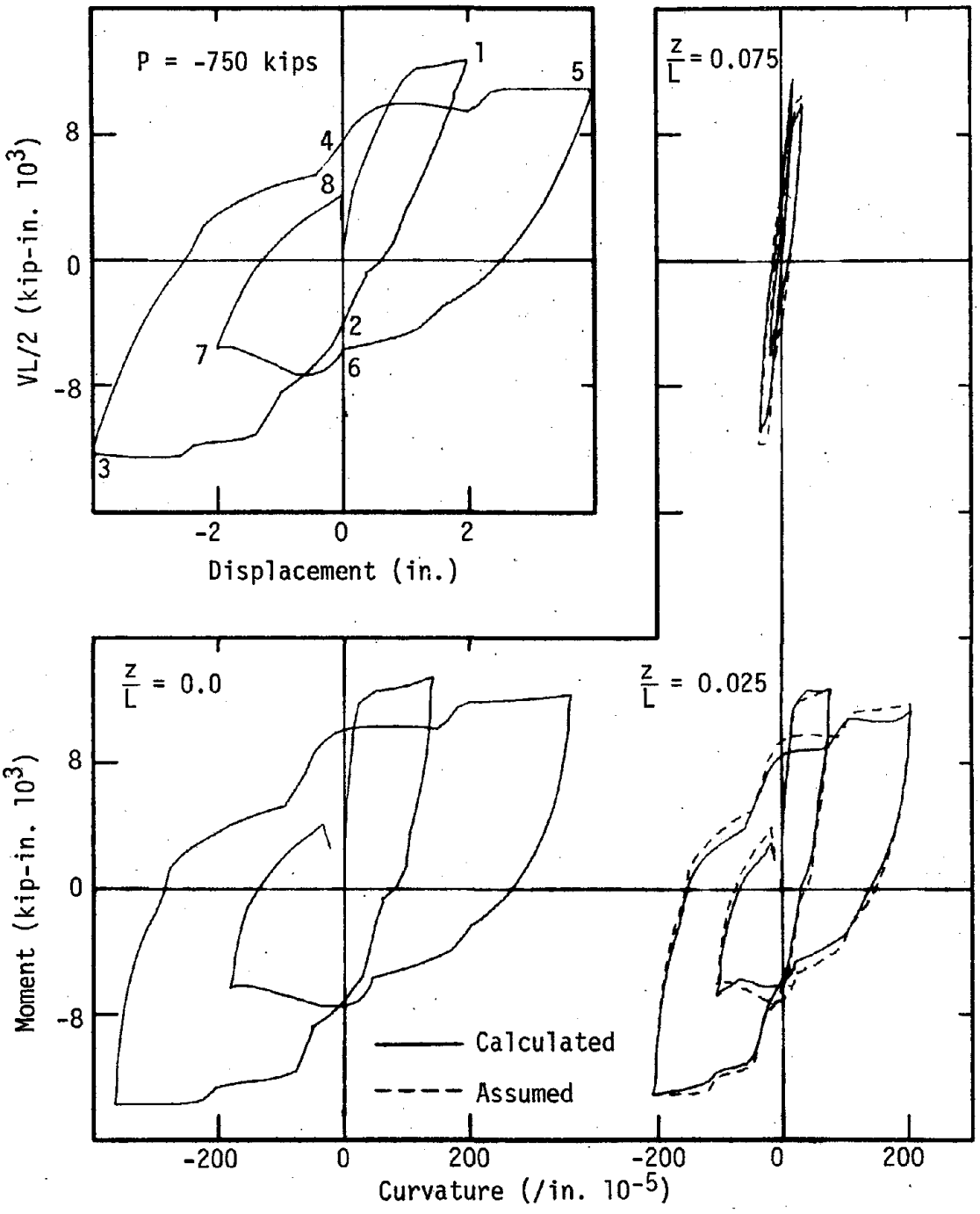

Fig. 2.30 Comparison of Assumed and Calculated Moment-Curvature Relationships Along Column Used in Deflection Calculations, Circular Column, Two-Dimensional Displacement History 2, Direction 1

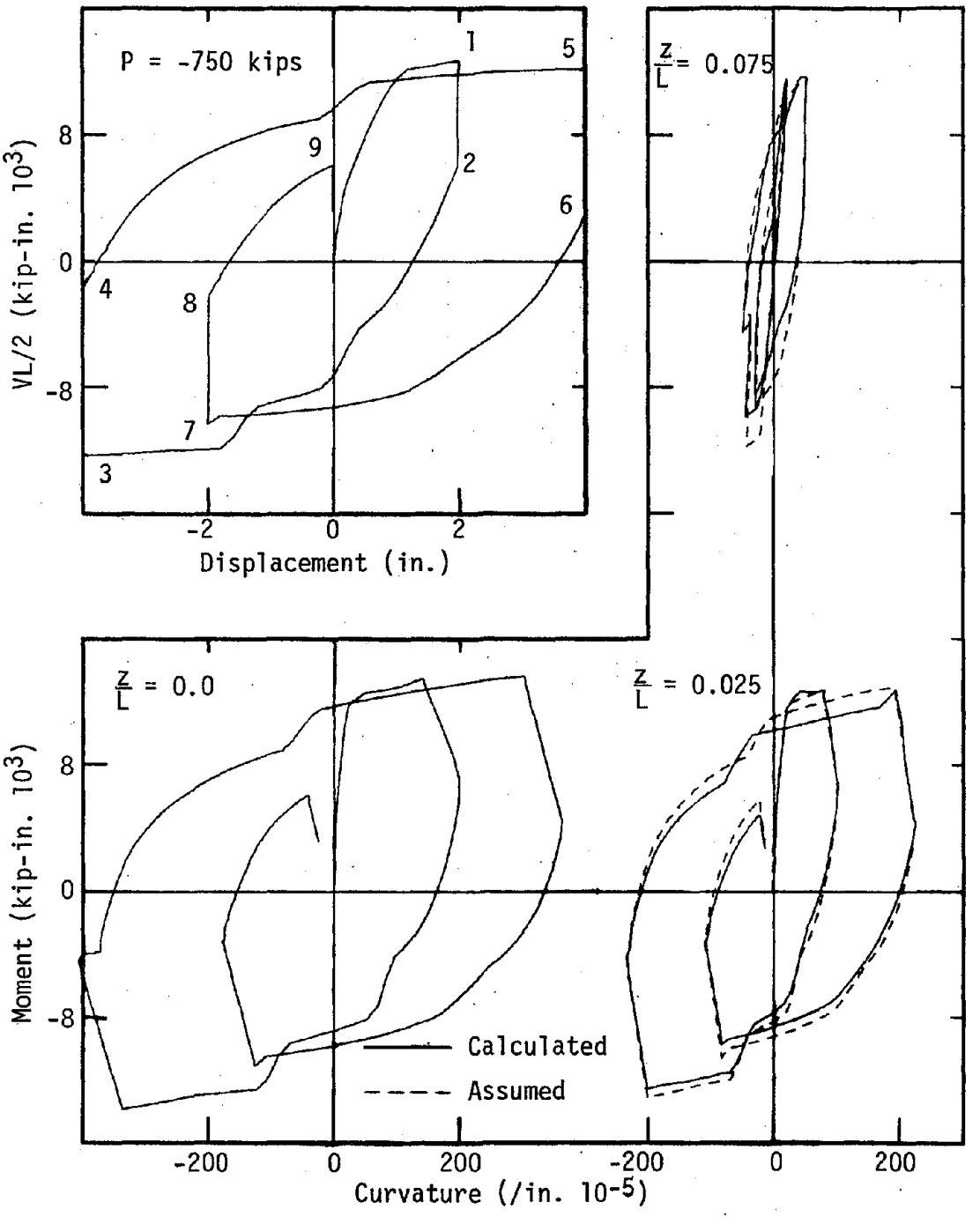

Fig. 2.31 Comparison of Assumed and Calculated Moment-Curvature Relationships Along Column Used in Deflection Calculations, Circular Column, Two-Dimensional Displacement History 3, Direction 1

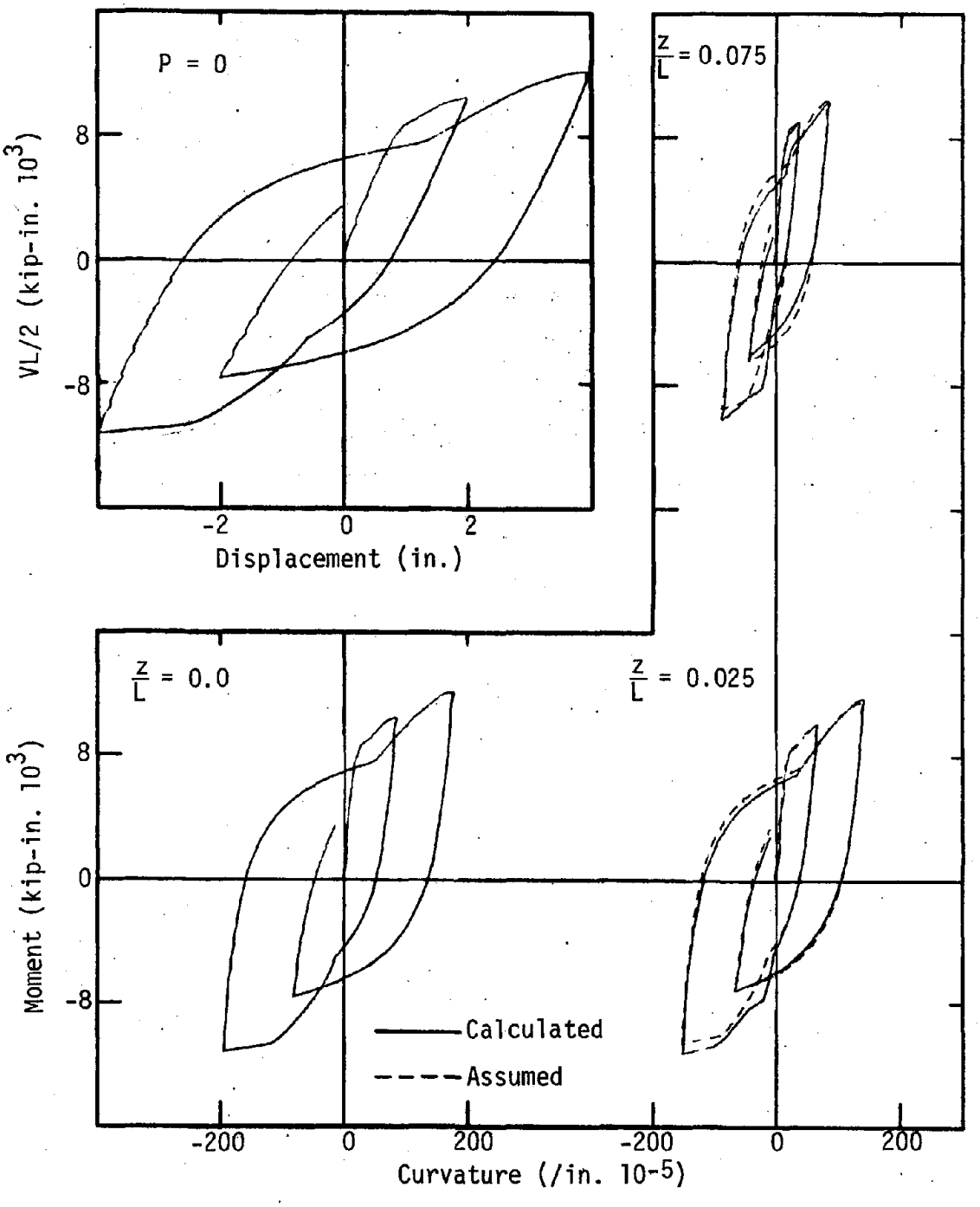

Fig. 2.32 Comparison of Assumed and Calculated Moment-Curvature Relationships Along Column Used in Deflection Calculations, Circular Column, One-Dimensional with P = 0

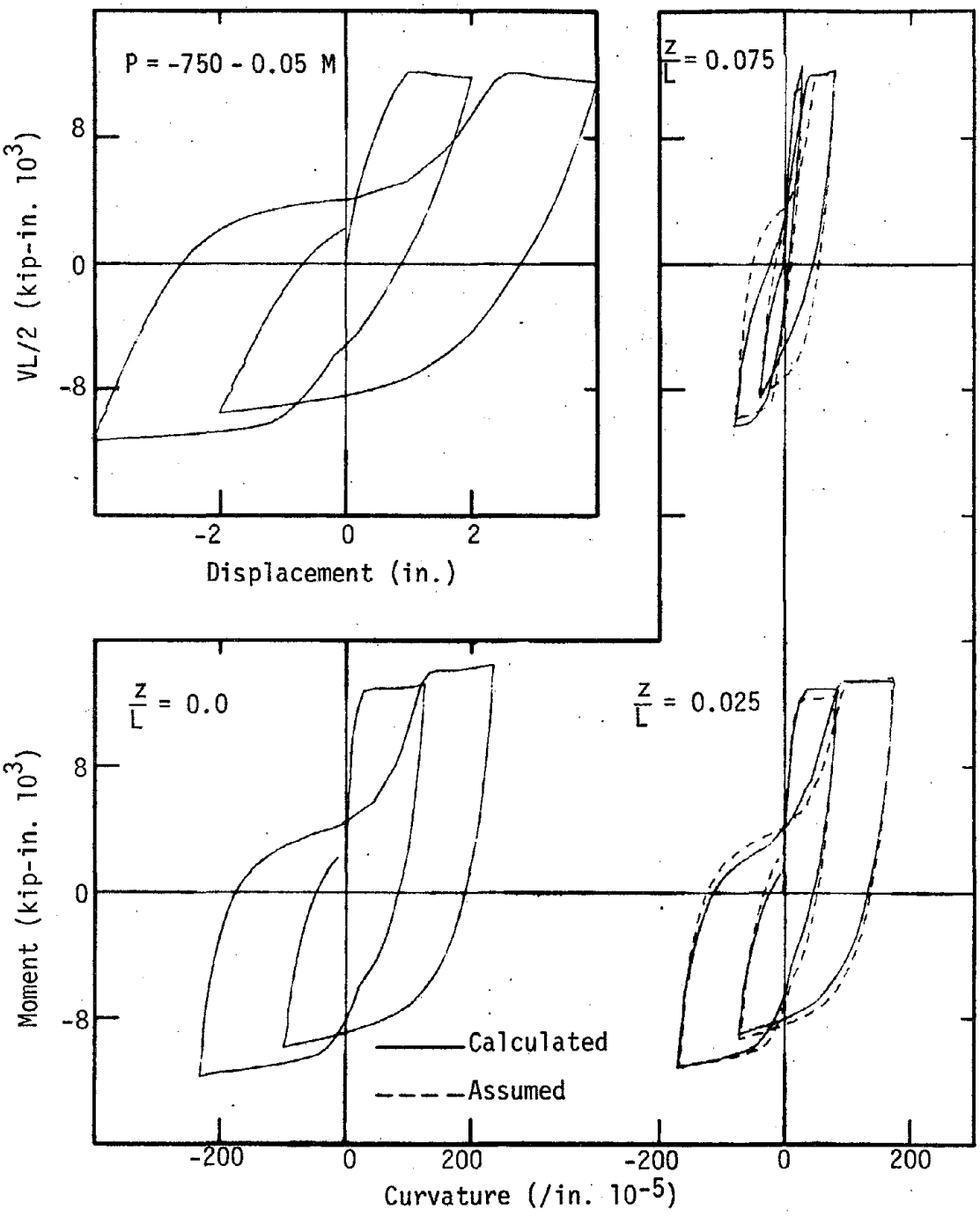

Fig. 2.33 Comparison of Assumed and Calculated Moment-Curvature Relationships Along Column Used in Deflection Calculations, Circular Column, One-Dimensional with Varying Axial Load

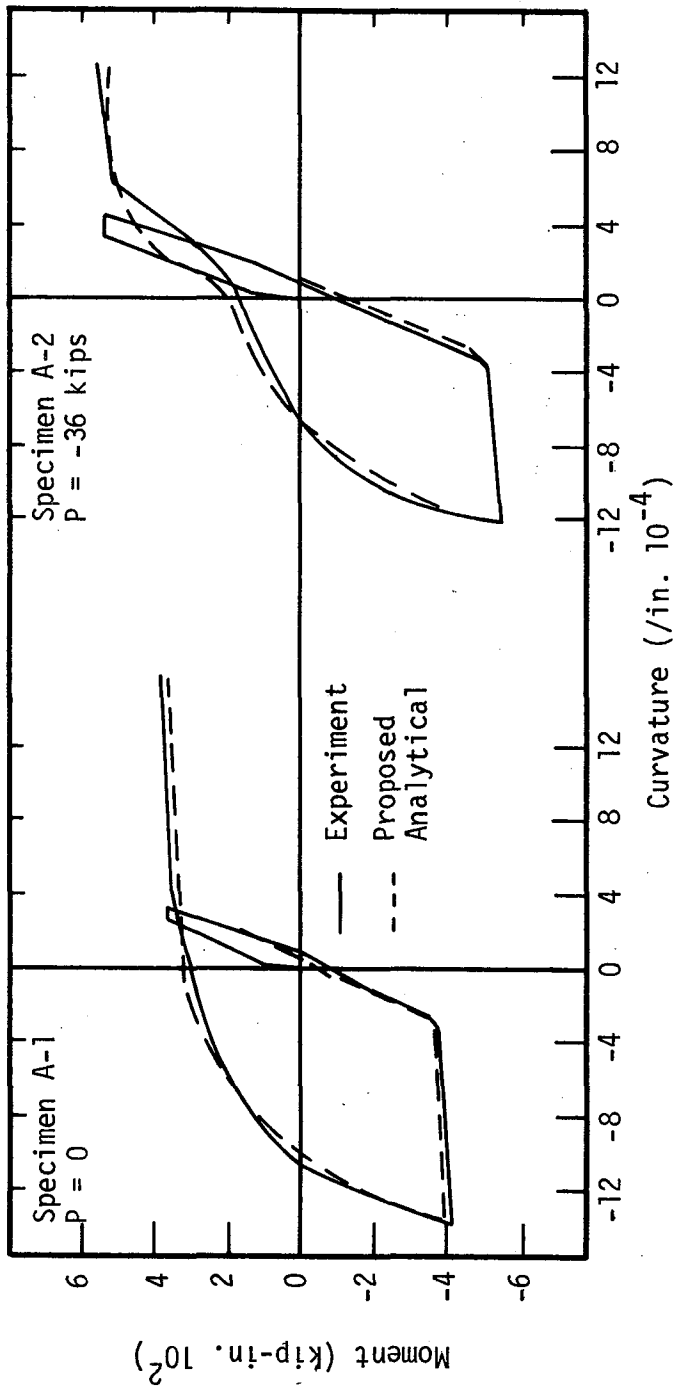

Fig. 2.34 Comparison of Analytical and Experimental Moment-Curvature Relationships, Aoyama's Tests (Ref. 3)

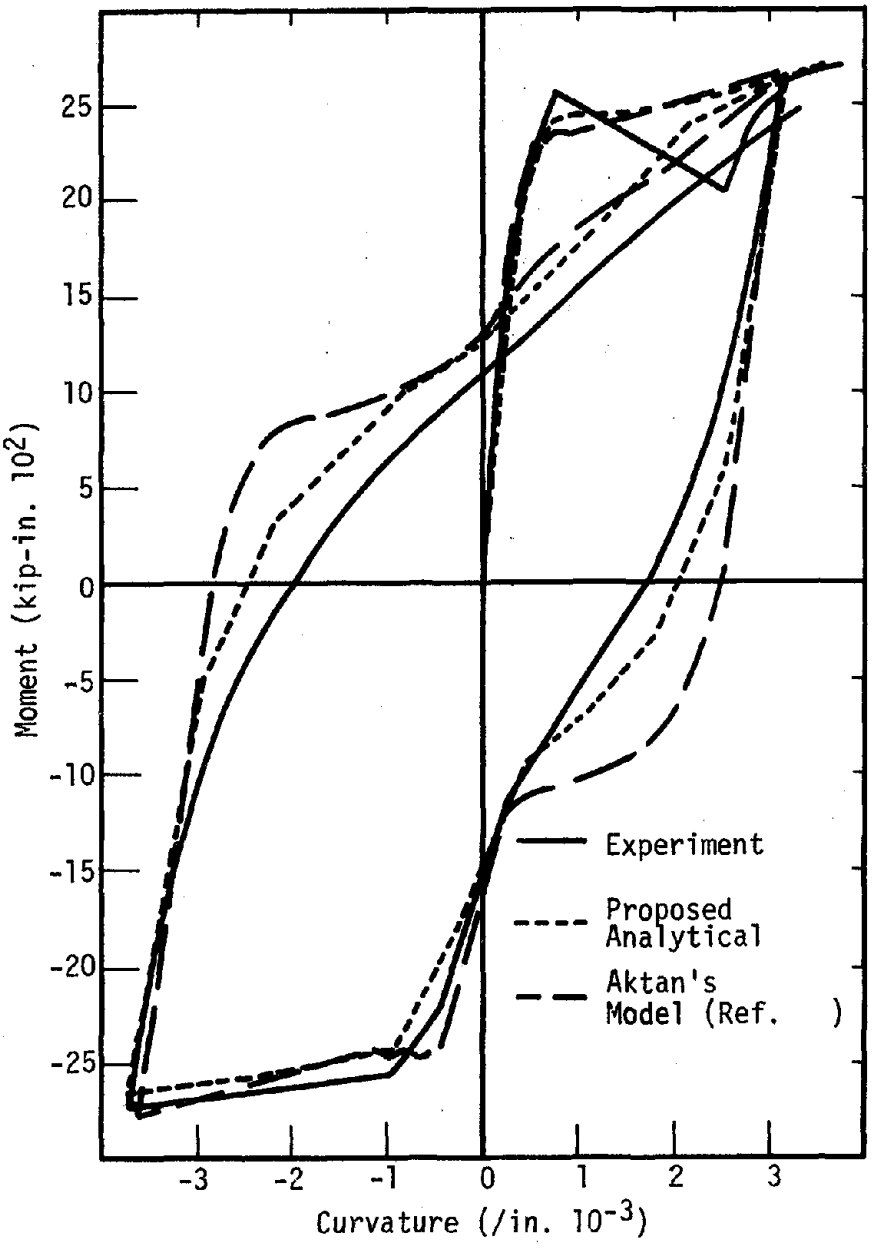

Fig. 2.35 Comparison of Analytical and Experimental Moment-Curvature Relationship, Karlsson's Specimen BK5 (Ref. 11)

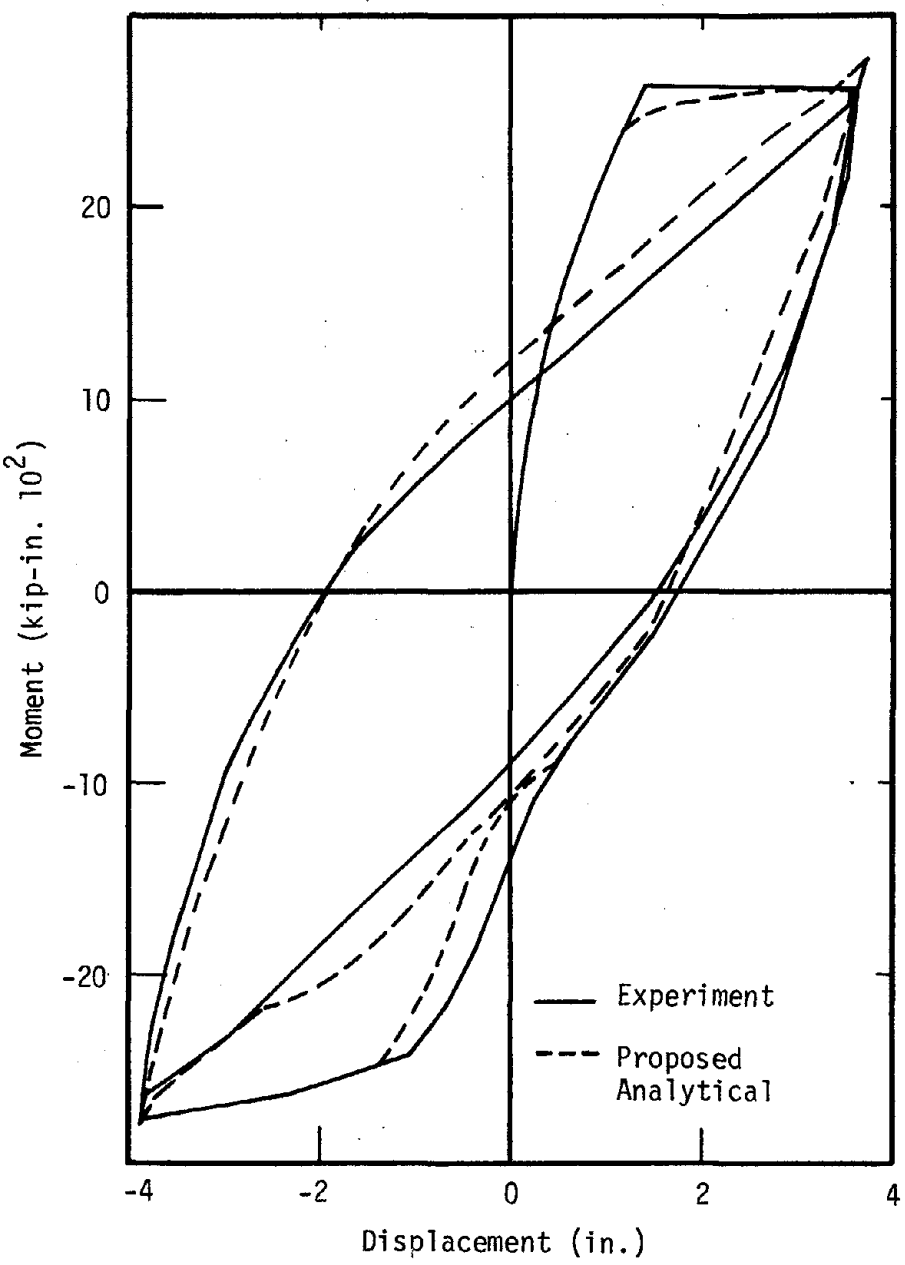

Fig. 2.36 Comparison of Analytical and Experimental Moment-Displacement Relationship, Karlsson's Specimen BK5 (Ref. 11)

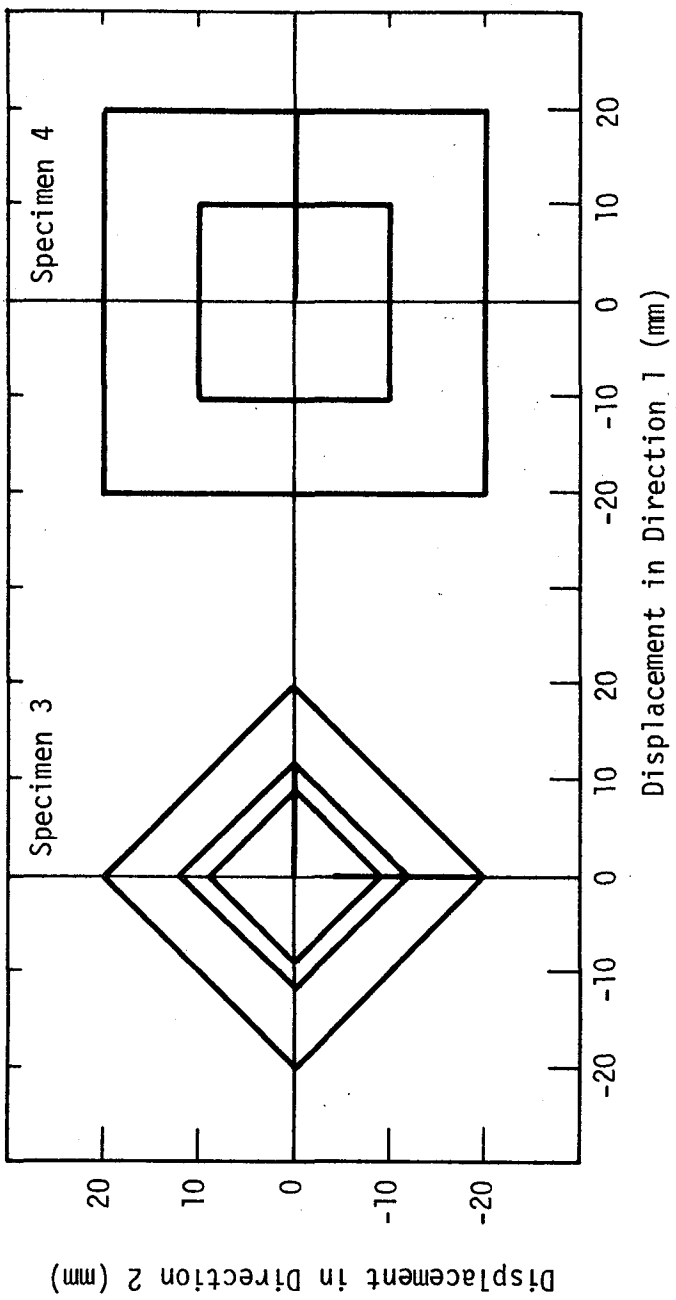

Fig. 2.37 Nominal Two-Dimensional Displacement Histories for Takizawa's Tests (Ref. 34)

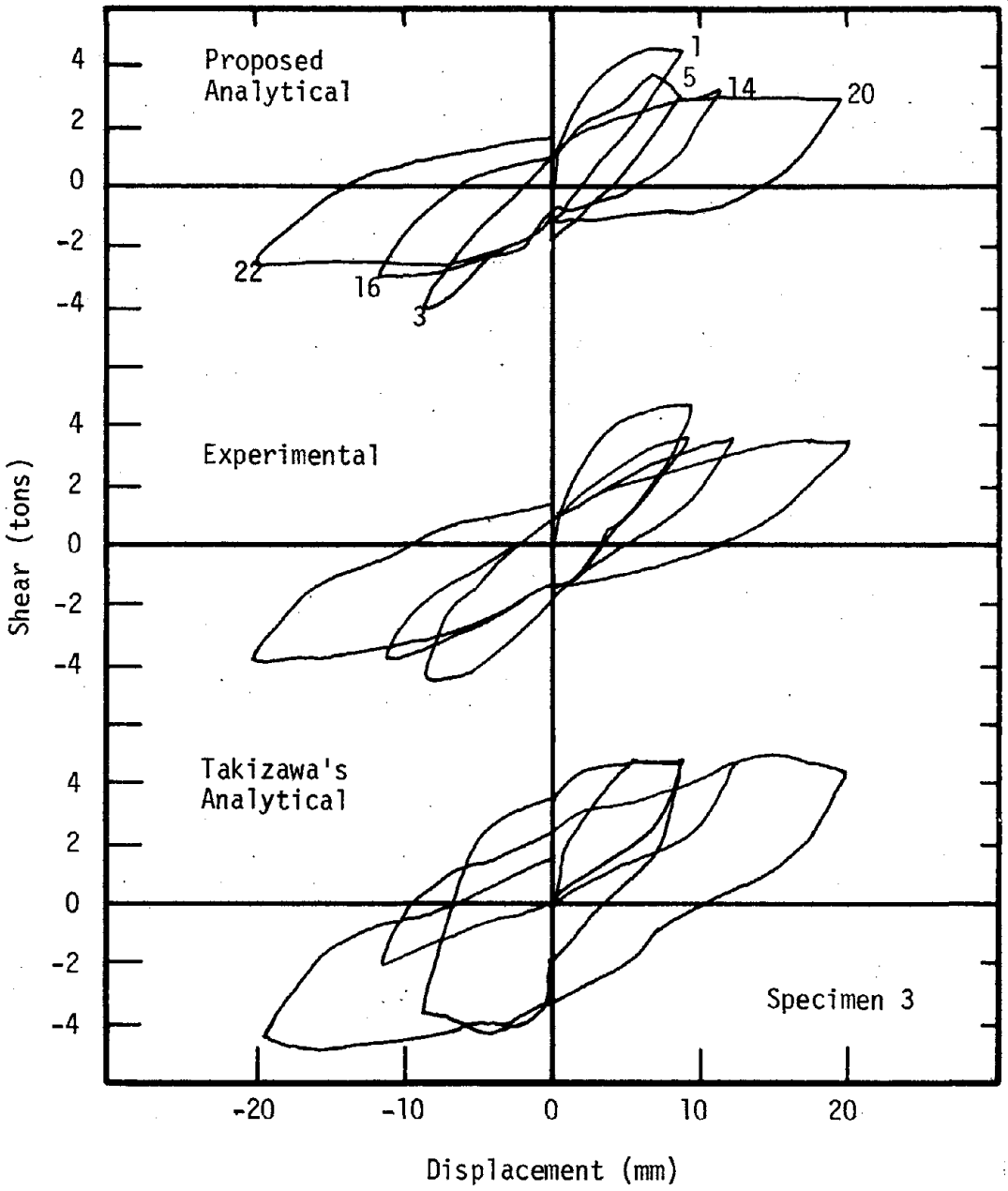

Fig. 2.38 Comparison of Analytical and Experimental Shear-Deflection Relationship, Takizawa's Tests (Ref. 34)

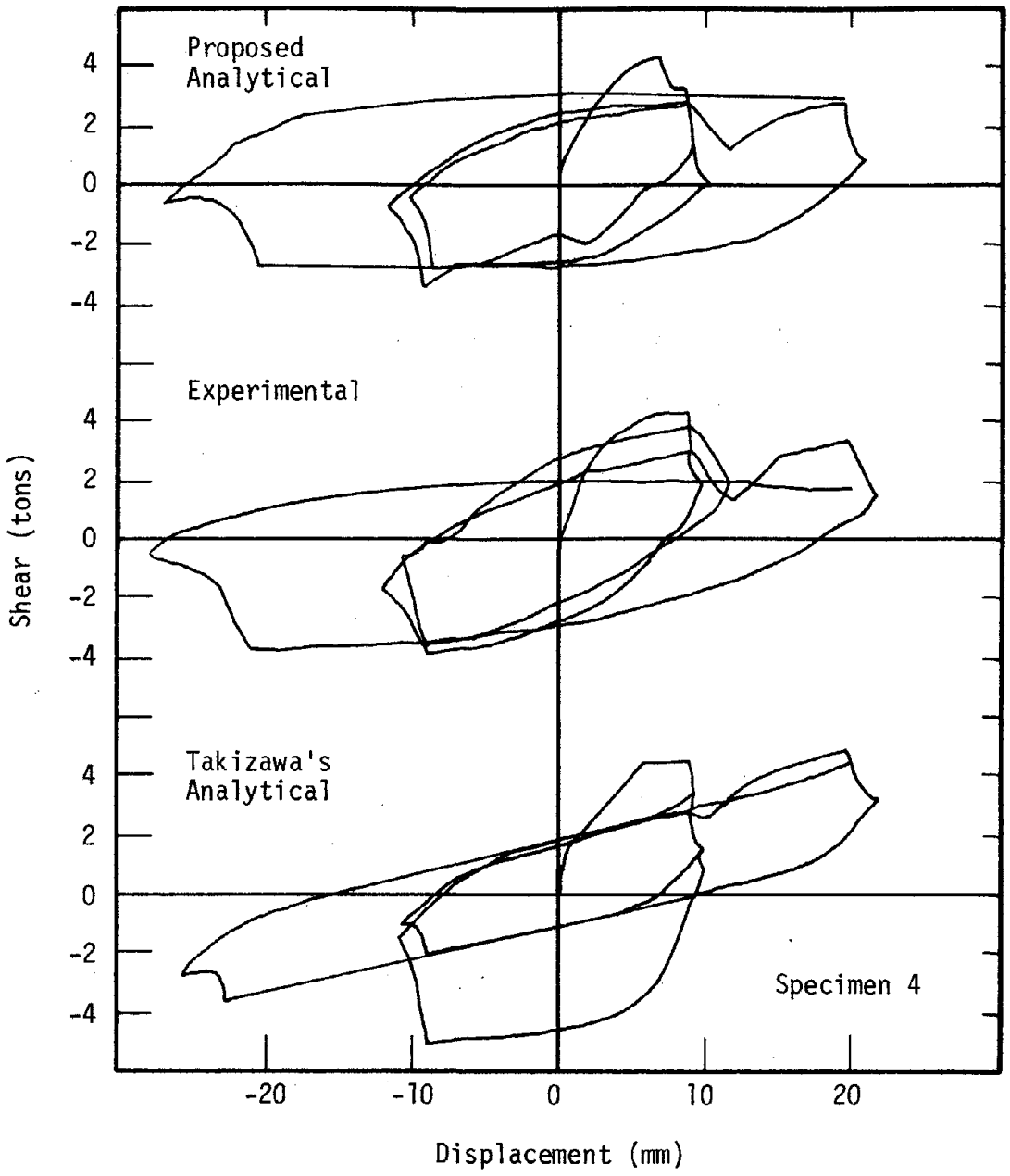

Fig. 2.38 (Continued)

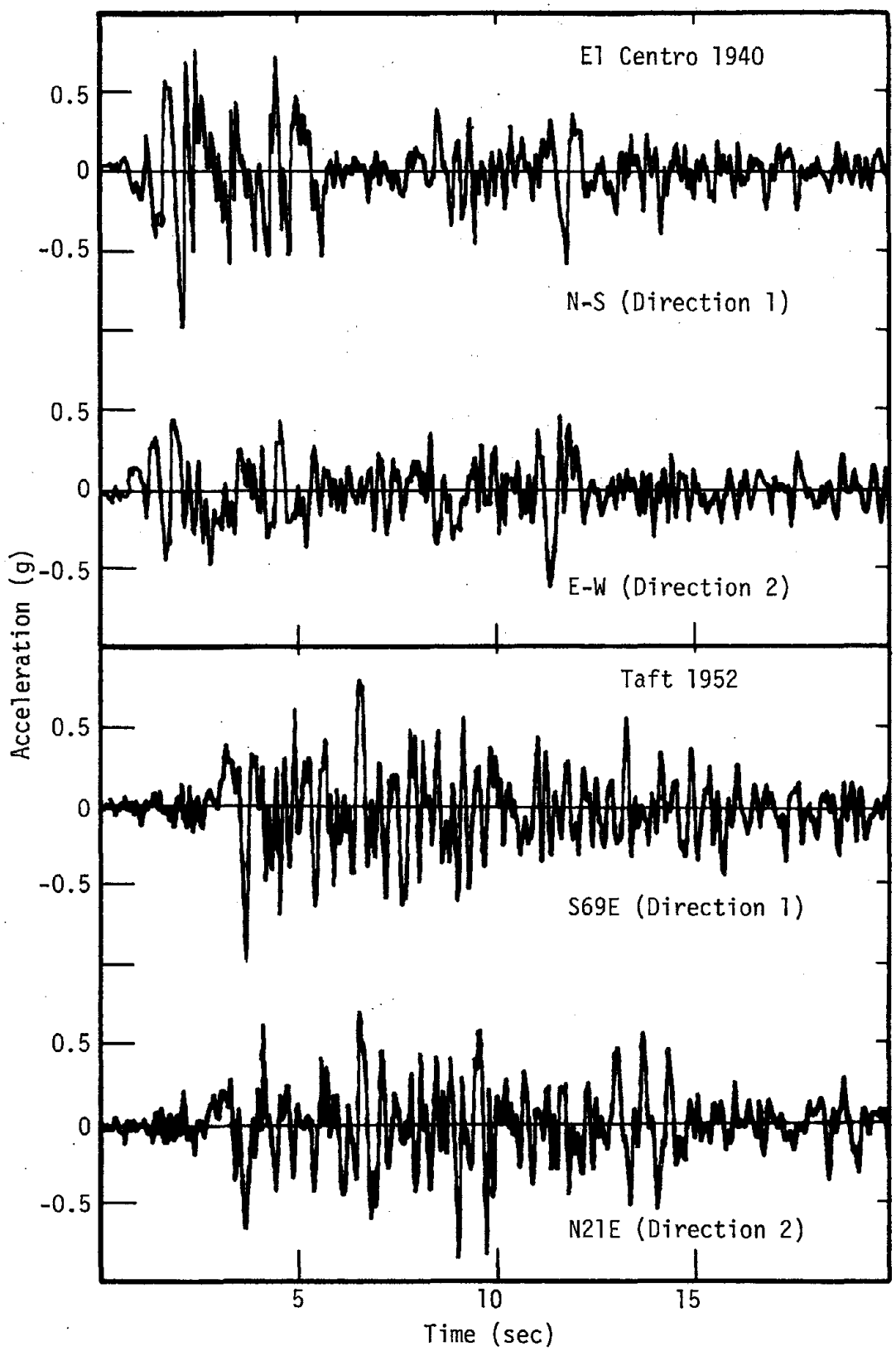

Fig. 3.1 Acceleration Records of Earthquakes Used in Study, Scaled to 1.0 g Peak Acceleration

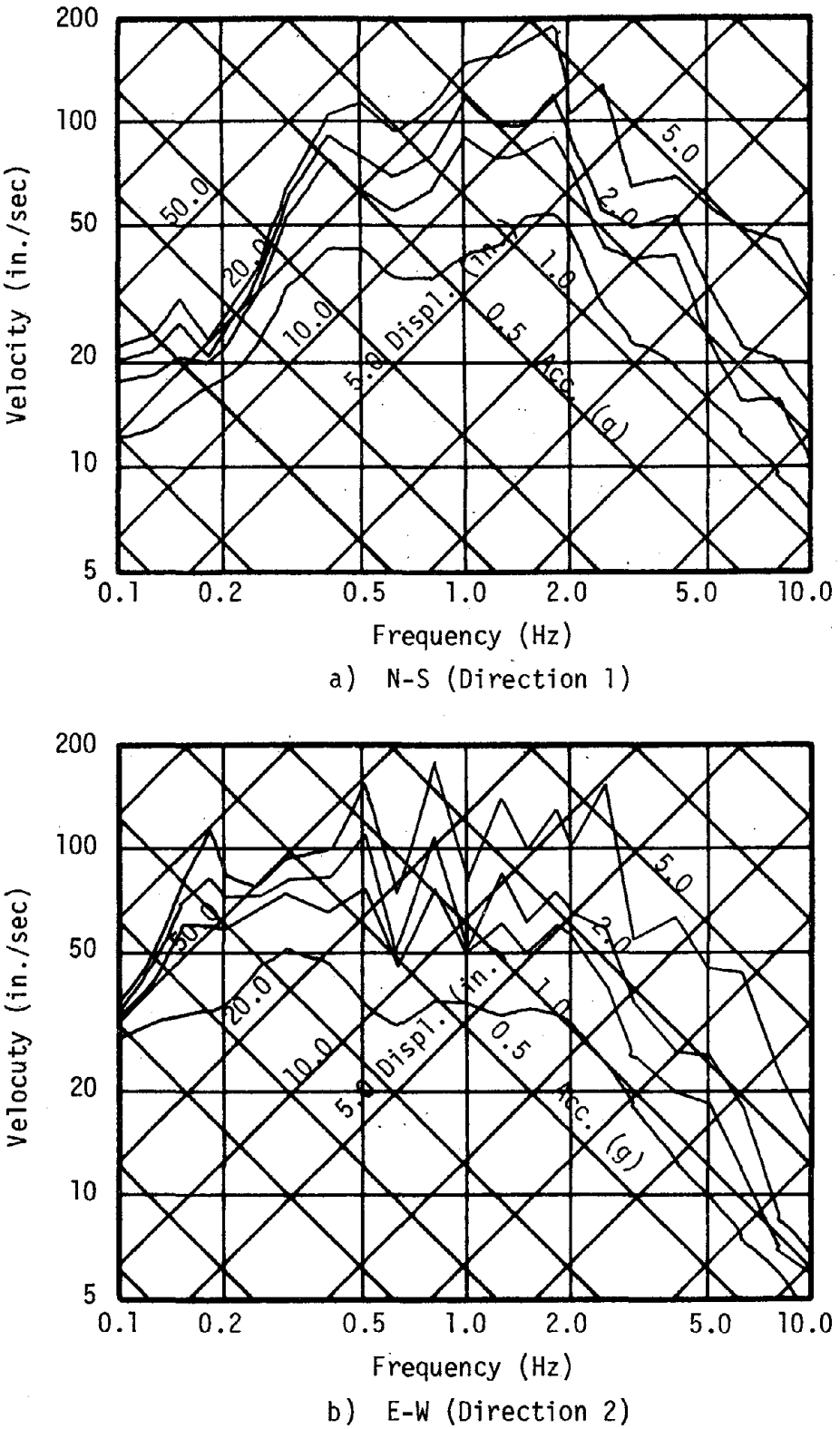

Fig. 3.2 20 Second Elastic Response Spectra, El Centro Record, Scaled to 1.0 g Peak Acceleration, 0%, 2%, 5%, and 20% Damping

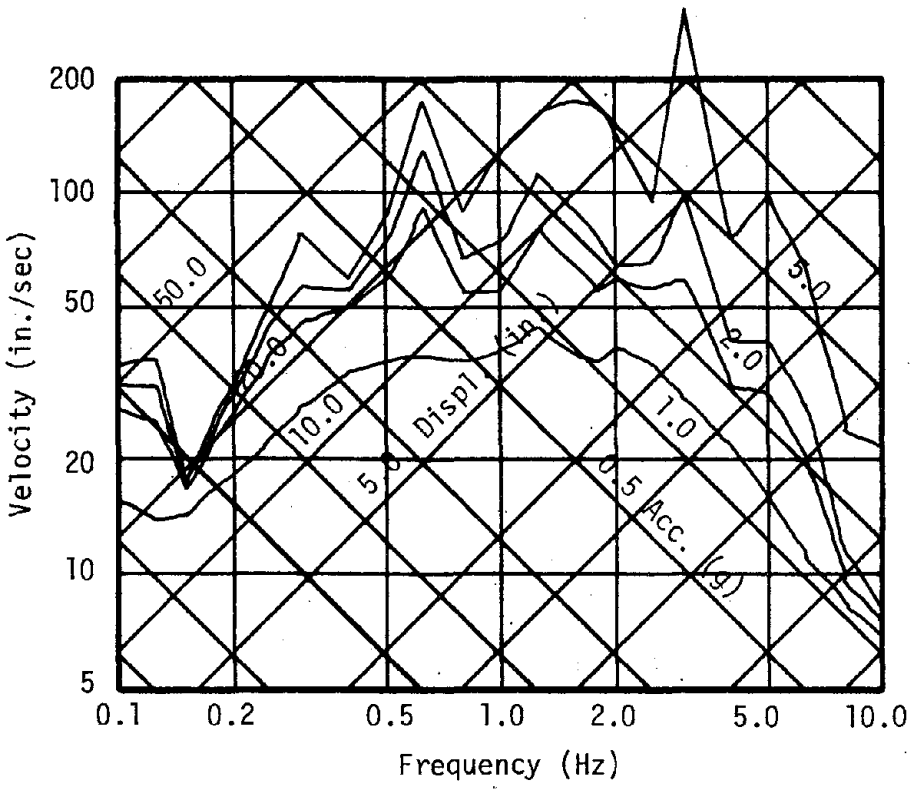

a) S69E (Direction 1)

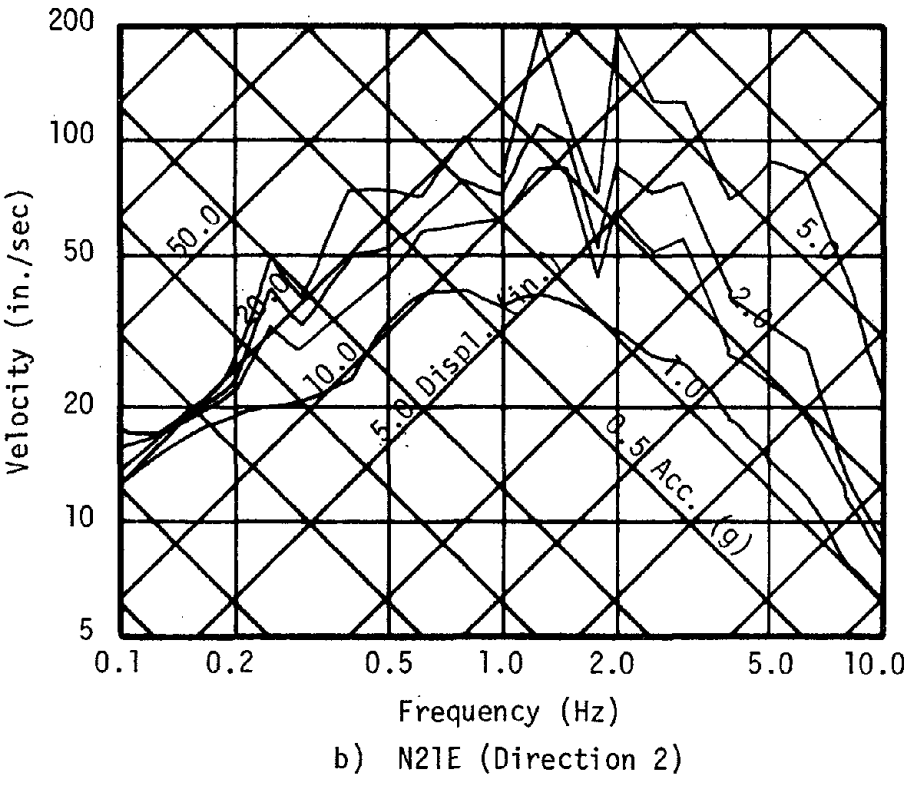

b) N21E (Direction 2)

Fig. 3.3 20 Second Elastic Response Spectra, Taft Record, Scaled to 1.0 g Peak Acceleration, 0%, 2%, 5% and 20% Damping

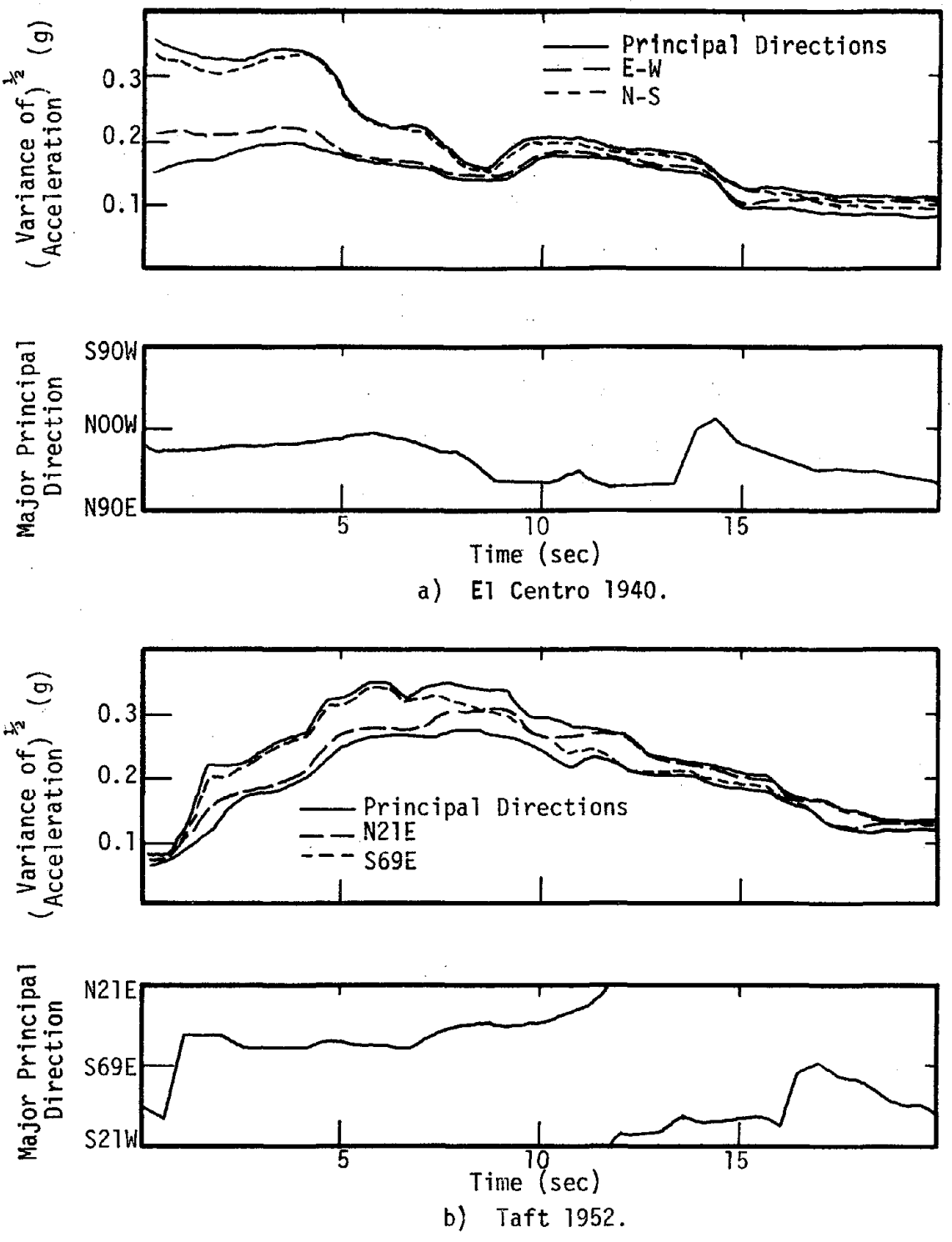

Fig. 3.4 Principal Directions and Variances of Earthquake Records Used, Scaled to 1.0 g Peak Acceleration

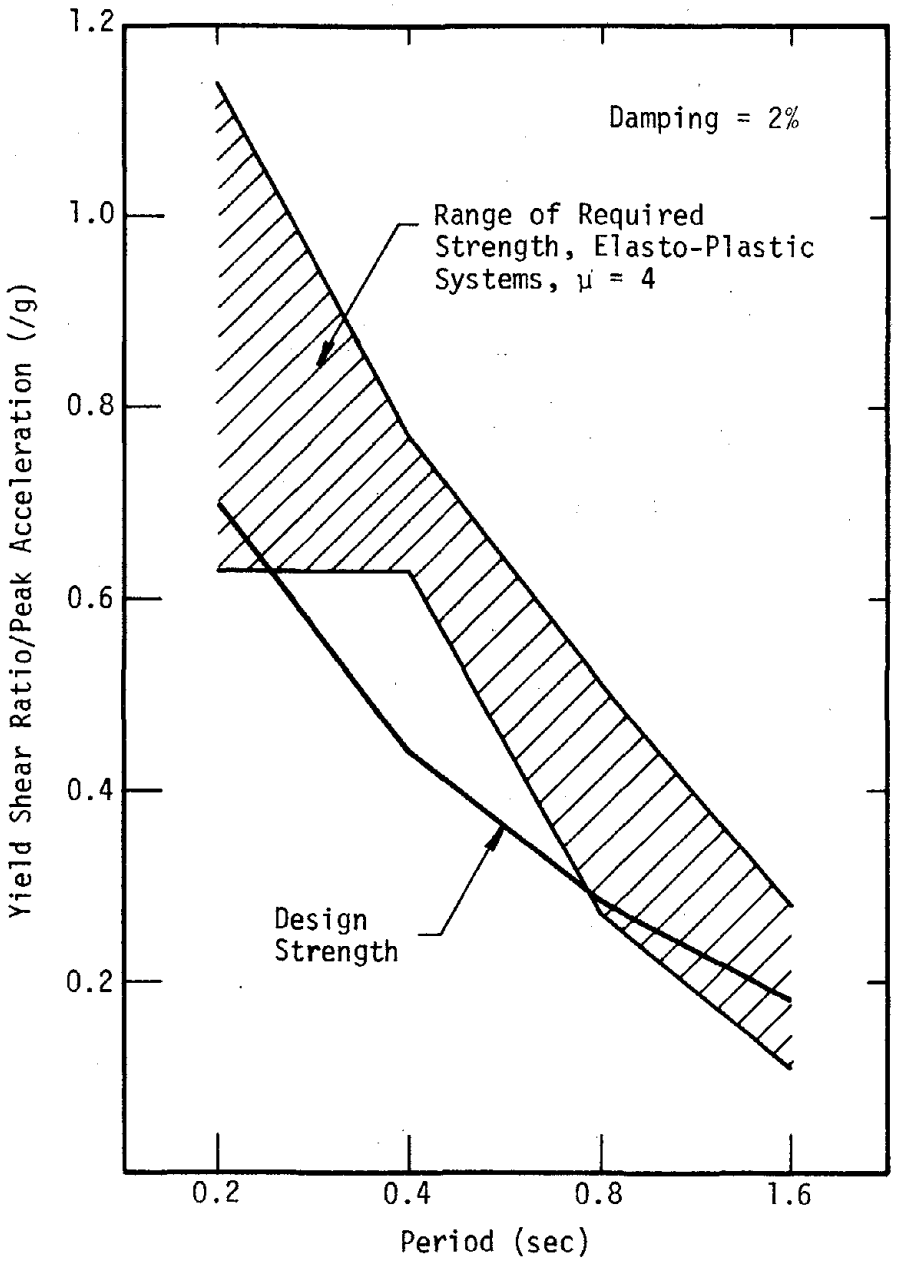

Fig. 3.5 Design Strength of Systems Compared with Required Strength of Elasto-Plastic Systems Subjected to El Centro and Taft Records, Calculated for $\mu = 4$

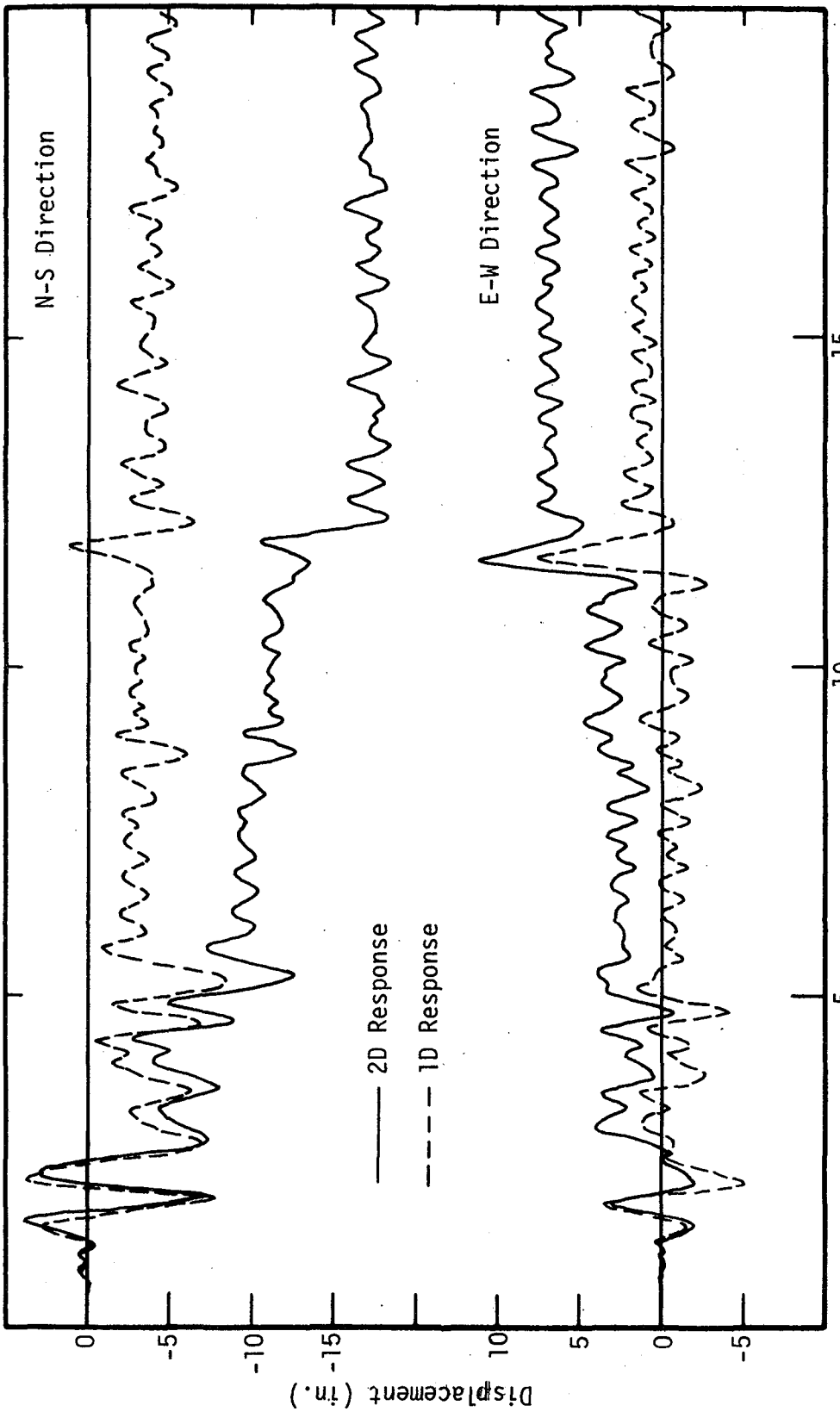

Fig. 3.6 Displacement Response, T = 0.4 System, El Centro Record

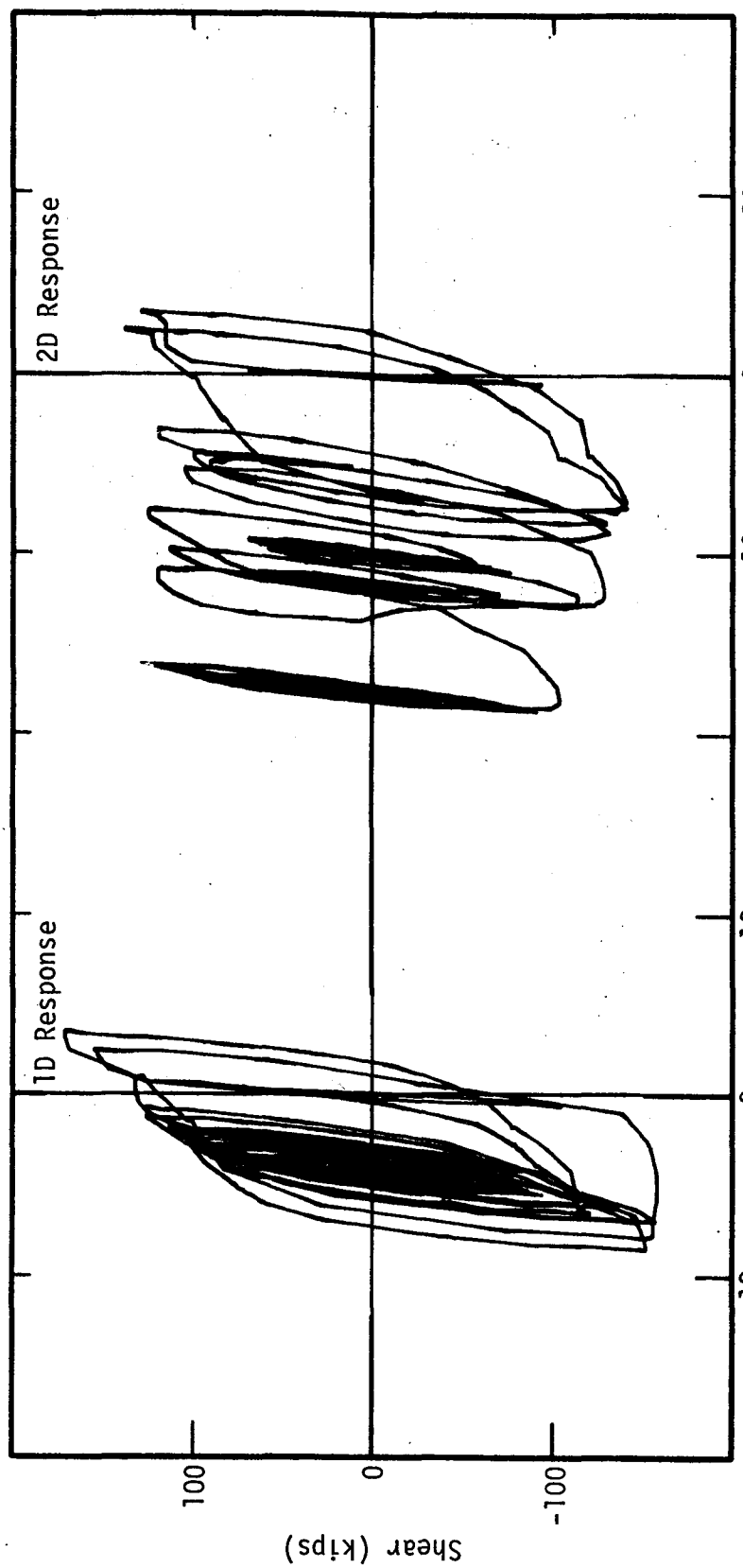

Fig. 3.7 Shear-Displacement Response, T = 0.4 System, El Centro N-S Record

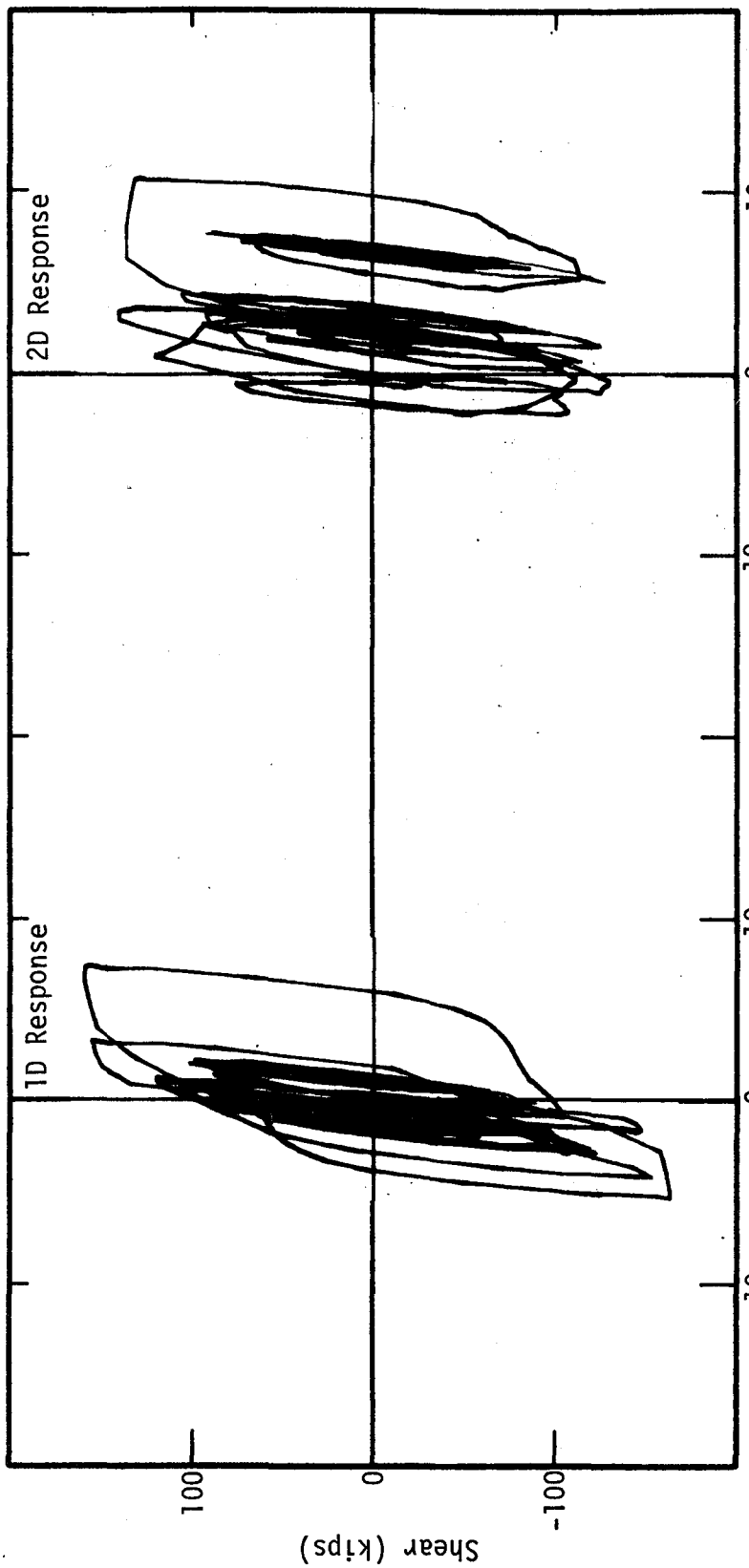

Fig. 3.8 Shear-Displacement Response, T = 0.4 System, El Centro E-W Record

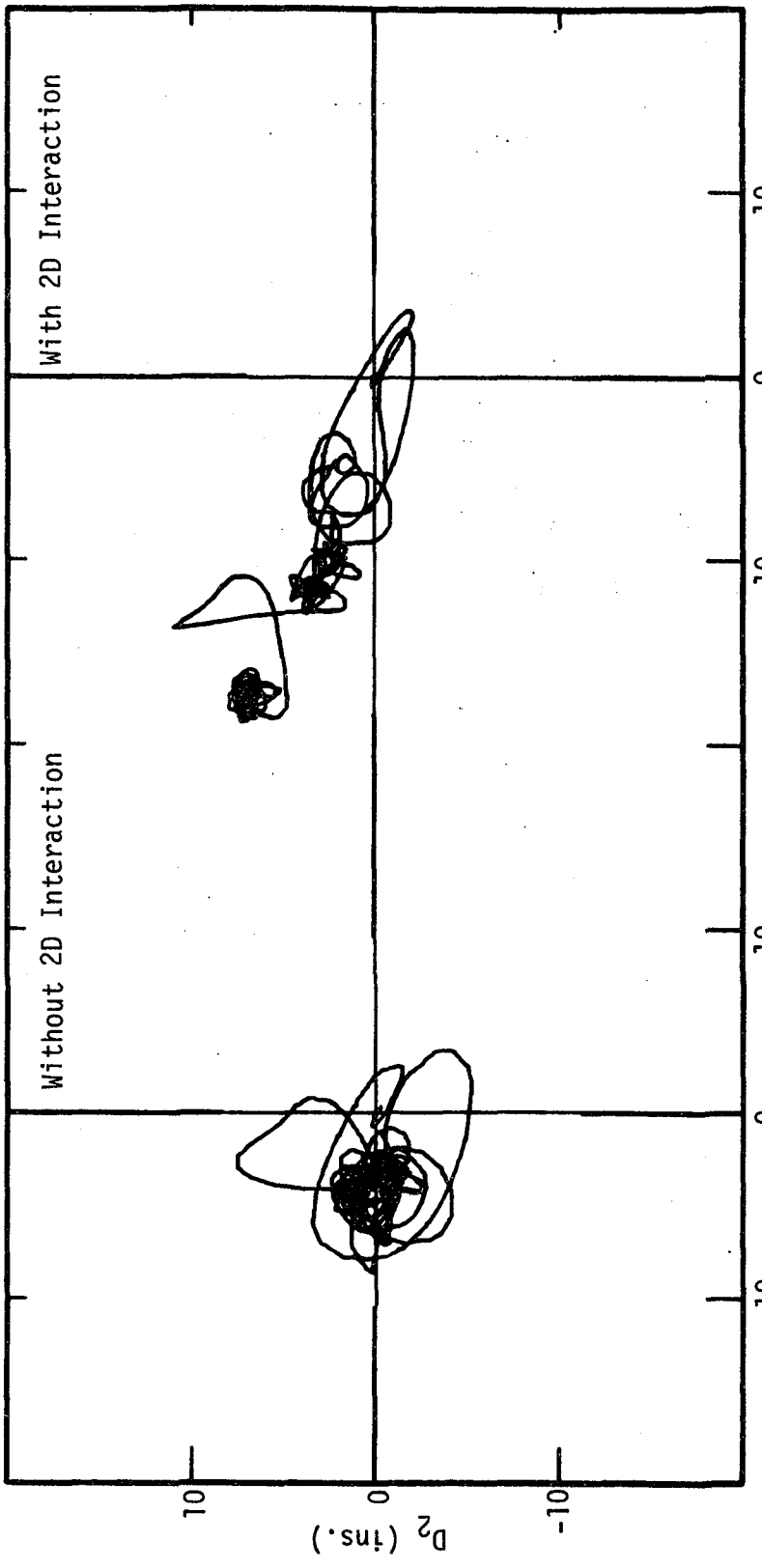

Fig. 3.9 2D Displacement Response of T = 0.4 System to the El Centro Record

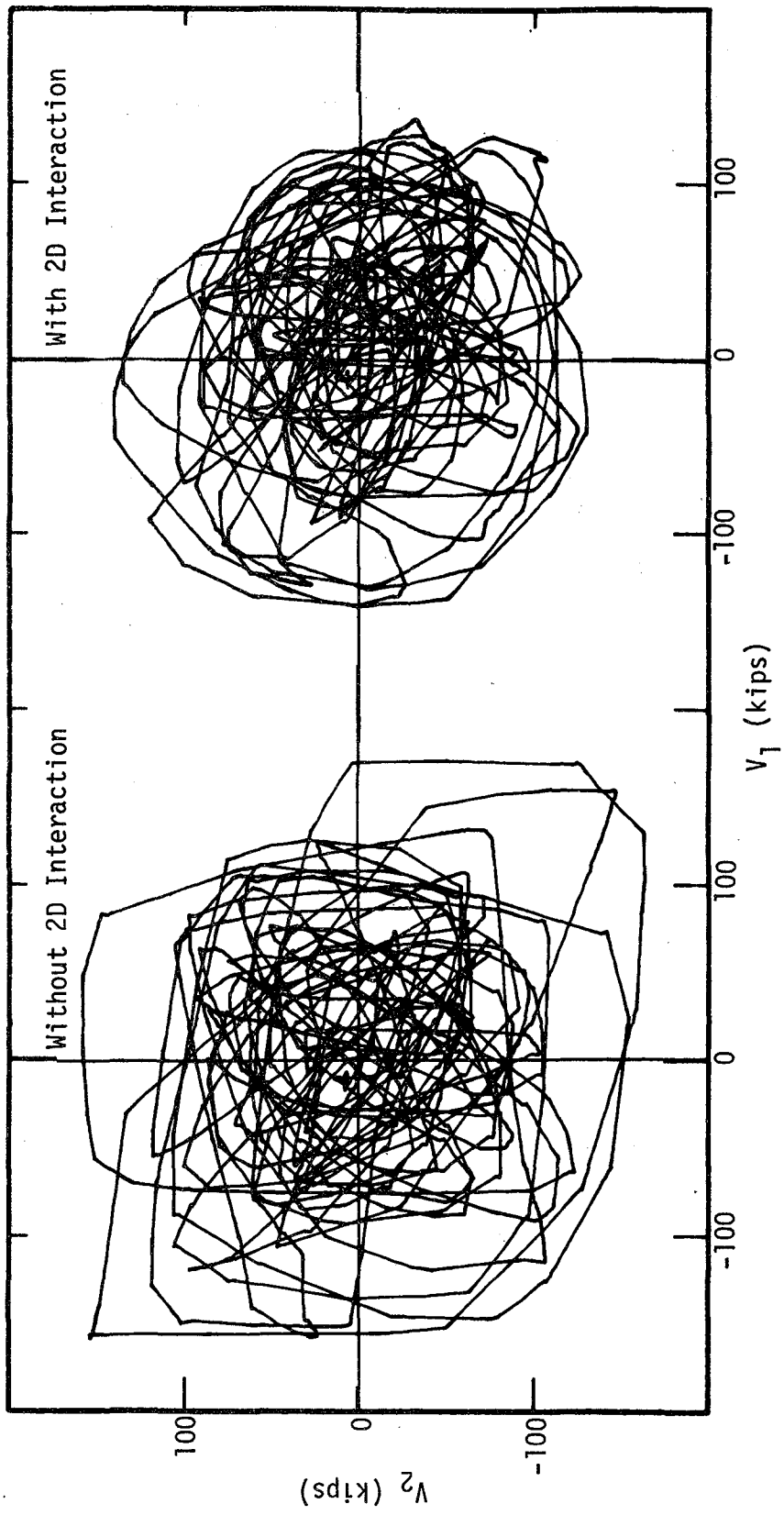

Fig. 3.10 2D Shear Response of T = 0.4 System to the El Centro Record

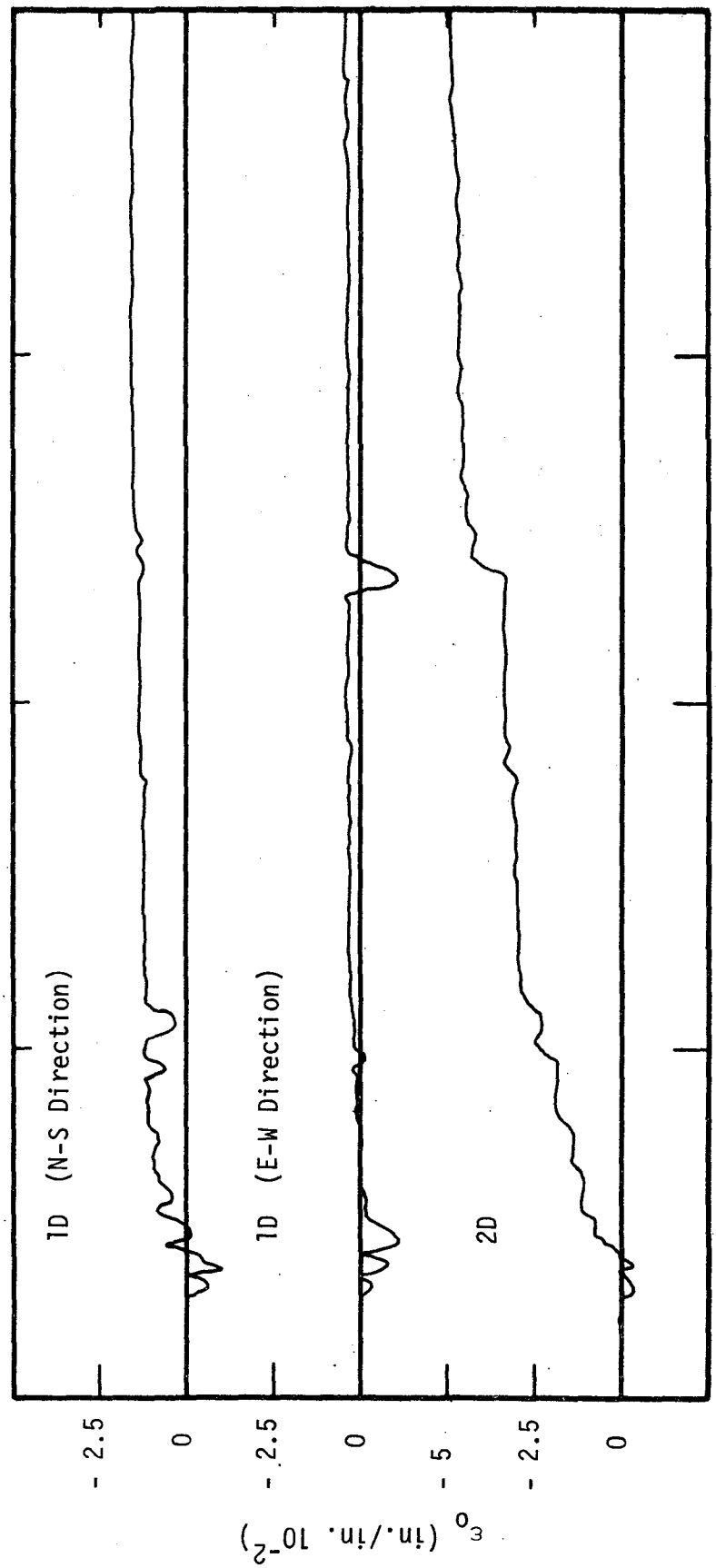

Fig. 3.11 Centroidal Strain-Time History, T = 0.4 System, El Centro Record

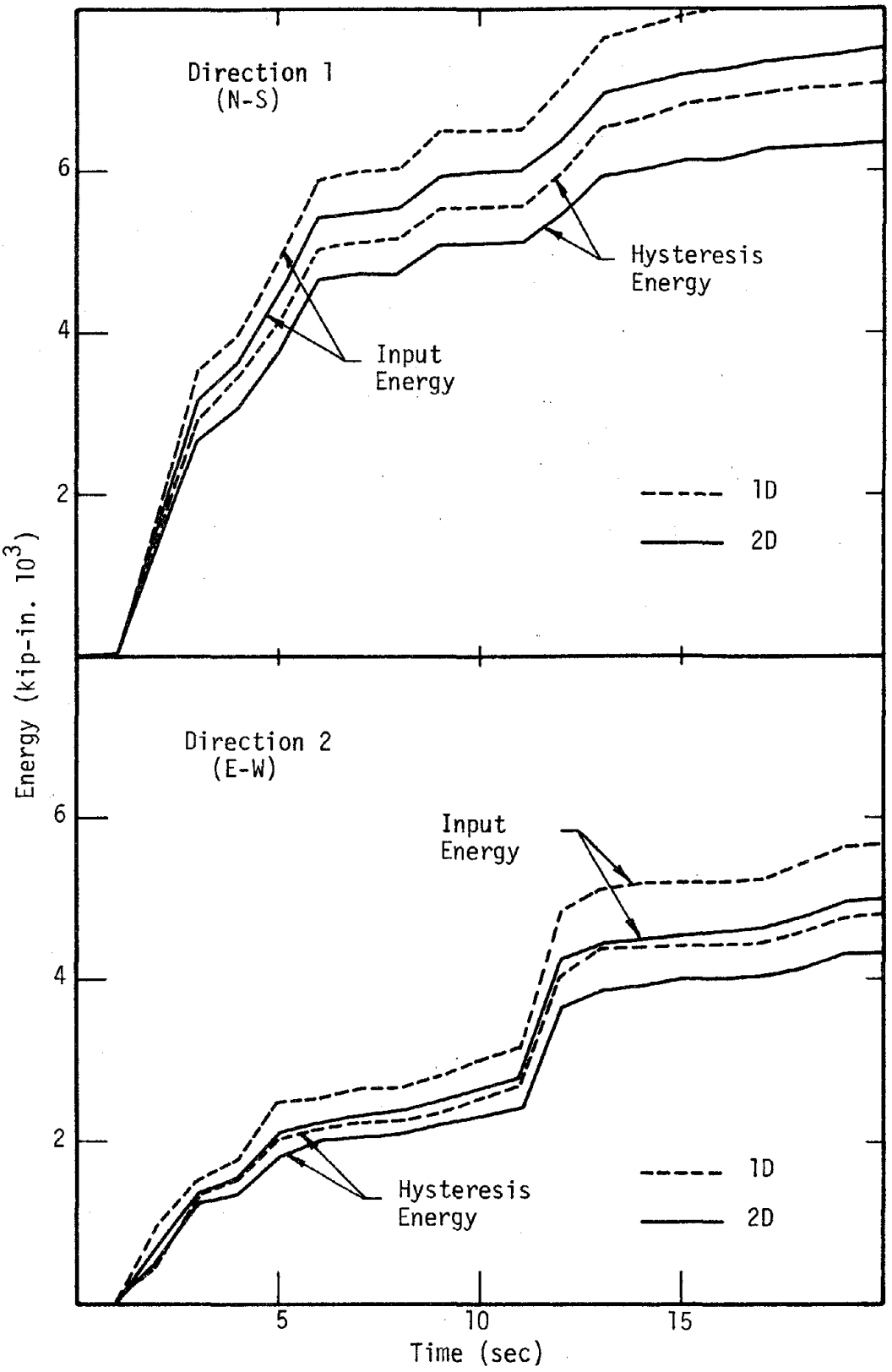

Fig. 3.12 Input and Hysteresis Energy-Time History, T = 0.4 System, El Centro Record

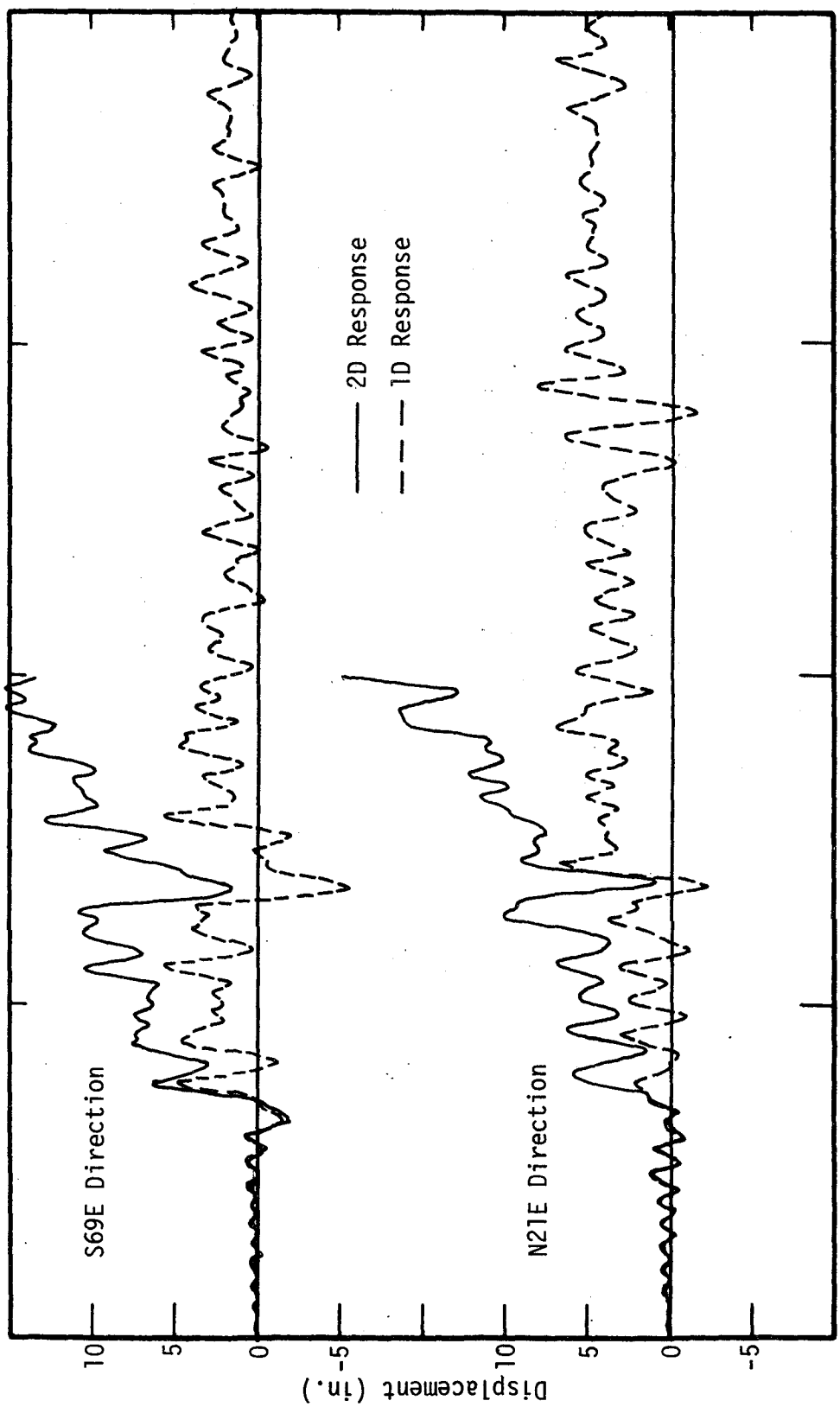

Fig. 3.13 Displacement Response, T = 0.4 System, Taft Record

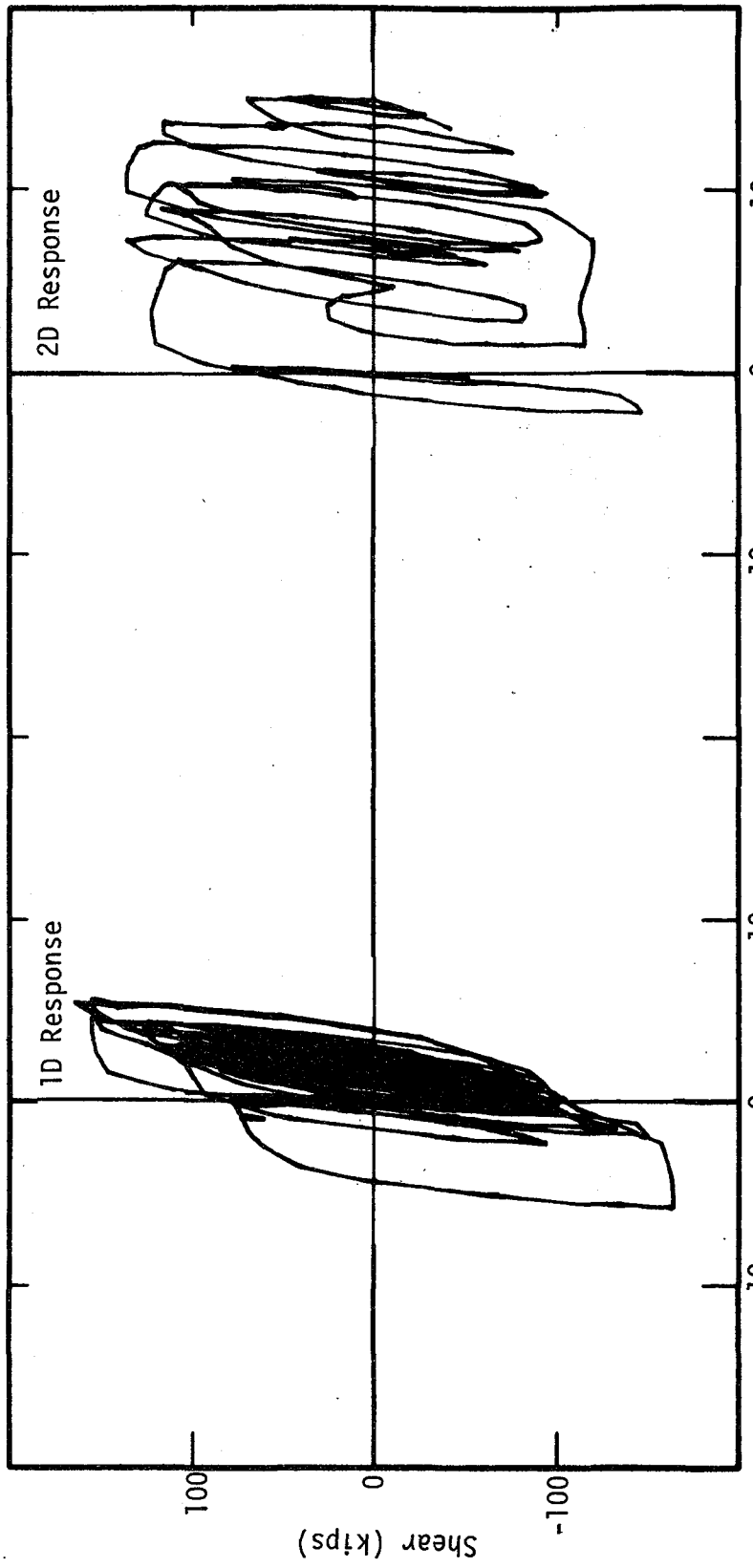

Fig. 3.14 Shear-Displacement Response, T = 0.4 System, Taft S69E Record

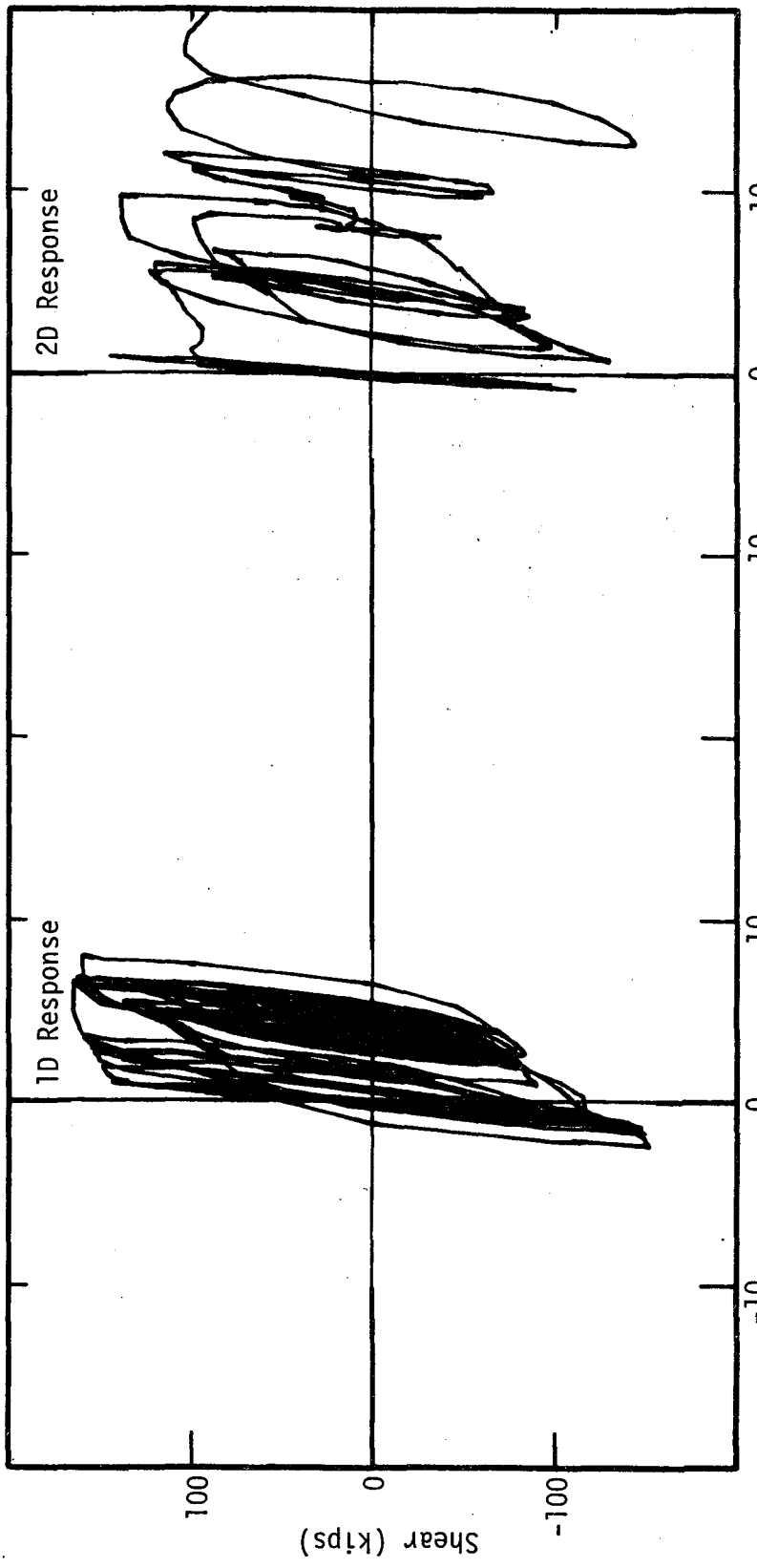

Fig. 3.15 Shear-Displacement Response, T = 0.4 System, Taft N21E Record

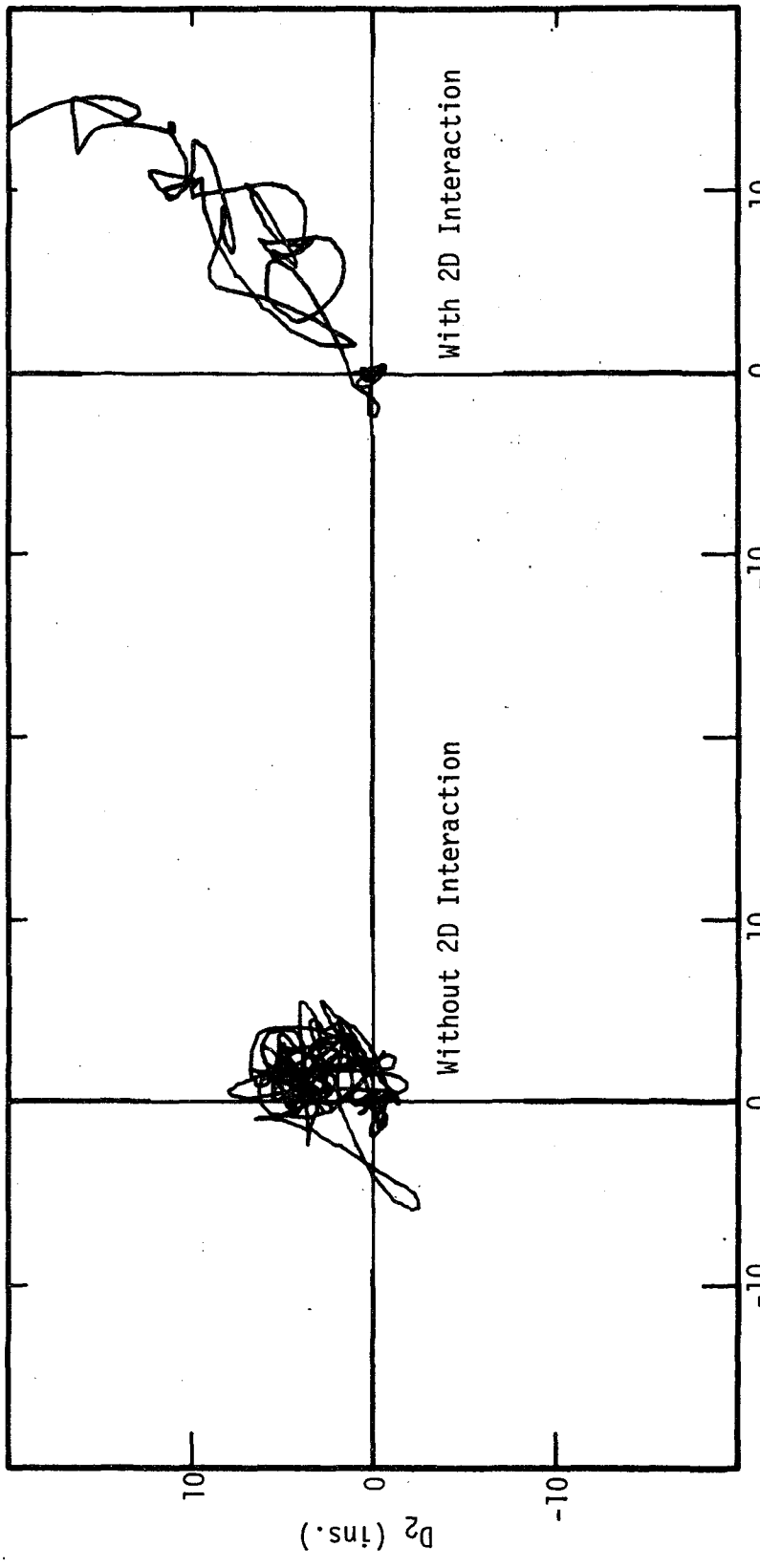

Fig. 3.16 2D Displacement Response of T = 0.4 System to the Taft Record

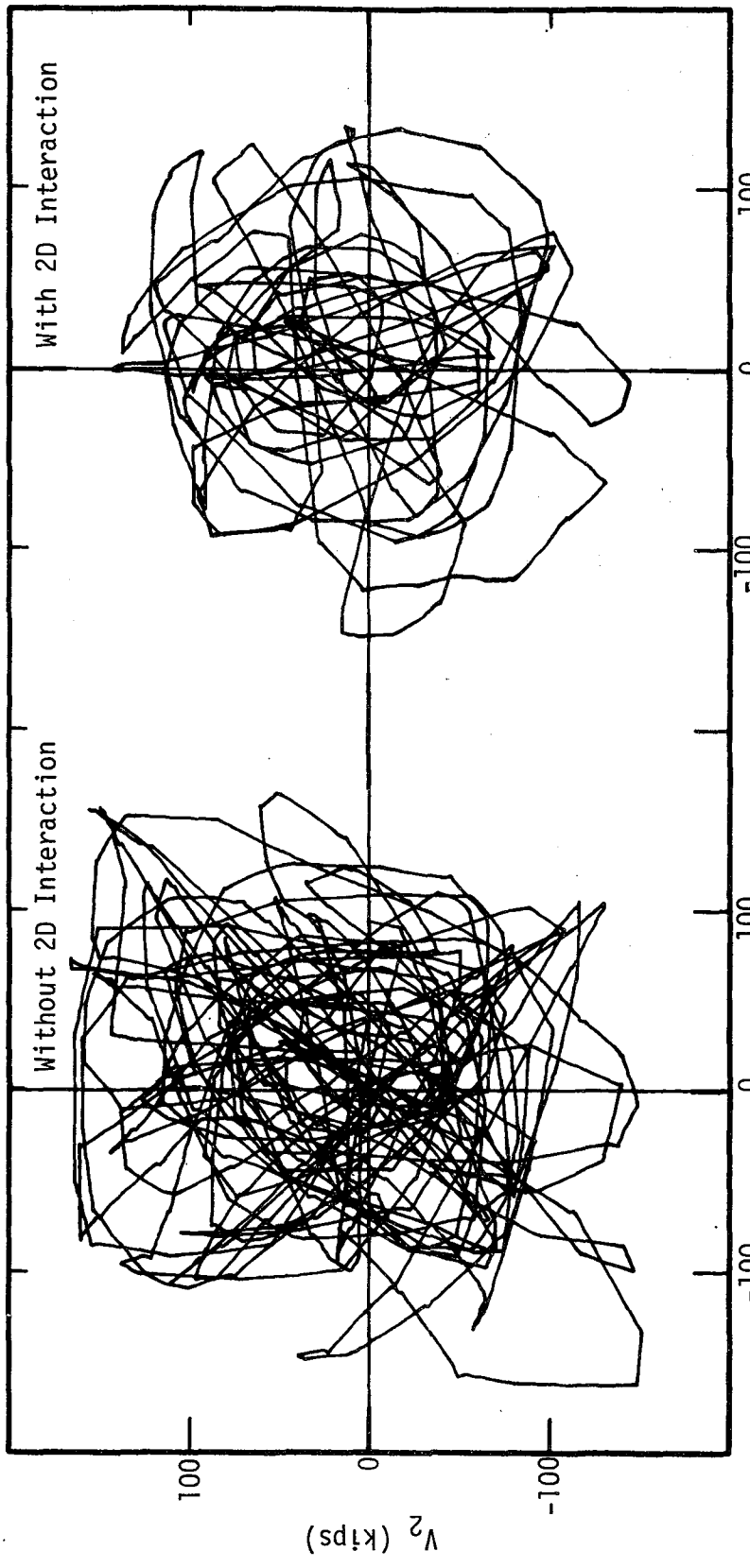

Fig. 3.17 2D Shear Response of T = 0.4 System to the Taft Record

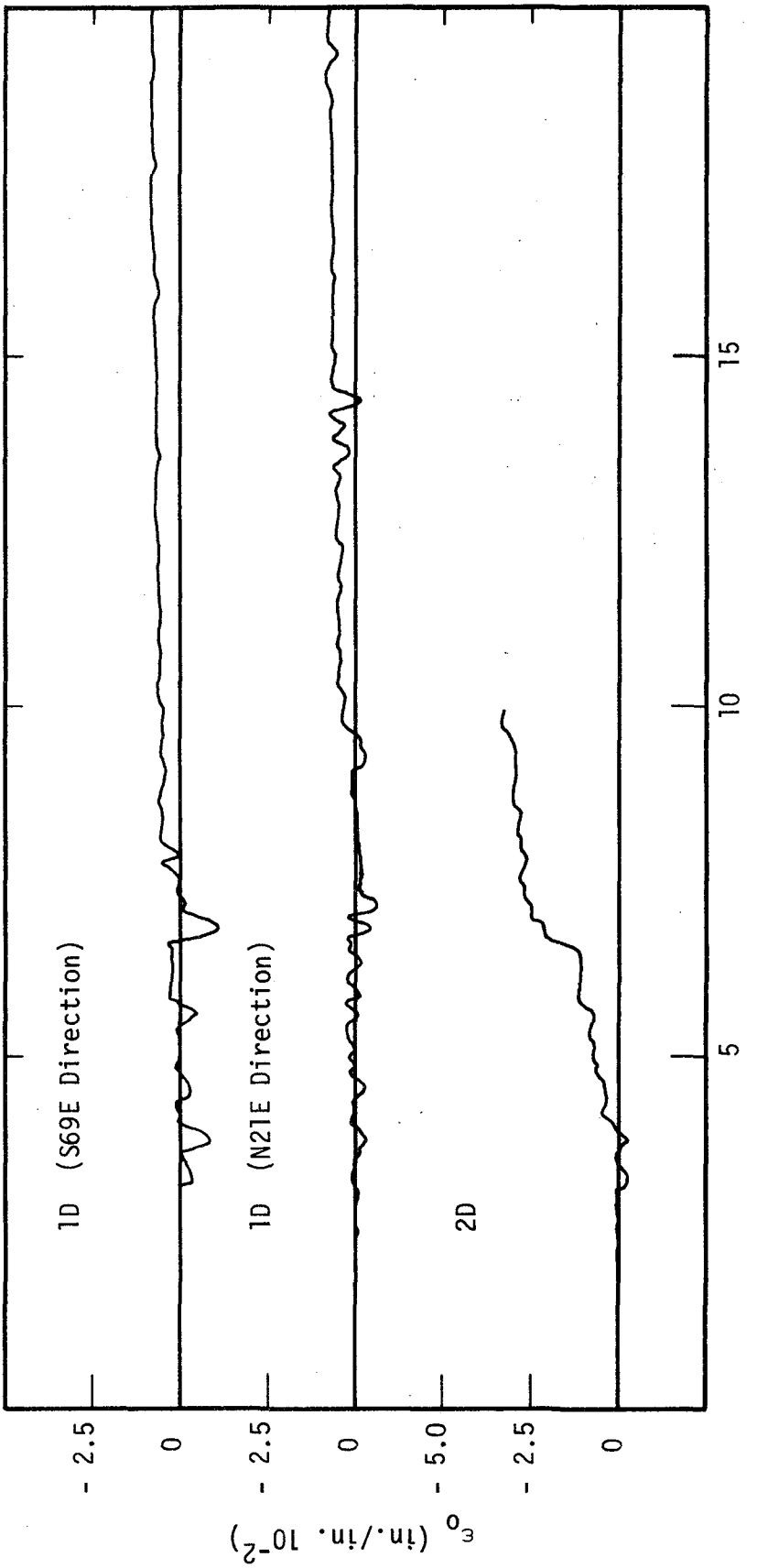

Fig. 3.18 Centroidal Strain-Time History, T = 0.4 System, Taft Record

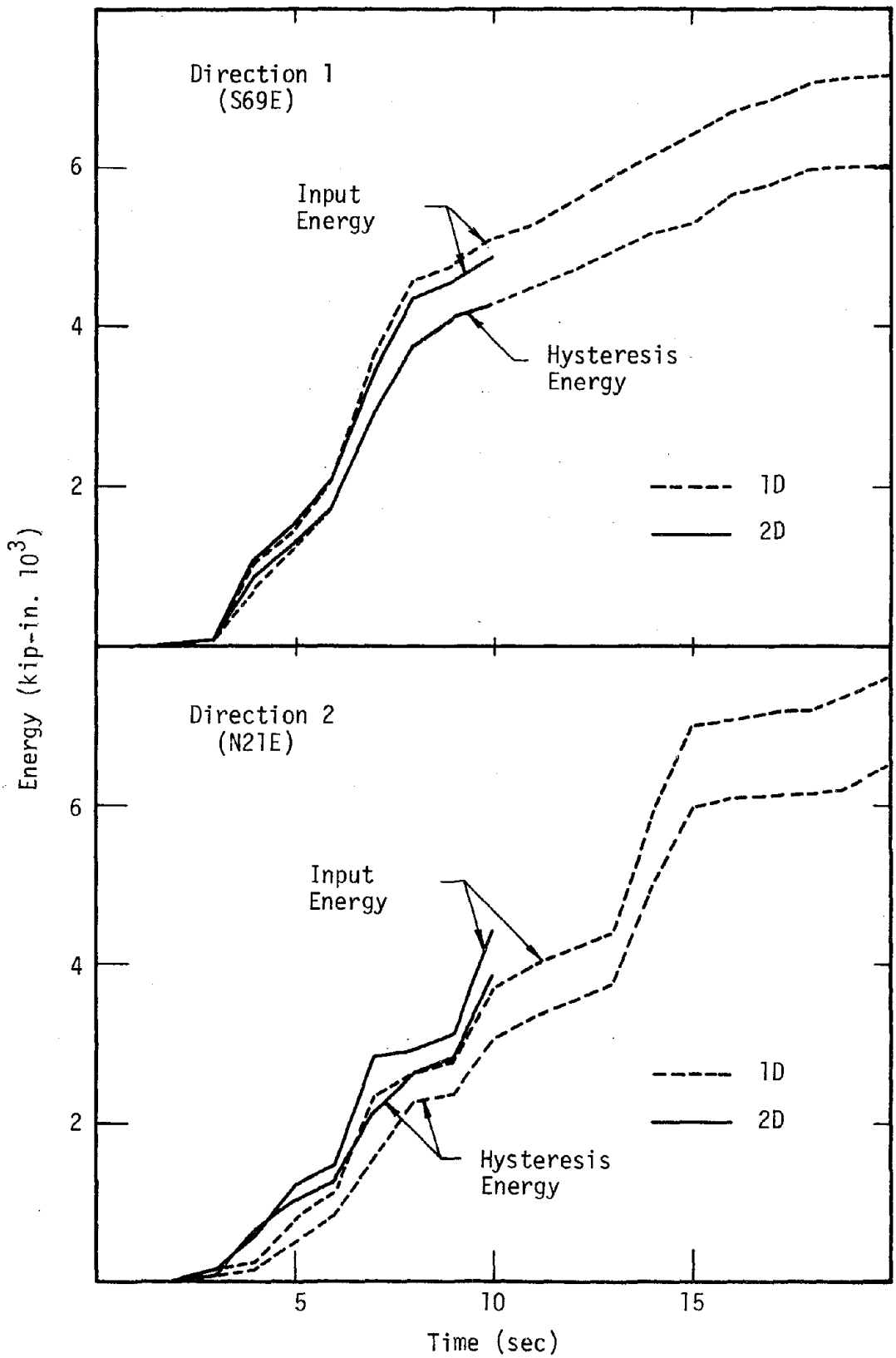

Fig. 3.19 Input and Hysteresis Energy-Time History, T = 0.4 System, Taft Record

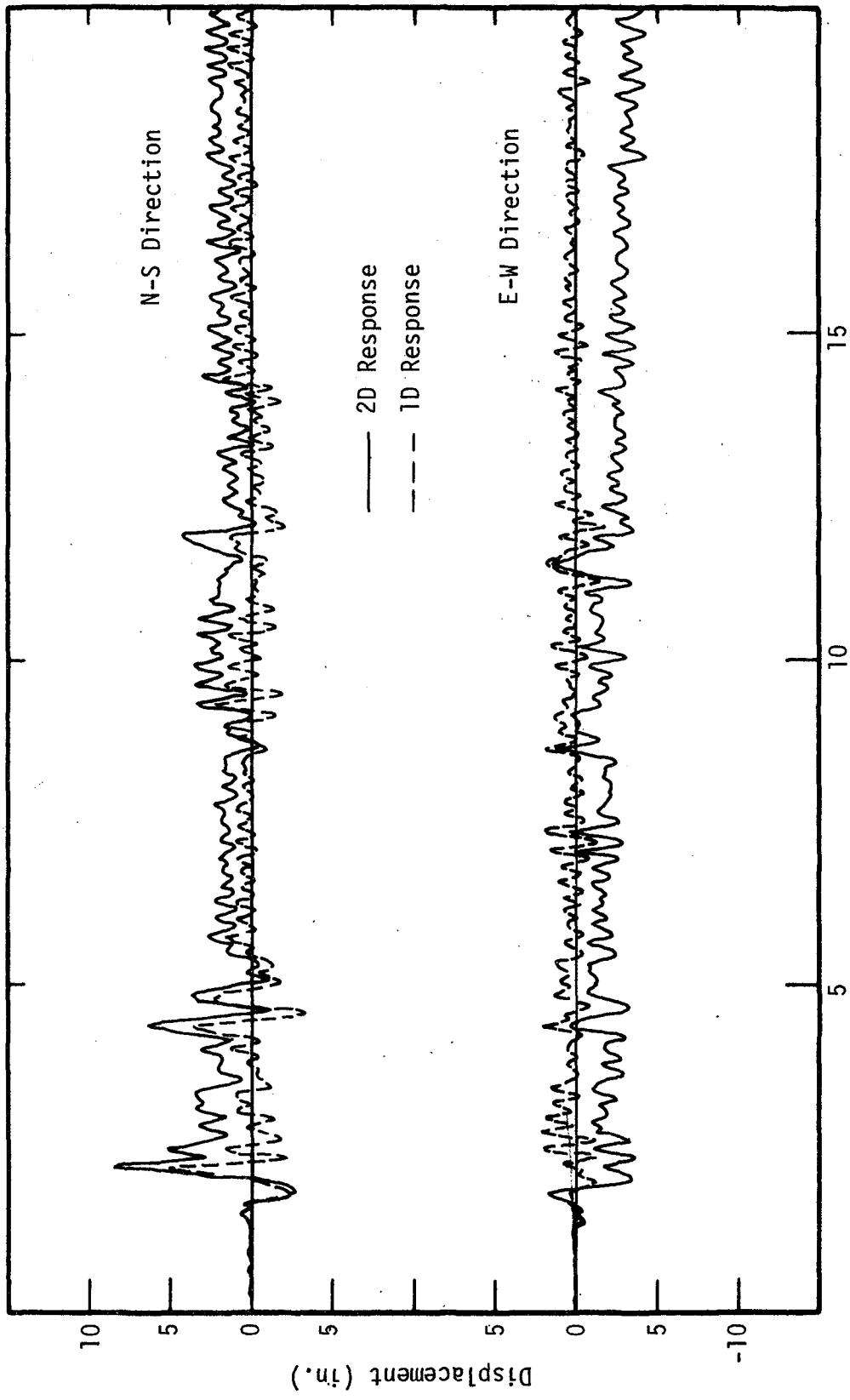

Fig. 3.20 Displacement Response, T = 0.2 System, El Centro Record

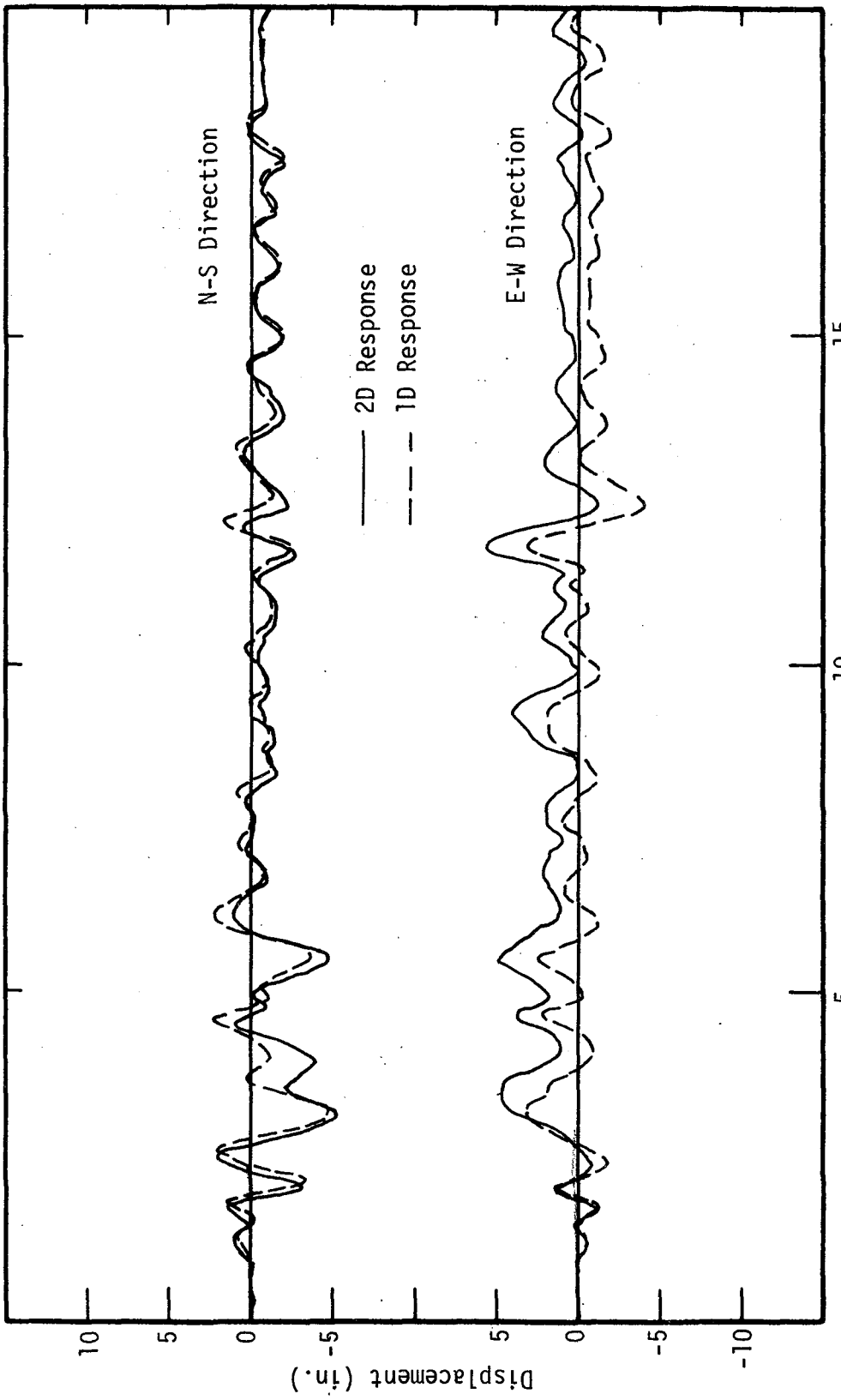

Fig. 3.21 Displacement Response, T = 0.8 System, El Centro Record

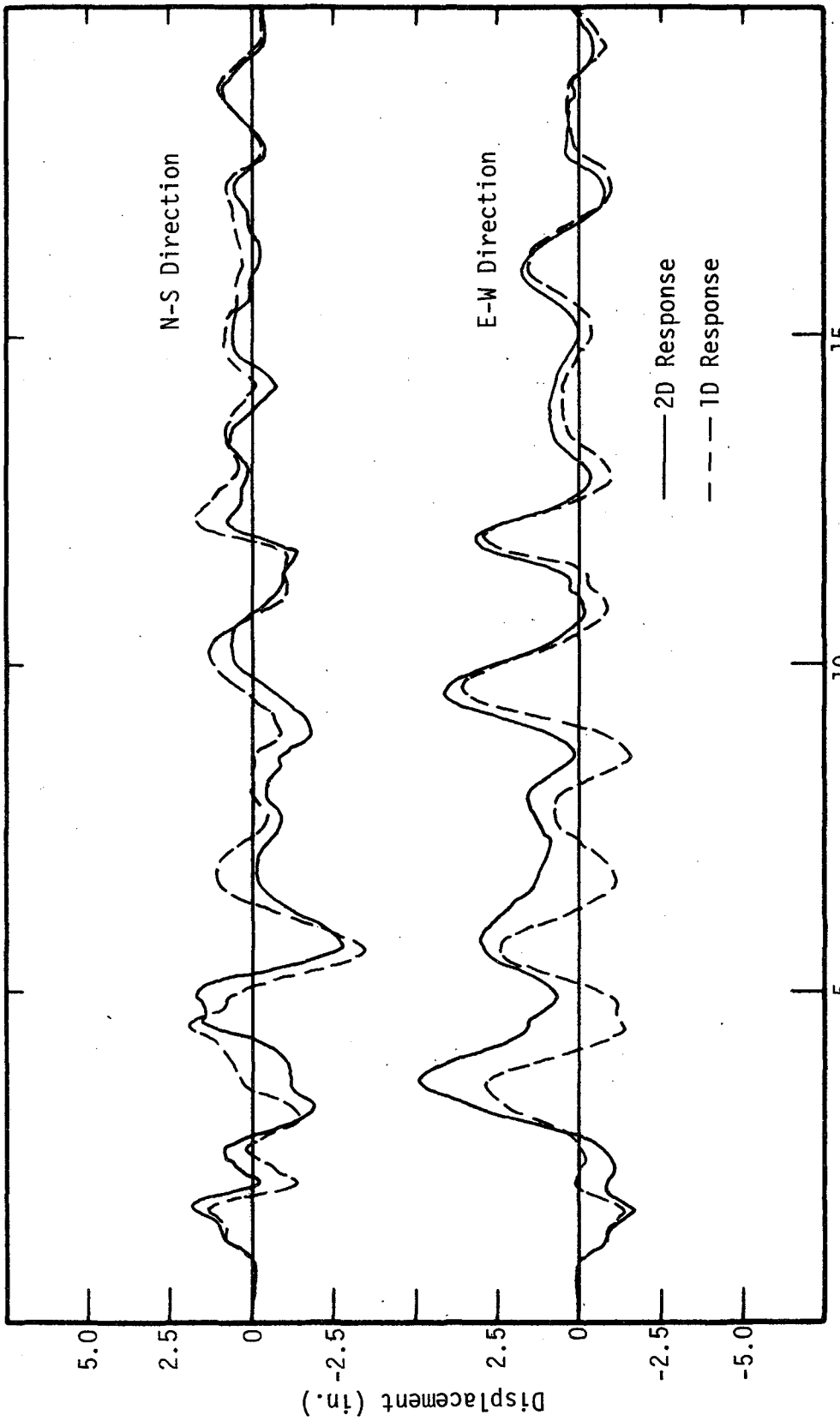

Fig. 3.22 Displacement Response, T = 1.6 System, El Centro Record

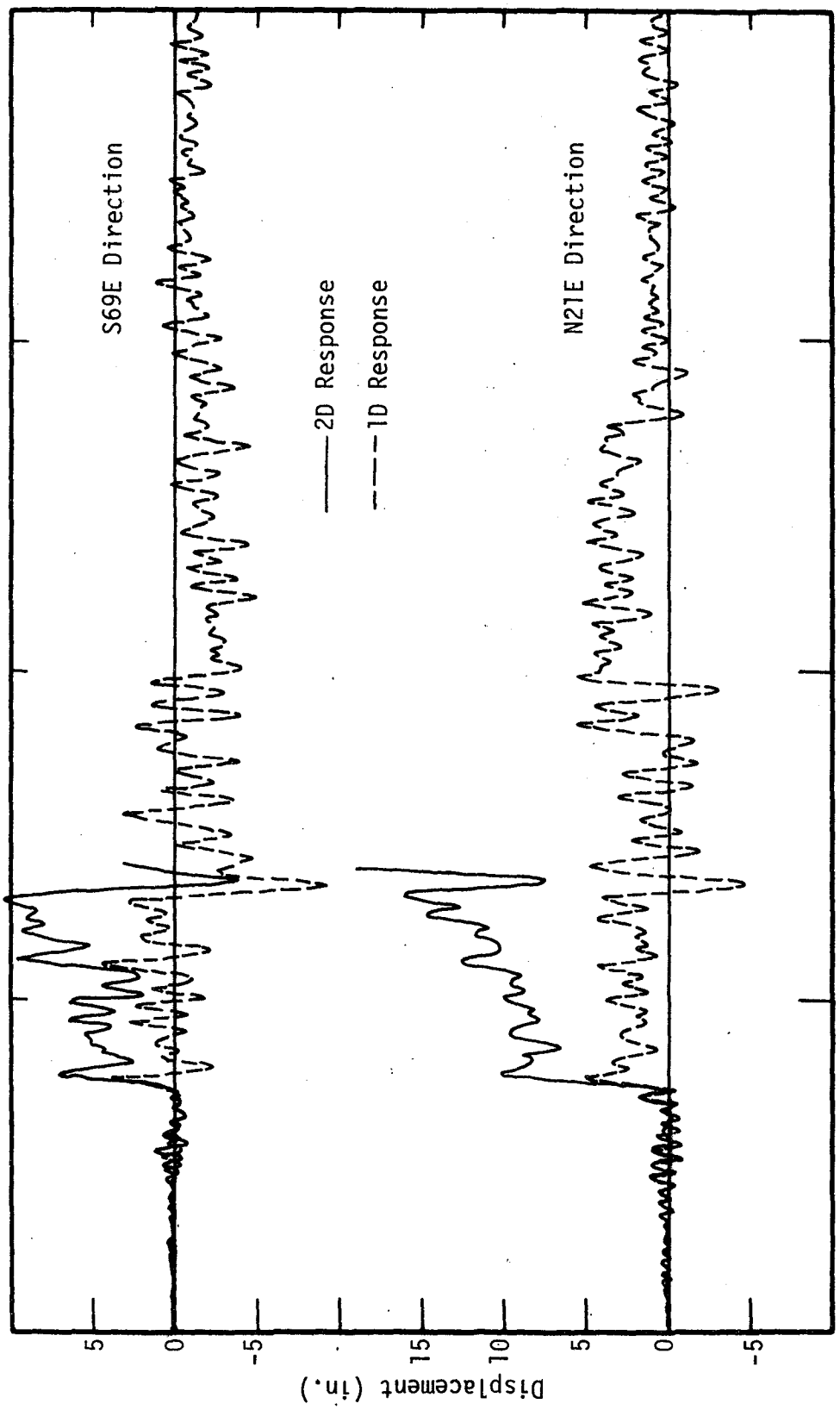

Fig. 3.23 Displacement Response, T = 0.2 System, Taft Record

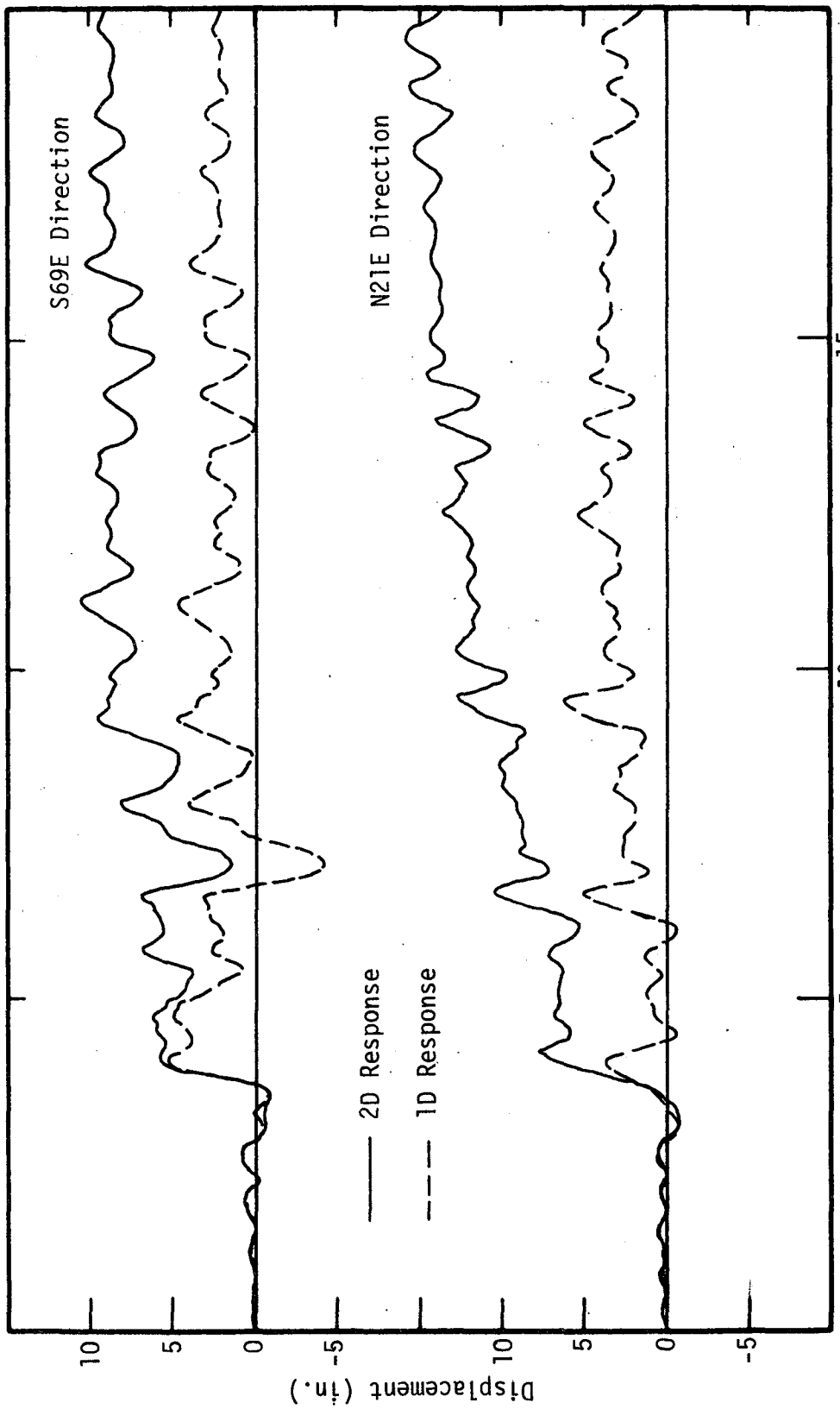

Fig. 3.24 Displacement Response, T = 0.8 System, Taft Record

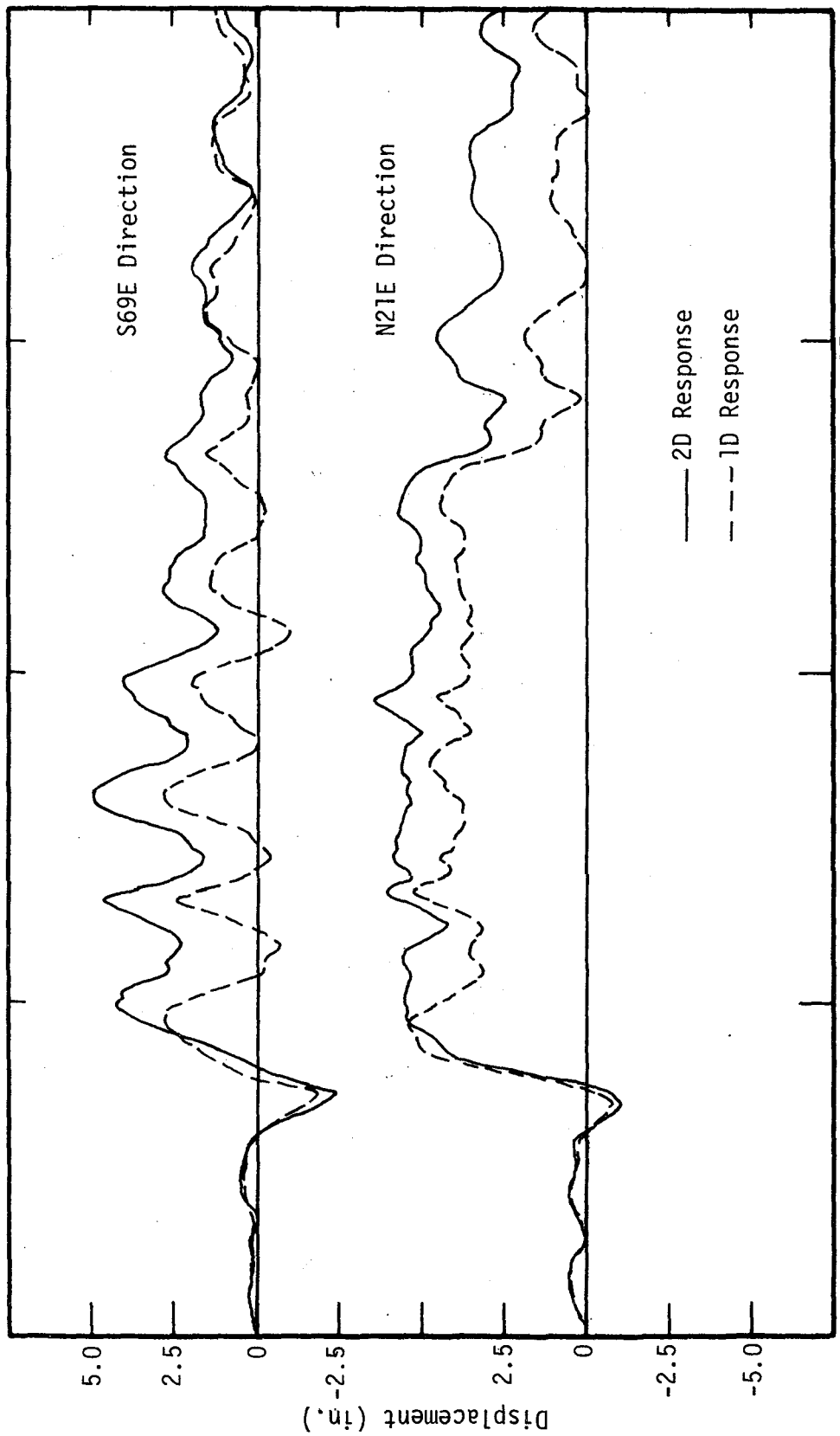

Fig. 3.25 Displacement Response, T = 1.6 System, Taft Record

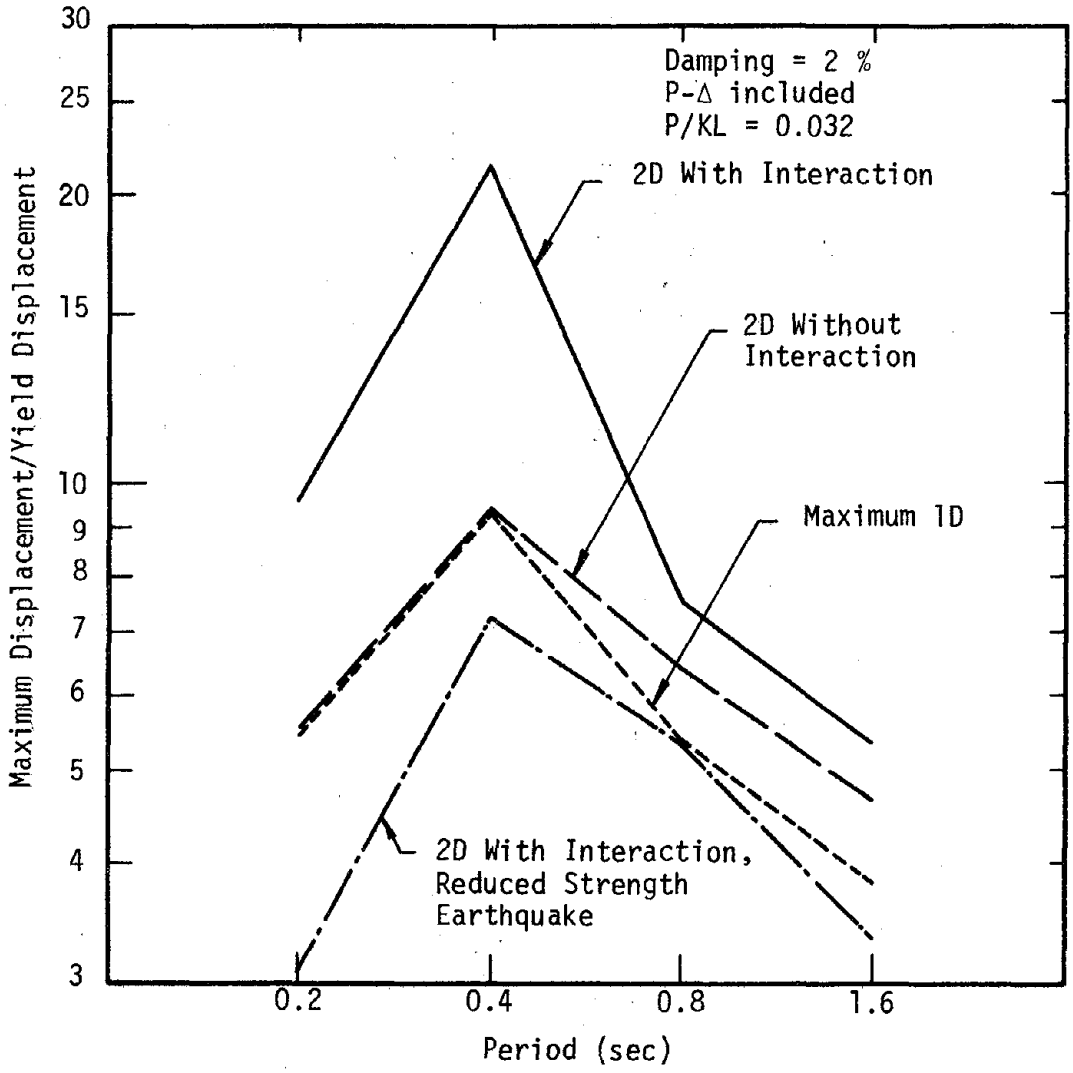

Fig. 3.26 Maximum Displacement Response of Systems with Design Strength, El Centro Record

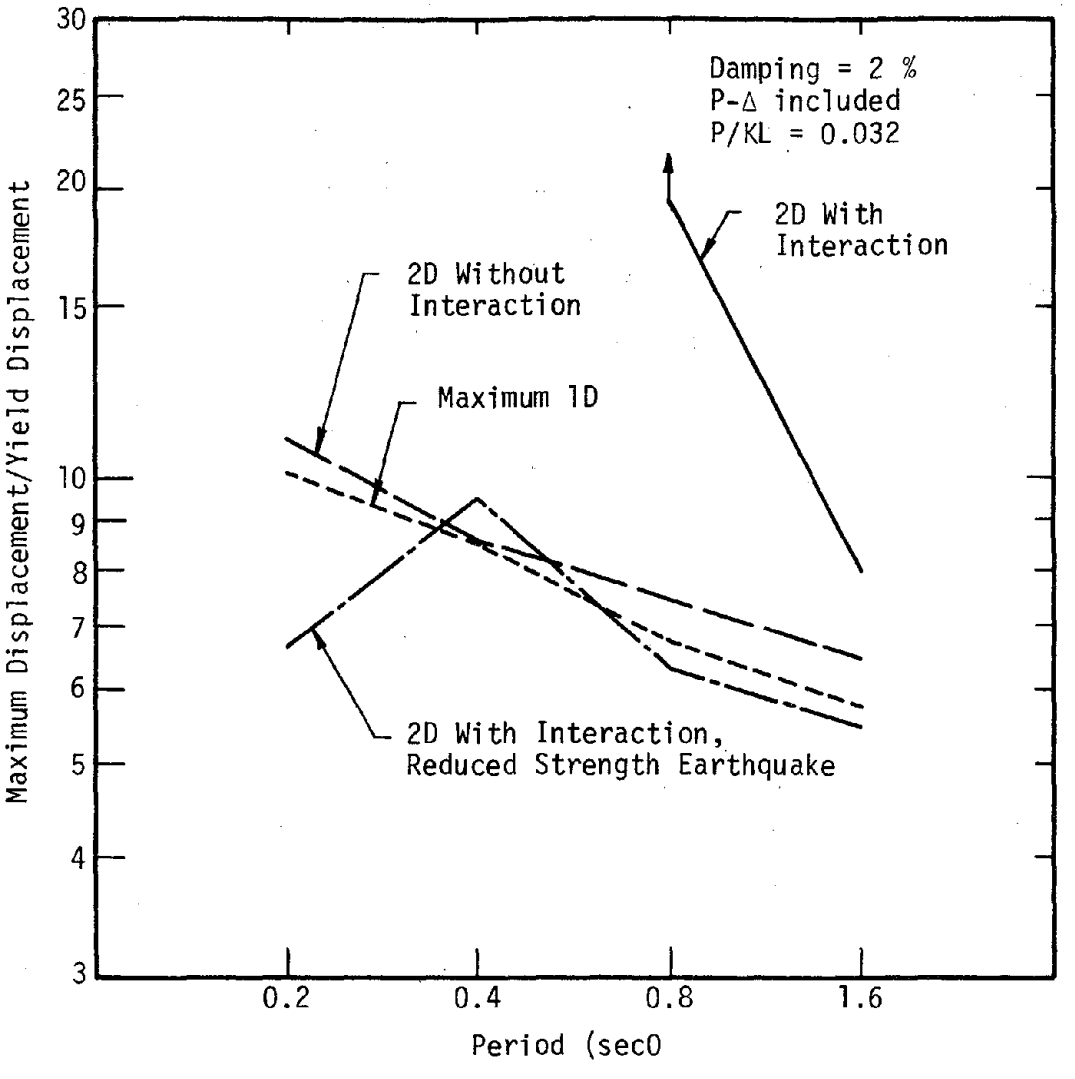

Fig. 3.27 **Maximum Displacement Response of Systems with Design Strength, Taft Record**

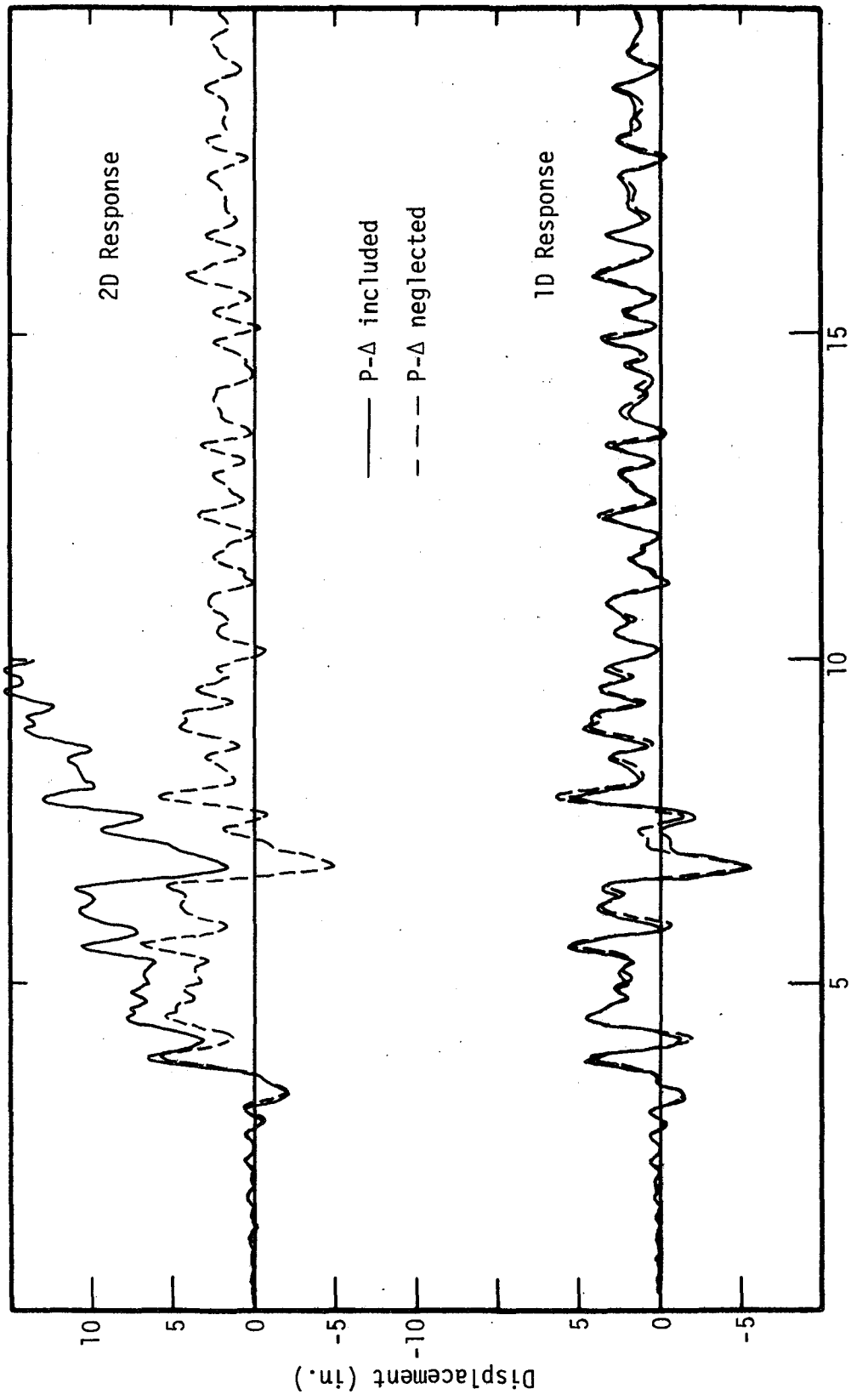

Fig. 3.28 Effect of P-Δ on Displacement Response, T = 0.4 System, Taft S69E Record

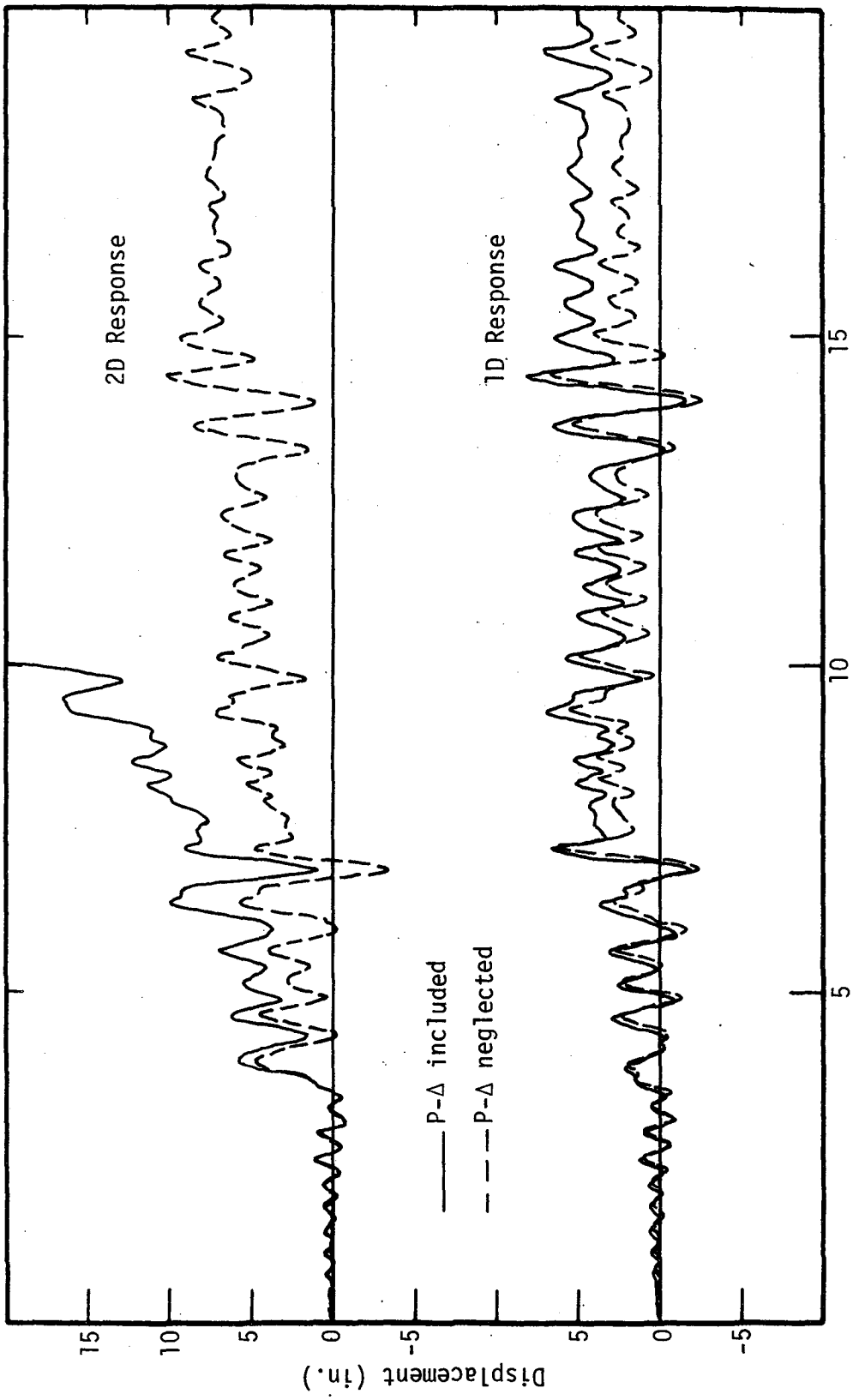

Fig. 3.29 Effect of P-Δ on Displacement Response, T = 0.4 System, Taft N21E Record

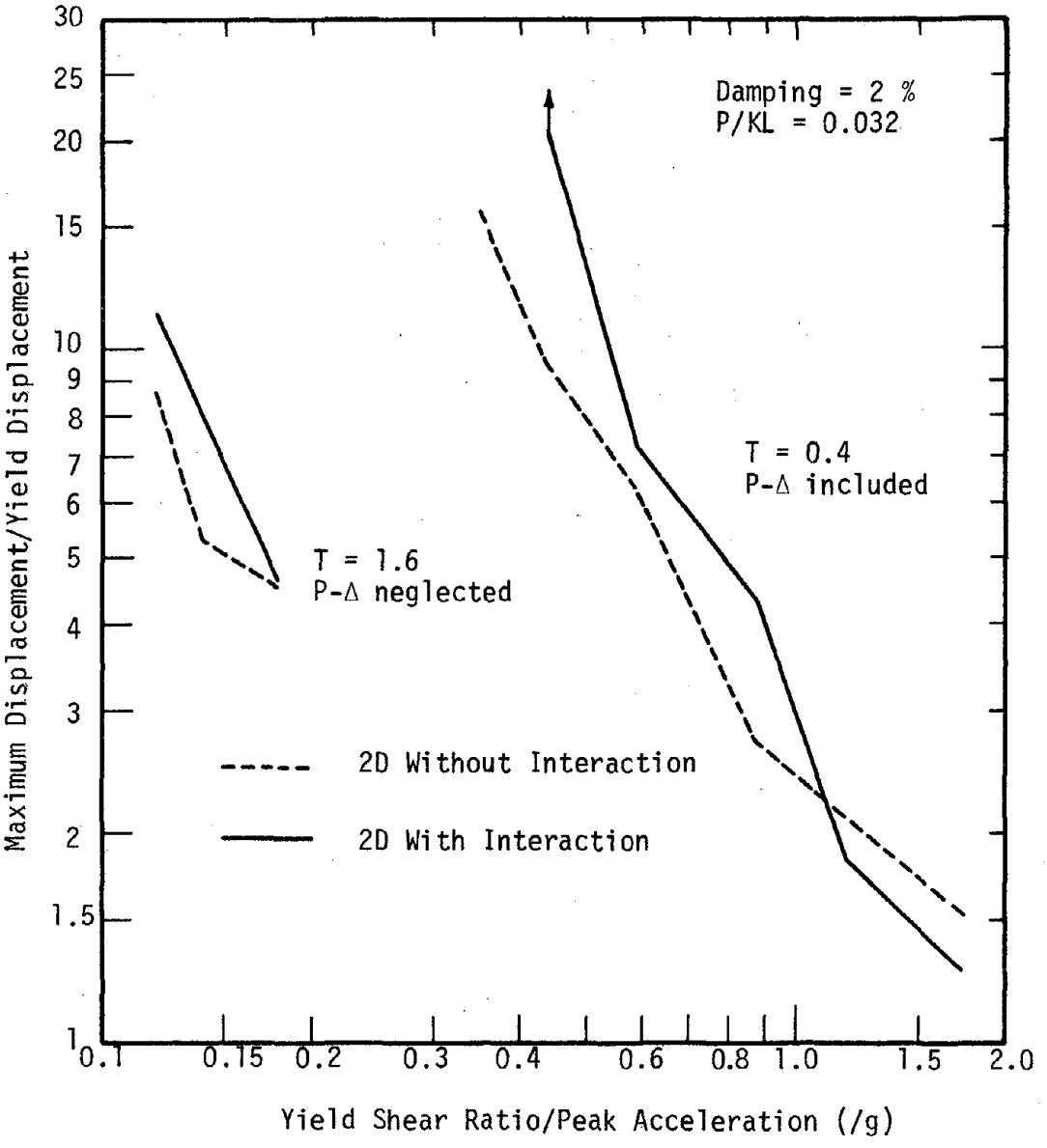

Fig. 3.30 Effect of System Strength on Maximum Displacement Response, El Centro Record

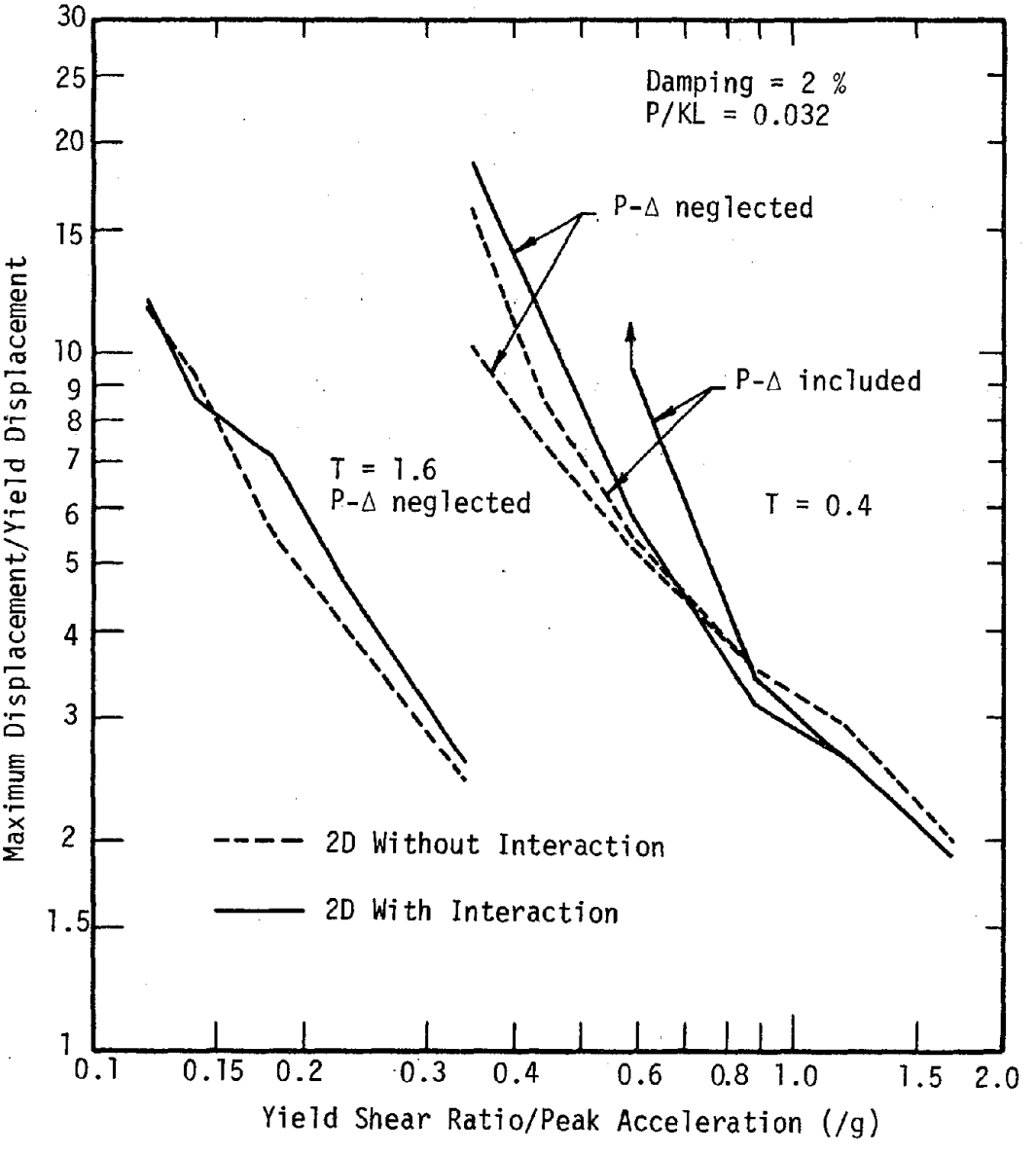

Fig. 3.31 Effect of System Strength on Maximum Displacement Response, Taft Record

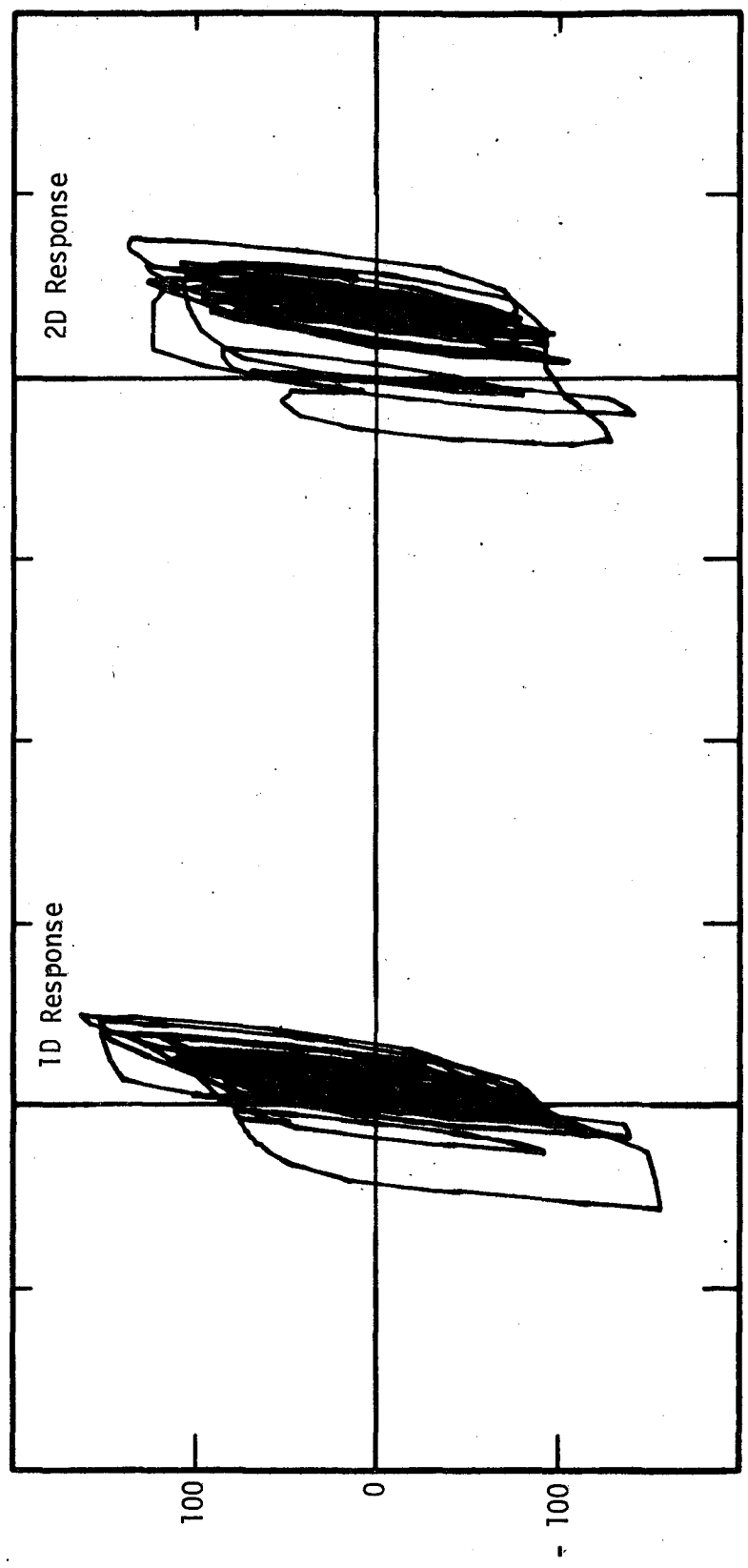

Fig. 3.32 Shear Displacement Response, P = - 562 kips, T = 0.4 System, Taft S69E Record

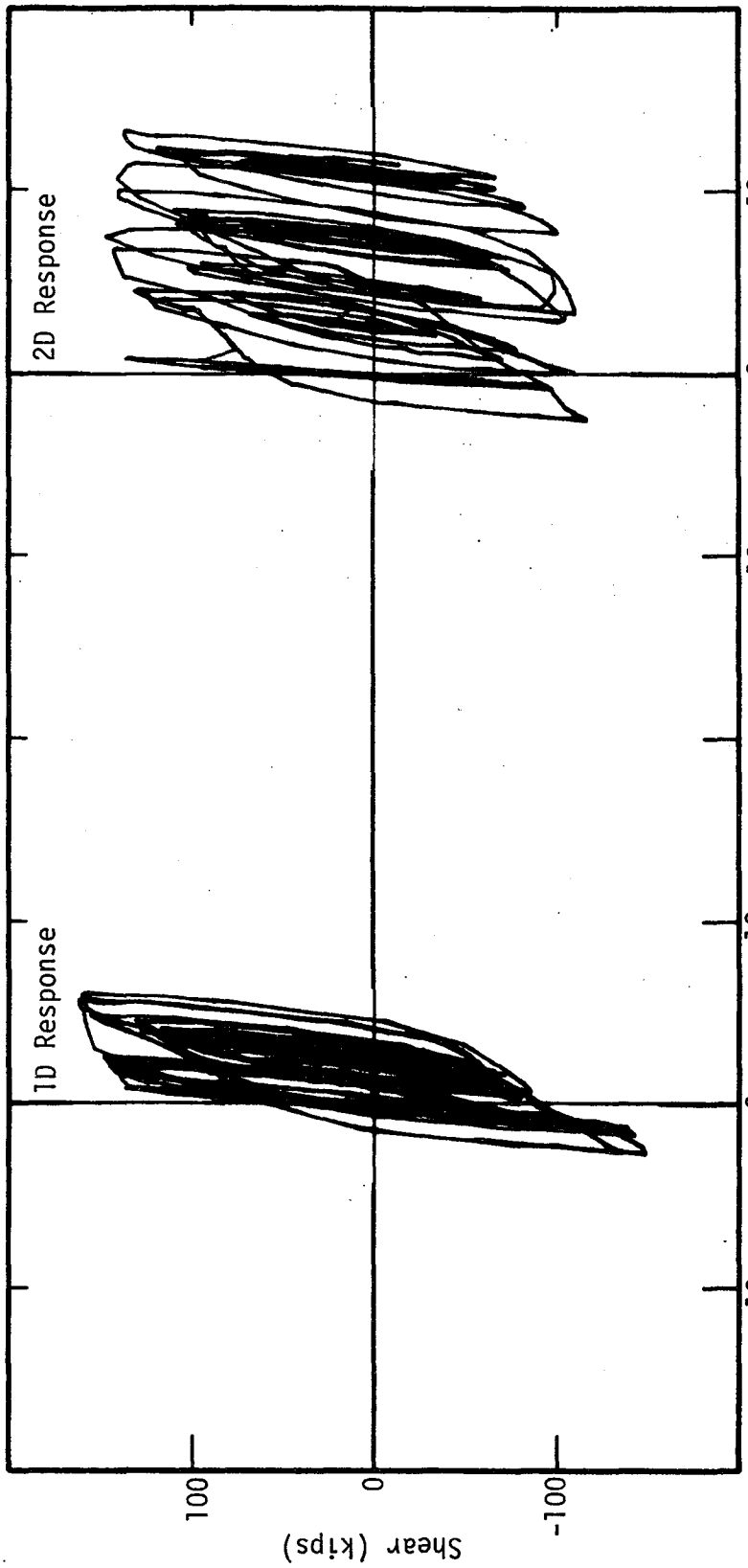

Fig. 3.33 Shear-Displacement Response, P = - 562 kips, T = 0.4 System, Taft N21E Record

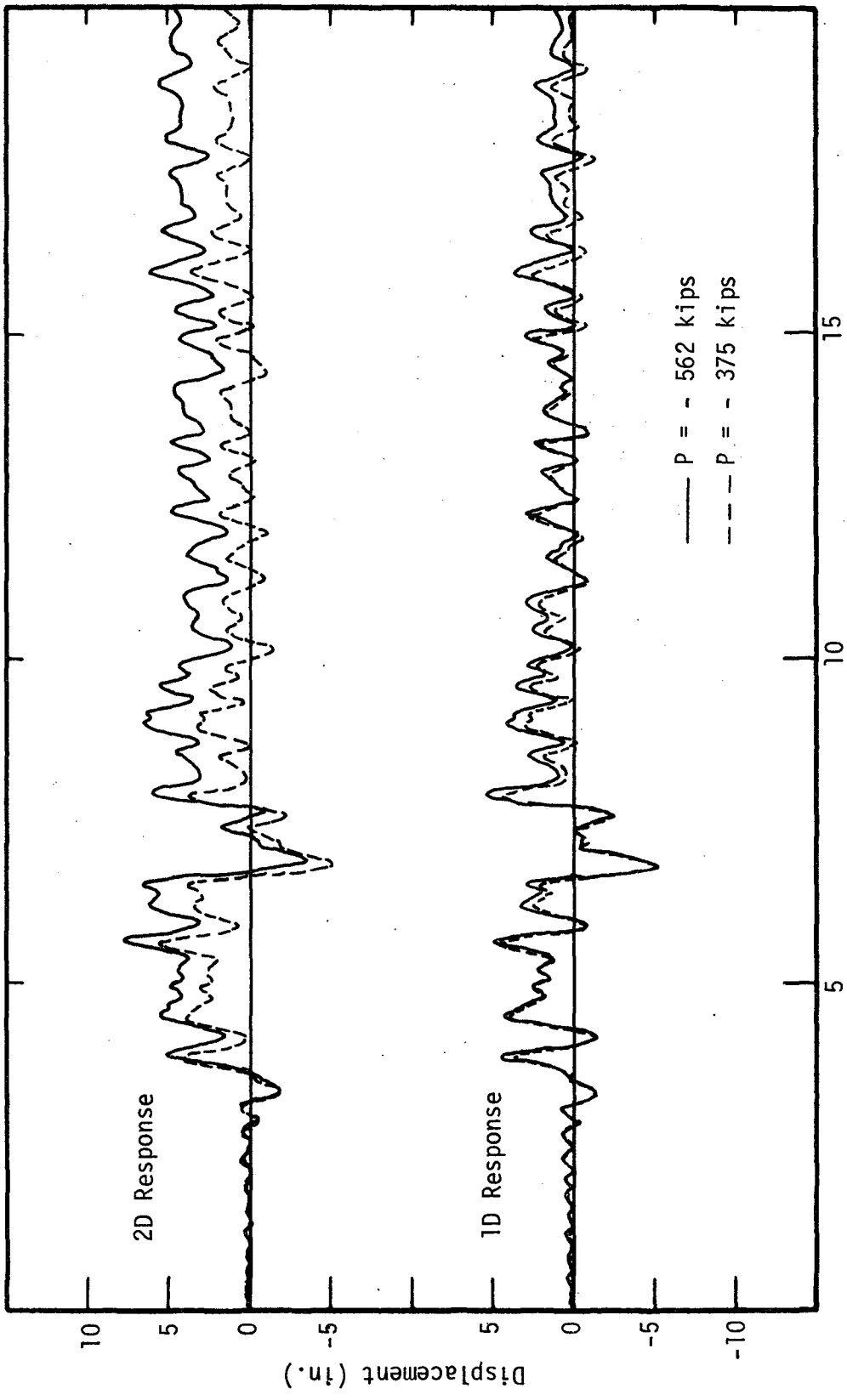

Fig. 3.34 Effect of Axial Load on Displacement Response, T = 0.4 System, Taft S69E Record

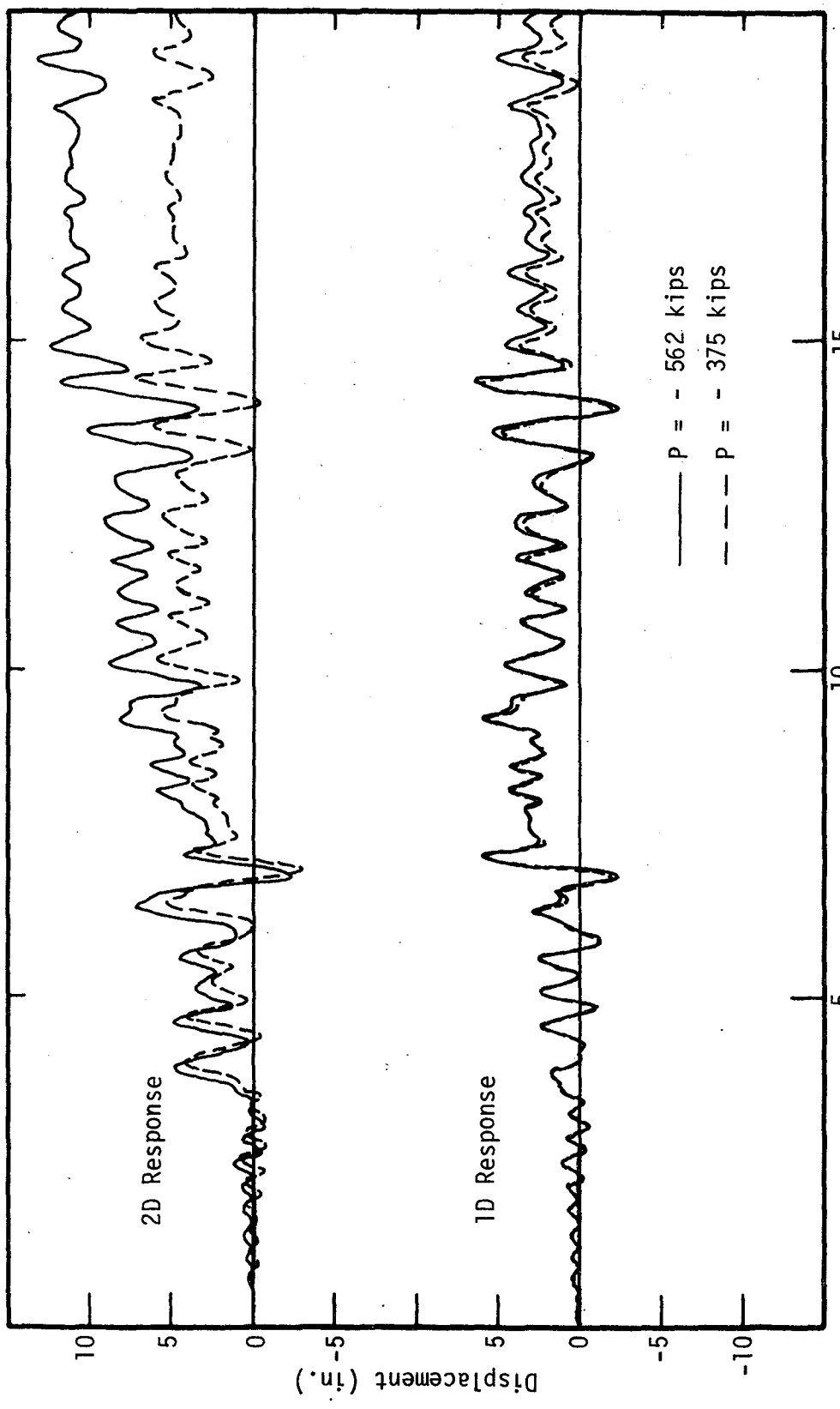

Fig. 3.35 Effect of Axial Load on Displacement Response, T = 0.4 System, Taft N21E Record

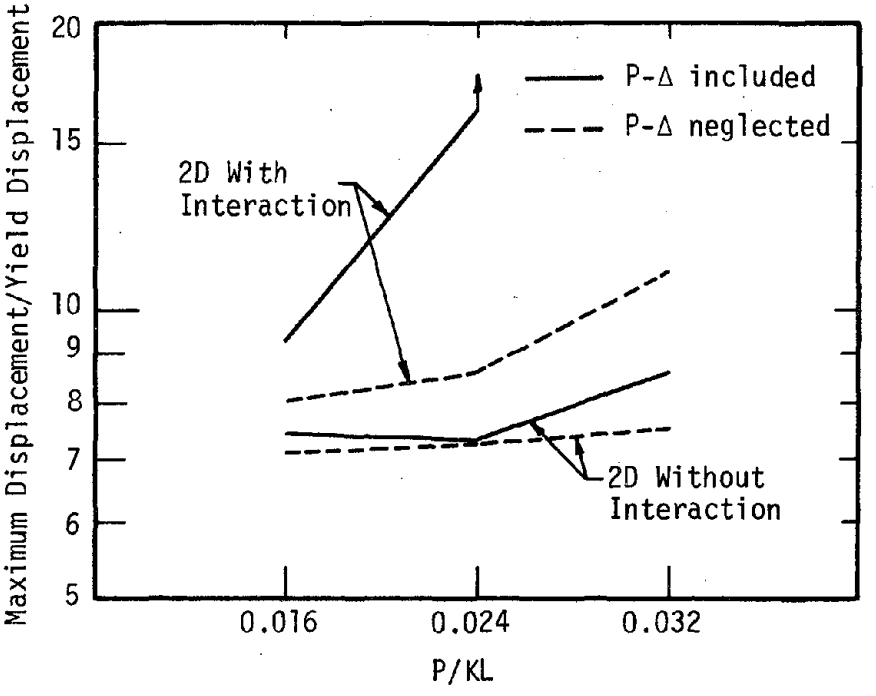

Fig. 3.36 Effect of Axial Load on Maximum Displacement Response, T = 0.4 System, Taft Record

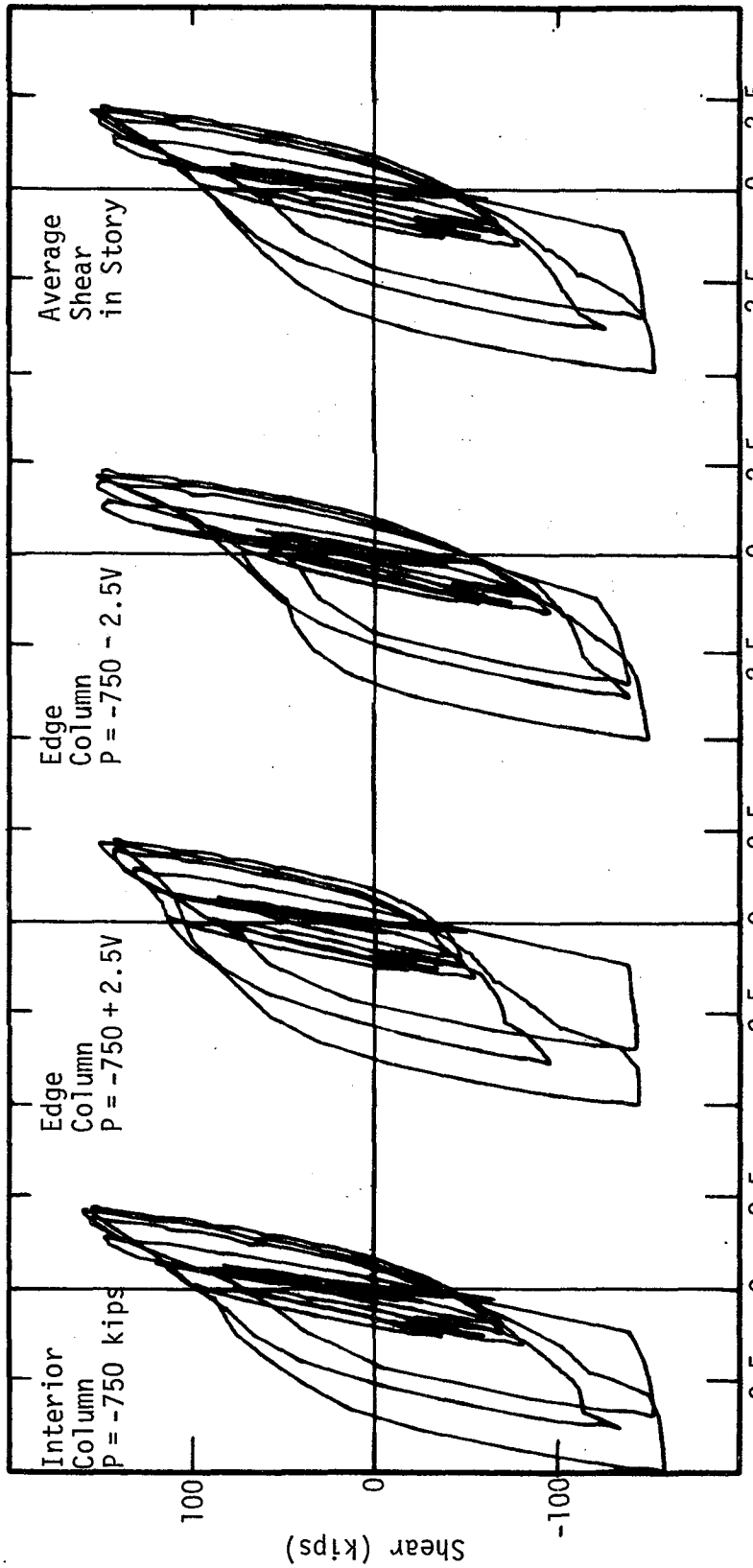

Fig. 3.37 Shear-Displacement Response of Edge Columns Subjected to 1D Displacement Response of T = 0.8 Interior Column to El Centro, N-S Record

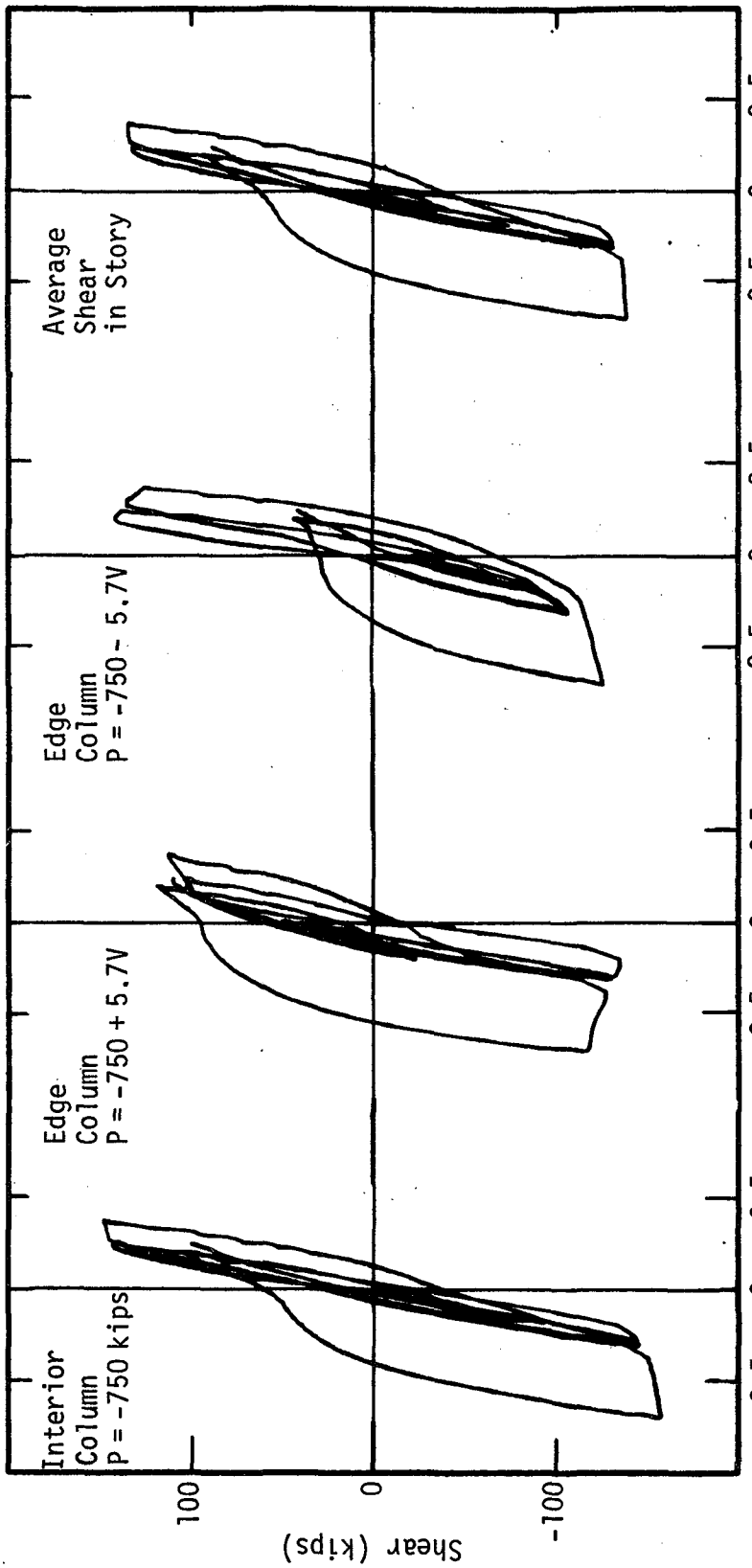

Fig. 3.38 Shear-Displacement Response of Edge Columns Subjected to 1D Displacement Response of T = 1.6 Interior Column to El Centro, N-S Record

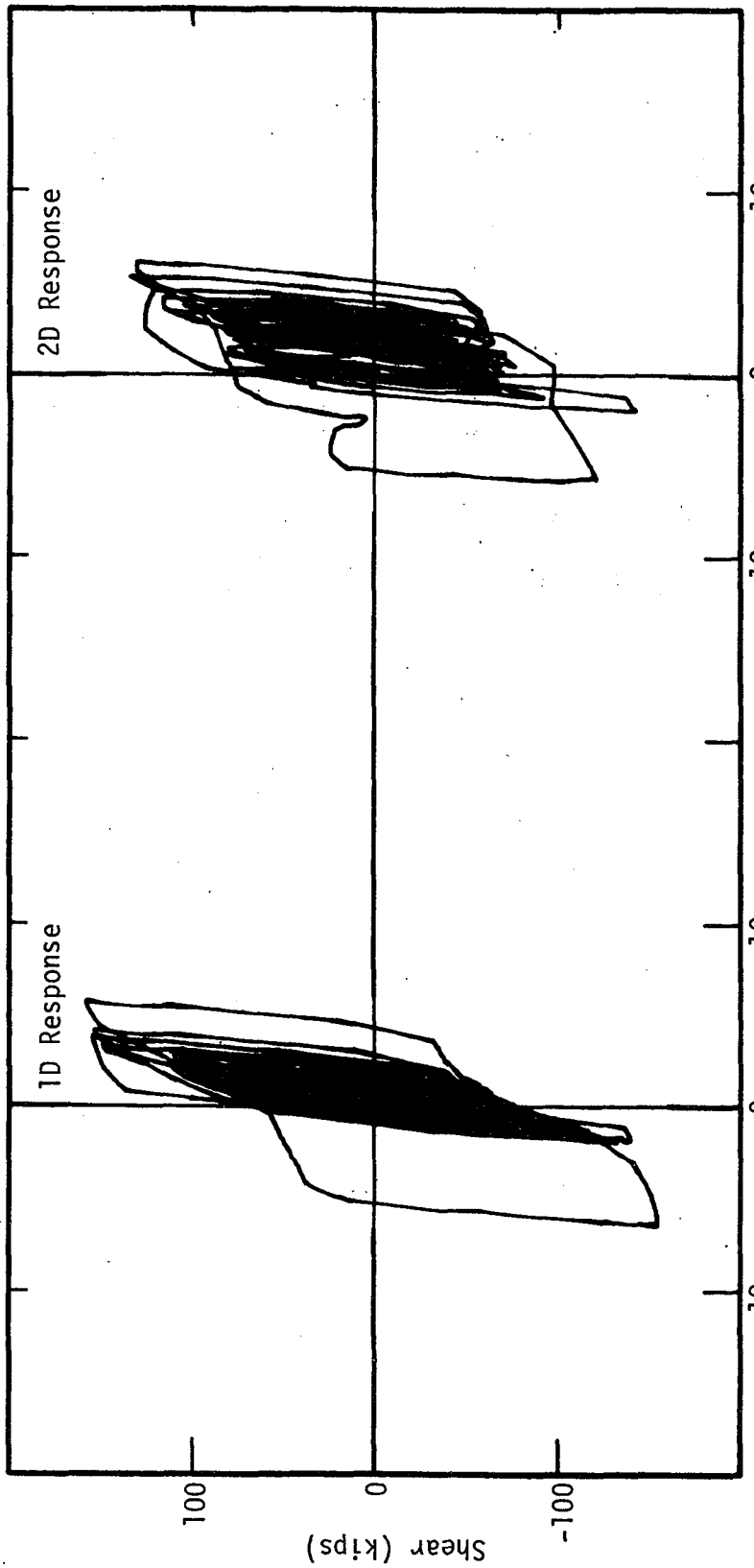

Fig. 3.39 Shear-Displacement Response, Bilinear Steel, 3% Hardening Slope, P = - 562, T = 0.4 System, Taft S69E Record

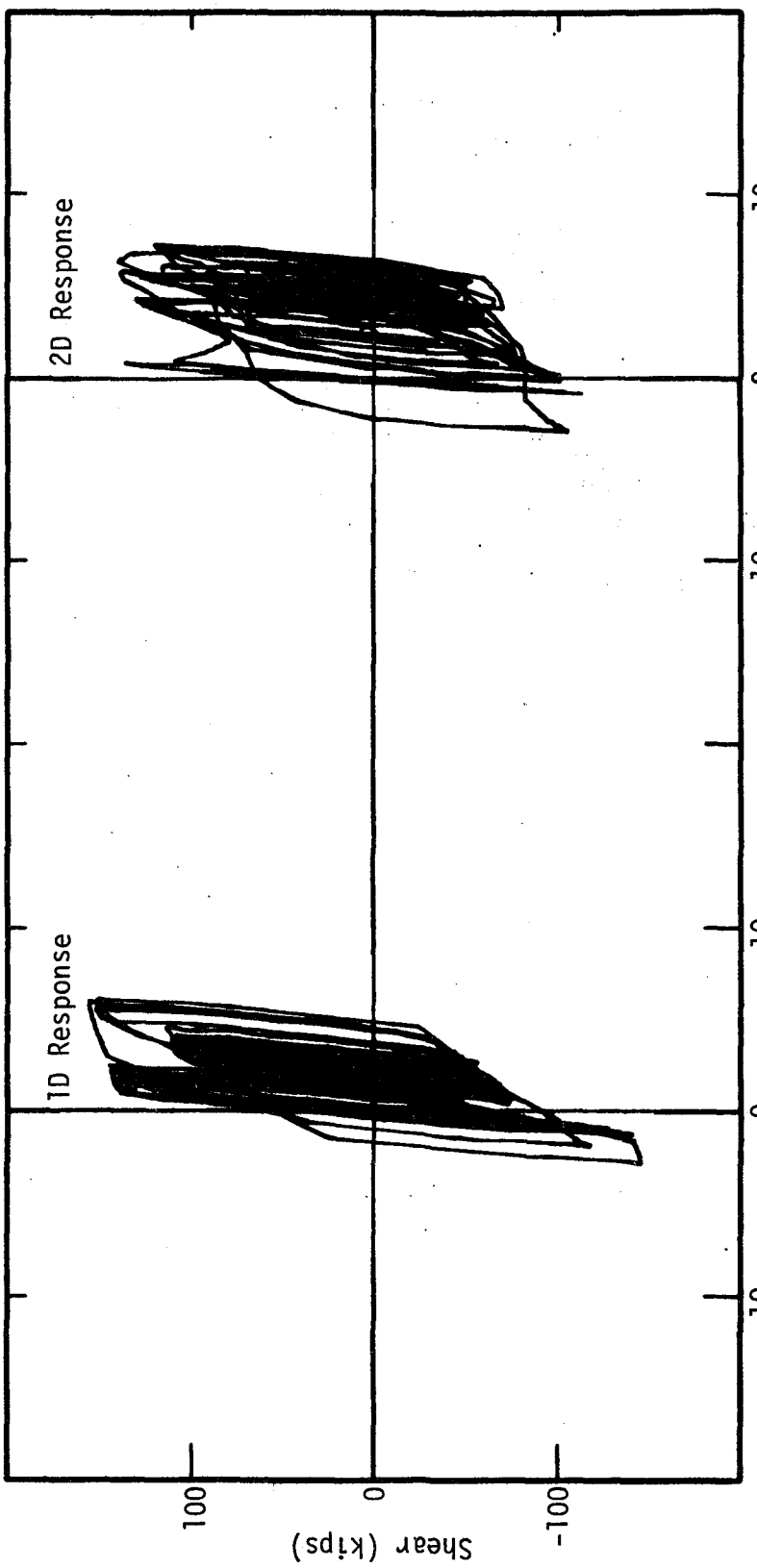

Fig. 3.40 Shear-Displacement Response, Bilinear Steel, 3% Hardening Slope, P = - 562, T = 0.4 System, Taft N21E Record

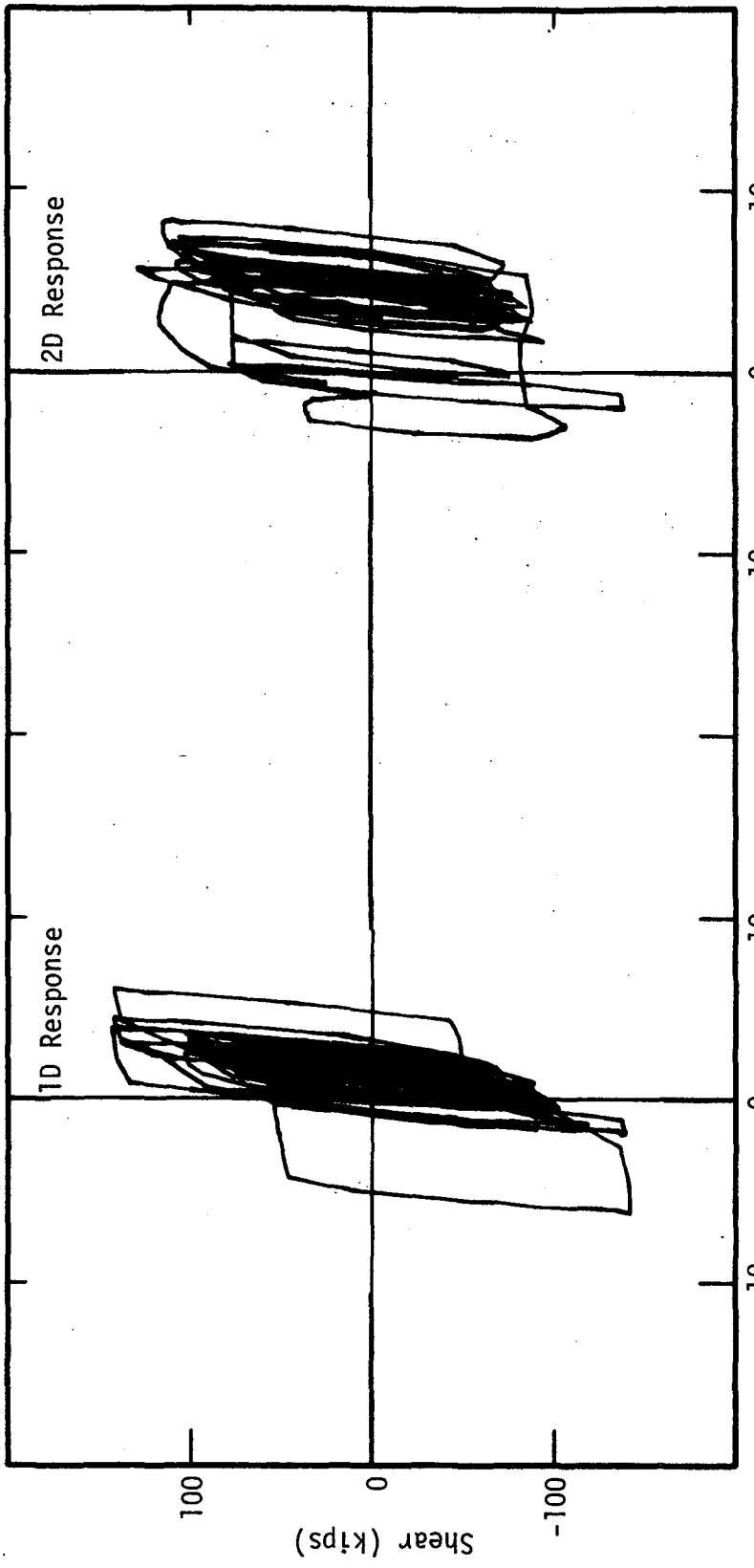

Fig. 3.41 Shear-Displacement Response, Bilinear Steel, 1.5% Hardening Slope, P = - 562, T = 0.4 System, Taft S69E Record

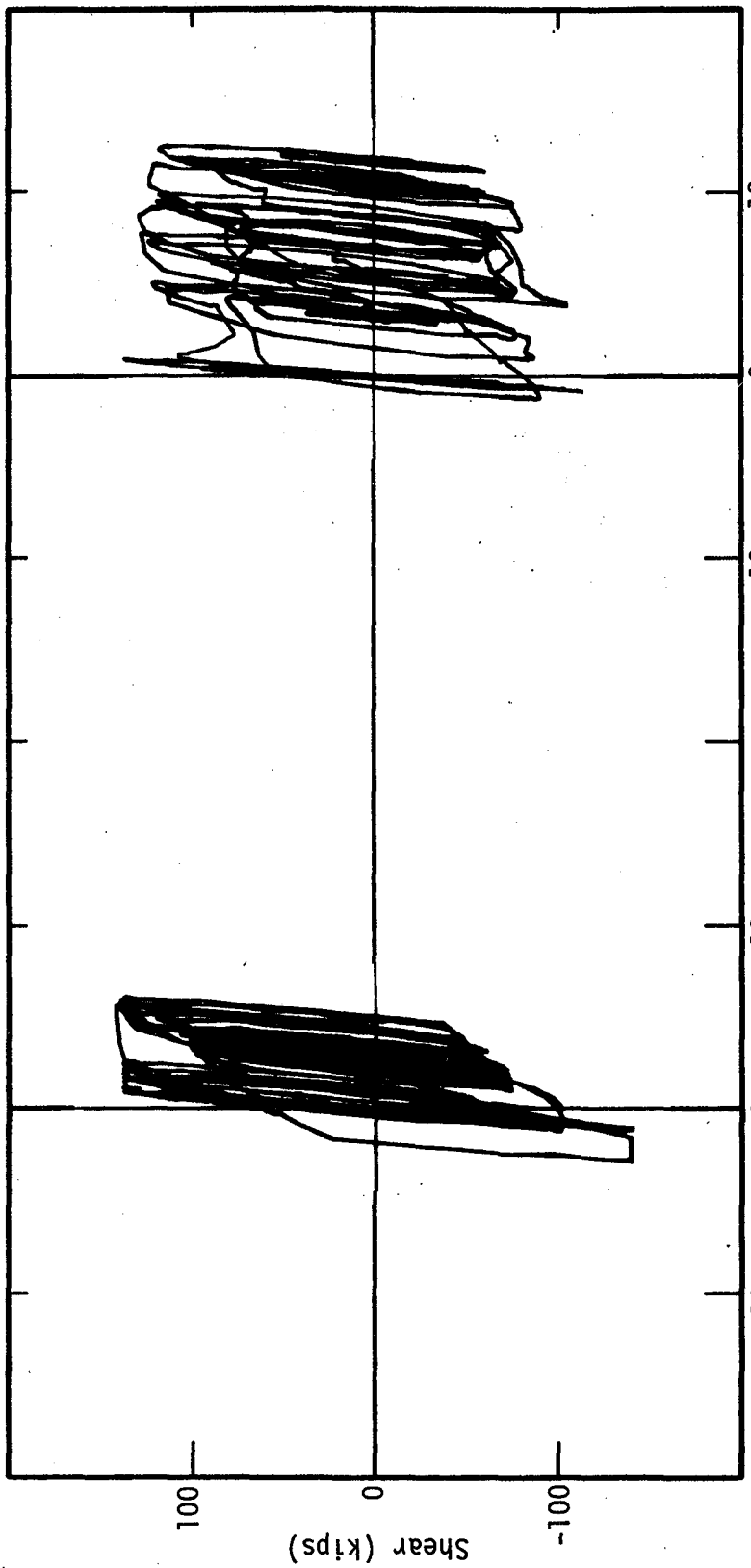

Fig. 3.42 Shear-Displacement Response, Bilinear Steel, 1.5% Hardening Slope, P = - 562, T = 0.4 System, Taft N21E Record

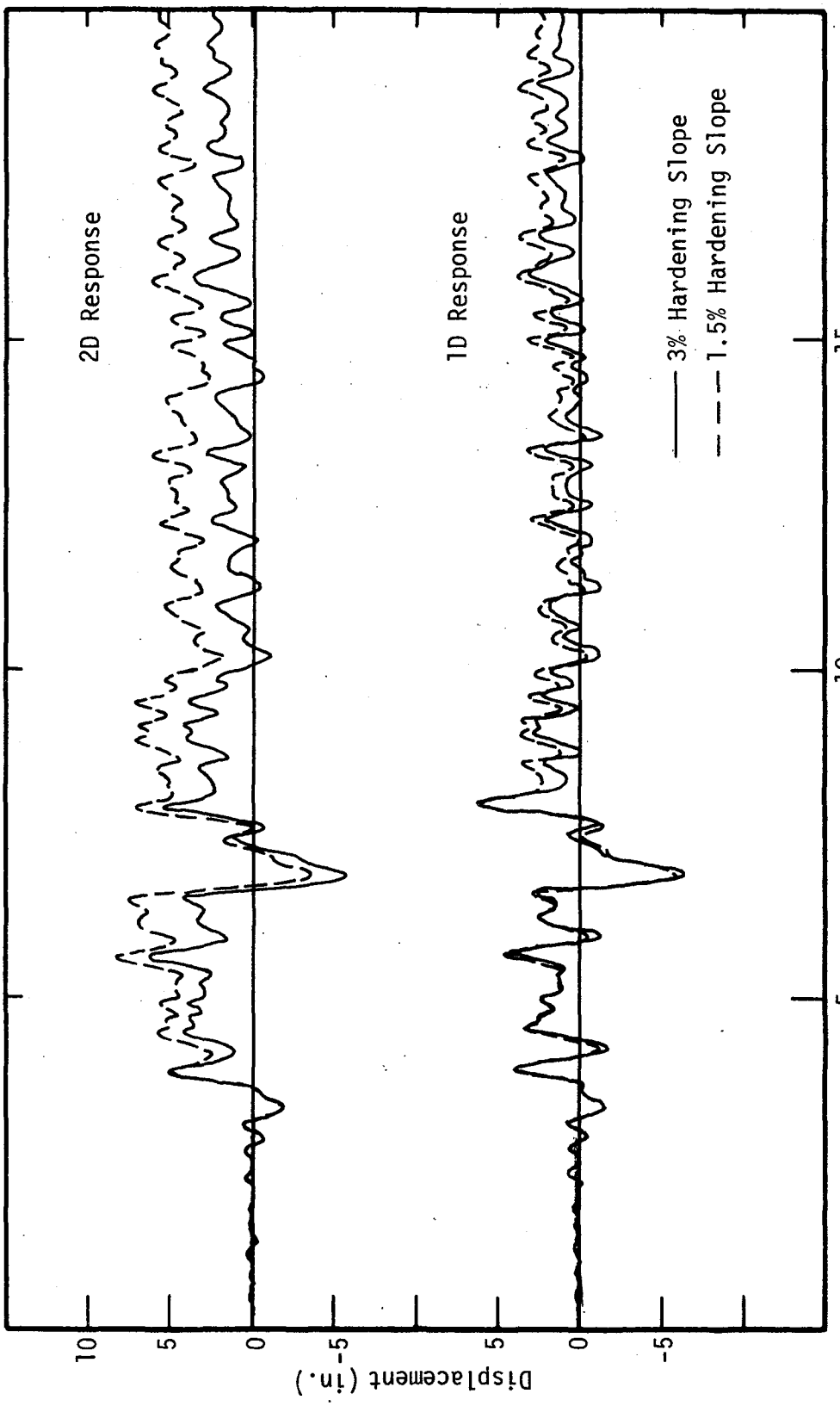

Fig. 3.43 Effect of Hardening Slope of Bilinear Steel on Displacement Response, P = - 562, T = 0.4 System, Taft S69E Record

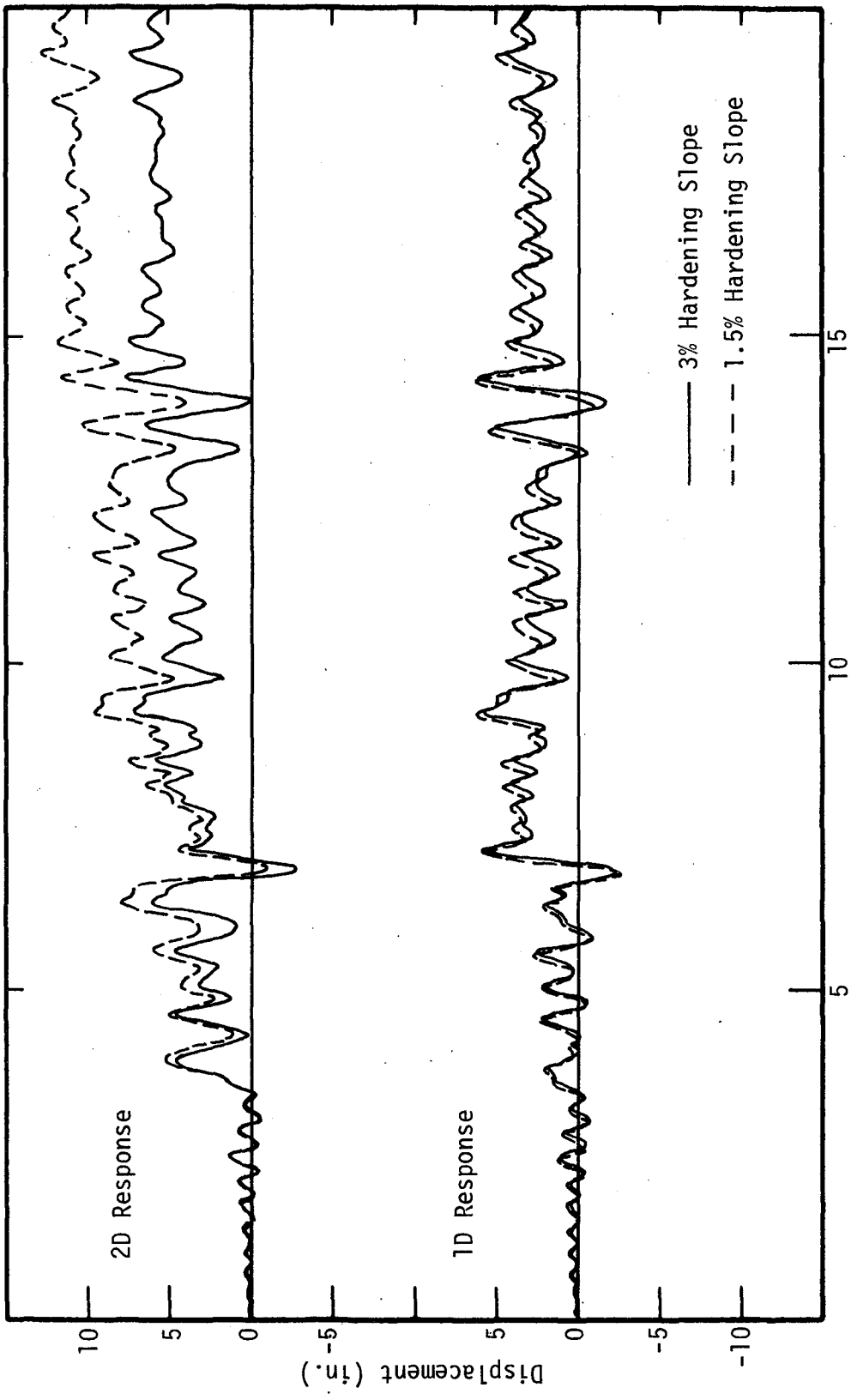

Fig. 3.44 Effect of Hardening Slope of Bilinear Steel on Displacement Response, P = - 562, T = 0.4 System, Taft N21E Record

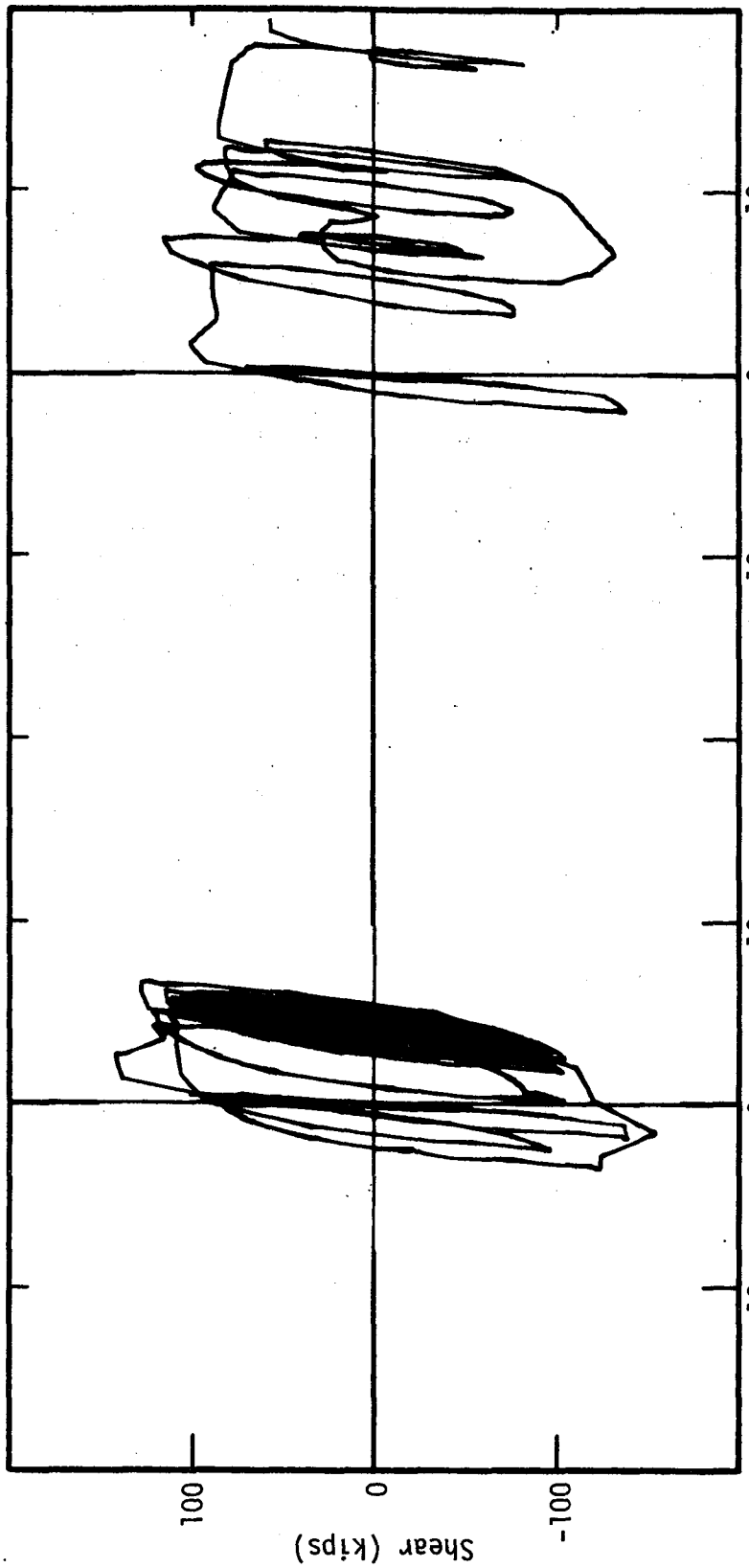

Fig. 3.45 Shear-Displacement Response, Concrete Confined by Ties, Ω = 40, P = - 562, T = 0.4 System, Taft S69E Record

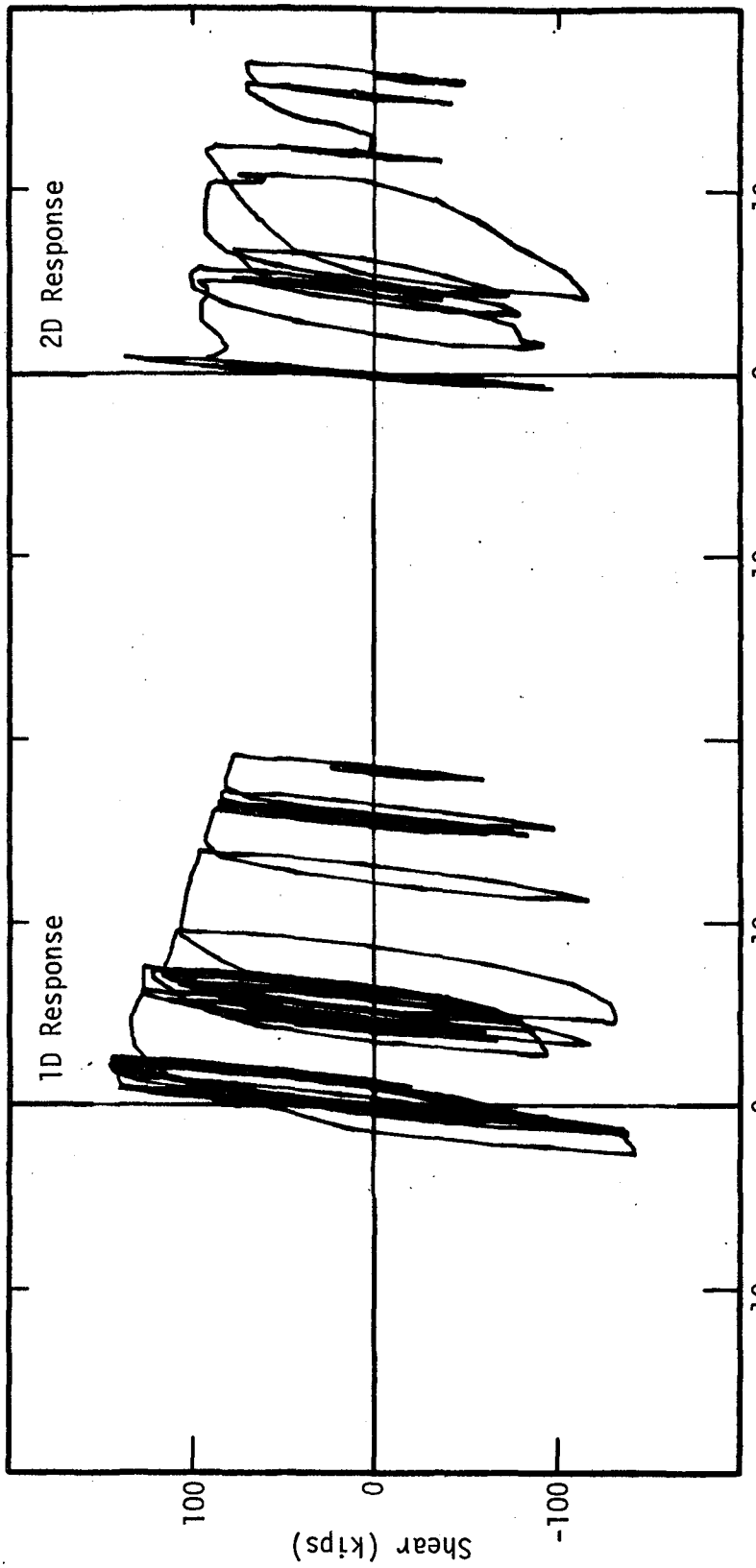

Fig. 3.46 Shear-Displacement Response, Concrete Confined by Ties, Ω = 40, P = - 562, T = 0.4 System, Taft N21E Record

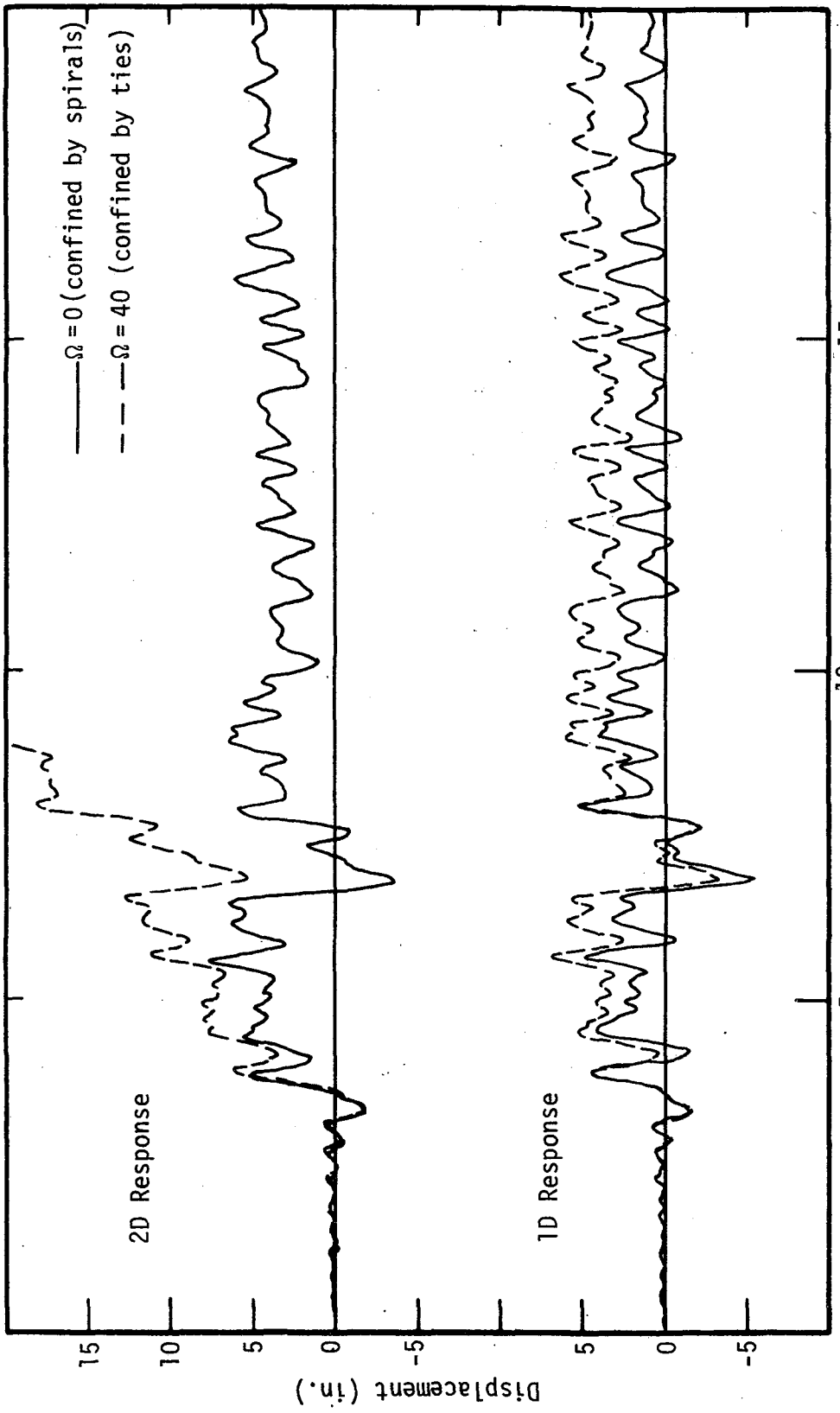

Fig. 3.47 Effect of Concrete Confinement on Displacement Response, P = - 562, T = 0.4 System, Taft S69E Record

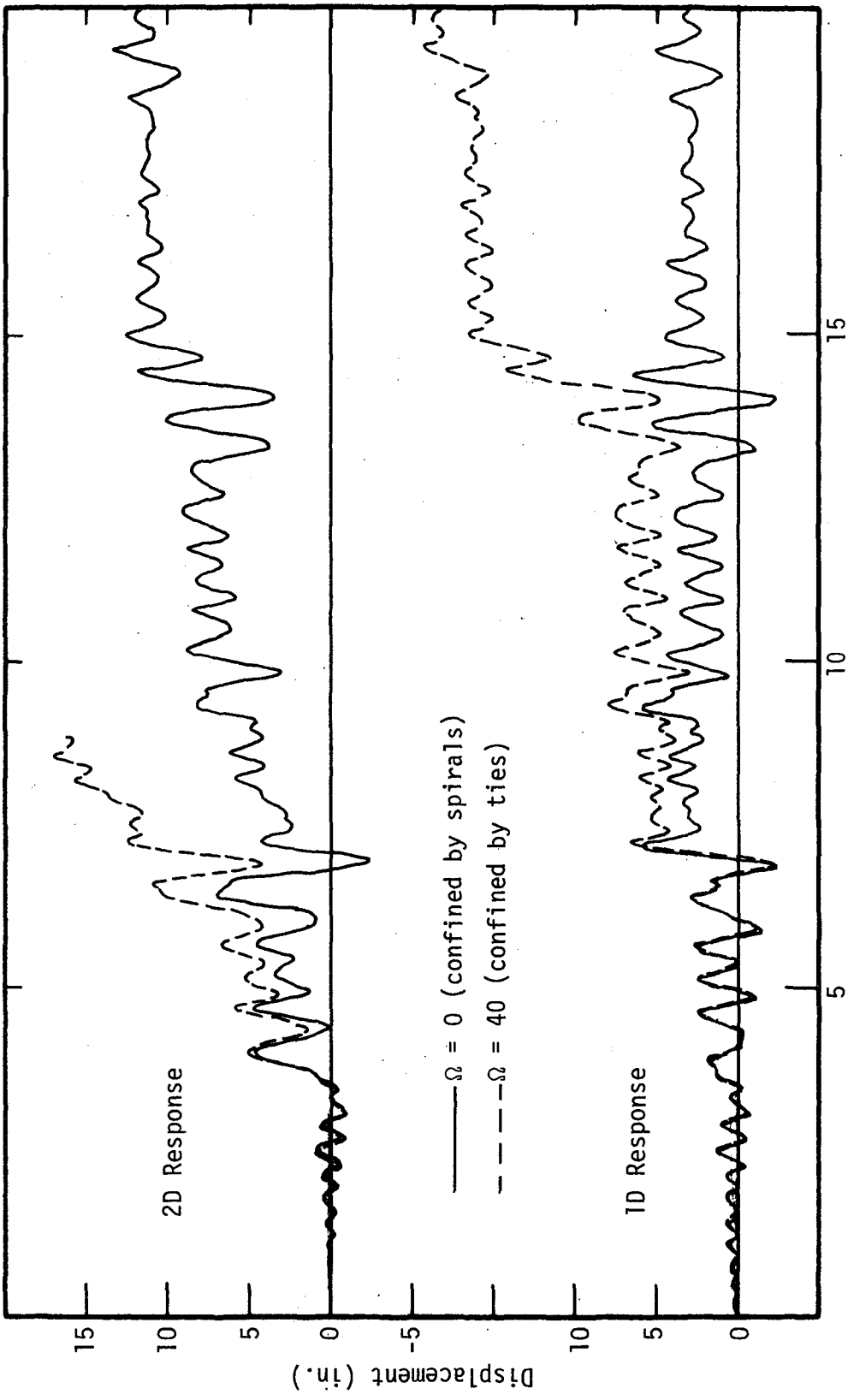

Fig. 3.48 Effect of Concrete Confinement on Displacement Response, P = - 562, T = 0.4 System, Taft N21E Record

APPENDIX A

MATERIAL HYSTERESIS RULES

A.1 Steel

The general relationship recommended by Richards and Abbott (24) was used to model stress-strain behavior of steel.

The rules used to determine the model are shown schematically in Figure 2.1, and are as follows:

For monotonic loading,

1. $\sigma = E\ \varepsilon \qquad |\varepsilon| < \varepsilon_y$ (A.1)

2. $\sigma = \sigma_y \qquad \varepsilon_y < |\varepsilon| < \varepsilon_{sh}$ (A.2)

3. $$\frac{\sigma}{\sigma_y} = \frac{(1-\alpha)\ \frac{\varepsilon}{\varepsilon_y}}{1 + \frac{|\varepsilon|}{\varepsilon_y\ \beta_{mon}}} + \alpha\ \frac{\varepsilon}{\varepsilon_y} \qquad \varepsilon_{sh} < |\varepsilon| \qquad \text{(A.3)}$$

but $|\sigma|$ not greater than σ_{ult}, and for all subsequent half-cycles,

4. $$\frac{\sigma-\sigma_i}{\sigma_y} = \frac{(1-\alpha)\ \frac{\varepsilon-\varepsilon_i}{\varepsilon_y}}{\left|1 + \left(\frac{|\varepsilon-\varepsilon_i|}{\varepsilon_y\ \beta_{cyc}}\right)^n\right|^{1/n}} + \alpha\ \frac{\varepsilon-\varepsilon_i}{\varepsilon_y} \qquad \text{(A.4)}$$

but $|\sigma|$ not greater than σ_{ult}.

5. Whenever an inner curve intersects an outer curve the outer curve is followed.

In the above equations,

σ = stress (positive in tension)

ε = strain

σ_y = yield stress

σ_{ult} = maximum stress attainable

ε_y = yield strain (corresponding to $\sigma = \sigma_y$ in Eq. A.1)

ε_{sh} = strain at beginning of strain hardening (corresponding to $\sigma = \sigma_y$ in Eq. A.3)

σ_i = stress at start of half-cycle

ε_i = strain at start of half-cycle

$\beta_{cyc} = a + b\,(\sigma_{max} - \sigma_{min})/\sigma_y$

$n = c + d\,(\sigma_{max} - \sigma_{min})/\sigma_y$

σ_{max} = maximum stress reached in any previous cycle, but not less than σ_y

σ_{min} = minimum stress reached in any previous cycle, but not more than $-\sigma_y$

and a, b, c, d, E, α and β_{mon} are constants.

The constants a, b, c, d, E, α, β_{mon}, σ_y and σ_{ult} have to be specified for each type of steel.

Also four strains, the strain in the previous step ε_{prev}, the maximum strain reached previously ε_{max}, the minimum strain reached previously ε_{min} and the strain at the beginning of the present half-cycle ε_i, and their corresponding stresses σ_{prev}, σ_{max}, σ_{min} and σ_i have to be retained as strain history parameters for each bar of steel.

The following values were used in this study whenever Grade 60 steel was assumed. These values were obtained from experiments reported by Aktan et al. (2).

$E = 29000$ ksi

$\alpha = 0.02$

$\beta_{mon} = 1.3$

$\beta_{cyc} = 0.9 + 0.6\ (\sigma_{max} - \sigma_{min})/\sigma_y$ but not greater than 2.75

$n = 0.9 + 0.3\ (\sigma_{max} - \sigma_{min})/\sigma_y$ but not greater than 1.8

$\sigma_{ult} = 1.7\ \sigma_y$

For Grade 40 steel some values had to be modified and are given below. These were obtained from experiments reported by Kent (13).

$\alpha = 0.01$

$\beta_{mon} = 1.15$

$\beta_{cyc} = 2.15$

$n = 2$

A.2 Concrete

The model used for the stress-strain relationship of concrete is a simplified version of the one used by Darwin (5). The basic rules of the model are shown in Figure 2.5. The model is characterized by an envelope curve (which also models monotonic loadings), and rules for loading reversals.

The slope of the envelope curve after maximum stress distinguishes between unconfined concrete, concrete confined by rectilinear ties and concrete confined by spiral reinforcement.

The following rules construct the envelope curve:

1. $\sigma = 0$ $\qquad \varepsilon \geq \varepsilon_t$ $\qquad$ (A.5)

2. $\sigma = E_o \varepsilon$ $\qquad \varepsilon_t \geq \varepsilon \geq 0$ $\qquad$ (A.6)

3. $\frac{\sigma}{\sigma_o} = 2 \frac{\varepsilon}{\varepsilon_o} - (\frac{\varepsilon}{\varepsilon_o})^2$ $\qquad 0 \geq \varepsilon \geq \varepsilon_o$ $\qquad$ (A.7)

4. $\frac{\sigma}{\sigma_o} = 1 - \Omega(\varepsilon - \varepsilon_o)$ $\qquad \varepsilon_o \geq \varepsilon \geq \varepsilon_{20}$ $\qquad$ (A.8)

   $\Omega = 0.0$ for concrete confined by spiral reinforcement

   $\Omega = \frac{0.5}{\varepsilon_o - \varepsilon_{50}}$ for concrete confined by rectilinear ties

   and for unconfined concrete Ω is obtained from Eq. A.8 by using $\varepsilon = \varepsilon_{20} = 4 \varepsilon_o$ for $\sigma = 0.2 \sigma_o$.

5. $\sigma = 0.2 \sigma_o$ for confined concrete

   $\sigma = 0.0$ for unconfined concrete $\qquad \varepsilon_{20} \geq \varepsilon$ $\qquad$ (A.9)

where,

σ = stress (positive in tension)

ε = strain

ε_t = tensile strain in concrete corresponding to tensile strength $\sigma_t = E_o \varepsilon_t$

σ_o = compressive strength of concrete

ε_o = strain corresponding to σ_o in Eq. A.7

$E_o = 2 \sigma_o / \varepsilon_o$

ε_{20} = strain at $\sigma = 0.2\ \sigma_o$ in Eq. A.8

ε_{50} = strain at $\sigma = 0.5\ \sigma_o$ in Eq. A.8. For concrete confined by rectilinear ties $\sigma_5 0 = 0.9\ A_v/s^2$

A_v = cross-sectional area of stirrup legs

s = spacing of stirrups

The rules for cyclic loading are described with reference to Figure 2.5. These rules are characterized by four points, which are the point of reversal from the envelope curve, given by the strain ε_{en}; the turning point, where slope of the unloading curve changes; the common point, where the unloading curve intersects the reloading curve; and the point on the strain axis where reloading begins, given by the plastic strain, ε_p.

Unloading from the envelope curve up to the turning point has slope E_o after which the unloading and reloading curves become parallel. The reloading line is defined by joining the plastic strain, ε_p with the common point and extending it to the envelope curve. Unloading and reloading between these two parallel lines is with the slope E_o. Unless the concrete has cracked previously loading in tension up to the tensile strength, σ_t can take place with a slope equal to the slope of the reloading line.

The plastic strain, ε_p is given by the following equation proposed by Karsan (12)

$$\frac{\varepsilon_p}{\varepsilon_o} = 0.145 \left(\frac{\varepsilon_{en}}{\varepsilon_o}\right)^2 + 0.13 \left(\frac{\varepsilon_{en}}{\varepsilon_o}\right) \qquad \text{(A.10)}$$

The common and turning points curves, joining all common and turning points respectively are assumed to be proportional to the envelope curve.

The constants σ_o, σ_t, ε_o, Ω and the ratios of the common and turning points curves to the envelope curve have to be specified for each type of concrete. The softening slope, may be specified directly or the lateral confinement of concrete from which it may be calculated can be specified.

Also the envelope strain ε_{en} and the stress ε_{prev} and strain ε_{prev} in the previous step have to be retained as strain history parameters for each point concrete stresses are being calculated for.

For the examples in this study the common points curve and the turning points curve were assumed to be 80 % and 50 % of the envelope curve, respectively.

APPENDIX B

CALCULATION OF MOMENT-CURVATURE-AXIAL LOAD RELATIONS

This appendix describes the procedure used in this study to calculate the resisting moments at a reinforced concrete section under a given set of biaxial curvatures and axial load. The axial load may be specified as a function of the resisting moments.

This procedure is used in the step by step calculation of the moment-curvature relationship at a section of a reinforced concrete column and it is assumed that the strain history parameters from the previous step, required in the stress-strain relations for steel and concrete are known (See Appendix A for details).

Referring to the axes shown in Fig. 2.8, the axial load P and the resisting moments M_1 and M_2 around the x and y axis respectively are given by

$$P = \int_A \sigma \, dA \tag{B.1}$$

$$M_1 = \int_A \sigma \, y \, dA \tag{B.2}$$

$$M_2 = \int_A -\sigma \, x \, dA \tag{B.3}$$

where σ is the stress and the integrals are evaluated over the area A of the reinforced concrete section.

The stress σ is obtained from hysteresis rules given in Appendix A, and may be written as

$$\sigma = \sigma \text{ (strain } \varepsilon\text{, strain history parameters, material properties)} \qquad \text{(B.4)}$$

The strain ε is given as

$$\varepsilon = \varepsilon_o + \phi_1 y - \phi_2 x \qquad \text{(B.5)}$$

where ε_o is the strain at the origin (the origin being located at the centroid of the concrete section) and ϕ_1 and ϕ_2 are the curvatures around x and y axis respectively. The assumption of linear strain distribution over the section and no bond-slip between steel and concrete is made in deriving Eq. B.5.

Since direct integration of Eqs. B.1-B.3 is complicated because of discontinuities in material properties and strain history parameters over the section they are evaluated as summations.

Equations B.1-B.3 can then be rewritten as

$$P = \sum_{i=1}^{N} \sigma_i A_i \qquad \text{(B.6)}$$

$$M_1 = \sum_{i=1}^{N} \sigma_i y_i A_i \qquad \text{(B.7)}$$

$$M_2 = \sum_{i=1}^{N} -\sigma_i x_i A_i \qquad \text{(B.8)}$$

where the area A of the reinforced concrete section is divided into N discrete areas A_i at locations (x_i, y_i). The evaluation of these areas and their locations is discussed in Section 2.3.1 of Chapter 2.

An inspection of Eqs. B.4-B.8 will reveal that given a set of curvatures, an axial load and strain history parameters from the previous step the evaluation of moments M_1 and M_2 from Eqs. B.7 and B.8 requires evaluation of the new centroidal strain ε_o from Eq. B.6.

Equation B.6 cannot be rewritten in a form from which ε_o can be directly calculated. Equation B.6 is, therefore, written in incremental form and an iterative procedure devised to calculate ε_o.

If the curvatures are held constant during a step, then

$$\Delta P = \sum_{i=1}^{N} E_{ti} \, \Delta\varepsilon_o \, A_i \qquad \text{(B.9)}$$

where ΔP is the change in axial load for a change $\Delta\varepsilon_o$ in the centroidal strain and E_{ti} is the tangent modulus for the discrete area A_i. This equation can be rewritten as

$$\Delta\varepsilon_o = \frac{P}{K_{tP}} \qquad \text{(B.10)}$$

where $K_{tP} = \sum_{i=1}^{N} E_{ti} \, A_i$ is the tangent stiffness of the column section to axial loads. The maximum value of K_{tP} occurs when the whole section is elastic. The minimum value for

computational purposes has been taken as 5% of the maximum value.

The procedure used to obtain ε_o and thus moments M_1 and M_2 from Eqs. B.7 and B.8, given the axial load, a set of curvatures and the strain history parameters is as follows:

1) Use ε_o from previous step and calculate P from Eq. B.6 using the new curvatures. The difference between the calculated P and the axial load required is ΔP.

2) Calculate $\Delta\varepsilon_o$ from Eq. B.10 using K_{tP} calculated from E_{ti} obtained in the previous call to the stress-strain routines.

3) Calculate new P from Eq. B.6 using $\Delta\varepsilon_o$ and obtain a new ΔP.

4) If ΔP in step 3 is of the same sign as in step 1 repeat steps 2-4 until the absolute value of ΔP is less than allowable tolerance in axial load. If ΔP in step 3 has changed sign interpolate for new ε_o using Eq. B.6 until the calculated P is within tolerance limits of the required axial load.

After the new ε_o is known the moments M_1 and M_2 are evaluated from Eqs. B.7 and B.8. If the required axial load is specified as a function of the moments, then M_1 and M_2 will have to be evaluated in steps 1, 3 and 4 also.

APPENDIX C

CALCULATION OF SHEAR-DEFLECTION-AXIAL LOAD RELATIONS

This appendix describes the procedure used in this study to calculate the shears in a reinforced concrete column, with both ends restrained against rotations, given a set of two-dimensional relative displacements between the ends.

This procedure is used for the step by step calculation of the shear-deflection relationship of a reinforced concrete column. A constant or a variable axial load dependent on the shears may be specified in each step.

It is assumed that the shears can be applied only at the ends of the column. Therefore, the bending moments vary linearly along the column in each of the two shear directions, and the shears can be obtained directly from the end moments. The moments about the same axis at either ends are also equal, because of rotational constraints at the ends. The point of contraflexure for both directions is, therefore, at the mid-length of the column. All deformations in the column are antisymmetrical about the point of contraflexure, thus, only one half of the column need be considered. This is the same as analyzing a cantilever column with half the length of the original column and half the relative displacement between the ends.

The moments at the fixed end of the column can be calculated from the curvatures at that section. However, the curvatures at the end section are now known in advance. Only the displacements (which are the moments of the curvature diagrams in each direction about the tip of the cantilever) are known. To be able to calculate the end curvatures from the displacements the distributions of the curvatures along the length of the column have to be assumed. These distributions of curvatures should be consistent with the assumption of linear bending moment diagrams along the length of the column.

In this study the cantilever column is assumed to consist of three segments in each of which a particular curvature distribution is assumed. The three segments are shown in Fig. 2.22 and are classified as uncracked, cracked but unyielded and yielded. The assumed distribution of curvatures in these segments is discussed in Section 2.3.2 of Chapter 2.

Although the shapes of the curvature diagrams along the length of the column have been assumed the end curvatures cannot be directly calculated from the given deflections. The reason is that the length of the segments and the values of the curvatures at the junctions of the segments are dependent on the end moments, the end moments being determined only after the end curvatures are known. An iterative procedure for obtaining the curvatures and thus the moments from the deflections is, therefore, used. The ratio between the change in

curvature in a particular direction and the change in the corresponding deflection in the immediately preceding step are used to predict the change in that curvature in the next step. This is if the change in deflection in that direction in the present step is of the same sign as in the preceding step. If the change is opposite in sign to the preceding step for any particular direction then the ratio for the elastic case which would be $12/L^2$ is used for prediction purposes in that direction. L/2 being the length of the cantilever column.

The complete procedure for calculating the moments from the given deflections in a particular step are:

1) In each direction compare the sign of the change in deflection in the present step with the previous step. If they are of the same sign use the ratio between the change in end curvature and the change in deflection from the previous step to predict new end curvature for that direction. If of opposite sign use ratio for elastic case.

2) Use procedure described in Appendix B to obtain end moments from the predicted end curvatures.

3) Obtain cracking and yielding moments and value of α required in Eq. 2.2 for rectangular sections, for the given axial load (if dependent on shears, axial load is calculated from the shears obtained from step 2) from a table of these values calculated in the beginning of the program. Also obtain

uncracked slope and the secant slope up to yield for the moment-curvature diagram for this axial load.

4) Identify sections where cracking or yielding has been initiated using cracking and yield curves shown in Figure 2.24 and change lengths of segments if required (the uncracked segment can only be shortened and the yielded segment can only be lengthened).

5) Calculate the curvatures at the junction of the segments from moments calculated in step 2 and slopes obtained in step 3.

6) Calculate the end deflections from the curvature diagrams calculated.

7) If the calculated deflections are within the allowable tolerance of the given deflections the moments calculated in step 2 are the required moments. If the calculated deflections are not within the allowable tolerance of the given values then new ratios between the change in curvature and the change in deflections are calculated and new curvatures predicted. Steps 2 to 7 are then repeated.

For computational purposes the minimum value of the ratio between change in curvature and change in deflection was assumed to be that for the elastic case ($12/L^2$). The maximum ratio was limited to ten times the minimum value.

The column is assumed to consist of only one segment if it is uncracked and of two segments if it has cracked but

not yielded. Also, if the column has yielded then for computational purposes the length of the yielded segment is taken as at least d/4, where d is the depth of the section.

It may be noted here that the numerical procedure outlined above gives results which are independent of the size of the step. However, the number of iterations required to predict the correct curvatures to satisfy the given deflections and to predict the centroidal strain to satisfy the given axial load will increase with increase in the size of the step.

APPENDIX D

PROCEDURE FOR DYNAMIC ANALYSIS

D.1 Introductory Comments

The procedure used in this study to obtain the response of a reinforced concrete column subjected to two-dimensional earthquake motion is given in this appendix. The reinforced concrete column is modeled with a single mass at the top with two translational degrees of freedom and fixed at the base, where the motion is applied. The determination of the mass for modeling different system periods is discussed in Section 3.3 of Chapter 3.

The equations of motion are given in the next section. Since the forcing function as well as the resisting forces cannot be described as a continuous function, a step by step procedure (17) is used to integrate the equations of motion in the time domain. Section D.3 describes the procedure for the solution of the equations. The shear-deflection relations for reinforced concrete columns developed in Chapter 2 are used to obtain the resisting forces.

D.2 Equations of Motion

For a single mass system with two translational degrees of freedom, subjected to base excitation, the

equation of motion in incremental form is

$$[M]\{\Delta\ddot{X}\} + [C]\{\Delta\dot{X}\} + \{\Delta F\} = -[M]\{\Delta\ddot{Y}\} + \{R\} \qquad (D.1)$$

where

$[M]$ is the diagonal, mass matrix,

$[C]$ is the diagonal, viscous damping matrix,

$\{\Delta\ddot{X}\}$ contains the incremental relative accelerations between mass and base,

$\{\Delta\dot{X}\}$ contains the incremental relative velocities between mass and base,

$\{\Delta\ddot{Y}\}$ contains the incremental base accelerations,

$\{\Delta F\}$ contains the changes in the resisting forces of the system, and

$\{R\}$ contains any unbalanced force left in previous time step.

Assuming a linear variation in the response acceleration between time t and t + Δt (β = 1/6 in Ref. 17) the response velocity $\{\dot{X}\}$ and displacement $\{X\}$ at time t + Δt can be written as:

$$\{\dot{X}\}_{t+\Delta t} = \{\dot{X}\}_t + \frac{\Delta t}{2}(\{\ddot{X}\}_t + \{\ddot{X}\}_{t+\Delta t})$$

$$\{X\}_{t+\Delta t} = \{X\}_t + \Delta t\{\dot{X}\}_t + \frac{\Delta t^2}{3}\{\ddot{X}\}_t + \frac{\Delta t^2}{6}\{\ddot{X}\}_{t+\Delta t} \qquad (D.2)$$

The incremental velocities and accelerations can be obtained from Eqs. D.2 in terms of the incremental displacements and responses at time t as

$$\{\Delta\dot{X}\} = \frac{3}{\Delta t}\{\Delta X\} - 3\{\dot{X}\}_t - \frac{\Delta t}{2}\{\ddot{X}\}_t$$

$$\{\Delta\ddot{X}\} = \frac{6}{(\Delta t)^2}\{\Delta X\} - \frac{6}{\Delta t}\{\dot{X}\}_t - 3\{\ddot{X}\}_t \qquad \text{(D.3)}$$

Substitution of Eqs. D.3 into Eq. D.1 gives

$$\left(\frac{6}{\Delta t^2}[M] + \frac{3}{\Delta t}[C]\right)\{\Delta X\}$$

$$= -[M]\{\Delta\ddot{Y}\} + \left(\frac{6}{\Delta t}[M] + 3[C]\right)\{\dot{X}\}_t$$

$$+ \left(3[M] + \frac{\Delta t}{2}[C]\right)\{\ddot{X}\}_t - \{\Delta F\} + \{R\}$$

which can be rewritten as

$$[K^*]\{\Delta X\} = \{Q\} - \{\Delta F\} \qquad \text{(D.4)}$$

where

$$[K^*] = \frac{6}{\Delta t^2}[M] + \frac{3}{\Delta t}[C]$$

and

$$\{Q\} = -[M]\{\Delta\ddot{Y}\} + \left(\frac{6}{\Delta t}[M] + 3[C]\right)\{\dot{X}\}_t$$

$$+ \left(3[M] + \frac{\Delta t}{2}[C]\right)\{\ddot{X}\}_t + \{R\}$$

[K*] may be called the dynamic stiffness matrix and {Q} the dynamic load vector. It may be noted that for the problem under consideration [K*] is diagonal and constant.

D.3 Procedure for Solution of Equations of Motion

The equations of motion in incremental form given by Eq. D.4 cannot be solved directly for the incremental displacement vector $\{\Delta X\}$, since the changes in the resisting forces $\{\Delta F\}$ are not known in advance. An iterative procedure is, therefore used to solve Eq. D.4. For the first iteration $\{\Delta F\}$ is assumed to be zero and $\{\Delta X\}$ evaluated from Eq. D.4. $\{\Delta F\}$ is then evaluated from the shear-deflection relations described in Appendix C using this value of $\{\Delta X\}$. Equation D.4 and the shear-deflection relations are solved successively until values of $\{\Delta F\}$ in consecutive iterations are within the allowable tolerance. The solution then proceeds to the next time step.

The complete procedure used in this study to obtain the response of a reinforced concrete column subjected to two-dimensional earthquake motion is as follows:

1) Initialize strain history parameters for the steel and the lumped concrete for the end section of the column. Initialize ε_o, the centroidal strain to the value for axial load only. Initialize lengths of yielded, unyielded and uncracked segments for shear-deflection calculations.

Initialize relative velocities and displacements for the system. Calculate mass and damping matrices for the system for the given period. Calculate dynamic stiffness [K*].

2) Calculate dynamic load vector {Q}.

3) Calculate {ΔX} from Eq. D.4 using value of {ΔF} evaluated in the previous iteration. If first iteration use {ΔF} equals zero.

4) From the value of {ΔX} obtained in step 3, predict changes in end curvatures using curvature/deflection ratios as explained in Appendix C. Calculate total end curvatures.

5) From predicted end curvatures, predict end moments iterating on ε_o as described in Appendix B, to obtain the required axial load within the allowable tolerance in axial load.

6) Using the end moments obtain lengths of uncracked, unyielded and yielded segments. Calculate curvatures at the junction of these segments and evaluate the deflections as described in Appendix C.

7) If {ΔX} obtained from Step 6 is within the allowable tolerance of deflection {ΔX} in step 3, proceed to step 8. If tolerance in deflection is exceeded calculate new curvature/ deflection ratios, predict further changes in curvatures and repeat steps 5 to 7.

8) From the end moments calculated in step 5, calculate changes in the resisting forces {ΔF}. If {ΔF} is within

allowable tolerance of $\{\Delta F\}$ used in step 3 then proceed to step 9. If tolerance level is exceeded repeat steps 3 to 8 using new value of $\{\Delta F\}$.

9) Repeat steps 2 to 9 for each step.

A flow-chart of the above procedure for a single time step is shown in Figure D.1.

D.4 Concluding Remarks

It may be noted that the procedure detailed in Section D.3 requires iterative solutions at three levels. The lowest level of iteration is for obtaining the centroidal strain ε_o for the end section of the column. A tolerance level for the error in the axial load is specified for these iterations. The next level of iteration is for calculating the end curvatures given a deflection increment. A tolerance level for the difference between the given and calculated deflection is specified. The highest level of iteration is for obtaining the change in relative displacements from the equations of motion (Eq. D.4). A tolerance level for the satisfaction of that equation is specified. A necessary condition for the iterations at a higher level to converge is that the maximum error introduced by the allowable tolerance at a lower level be less than the allowable tolerance at the higher level. This conditions should be considered when specifying tolerances.

The tolerances allowed in this study were 5 kips for axial load, 0.005 inches for deflection and 1 kip for the unbalance in the equation of motion. These can be compared with 3600 kips axial load capacity, 0.93 inches yield displacement and 131 kips yield shear.

The average number of iterations required for each time step were 1.8 to obtain $\{\Delta X\}$ from the equations of motion. This in turn required a total of 3.0 iterations per time step to obtain curvatures from deflections. This further required a total of 6.5 iterations per time step to obtain ε_o to satisfy the axial load.

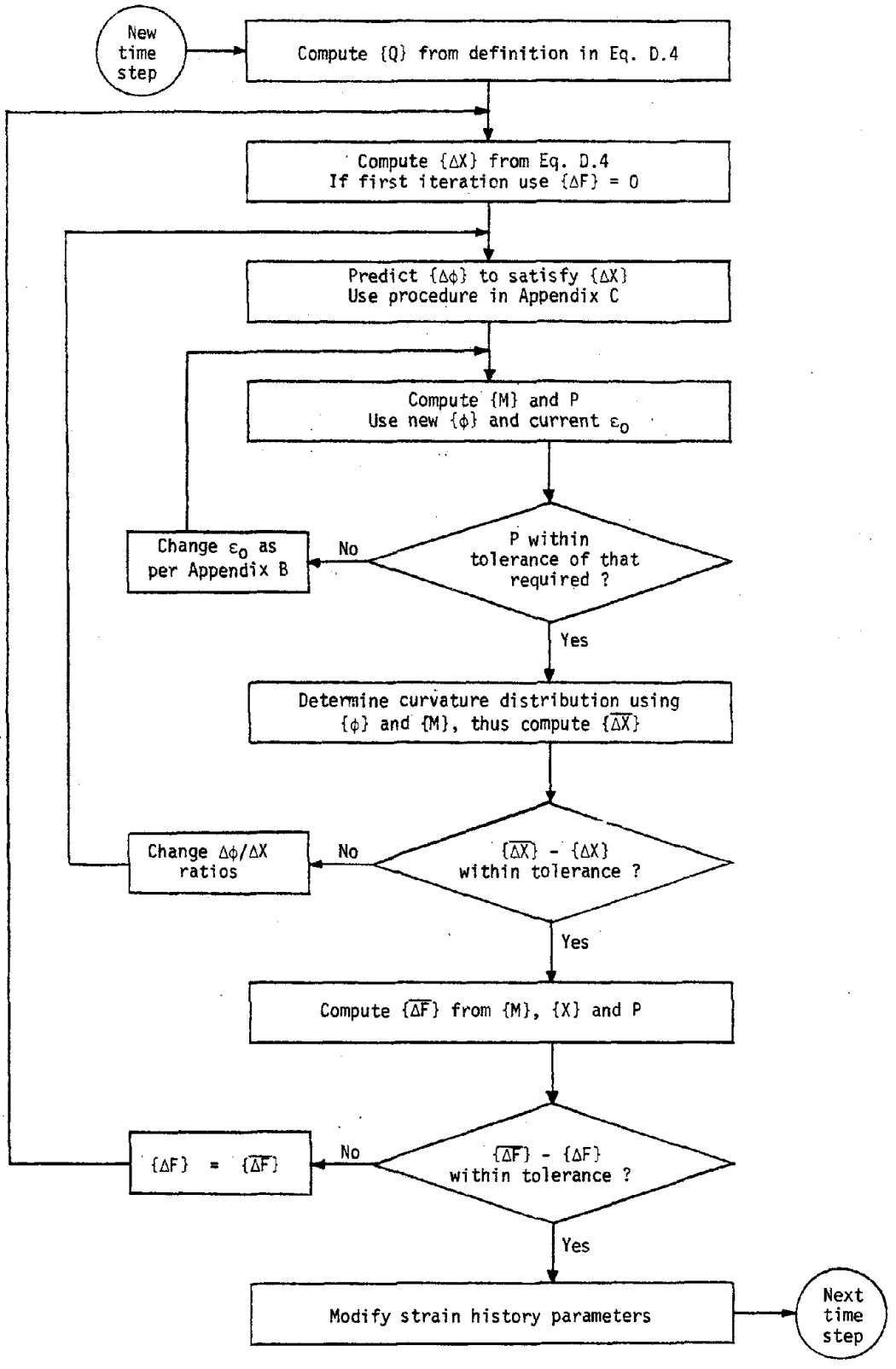

Fig. D.1 Flow-Chart of Calculation Procedure for Single Time Step

APPENDIX E

NOTATIONS

The following symbols are used in the study:

A_i = ith discrete area in section

A_{max} = peak acceleration recorded during an earthquake

A_s = area of longitudinal steel in the section

A_v = cross-sectional area of stirrup legs

$[C]$ = 2 x 2 viscous damping matrix of the system

D_1 = displacement in Direction 1

D_2 = displacement in Direction 2

E = modulus of elasticity of steel

E_o = initial modulus of concrete

E_{t_i} = tangent modulus of ith discrete area in the section

$\{F\}$ = 2 x 1 vector of shear resistance of column

K = uniaxial secant stiffness up to yield for the column

K_{tp} = tangent stiffness of column section to axial loads

$[K^*]$ = 2 x 2 dynamic stiffness matrix of the system

L = length of fixed-fixed column

M = moment at a section

$\{M\}$ = 2 x 2 mass matrix of the system

M_1 = moment around Direction 1 at a section

M_2 = moment around Direction 2 at a section

M_{cr} = initial cracking moment for a section

M_{cr1} = uniaxial cracking moment for a section in Direction 1

M_{cr2} = uniaxial cracking moment for a section in Direction 2

M_y = uniaxial yield moment for a section

M_{y1} = uniaxial yield moment for a section in Direction 1

M_{y2} = uniaxial yield moment for a section in Direction 2

P = axial load on the column (positive in tension)

$\{Q\}$ = 2 x 1 dynamic load vector

$\{R\}$ = 2 x 1 vector containing imbalance in equation of motion in the previous time step

T = period of the system

V = shear resistance of the column

V_1 = shear resistance of the column in Direction 1

V_2 = shear resistance of the column in Direction 2

V_y = shear resistance of the column at yield

$\{X\}$ = 2 x 1 vector of relative displacements between mass and base

$\{\dot{X}\}$ = 2 x 1 vector of relative velocities between mass and base

$\{\ddot{X}\}$ = 2 x 1 vector of relative accelerations between mass and base

$\{\ddot{Y}\}$ = 2 x 1 vector of ground accelerations

a_i = ground acceleration in direction i

a_j = ground acceleration in direction j

$\bar{a}_i$ = average of ground acceleration in direction i over the duration of the record

$\bar{a}_j$ = average of ground acceleration in direction j over the duration of the record

c = yield shear ratio = Vy/mg

cov_{ij} = covariance of accelerations in directions i and j

d = depth of column section

f'_c = cylinder strength of concrete

g = acceleration due to gravity

k_{cr} = uniaxial stiffness up to cracking for a section

k_y = uniaxial secant stiffness up to yield for a section

m = mass on column top

m_1 = moment in a particular direction at junction of segments 1 and 2

m_2 = moment in a particular direction at junction of segments 2 and 3

m_3 = moment in a particular direction at column end

n = shape parameter for steel stress-strain curve

r = radius of circular sections

s = stirrup spacing

t = time

t_o = time were variances or covariances are being computed

u_y = uniaxial yield displacement of the column

x = x-coordinate measured from centroid of concrete section

x_i = x-coordinate of ith discrete area in the section

y = y-coordinate measured from centroid of concrete section

y_i = y-coordinate of ith discrete area in the section

z = z-coordinate measured along column axis from column end

Δ = column displacement used for gravity effects

Δ = increment in a quantity

Ω = softening slope of the concrete envelope curve

α = shape parameter for yield determination at a section

α = parameter representing strain-hardening slope for steel stress-strain curve

β = coefficient in Newmark's β-method

β_{cyc} = strength parameter for steel cyclic stress-strain curve

β_{mon} = strength parameter for steel monstonic stress-strain curve

ε = strain (positive in tension)

ε_o = centroidal strain of the section

ε_o = strain at maximum stress in concrete

ε_{20} = strain in concrete when stress reaches 20 % of maximum on the descending branch of the envelope curve

ε_{50} = strain in concrete when stress reaches 50 % of maximum on the descending branch of the envelope curve

ε_{en} = strain on envelope curve of concrete from where reversal took place

ε_i = steel strain at last reversal

ε_{max} = maximum steel strain reached previously

ε_{min} = minimum steel strain reached previously

ε_p = plastic strain of concrete

ε_{prev} = strain at previous time step

ε_{sh} = strain at beginning of strain-hardening in steel

ε_t = strain corresponding to tensile strength of concrete

ε_y = yield strain of steel

μ = displacement ductility

σ = stress (positive in tension)

σ_o = compressive strength of concrete

σ_i = steel stress at last reversal

σ_{max} = maximum steel stress reached previously

σ_{min} = minimum steel stress reached previously

σ_t = tensile strength of concrete

σ_{ult} = maximum possible stress in steel

σ_y = yield stress of steel

$\{\phi\}$ = 2 x 1 vector of curvatures at end sections of columns

ϕ_1 = curvature in a particular direction at junction of segments 1 and 2

ϕ_2 = curvature in a particular direction at junction of segments 2 and 3